UNIVERSITY of LONDON,
IMPERIAL COLLEGE of SCIENCE AND TECHNOLOGY
PHYSICS DEPARTMENT,
BIOPHYSICS SECTION.

COLOUR MECHANISMS IN NORMAL AND DEFECTIVE HUMAN VISION

BY

ISOBEL MARY BLYTHE

Thesis submitted for the degree of Doctor of Philosophy
of the University of London

1984

TABLE OF CONTENTS

		Page Number
ABSTRACT		3
CHAPTER 1	General Introduction	5
CHAPTER 2	Experimental Apparatus	34
CHAPTER 3	Post-receptoral inhibitory responses in subjects with normal colour vision	57
CHAPTER 4	Visual responses of congenital red-green colour defective subjects	90
CHAPTER 5	Visual responses of a subject with an unusual defect associated with chromatic light stimuli	156
CHAPTER 6	Summary and General Conclusions	180
APPENDIX A	Data recording circuit	183
APPENDIX B	Representation of a desaturated stimulus in terms of chromatic and achromatic components.	185
REFERENCES		187
ACKNOWLEDGEMENTS		198

ABSTRACT

This thesis describes a psychophysical investigation into several aspects of human colour vision. The introductory chapter contains a review of relevant psychophysical and electrophysiological studies of the vertebrate visual system. The apparatus employed in the present study, some of which was newly constructed or modified from existing equipment, is described in chapter two.

The third chapter begins with a brief review of some binocular adaptation experiments, based on the contrast threshold elevation effect (Blakemore and Campbell, 1969 b), and the associated binocular inhibitory effect (Ruddock and Wigley, 1976). It has been shown that application of these methods reveals three independent spectral response mechanisms: two red-green opponent and one short-wavelength sensitive. New data relating to these post-receptoral chromatic responses is presented, and a method for the calculation of the spectral sensitivities of these mechanisms is proposed.

In subjects with normal colour vision, the most consistent results are obtained in measurement of the red-green opponent post-receptoral mechanism, the spectral sensitivity of which is described by the subtraction of the green-sensitive cone response from the red-sensitive cone response, and data for this mechanisms measured for red-green dichromats and anomalous trichromats is described in chapter four. It is shown that dichromats have no wavelength dependent response, which is consistent with

their lacking one or other of the red and green photopigments. The deuteranomalous trichromats nearly all obtained similar results to the normal and this is analysed with respect to the current theories of anomalous trichromacy. Data for the change in the Rayleigh match of normal and anomalous trichromats when subjected to intense bleaching lights are also presented, as are the wavelength discrimination curves for the colour defective observers.

The remainder of the thesis describes the visual responses of a subject (MW) who has a rare central colour vision defect. This defect is associated with a strong inhibitory response to chromatic, and in particular long-wavelength, stimuli which suppresses the detection of other high-contrast stimuli.

CHAPTER ONE

General Introduction

Section		Page
1.1	Gross Anatomy of the Visual System	6
1.2	Structure of the Retina	8
1.3	Receptor Photopigments	10
1.4	Chromatic Coding of Neural Signals	11
1.4.1	S-Potentials	12
1.4.2	Ganglion Cells	13
1.4.3	L G N	15
1.4.4	Striate Cortex	16
1.4.5	Prestriate Cortex	18
1.5	Colour Matching	18
1.5.1	The W.D. Wright System of Colour Matching	20
1.5.2	The C.I.E. System	21
1.6	Colour Deficiencies	24
1.6.1	Dichromats	26
1.6.2	Anomalous Trichromats	26
1.7	Spatially Structured Stimuli	30
1.7.1	Contrast Threshold Elevation Effect	31

1.1 Gross Anatomy of the Visual System

A schematic diagram of the visual pathways is shown in fig. 1.1a. Light from the external visual field is focused by the lens on to the retina, thus forming an inverted two-dimensional image. Light is absorbed by the photoreceptors which are situated at the back of the eye and phototransduction takes place, thus converting light energy into graded electrical potentials. There are two classes of receptor; rods which are responsible for low acuity, monochromatic vision at low illumination levels (scotopic conditions) and cones which are responsible for colour vision and high visual acuity at high illumination levels, e.g. daylight (photopic conditions). Under photopic conditions the retinal image is centred at the fovea which is almost entirely populated by cones and is thus an area of high spatial resolution and colour discrimination.

After complex processing by the various neural layers of the retina, signals pass along the optic nerve fibres which connect the retina to the lateral geniculate nucleus (LGN) via the optic chiasma. Here partial decussation of the fibres occurs, such that fibres from the nasal half-field of the retinae of both eyes cross to the opposite side of the brain and those from the temporal half-field continue to the same side. The external visual field is divided into two along the vertical meridian, each half being separately represented in the visual cortex. The two separate half-fields are brought together by the fibres of the corpus callosum, which link the two halves of the brain.

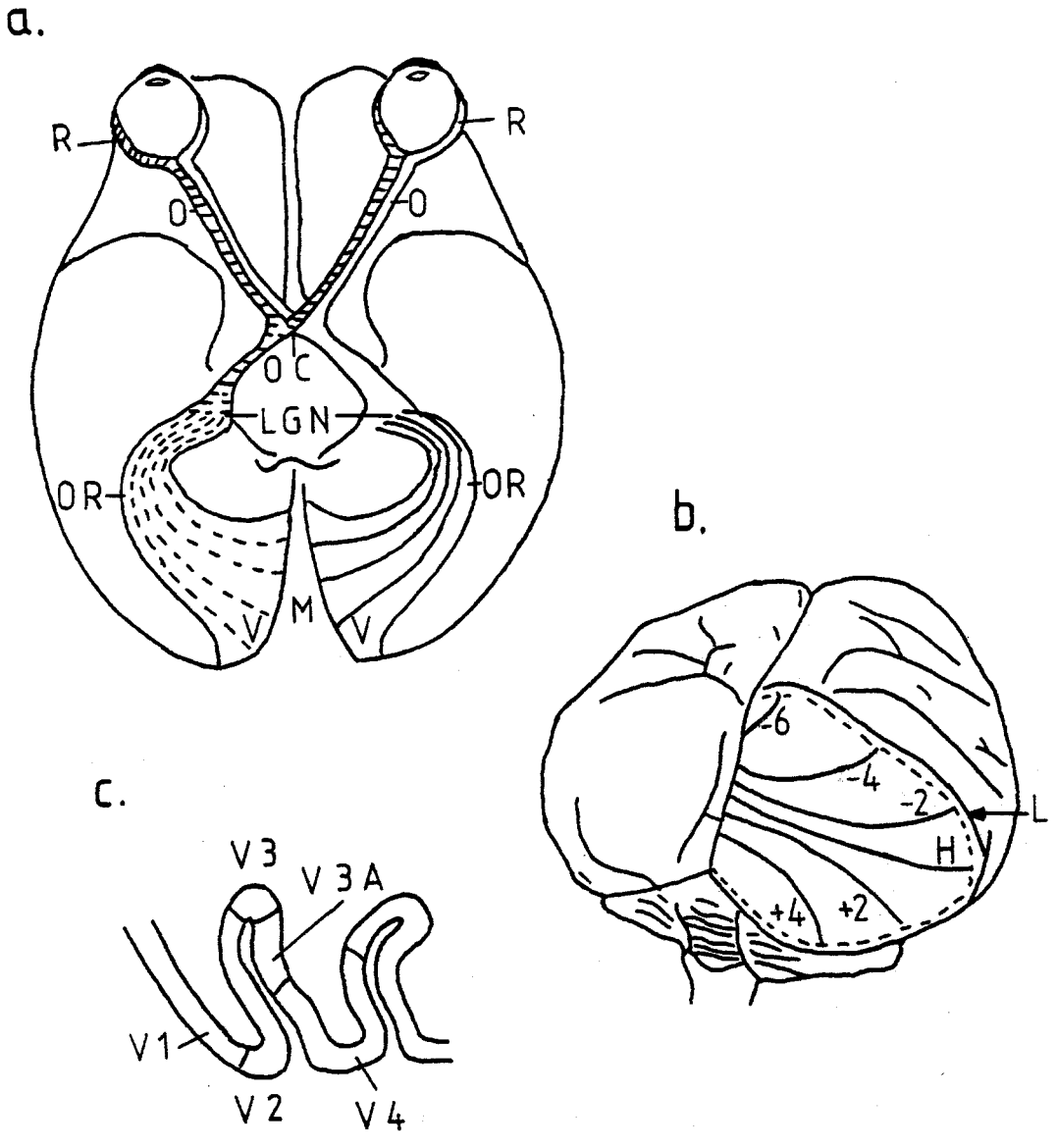


Fig. 1.1a Schematic view from underneath the brain of the primate visual system. R, Retina; O, optic nerve; OC, optic chiasma; LGN, lateral geniculate nucleus; OR, optic radiation; V, visual cortex; M, midline dividing the two halves of the brain.

b. View of the back of the primate brain showing the mapping of the visual field on to the striate cortex. Continuous lines show the mapping of lines parallel to the horizontal meridian at different degrees of eccentricity. The vertical meridian (dotted line) runs along the border of the lunate sulcus (L) which marks the limit of the striate cortex.

c. Horizontal section through the striate and prestriate cortex showing the different visual areas.

In the primate, axons from cells in the LGN project to the striate visual cortex (area 17 or V1), where there is a point-to-point map of the external visual field (fig. 1.1b), which is distorted such that the representation of the foveal area comprises a disproportionately large cortical area. The striate cortex projects to the prestriate cortex where further functional maps have been identified (Zeki, 1978), as illustrated in fig. 1.1c. V2 receives input from V1 and V3 is a mirror image of V2. V4 is not an ordered map and contains a high proportion of colour selective cells.

1.2 Structure of the Retina

Fig. 1.2 shows a schematic drawing of the primate retina (Dowling and Boycott, 1966) obtained from electron microscopic studies. There are two synaptic layers, the outer and inner plexiform layers. The outer plexiform layer contains vertical synapses between the photoreceptors and the bipolar cells. Rods synapse with only one type of bipolar cell, the rod bipolar cell, which pools signals from many separate rod receptors, thus increasing absolute sensitivity but reducing visual acuity (Boycott & Dowling, 1969). Cones, however, synapse with two distinct bipolar cells, the midget and the flat or diffuse cone bipolar cells. A midget bipolar usually connects to only one cone, whereas a flat bipolar connects to about seven cones. Thus, the two classes of photoreceptor in the primate retina have separate bipolar pathways. Horizontal cells also synapse with rods and cones, and send long extensions laterally across the retina.

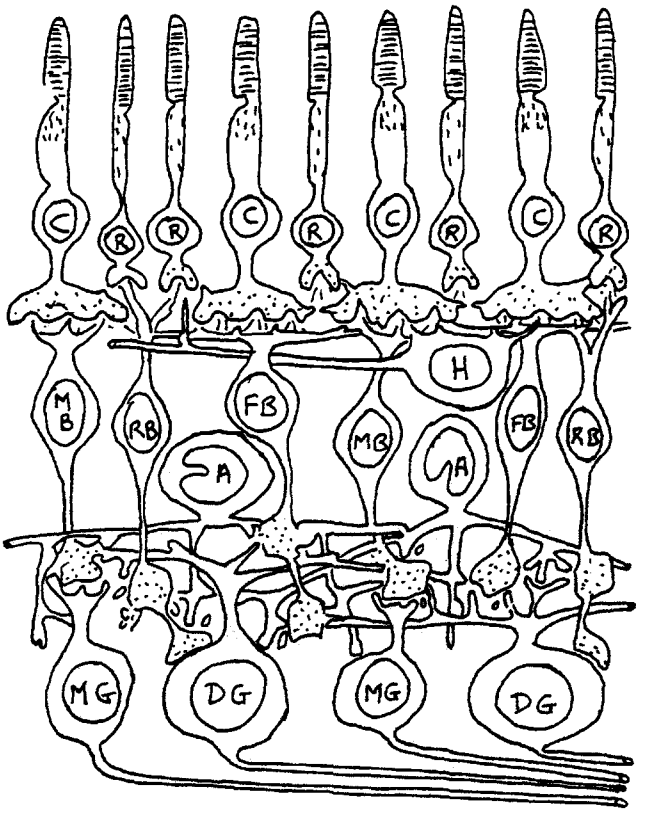


Fig. 1.2 Schematic section through the primate retina. R, rod photoreceptors; C, cone photoreceptors; H, horizontal cells; MB, midget bipolar cells; RB, rod bipolar cells; FB, flat bipolar cell; A, amacrine cells; MG, midget ganglion cells; DG, diffuse ganglion cells. From Dowling and Boycott, 1966.

In the inner plexiform layer, ganglion cells synapse with amacrine and bipolar cells. Each midget ganglion cell contacts a single midget cone bipolar cell; amacrine cells have synaptic contact with all classes of bipolar cell, with ganglion cells, and also with each other.

1.3 Receptor Photopigments

The rod photopigment, rhodopsin, has been extracted and chemically analysed (Wald, 1968). It has been shown that the pigment absorption spectrum closely follows the human scotopic sensitivity function, and that rod pigments extracted from different species have identical absorption spectra, when plotted as a function of stimulus frequency, except that the position of peak absorption varies (Dartnall, 1952).

There is, however, much less information available concerning the cone photopigments, which have proved difficult to extract and identify. The most direct method of measuring cone absorption spectra has been the microspectrophotometric technique of Marks, Dobelle and MacNichol, 1964 and Brown and Wald, 1964. This revealed the presence of three types of cone receptor in the excised parafoveal human and monkey retina (see Fig. 1.3), with peak sensitivities at 445 - 450 nm, 525 - 535 nm, and 555 - 570 nm. More recent microspectrophotometric investigations (Bowmaker et al, 1978; Bowmaker and Mollon, 1980) have confirmed these findings in the monkey retina, using larger samples of cones. They, too, found three classes of cones with maximum sensitivities at 415- 420 nm, 535 nm and 565 nm.

Information regarding the cone photopigments has also been obtained by fundus reflectometry (Rushton, 1963: 1965), where the light intensity of different wavelengths reflected from the back of the eye is measured before and after

bleaching of the photopigments, thus enabling the sensitivity of the photopigments to be deduced. This method has revealed interesting information concerning dichromatic colour defective subjects, who have only one pigment active in the long-wavelength region of the spectrum, but cannot separate absorption in the two normal middle - and long - wavelength sensitive mechanisms.

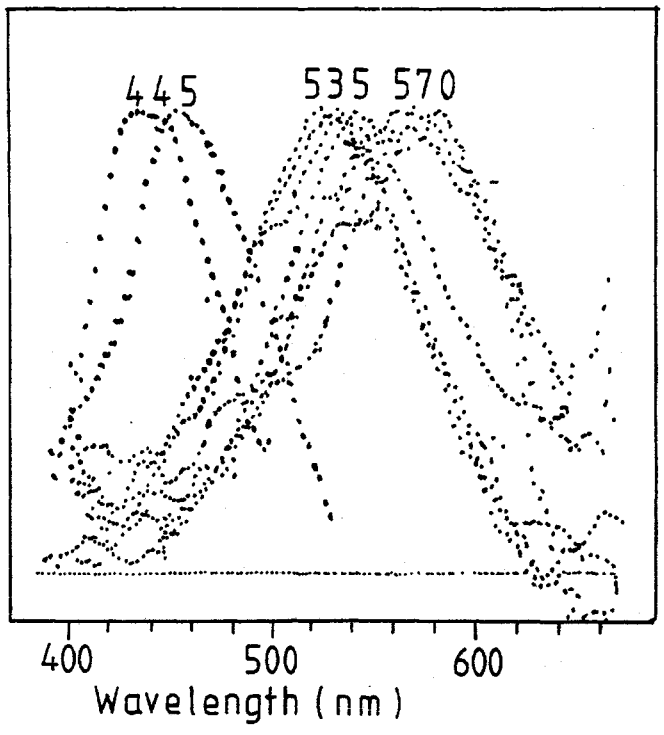


Fig. 1.3 Difference spectra recorded from ten primate parafoveal cones.
From Marks, Dobelle and MacNichol, 1964.

1.4 Chromatic Coding of Neural Signals

In the nineteenth century, there were two rival theories of colour vision; the trichromatic theory advocated by Helmholtz and Maxwell, and proposed by Young (1802), who stated that it was almost impossible to

conceive of an infinite number of receptors at each sensitive point of the retina and suggested that the number was limited to three. The "rival" theory of opponent colours was proposed by Hering (1885), and it was originally supposed that colour vision was mediated by three substances which were either broken down or regenerated by pairs of complementary radiations: light and dark, red and green, yellow and blue. This theory, as a description of retinal receptors, is wrong, but it is believed that colour information is coded as opponent-colour responses at later stages of the retina and visual pathways.

1.4.1. S - Potentials

The first evidence of opponent-colour responses in the visual system are the so-called Slow-Potentials (S-Potentials) recorded by Svaetichin(1953)in the isolated carp retina. He found two different types of graded photopic response: the luminosity (L-type) response which was hyperpolarising independent of stimulus wavelength, and the chromaticity-type response (Y-B, R-G) which has two maxima of opposite sign centred about a neutral point (the stimulus wavelength which causes no change of the "unit's" D.C. potential). The chromatic responses appear to be combinations of two separate potentials of opposite sign "subtracted" from one another. Svaetichin originally supposed that these S-potentials were cone responses, but later (Svaetichin and MacNichol, 1958) suggested that they arose in the horizontal cell layer (the chromatic response possibly being the bipolar cell response). Electrophysio-

logical and histological studies on the carp by Kaneko (1970) and Oikawa et al (1959), and the cat (Steinberg and Schmidt, 1970) confirmed that the site of origin of the S-Potentials was the horizontal cell layer.

1.4.2 Ganglion Cells

The ganglion cells, whose axons form the optic nerve fibres, tend to have concentrically organised receptive fields. Kuffler (1953) noted that the general functional organisation of ganglion cells in the cat retina is a central area of low threshold and a surround area whose response to stimuli is opposite to the centre response. Wagner, MacNichol and Wolbarsht (1960), when studying ganglion cells in the goldfish retina, noted that a change in wavelength of the light stimulus could convert a pure 'on' response to a pure 'off' response. A later study by Daw (1968) showed that these cells were in a minority and that most ganglion cells have a more complex receptive field structure. 49% of the cells studied had a centre-surround antagonistic organisation, such that the cell gave an 'on' response to red light and an 'off' response to green in the centre, and an 'off' response to red and an 'on' to green in the surround. Such units are appropriate for the detection of simultaneous colour contrast and imply a degree of specialisation at the ganglion cell level. Enroth-Cugell and Robson (1966), from studies on the cat retina, classified ganglion cells into two groups on the basis of the interaction between signals arising in the centre and the surround of the receptive field: X - which appear to

have linear summation over their receptive fields and Y - which have non-linear summation.

Michael (1968), recording from the optic nerve fibres of the ground squirrel, found two types of colour-opponent cells; green 'off', blue 'on' or blue 'off', green 'on'. No red/green opponent responses were observed

Hubel and Wiesel (1960) found that the receptive fields of optic nerve fibres in the spider monkey were organised in a manner similar to those described by Kuffler in the cat, i.e. they had a concentric centre-surround antagonistic organisation. A later study by Gouras (1968) on the rhesus monkey revealed two types of ganglion cell, phasic and tonic, possibly corresponding to the X and Y cells of Enroth-Cugell and Robson. Phasic cells respond transiently at the onset of light stimulation, have no maintained discharge and receive signals from the red - and green - sensitive cone mechanisms, both of which are excitatory in the centre and inhibitory in the surround. Tonic cells discharge continuously to maintained stimulation of appropriate wavelength, and receive excitatory input from only one cone mechanism in the centre and inhibitory input from another cone mechanism in the periphery of the receptive field. They outnumber the phasic cells and are relatively more common towards the foveal area. Gouras (1969) suggested that these tonic cells are the same as Polyak's (1941) anatomical class of monosynaptic or individual ganglion cells,and Boycott and Dowling's (1969) midget ganglion cells. These are among the smallest

ganglion cells, making direct contact with a single bipolar, which in turn synapses with a single cone.

De Monasterio, Gouras and Tolhurst (1975) looked at the criteria for distinguishing colour-opponent, from spectrally non-opponent cells in the rhesus monkey retina,on the basis of the cone inputs they receive. They found that one third of the colour-opponent cells studied did not show colour opponency in the presence of neutral backgrounds and only revealed this behaviour in the presence of chromatic adaptation. They termed this characteristic 'concealed colour opponency' and found that the proportion of such cells increased towards the pheripheral areas of the retina.

De Monasterio (1978 a, b), recording from X and Y cells in the macaque retina, found that X cells had opponent-colour responses that had centre and surround responses mediated by input from different cone mechanisms, whereas most Y cells had centre and surround responses mediated by input from the same type of cone mechanism and were thus spectrally non-opponent. These results were consistent with those of Gouras (1968), but de Monasterio also found a small proportion of Y cells where one of the types of cone input present in one region of the receptive field was absent in the other region . Thus, there are a small proportion of colour-opponent Y cells present in the monkey retina.

1.4.3 LGN

The receptive fields of lateral geniculate cells appear to be organised in much the same way as the

ganglion cells. De Valois, Abramov and Jacobs (1966), and Wiesel and Hubel (1966) recorded from cells in the LGN of the macaque monkey and divided the responses into two general classes: spectrally opponent and spectrally non-opponent cells. Chromatic adaptation experiments by Hubel and Wiesel suggested that the spectrally opponent cells had connections with one cone mechanism in the field centre and another in the surround. De Valois et al suggested that the non-opponent cells transmit brightness information whereas the opponent cells transmit information about colour, the hue of the stimulus being determined by the relative responses of the different types of opponent cells. Padmos and Norren (1975), however, contended that because the majority of 'non-opponent' cells show antagonistic red-green cone interactions, the existence of a separate luminosity channel is doubtful.

1.4.4 Striate Cortex

Lennox-Buchthal (1962) studied the responses of single units in the monkey striate cortex to flashes of monochromatic light and found that about 50% of the units had narrow-band spectral sensitivities, which implies that they are colour opponent. Many cortical cells must have been missed in this study due to the large-field stimuli.

The breakthrough in studying cells in the striate cortex came from Hubel and Wiesel (1962, 1968) who used line stimuli on cortical cells in cat and monkey. They found that most cells could be categorised as simple, complex or hypercomplex. Simple cells were defined as

having receptive fields with spatially distinct 'on' and 'off' areas separated by parallel straight lines, i.e. bars or edges. Complex cells show no separation of receptive fields into excitatory and inhibitory parts. As for simple cells, a line stimulus (bar or edge) in a particular orientation evokes optimum response, but whereas for the simple cell the position of the stimulus is crucial, in the complex cell a response is evoked by a correctly oriented line on any part of the receptive field. Complex cells are also often selective for movement. Hypercomplex cells also respond to correctly oriented line stimuli, but extending the line beyond the activating part of the receptive field in one or both directions causes a marked fall-off in response.

Hubel and Wiesel found only a few colour opponent cells. This may have been due to the fact that they were studying the cortical representation of the parafovea rather than the fovea. Gouras (1970) and Michael (1978), however, discovered several different types of opponent-colour cells in the monkey striate cortex. One such cell was excited by the blue - and green - sensitive cone mechanisms at stimulus onset and by the red-sensitive cone mechanism at stimulus offset. Thirteen of the twenty-seven cortical cells recorded from by Gouras received signals from three different cone mechanisms. He also found that these colour-sensitive cells showed only transient responses. Gouras (1974) found that the majority of cells in layer 4B of the striate cortex are colour-opponent and do not show orientation or directional selectivity, whereas the majority

of cells in the outer layers exhibit considerable spatial selectivity without apparent colour-opponency.

1.4.5 Prestriate Cortex

The prestriate cortex of the monkey contains many different visual areas receiving direct inputs from the striate cortex (fig. 1.1c). Different areas appear to be specialised for the representation of different features of the environment (Zeki, 1978). For example, most orientation selective cells are grouped into three areas: V2, V3 and V3A. The V4 complex, however, contains few orientation selective cells but has a large proportion of cells which are colour specific; that is they respond to one part of the spectrum only. Cells have been discovered whose responses appear to correlate with human colour perception (Zeki, 1980). A red-sensitive cell, for example, responded only to a red object when it was illuminated with white light and not red light alone. Thus it appears possible to equate the responses of cells at this level with the perception of colour.

The data described so far have been obtained from anatomical and electrophysiological studies on animals and much can be inferred from this about the human visual system. There is, however, an alternative approach in the form of psychophysics, where the responses of human observers to known stimuli are measured and analysed, and this is dealt with in the following sections.

1.5 Colour Matching

The eye is sometimes unable to distinguish totally

different mixtures of monochromatic lights: for example, a yellow light may appear identical to a mixture of red and green lights. The two composite stimuli have entirely different spectral composition but appear the same in colour and intensity to the observer, and constitute a metameric match.

Colour matches are often made using the sensitive foveal area. The observer views a small field divided into two halves, each of which contains spectrally different stimuli. With this arrangement it is possible for most observers to make a match of any spectral light with a mixture of three matching stimuli, usually red, green and blue. Human colour vision is therefore trivariant and this implies that there must be at least three kinds of photoreceptor involved in the process, with at least three different photopigments. It is well known that the cones are responsible for colour vision, particularly because the fovea, which is the area of the retina most sensitive to changes in colour, has few or no rods present. It is possible that there may be more than three pigments and that the trivariance may occur at a later stage in the visual system. The experimental evidence that is available, in particular from fundus reflectometry and microspectrophotometry (section 1.3), suggests, however, that there are only three cone photopigments located separately in different spectral classes of cone. This implies that colour matches should be undisturbed by adaptation, and it is indeed found that significant changes in the appearance of colour can be

produced by adaptation to coloured lights without upsetting colour matches. Colour matches can be disturbed, however, by adaptation to very intense bleaching lights (Wright, 1936; Brindley, 1953).

1.5.1 The W.D. Wright System of Colour Matching

A system of colour matching (Wright, 1946) involves matching a spectral stimulus (C) with a mixture of monochromatic red (R), green (G) and blue (B) stimuli. The colour match can be expressed algebraically,

$$C\,(C) = R\,(R) + G\,(G) + B\,(B) \qquad \text{Equation 1.1}$$

where C units of stimulus (C) appear identical to a mixture of R units of (R), G units of (G) and B units of (B), and C = R + G + B.

If two separate matches are made for two distinct colours (C_1) and (C_2), then

$$C_1(C_1) = R_1(R) + G_1(G) + B_1(B)$$

$$C_2(C_2) = R_2(R) + G_2(G) + B_2(B)$$

and if (C_1) and (C_2) are mixed together,

$$C_1(C_1) + C_2(C_2) = R(R) + G(G) + B(B)$$

If colorimetric addivity holds, it is necessary for the following relations to be true:

$$R = R_1 + R_2\,,\quad G = G_1 + G_2,\quad B = B_1 + B_2$$

It is found experimentally that this is the case and the hypothesis that colour matching is additive holds for many experimental conditions.

Wright (1928) obtained colour matching data for a 2° centrally fixated field using three near-monochromatic matching stimuli; R, 650 nm; G, 530 nm; B, 460 nm.

Using equation 1.1 he defined the chromaticity coordinates r, g and b as,

$$r = \frac{R}{R+G+B}, \quad g = \frac{G}{R+G+B}, \quad b = \frac{B}{R+G+B} \qquad \text{Equations 1.2}$$

such that $r+g+b = 1$. Wright's system of units were chosen such that $r = g$ for a test stimulus of wavelength 582.5 nm and $g = b$ for a test stimulus of wavelength 494 nm. His mean colour-matching results are shown in fig. 1.4

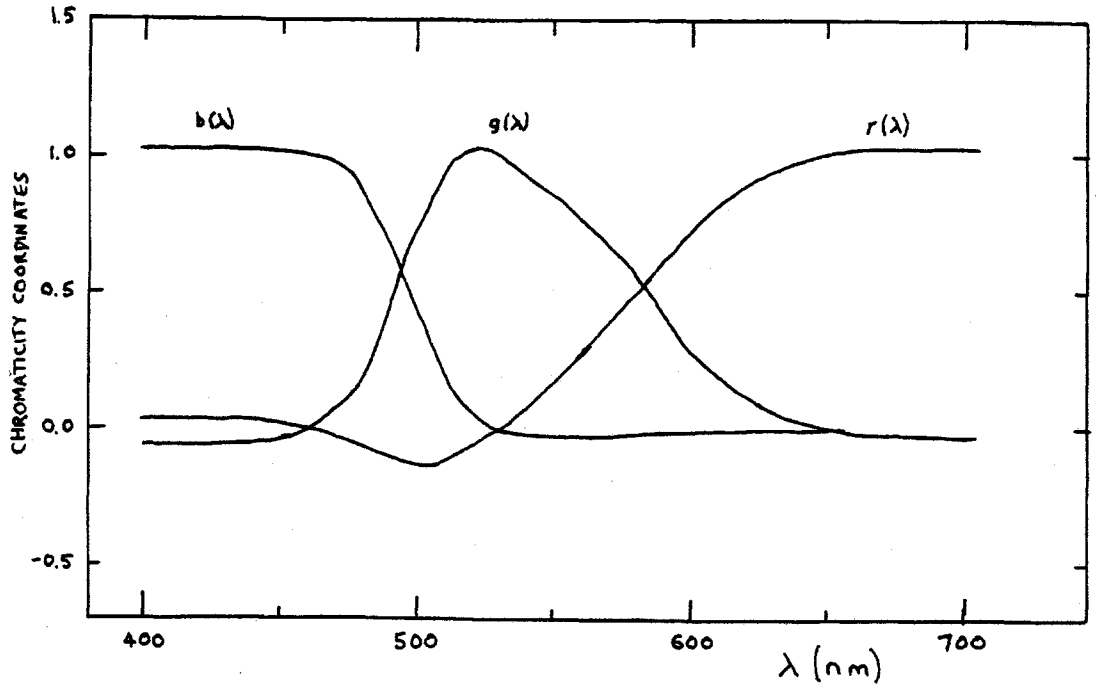


Fig. 1.4 Wright's colour matching results. The normalised chromaticity co-ordinates r, g and b are plotted against wavelength, λ, in nm.
From Wright, 1946.

Colour mixture curves were derived from these colour matching data (Wright, 1928) which define the relative luminance of the three matching stimuli (650 nm, 530 nm, and 460 nm) required to match a spectral stimulus of wavelength, λ.

1.5.2 The C.I.E. System

Wright's colour mixture curves were combined with the similar data of Guild (1931) to define the standard observer

of the Commision Internationale de l'Eclairage (C.I.E.) in 1931. The matching stimuli used in this definition were 700 nm (red),546.1 nm (green) and 435.8 nm (blue) and their units were adjusted to be equal in a colour match of an equal energy white. The resulting curves (fig.1.5a), obtained for a 2° field, define the relative amounts of the three radiations required to match each wavelength in the equal energy spectrum; $\bar{r}$, $\bar{g}$, $\bar{b}$ are the colour matching functions, sometimes referred to as the distribution coefficients or spectral tristimulus values.

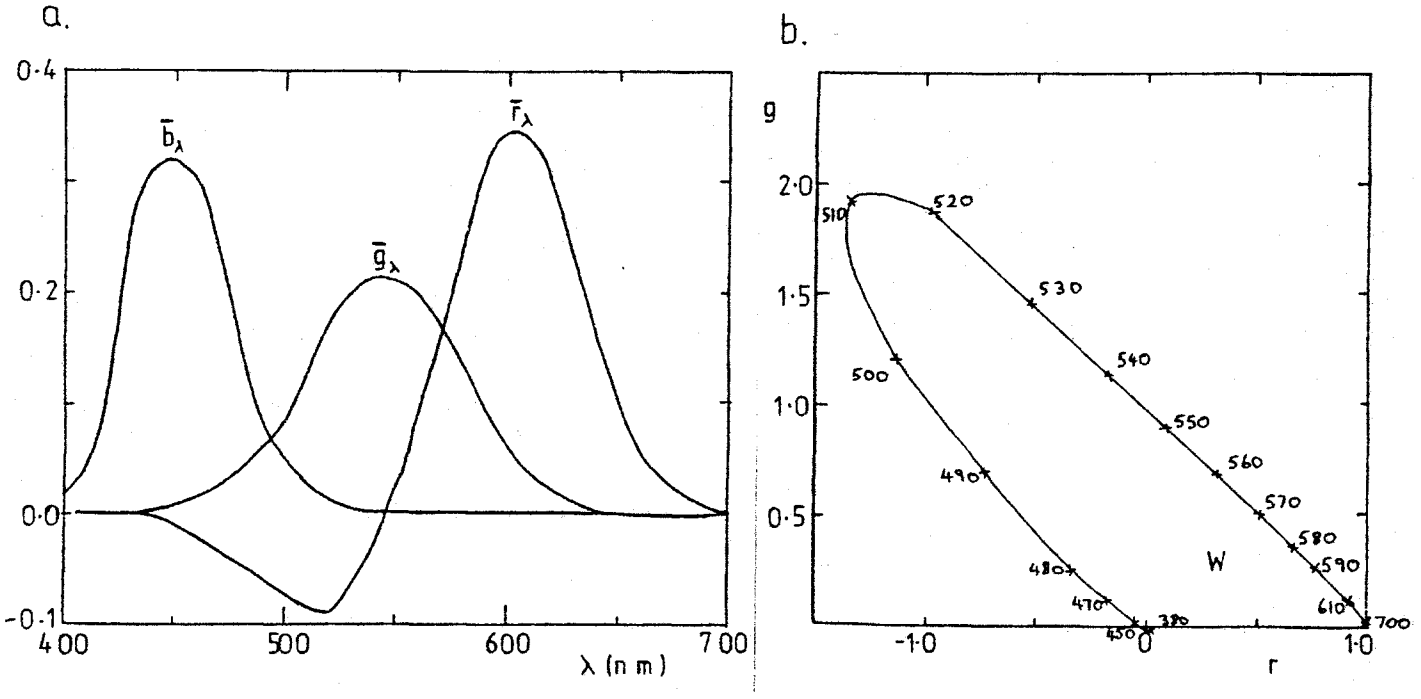


Fig. 1.5 Data for the C.I.E.1931 standard colorimetric observer in the system defined by matching stimuli R(700 nm), G(546.1 nm) and B(435.8 nm).

a. Colour-matching functions $\bar{r}_\lambda$, $\bar{g}_\lambda$, $\bar{b}_\lambda$ are plotted against wavelength, λ ,in nm.

b. The corresponding chromaticity diagram. The unit green coordinate, g, is plotted against the unit red coordinate, r. The blue coordinate can be inferred at each point using the relationship r + g + b = 1. W is the position of the equal energy white. The continuous curve corresponds to the spectrum

locus, with wavelengths marked in nm, and any real stimuli lie within the area bounded by this curve and the r-axis. The units have been adjusted to be equal in a colour match on an equal energy white and the standard data were obtained using a 2^{o} field. Data taken from Wyszecki and Stiles, 1982.

The system can also be defined in terms of chromaticity coordinates, as defined in the W.D. Wright system by equation 1.2. It is clear from the definition of the chromaticity coordinates that r + g + b = 1, and thus to define any stimulus it is necessary to specify only two coordinates, by convention r and g, as shown in fig. 1.5.b.

The colour matching functions $\bar{r}_\lambda$, $\bar{g}_\lambda$, $\bar{b}_\lambda$ and the corresponding chromaticity coordinates r, g, b include negative values. This is not always practically convenient and so the C.I.E. adopted a new coordinate system, which is a transformation of the old (R G B) system, based on matching stimuli X, Y and Z. These are 'imaginary' stimuli which lie outside the spectrum locus on the RGB chromaticity diagram and have been chosen such that the chromaticity coordinates x, y, z and the corresponding tristimulus values X, Y, Z of any real colour stimulus are never negative. This is the basis of the standard international (XYZ) system as defined by the C.I.E. in 1931. The chromaticity coordinates are defined in terms of the tristimulus values:

$$x = \frac{X}{X+Y+Z}, \qquad y = \frac{Y}{X+Y+Z}, \qquad z = \frac{Z}{X+Y+Z} \quad \text{Equations 1.3}$$

and the chromaticity of any colour is specified by only two unit coordinates, e.g. x and y (fig. 1.6).

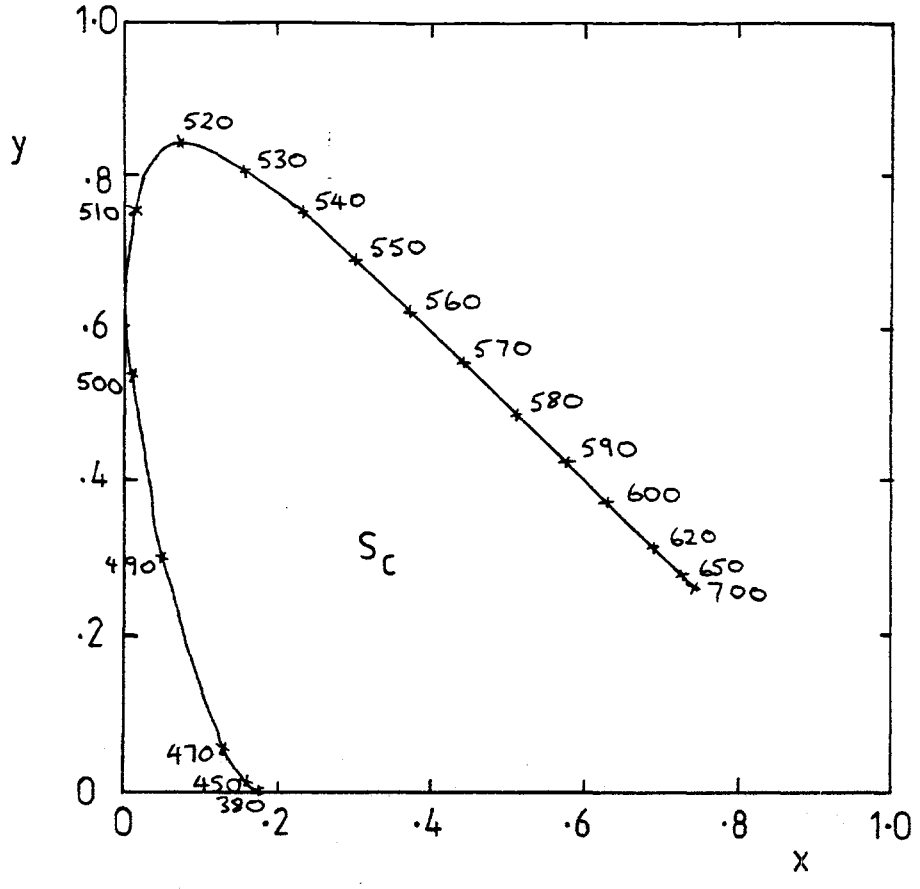


Fig. 1.6 Tristimulus space based on the C.I.E. stimuli X, Y, Z showing the spectrum locus with wavelengths marked in nm. Sc is one of the standard illuminants defined by the C.I.E. and represents natural daylight.

A colour is defined completely in terms of this system by three coefficients x, y and Y which is the brightness or luminance factor.

1.6 Colour Deficiencies

Experimental colour matches are subject to significant inter-observer variation. In many cases these variations may result from observer differences in transmission characteristics of the ocular media and retina, in particular the macular pigment, which is a yellow pigment covering an area of up to 5° from the fovea centralis, and the crystalline lens. Ruddock (1965) computed the change in the W.D. Wright chromaticity coordinates of the C.I.E. standard illuminant S

which result from age changes in lens transmission or from changes in the optical density of the macular pigment. Experimental data show that age changes in colour matching correspond closely to the calculated changes arising from increased lens absorption (Ruddock,1963). Similarly, Ishak (1952) correlated colour matching differences between English and Egyptian observers with differences in the optical density of the macular pigment. Thus, most inter-observer variability in colour-matching can be accounted for by differences in absorption of the ocular media and it can be assumed that the majority of observers have essentially the same mechanisms mediating colour perception. There is, however, a significant proportion of the population (about 8% of men and 0.4% of women) who differ significantly from 'normal'. Thus they make colour matches which lie outside the normal range and their discrimination of colour is significantly impaired, and they are therefore known as 'colour defective' (or, popularly, 'colour blind'). The commonest type of colour deficiency involves discrimination of the red-green spectral colours and is congenital. It can take several typical forms and such observers can be classified according to their colour matching characteristics, in particular with respect to the proportion of green and red lights they require to match a spectral yellow. Such a match is known as a Rayleigh match and is stable among normal observers, as the crystalline lens and macular pigment are effectively transparent in that region of the spectrum. Thus it is an effective method of classifying red-green colour defective subjects:

1.6.1 Dichromats

Dichromats can match any monochromatic light with a mixture of only two matching stimuli, for example red and blue. The two most common forms of dichromacy are protanopia and deuteranopia, each occurring in 1% of the male population. Both classes of observer confuse all spectral stimuli with wavelength greater than 530 nm (see fig. 1.7a). Protanopes can be distinguished from deuteranopes in that they are insensitive to red lights; thus they need a very intense red light to match a green light, and their overall photopic sensitivity curve is displaced towards the blue end of the spectrum with respect to the normal curve (Pitt, 1944), whilst the deuteranopic curve is shifted towards the red end (see fig. 1.7b). Young (1807) suggested that Dalton's defect (1798) was due to a lack of the red mechanism. Rushton (1963, 1965) studied the pigments of both protanopes and deuteranopes using fundus reflectometry. He concluded that the red pigment 'erythrolabe' was absent from the retina of the protanopes and the green pigment 'chlorolabe' was missing in deuteranopes. In other words, protanopia and deuteranopia seem to be associated with the lack of the red and green photopigments respectively.

1.6.2 Anomalous Trichromats

The commonest type of colour defect is anomalous trichromacy. Such observers require three primaries to match any spectral colour, but their wavelength discrimination is impaired and their colour matching is abnormal. They are classified according to their colour matching characteristics into groups which correspond to the different types of dichromacy, i.e. protanomalous and deuteranomalous. They have

reduced discrimination in the red-yellow-green part of the spectrum and range from the nearly normal to the nearly dichromatic.

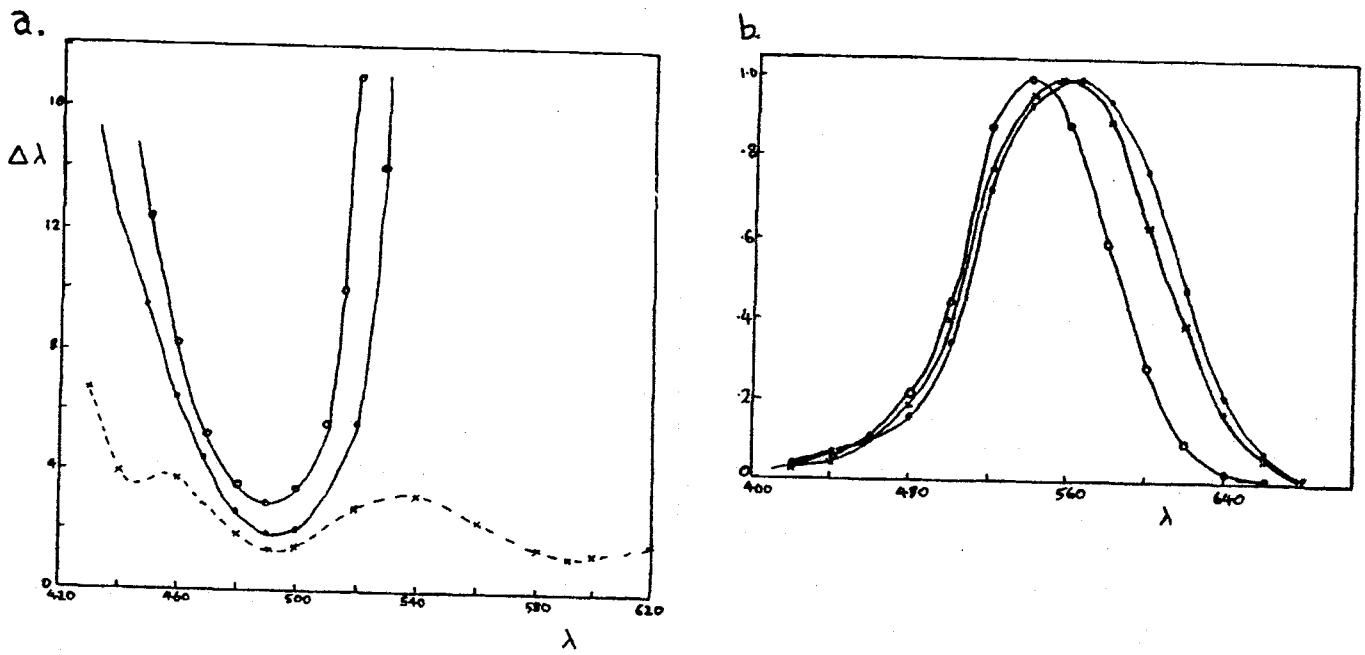


Fig. 1.7 a. Wavelength discrimination curves for • deuteranopic, o protanopic, × normal subjects. Just noticeable difference in wavelength, $\Delta\lambda$ in nm, is plotted against wavelength, λ , in nm.

b. Photopic sensitivity curves for • deuteranopic, o protanopic and × normal subjects. Relative luminosity is plotted against wavelength, λ. Each point is the mean of six observers. Data taken from Wright, 1946.

Anomalous trichromats differ from dichromats in one important respect in that they do not accept metameric matches made by normal observers, a feature first noted by Rayleigh (1881). Protanomalous observers require more red than normal in a Rayleigh match, whilst deuteranomalous observers require more green.

Nelson (1938) undertook a statistical survey of anomalous trichromats using a Nagel anomaloscope, an instrument which provides a bipartite field, one half a monochromatic yellow of variable intensity, the other half a mixture of red and green with variable red : green ratio. The results of this survey, plotted as percentage of observers against log red/green (fig. 1.8) show a continuous distribution curve with a dip on the deuteranomalous side of normal.

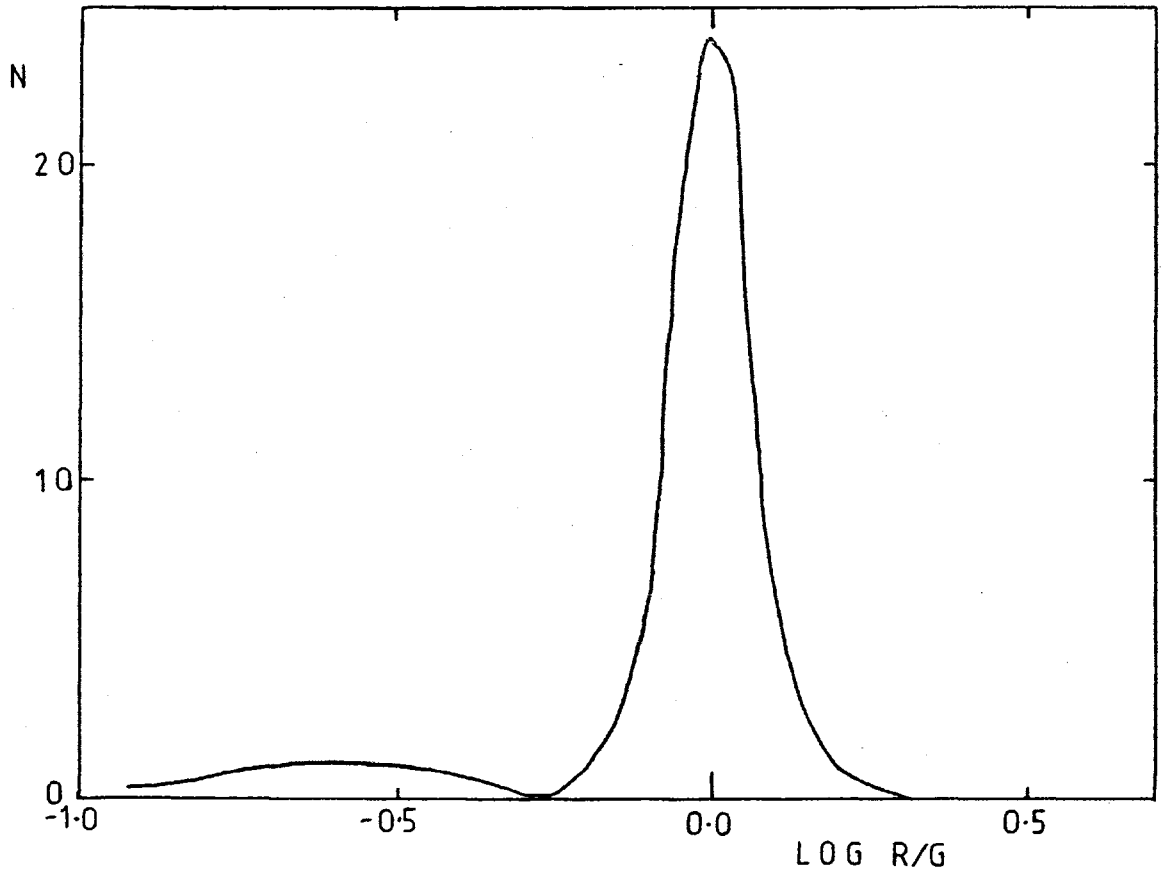


Fig. 1.8 Distribution of R/G ratio for the Nagel match. Number of observers, as a percentage, is plotted against the log. of the red : green ratio required to match a fixed yellow.
From Nelson, 1938.

The continuous form of this Nagel distribution curve suggests that anomalous trichromacy is an intermediate state

between normal trichromacy and dichromacy. Nelson concluded that the symmetrical shape of the deuteranomalous maximum supported this idea, with a perferential state corresponding to the position of the deuteranomalous maximum. He also concluded, from detailed studies on selected anomalous observers, that if the hue discrimination curves are taken as a guide to the degree of the deficiency, then the other characteristics (such as the log R/G ratio) cannot be treated as an obvious measure of the defect.

McKeon and Wright (1940) studied the characteristics of eleven protanomalous subjects and found that although the hue discrimination results yielded a family of curves ranging between that of the normal trichromat and that of the protanope, the luminosity curves varied little from observer to observer and were in fact almost identical to that of the protanope. They asserted that it was difficult to reconcile this result with the, till then, usual conception that different degrees of protanomaly arose from the magnitude of the red response varying from one observer to another. This explanation of anomalous trichromacy can also be rejected on the grounds that a simple loss of sensitivity of one mechanism would not cause an observer to reject a normal colour match.

Two other explanations of anomalous trichromacy have been proposed: the abnormal spectral sensitivity may be due to an inert screening pigment, or to directional differences of the cones (Stiles - Crawford effect). These explanations were refuted by Alpern and Torii (1968) in a series of experiments on protanomalous subjects, including measurements employing fundus

reflectometry and the trans-scleral illumination technique of Brindley and Rushton (1959). The retina was illuminated from behind by pressing the tip of a glass rod optical fibre against the sclera to provide a red/green mixture and a comparison yellow field. Protanomalous matches were still too red despite the fact that the matching fields came from behind the retina, thus eliminating the possibility that the colour deficiency is due to any inert filter residing somewhere between the cone outer segments and the cornea.

The only consistent explanation of anomalous trichromacy, therefore, is that the absorption spectrum of at least one cone mechanism must be different to that of the cones in the normal retina.

1.7 Spatially Structured Stimuli

Psychophysical techniques can also be used to study responses to spatially structured targets. The existence of size-tuned mechanisms in the human visual system has been inferred from a series of psychophysical experiments. Westheimer (1965, 1967) has shown that the contrast threshold for the detection of a small test spot of constant size superimposed on a circular background of variable size increases to a maximum and then decreases, indicating a receptive field organisation with excitatory and inhibitory regions. Similar antagonistic responses have been obtained from experiments involving the visibility of various types of test stimuli, including thin lines (Fiorentini and Mazzantini,1966), rectangles of various widths (Thomas, Padilla and Rourke, 1969) and squares (Bagrash, Kerr and Thomas, 1971). A highly

productive technique has been the use of square-wave and sine-wave gratings as the visual stimuli, such as the adaptation experiments described in the following section.

1.7.1 Contrast Threshold Elevation Effect

Adaptation to a high contrast, sine-wave grating significantly raises the contrast threshold for detection of a test grating of similar spatial frequency and orientation (Gilinsky, 1968; Pantle and Sekuler 1968, 1969: Blakemore and Campbell, 1969 a,b). This effect is illustrated in fig. 1.9.

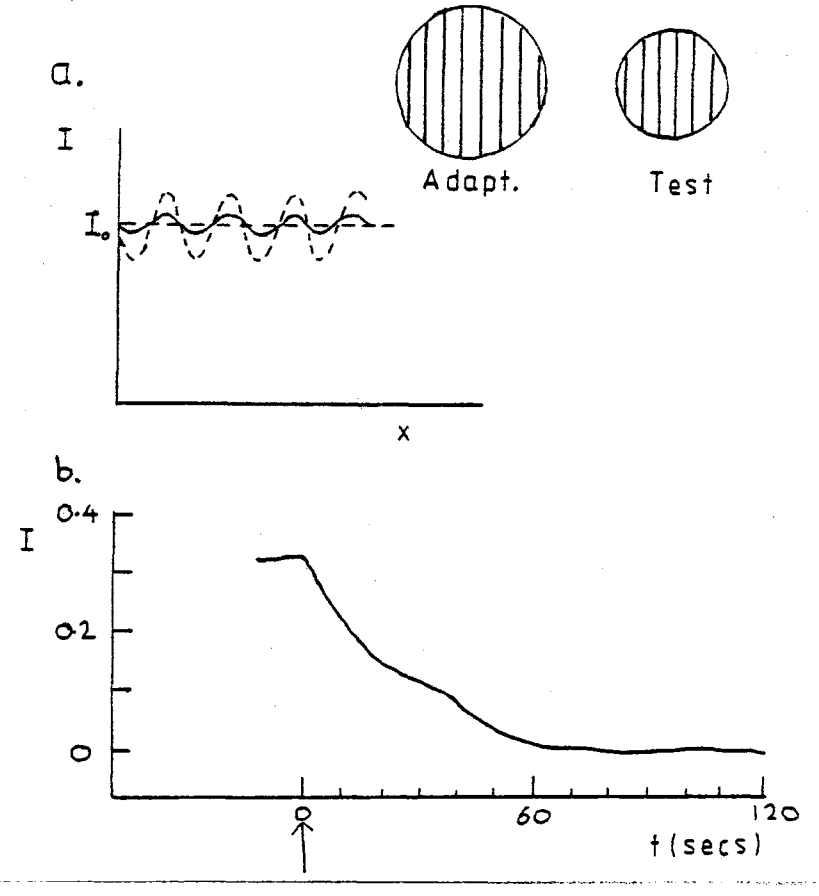


Fig. 1.9 Diagram showing the contrast threshold elevation effect. a. Threshold illumination level for the detection of a low contrast test grating, I, is plotted against spatial distribution, x, both before adaptation (continuous curve) and after adaptation (dashed curve) to a high contrast grating of the same spatial frequency as the test. The inset shows the test and adaptation stimuli. b. Threshold illumination for detection of the test, I, is plotted against time after offset of the adaptation stimulus (marked by the arrow).

The effect is transient (fig.1.9b), with the elevation of contrast threshold decaying back to its pre-adaptation value over about one minute. The effect can equally well be obtained with square-wave gratings, i.e. sets of light and dark bars with light : dark ratio 1 : 1 and is specific to bar width and orientation as shown in fig. 1.10 (Maudarbocus and Ruddock, 1973).

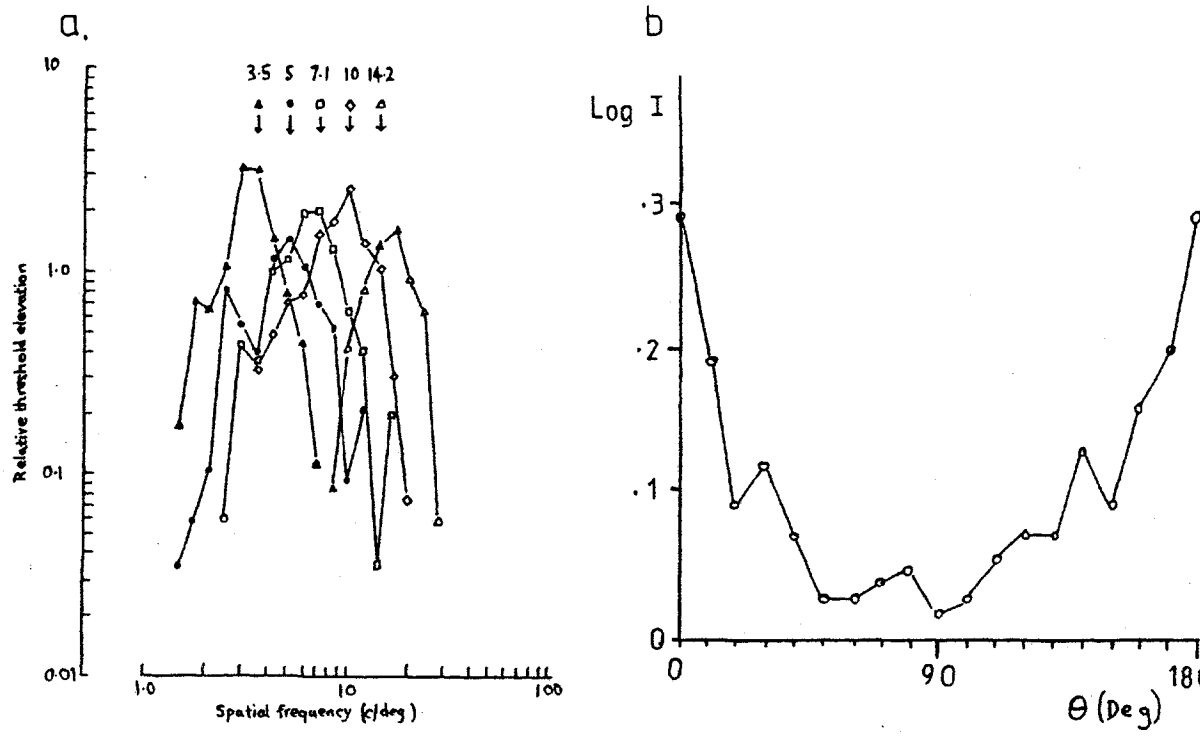


Fig. 1.10 a.Relative threshold illumination level, I, plotted against spatial frequency of the test, f, in cycles/deg for five adaptation gratings (spatial frequencies marked by the arrows). From Blakemore and Campbell, 1969b.

b. Threshold illumination for detection of a vertical test grating, I, plotted against angle of orientation from the vertical, θ , of the adaptation grating of the same bar width as the test. From Maudarbocus, 1973.

These results suggest that the mechanism responsible for detection of a given test grating is affected by only a

limited range of adaptation frequencies, and that maximum threshold elevation is obtained when the test and adaptation gratings have the same bar width and orientation.

The effect is observed for all resolvable gratings; the amplitude is constant for spatial frequencies < 15 cycles /deg and falls off slowly for high spatial frequencies (Maudarbocus, 1973) as shown in fig.1.11. It can be dichoptically transferred, i.e. adapting one eye raises the contrast threshold for a matched test grating in the other eye.

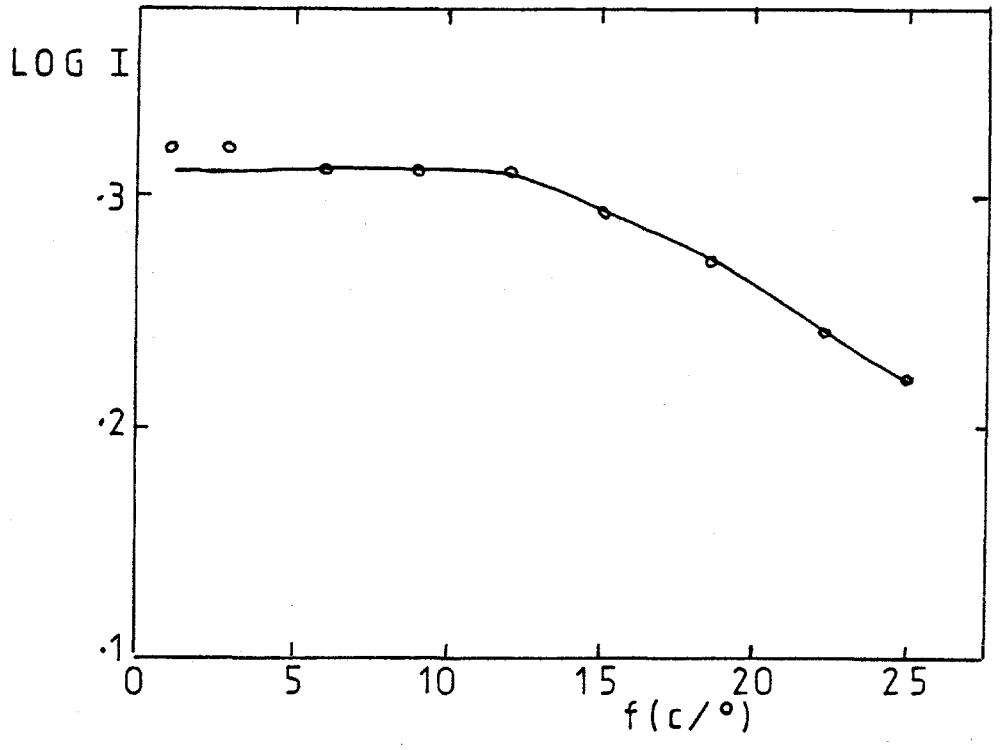


Fig. 1.11 Log threshold illumination level for detection of a test grating, log I, plotted against spatial frequency of matched test and adaptation gratings.
From Maudarbocus, 1973.

These responses are non-wavelength selective and correlate closely with the responses of single neurones in the striate cortex observed by Hubel and Wiesel (1962, 1968) described in section 1.4.3 (Maffei, Fiorentini and Bisti, 1973).

CHAPTER TWO

The Experimental Apparatus

Section		Page
2.1	4-Channel Maxwellian Viewing System	35
2.2	Outline of the 4-Channel System	36
2.3	Stabilised Power Supply	38
2.4	Shutter Control Unit	38
2.5	Neutral Density Wedge Drive	38
2.6	Data Recording Equipment	39
2.7	Calibrations	40
2.8	Magnification of the System	42
2.9	Experimental Procedure	43
2.10	General Outline of the Wright Colorimeter	46
2.11	Calibration of the Colorimeter	49
2.12	Experimental Arrangement for the Bleaching Experiments	51
2.13	Experimental Procedure	53

Experiments on contrast threshold elevation to be described in this thesis were all carried out on a 4-channel Maxwellian viewing system. This apparatus was originally constructed by Dr. V.A. Barbur, with several modifications introduced by the present author. The wavelength discriminations and colour matching experiments were performed on the Wright tristimulus colorimeter.

2.1 4-Channel Maxwellian Viewing System

A Maxwellian viewing system images a light source in the eye's pupil, so that the viewing lens appears uniformly illuminated. It has the advantage that whilst the retinal illuminance attainable can be equal to that for direct viewing of the light source, the area of the retina so illuminated may be larger (Westheimer, 1966). The basic arrangement used in this system is shown in fig. 2.1

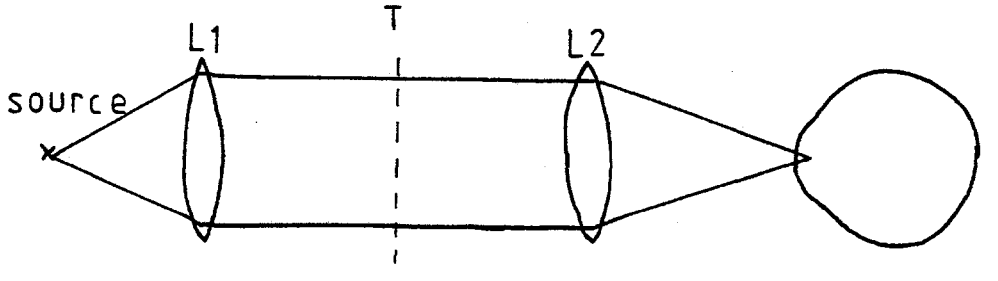


Fig.2.1 A simple Maxwellian viewing system. Light from the source is collimated by lens L1 and imaged on to the pupil by L2. The target, T, may be anywhere between L1 and L2, the exact position depending on the accommodation of the observer

2.2 Outline of the 4-Channel System

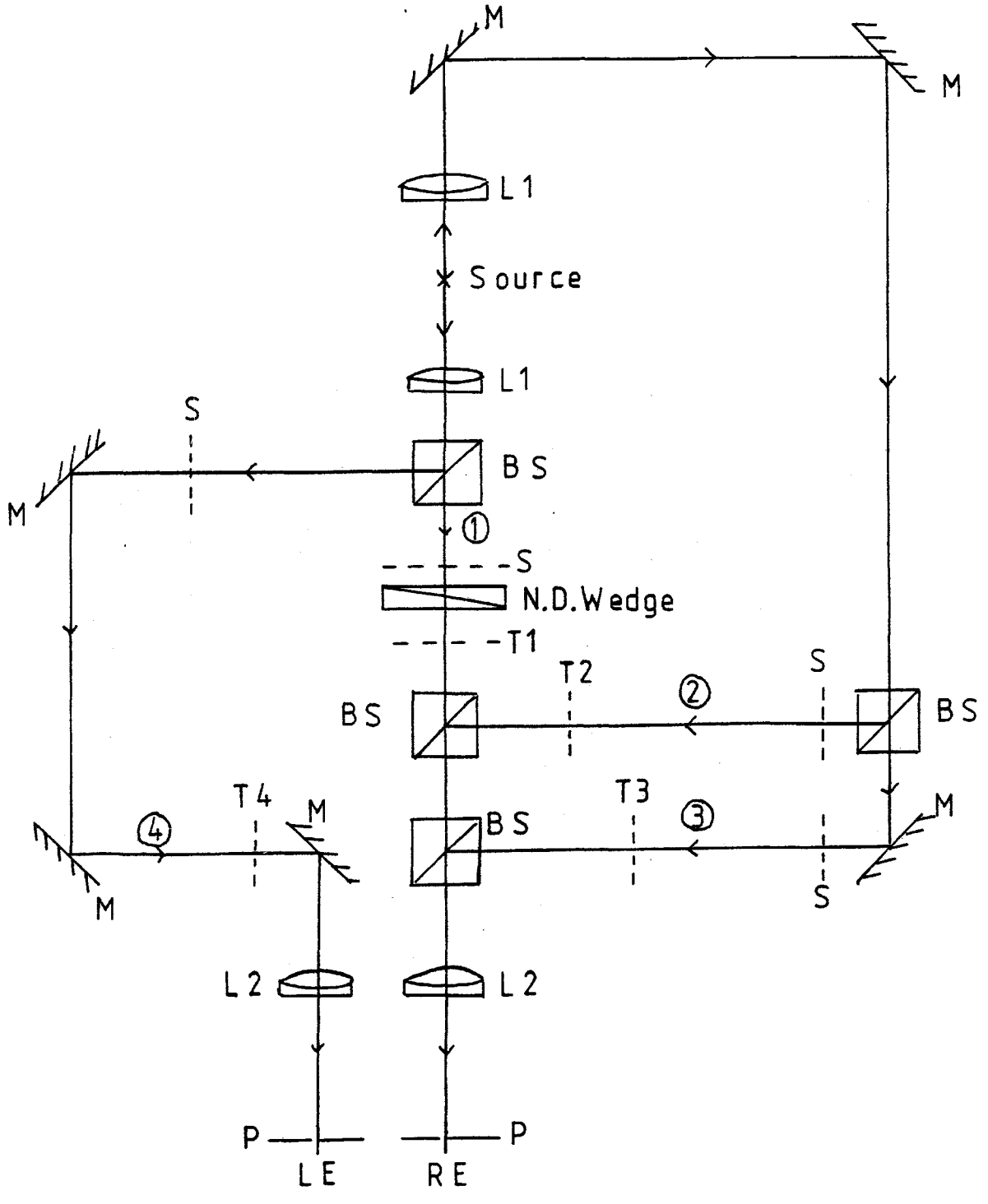


Fig.2.2 The Maxwellian viewing system

In the 4-channel system (fig.2.2) the white light source was a 150 W tungsten-halogen lamp, which was driven by a 24V D.C. stabilised power supply, and was fan-cooled. Fig. 2.2 shows the arrangement of beam-splitters (B.S.) and front-silvered mirrors (M) which provided up to four separate channels. Collimating lenses (L1) on each side of the source produced two parallel beams of light, propagating in opposite directions. A beam splitter was placed in each beam, thus providing the four channels. One channel was focused on to the left eye, while the other three were eventually recombined and focused on to the right eye. Artificial pupils (P), of 2 mm diameter, were positioned in front of the two eyes. The object planes (T1-4) were at the foci of the final lenses (L2), thus providing virtual images at infinity, but the targets could be moved if necessary to compensate for any refractive error of the observer.

The intensity of each channel could be adjusted stepwise by the experimenter by the insertion of neutral density filters, and the intensity of beam 1 could be varied in a continuous fashion by the observer, using a motor-driven, acetate neutral density wedge (Kodak). The wavelength of each beam could be controlled with interference filters (Balzer, type B40, bandwidth±5 nm). The target stimuli were generated on microfilm, with programs written for the University of London C.D.C. computer, and plotted on 35mm film. These computed patterns were then reproduced on high contrast Kodalith film and mounted in double-sided slide holders. The presentation of targets to the observer was controlled using rotary

solenoid shutters (S), driven by a specially constructed Timer unit in a pre-determined sequence. The observer's head was maintained in position by means of a dental clamp.

2.3 Stabilised Power Supply

A stabilised power supply which incorporated a current-limited device was used to drive the white light source (Nunn, 1978). This provided a steady 24V D.C. supply and limited the output current to 10 Amps. Also included in the design was a resistor/capacitor circuit which allowed a gradual rise to maximum voltage when the equipment was turned on and, similarly, a gradual decrease to zero when it was turned off. This was to prevent sudden transients occurring, thus lengthening the lifetime of the lamp.

2.4. Shutter Control Unit

A timer unit, based on timing elements type No. ZN 1034E and Darlington amplifier circuits, type No. ZN 6385, was used to drive the electromagnetic shutters (Waterfield, 1980). Up to three shutters could be controlled independently, to determine the relative time of opening and rate of opening of each. The required sequence could be pre-set by the experimenter, and initiated by either the experimenter or the observer by means of a control switch.

2.5. Neutral Density Wedge Drive

The neutral density wedge was connected, via gears, to a linear coil motor which could be driven in either direction, depending on the sign of the applied voltage. The speed of the motor in either direction depended on the variable resistors and was adjusted to be as slow as possible

in the direction corresponding to decreasing intensity of the target beam, thus enabling the observer to make accurate threshold settings.

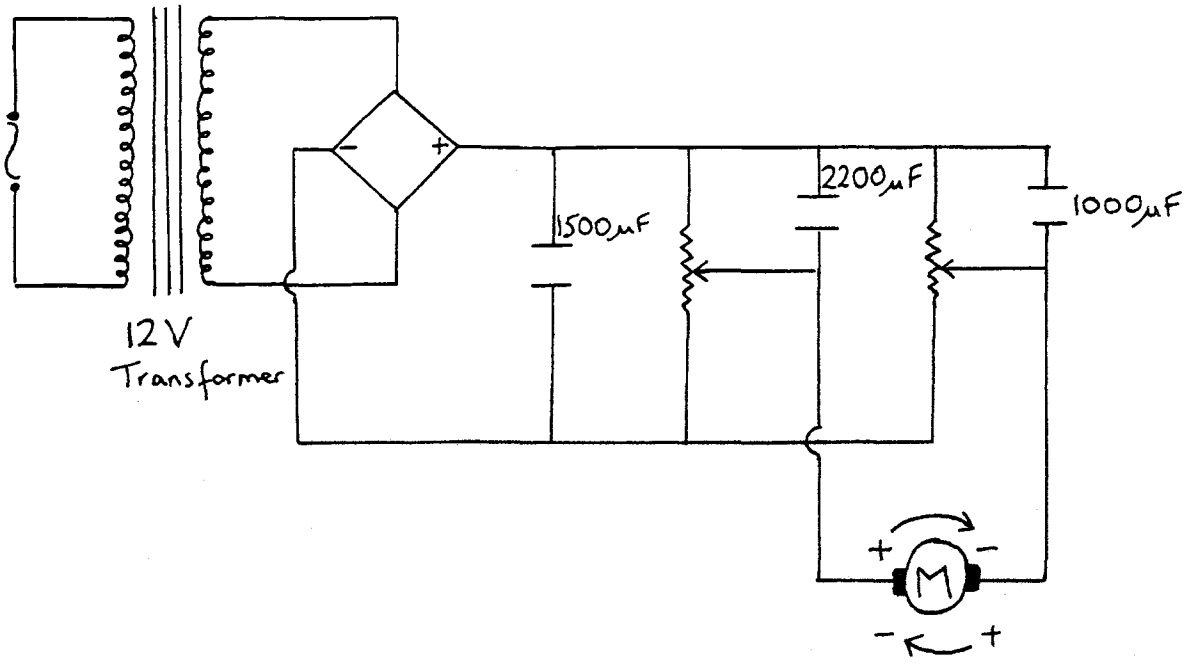


Fig. 2.3 Schematic representation of the neutral density wedge drive.

2.6. Data Recording Equipment

The intensity of the test beam was controlled by the observer using the calibrated, motor-driven, neutral density wedge. A 10-turn potentiometer, with a constant applied voltage, was connected via gears to the wedge. The change in voltage from the potentiometer was displayed on a digital multimeter (DANA, model 3800B) and printed out on a digital printer (CREDSHIRE, model DP 100). The value of this change corresponded to the position of the neutral density wedge and thus to the intensity of the target beam. The recordings were made on a sample and hold circuit (Appendix A) which provided two print sequences, black type or red type, and paper feed. These sequences could be

initiated by the observer, using the appropriate switches on a control box. A counter unit and buzzer were also incorporated into the circuit (Waterfield, 1980). This was designed to count a fixed number of measurements, which could be set between 1 and 9 at the beginning of the experiment, and to produce an audible 20 m sec signal at the end of each set of measurements.

The power supply to the wedge motor was kept completely separate from the 5V supply for the recording equipment in order to avoid signals generated in the sample and hold circuit by the back emf from the motor.

2.7 Calibrations

The source intensity at the exit pupil was measured in candelas with a digital photometer/radiometer unit (MACAM PR 3010) fitted with a filter which approximately matches the CIE photopic curve. The unit of retinal illuminance used throughout this study is the troland, being the retinal illumination level produced by a surface of luminance 1 cd/m^2 viewed through a pupil of 1 mm^2 area, i.e. 10^6 lumens/sterad. visual angle. Retinal illumination levels in trolands were obtained from the measurements in candelas by multiplication by 10^6, and the logarithms of these values were usually used.

The intensity of the individual beams could be reduced using neutral density filters. These were Wratten gelatin filters mounted between two plates of neutral glass and were calibrated *in situ* using the photometer unit. The monochromatic stimuli required for various experiments were

provided by Balzer (type B40) interference filters, with a bandwidth of ± 5 nm and shoulders of < 1% of the maximum transmission. The spectral transmissions of the filters were checked on a Beckman recording spectrophotometer (model DK 2). Fig. 2.4 shows the relative energy of the spectral distribution emitted by the source through the relevant interference filters, measured by positioning the radiometer at the exit pupil of the system.

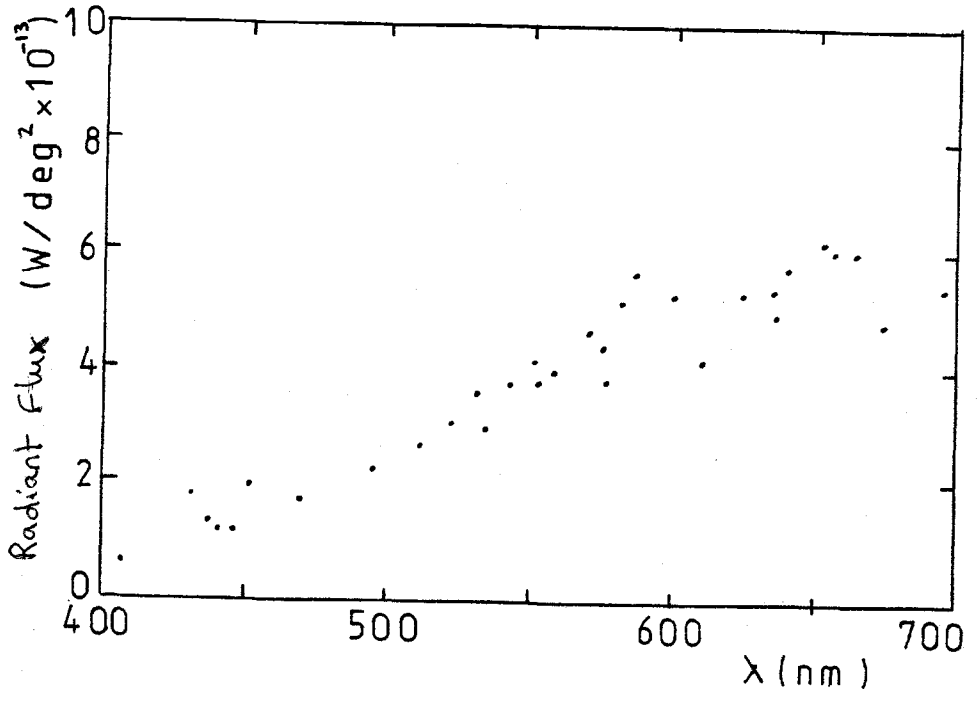


Fig. 2.4. Spectral distribution of light emitted from the source. The relative flux transmitted through the relevant interference filters, in Watts / deg^2, is plotted against wavelength, λ, in nm.

The neutral density wedge was calibrated <u>in situ</u> using the photometer unit, at approximately twenty positions along its length. Fig. 2.5 shows the relative transmission of the wedge plotted against the reading on the digital multimeter. The wedge was calibrated using white light as it was considered effectively neutral for wavelengths > 500 nm.

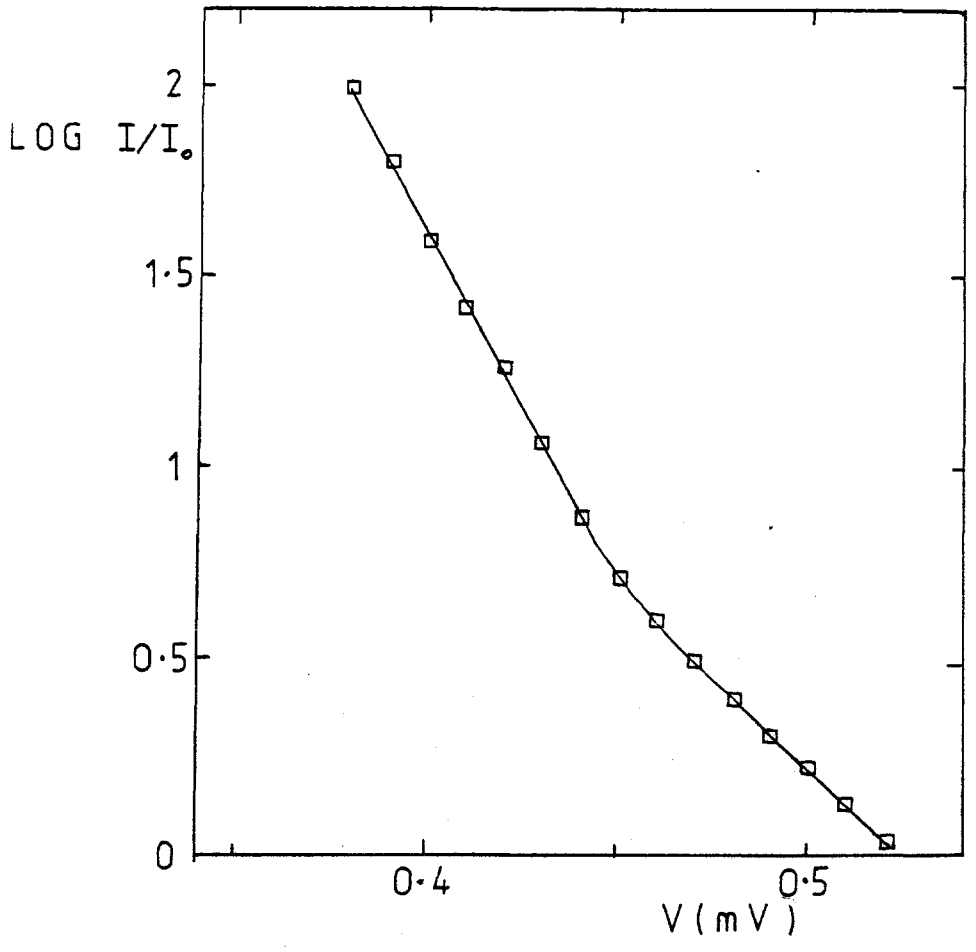


Fig. 2.5 Calibration curve for the neutral density wedge. Relative transmission, log I/I_o , is plotted against voltage, in mV.

The calibration is not completely linear, but was found to be unchanged each time it was repeated.

2.8 Magnification of the System

It is possible to obtain a conversion factor for the Maxwellian optical system which relates the object grating bar width, x , expressed in mm, to the imaged grating bar width, d , expressed in degrees of visual angle, and the equivalent spatial frequency, f, (defined as $^1/_{2d}$) in cycles /degree.

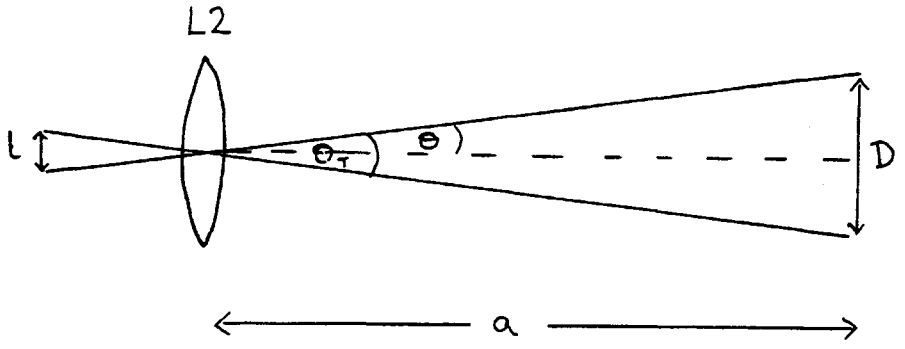


Fig. 2.6 Schematic diagram showing the magnification of an object (1 mm) by the final lens L2.

The magnification of the system can be calculated by placing a known object (1 mm) at the focus of the final lens L2 and measuring the image size (Dmm) at a distance 'a' (usually 100 mm) away from L2. Then,

$$\theta_T = 2 \tan^{-1} \frac{D}{2a}$$

θ_T / l = deg/mm in object space, i.e. each degree = l/θ_T mm

If x mm is the object grating bar width, then the imaged grating bar width, d = $x\,\theta_T/l$ degrees of visual angle.

Thus, the spatial frequency of the grating stimulus, f, is given by $1/2x\theta_T/l$, i.e. f = $l/2x\theta_T$ cycles/degree.

The conversion factor for the system, therefore, is .

Actual measurements on the system reveal that $l/2\theta_T$ = 2.05 mm/deg.

2.9 Experimental Procedure

Adaptation effects for linear square-wave gratings of different

spatial frequencies (where spatial frequency is defined as the inverse of twice the grating bar width) and wavelengths are approximately equal, provided that the grating illuminations are set at the same suprathreshold level (Maudarbocus and Ruddock, 1973). Threshold illumination levels for detection of different monochromatic gratings and spot matrices were determined by reducing the illumination of the target until it was just no longer visible. The illumination level could then be raised to a required suprathreshold level by removing the appropriate neutral density filters.

In all the adaptation experiments, the observer was initially adapted for two minutes, after which the shutter mechanism was operated allowing the test to be presented for 2 seconds. The transient nature of the adaptation effect is such that the adaptation stimuli must be viewed cyclically with the test stimulus, in order to maintain the maximum effect. Thus, after the initial 2 minute period, the adaptation and test stimuli were presented alternately for 15 s and 2 s respectively. In general, the adaptation stimuli were either square-waveform gratings or spot matrices of $>$ 98% contrast. The test was composed of a near threshold grating structure superimposed on a uniform field, the illumination level of which was equal to that of the adaptation stimulus (fig. 2.7). Thus when the test and adaptation stimuli were alternated, there was no change in the average retinal illumination level, and hence in retinal adaptation.

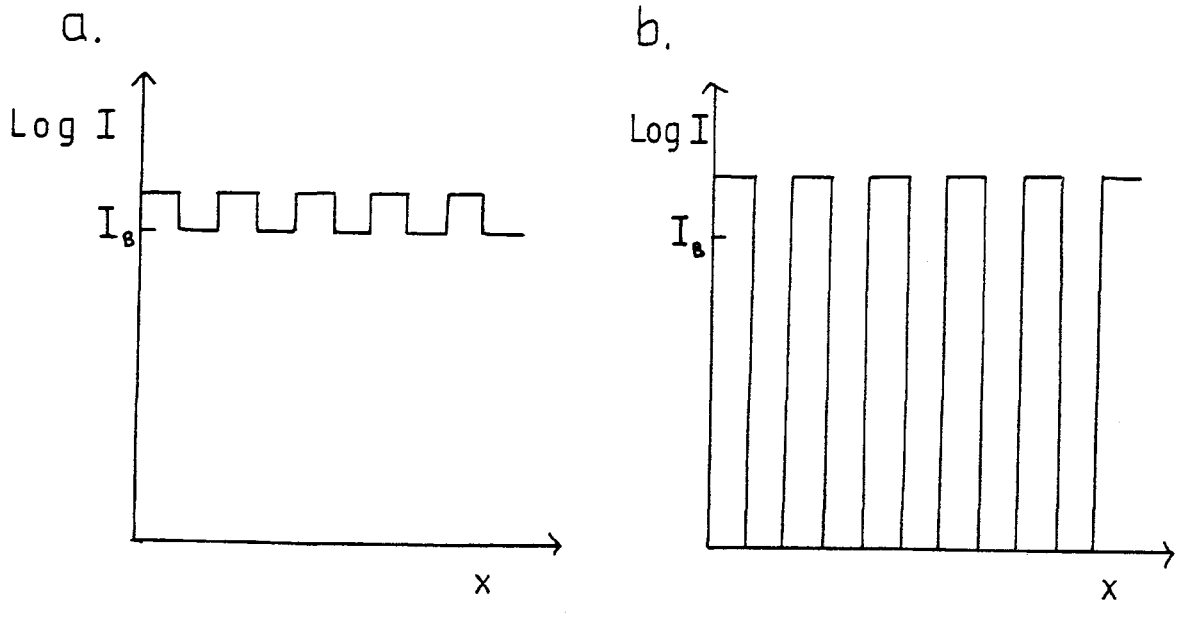


Fig. 2.7 Schematic diagram showing the illumination profile of a. the test stimulus and b. the adaptation stimulus. Illuminance, log I, is plotted as a function of spatial distribution, x. Log I_B is the illumination level of the uniform field component of the test and also the average illumination level of the adaptation grating.

The observer was instructed to view the test when it appeared and to decide whether or not the structure was visible. If he could detect the target he reduced the illumination level of the structured component of the test, using the motor-driven neutral density wedge, and continued in this manner until the threshold setting was reached, i.e. until the test structure was just no longer visible. The position of the wedge, corresponding to threshold illumination, Log I_t, was then recorded by depression of the appropriate switch on the control box. Finally the wedge was reset to a random position and the process repeated four or five times to

obtain an accurate measure of the threshold and an estimate of the standard error.

Similarly, threshold illumination Log I_t was measured after adaptation to a uniform field of average illumination level equal to that of the adaptation grating or spot matrix. This threshold level was subsequently subtracted from all other threshold measurements in the same experimental run, so that Log I_t = 0 after adaptation to a uniform field provided a base line for the data.

The Wright Colorimeter

2.10 General Outline

Wavelength discrimination, spectral sensitivity and colour matching experiments were performed on the Wright colorimeter (Wright, 1946). This is a versatile optical system illustrated in fig. 2.8, which provides a bipartite field; one half consisting of up to three near-monochromatic matching stimuli and the other of a near-monochromatic test stimulus.

The 100V quartz-halogen source, S1, is focussed on to the slit of a collimator and a parallel beam of light produced by L2. This beam passes through the upper half of the two 60° prisms P1 and P2 and is split into two by the dividing mirror, D, shown in fig. 2.9.

Half of the incident beam is reflected by P_1 and is focused as a spectrum in W1, the other half passes through P_2 and is focused at W2. Reflecting prisms, R, are mounted in W1 and W2 and cause selected components of the beams to retrace their paths, but at a slightly lower

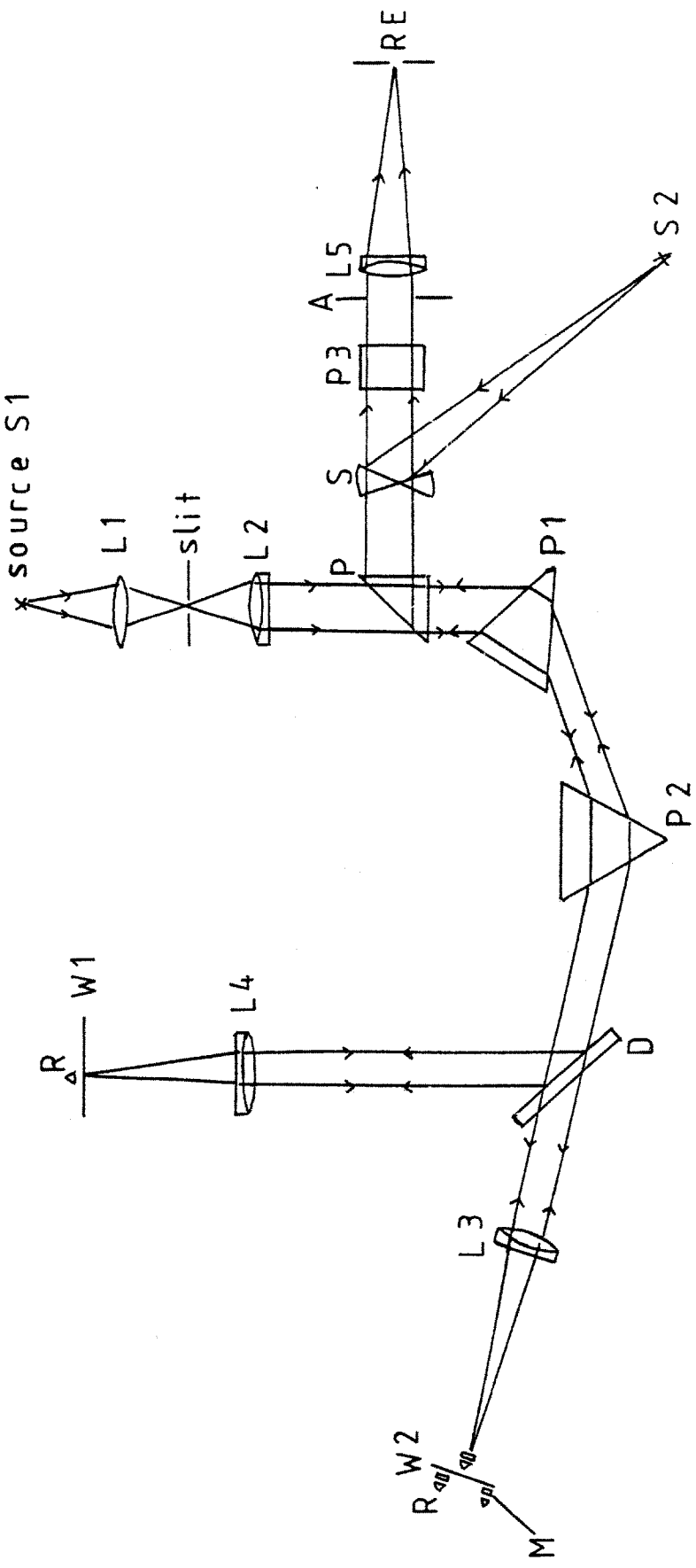


Fig. 2.8 The Wright colorimeter.

level. Light from W1 is reflected by q_1, and light from W2 passes through q_2, both beams again going through the dispersing prisms P1 and P2, thus neutralising the original dispersion and making the two beams parallel. The two vertically displaced beams are reflected onto the photometer prism, P3 (fig. 2.10), which provides a sharp edge between the two halves of the field, then pass through the rectangular aperture, A, and are finally focused onto the exit pupil. The bipartite field as seen by the observer, whose head is maintained in position by use of a dental clamp, is shown in fig 2.11.

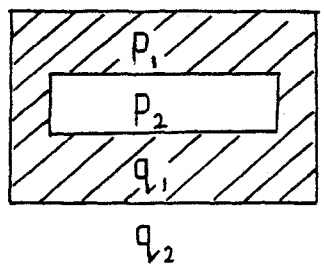


Fig. 2.9 The Divided Mirror, D, viewed from the source side.

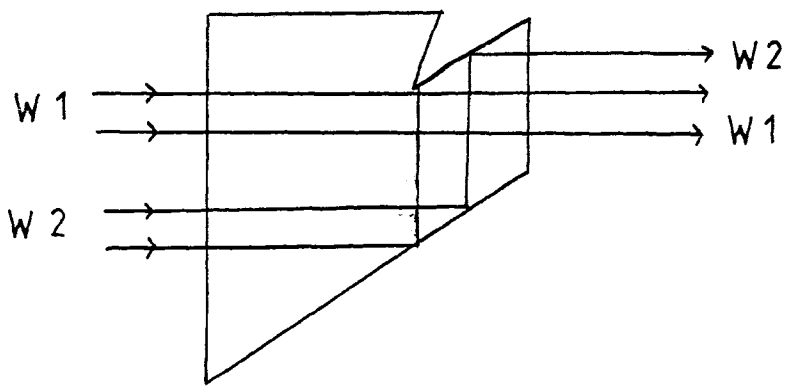


Fig. 2.10 Side view of the photometer prism, P3, showing how the two beams, W1 and W2, are brought to a sharp edge

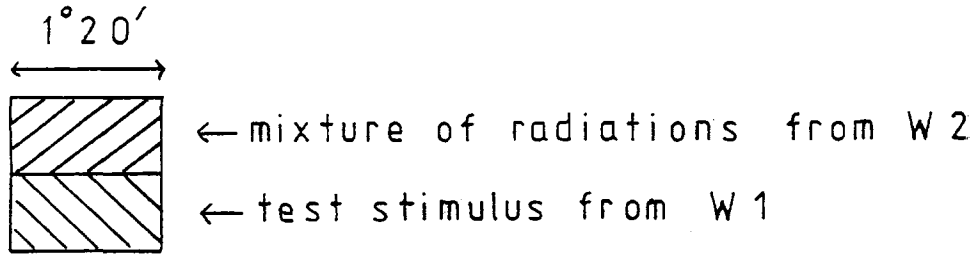


Fig. 2.11 The bipartite visual field of the colorimeter, as viewed by the observer.

The intensity of the three matching stimuli can be controlled by the observer by manipulating control knobs that are connected via pulleys to the three photometer wedges, M, mounted in front of the reflecting prisms in the W2 spectrum (fig 2.8). A secondary source, S2, and a rotating sector S, are available for flicker photometric experiments.

2.11 Calibration of the Colorimeter Wavelength

The prisms and wedges in W1 and W2 were mounted on a horizontal bed marked with a linear scale, along which the prisms could be moved, and the wavelengths of the dispersion spectrum corresponding to different points on the linear scale were calibrated with spectral line sources. The source S1 was removed and a mercury lamp put in its place, thus producing spectral lines at W2 and W1. The two scales were calibrated separately by moving the reflecting prisms along until the observer could detect one of the mercury lines and the corresponding scale reading was recorded.

Cadmium and sodium lamps were also used to give readings over the full range of the spectrum and thus increase the accuracy of the calibration, which is shown in fig. 2.12.

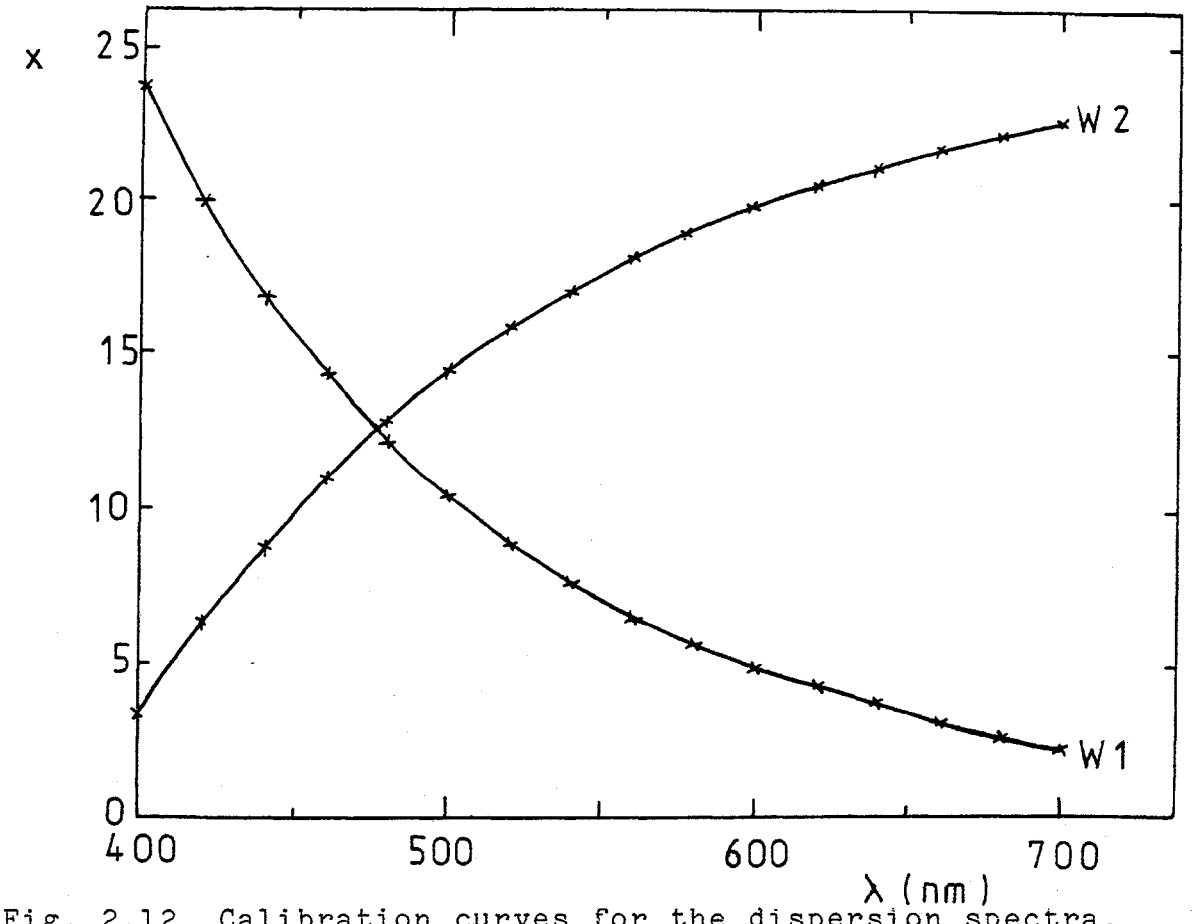


Fig. 2.12 Calibration curves for the dispersion spectra. Scale reading, x, is plotted against wavelength, λ.

Cauchy's dispersion equation, equation 2.1, gave a reasonably good representation of the graphs obtained and was used to generate values of x for wavelengths between 400 nm and 700 nm.

$$n = A + \frac{B}{\lambda^2} + \frac{C}{\lambda^4} \qquad \text{Equation 2.1}$$

where n is the refractive index of the medium, i.e. glass, and is proportional to the scale reading, x. A, B and C are constants, and λ is the wavelength of light at position x.

Photometer Wedges

The three photometer wedges were calibrated in situ by means

of a photomultiplier (EMI, type 9558) placed at the exit pupil of the colorimeter. Fig. 2.13 shows the calibration data for all three wedges, set at 650 nm, 530 nm and 460 nm.

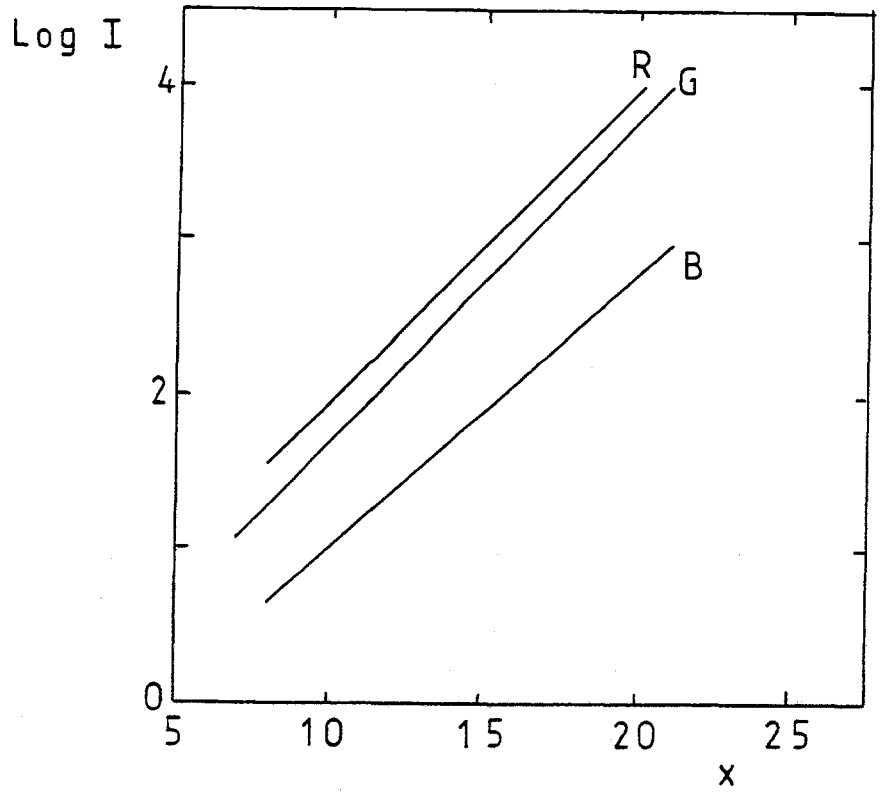


Fig. 2.13 Calibration curves for the three photometer wedges. Log transmitted illuminance, I, is plotted against wedge scale reading, x. Wedges calibrated: R at 650 nm, G at 530 nm and B at 460 nm.

N.P.L. calibrated

The photomultiplier was also used to obtain the spectral output of the source, S1, measured at the exit pupil (fig. 2.14)

2.12 Experimental Arrangement for the Bleaching Experiment

The bleaching experiments required the introduction of another white light source , S3; thus a 150V D.C. quartz-halogen lamp, driven by the stabilised power supply described in section 2.3, was introduced into the system as shown in fig. 2.15

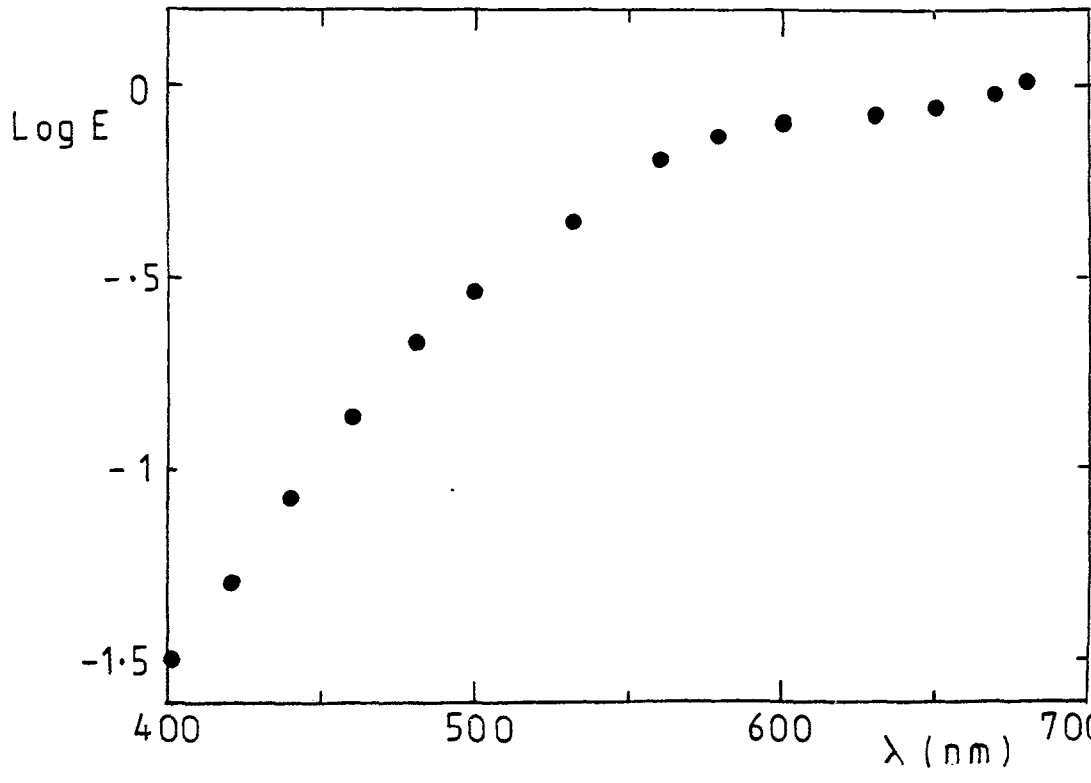


Fig. 2.14 Spectral output of the source, S1. Log relative irradiance, E, is plotted against wavelength ,λ in nm.

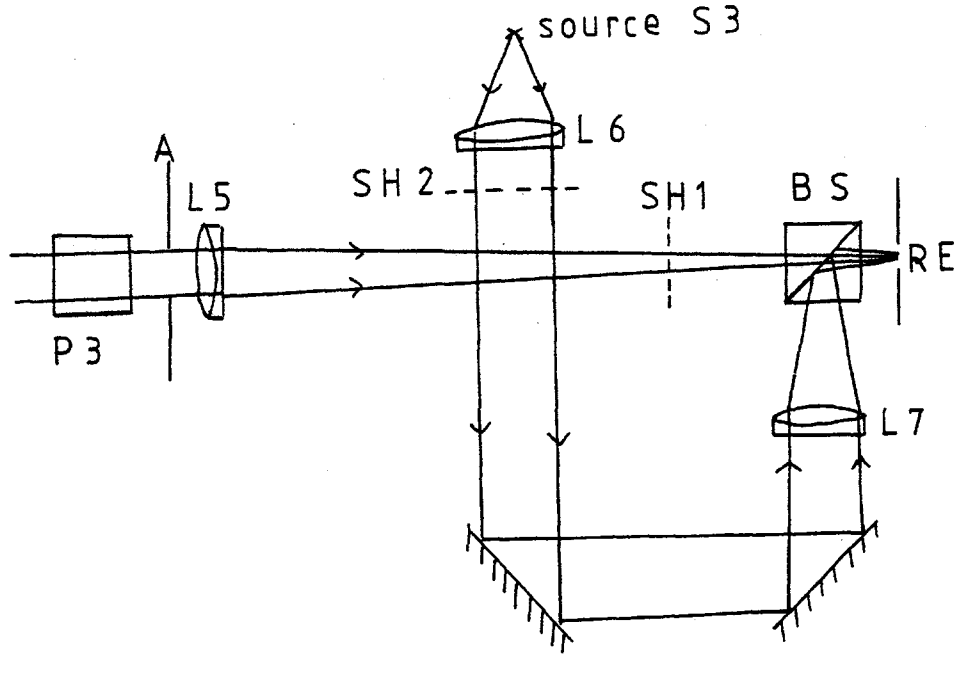


Fig. 2.15 Modification to the Wright colorimeter: described in text.

Light from the source S3 is collimated by L6, reflected onto the final lens L7, and combined with the bipartite field by a beamsplitter, B.S. Neutral density filters can be inserted to control the intensity of the bleaching field and broad band gelatin filters used to select the required colour. The combined fields as seen by the observer are shown in fig. 2.16. Manually controlled shutters SH1 and SH2 were used to control the presentation of the stimuli to the observer.

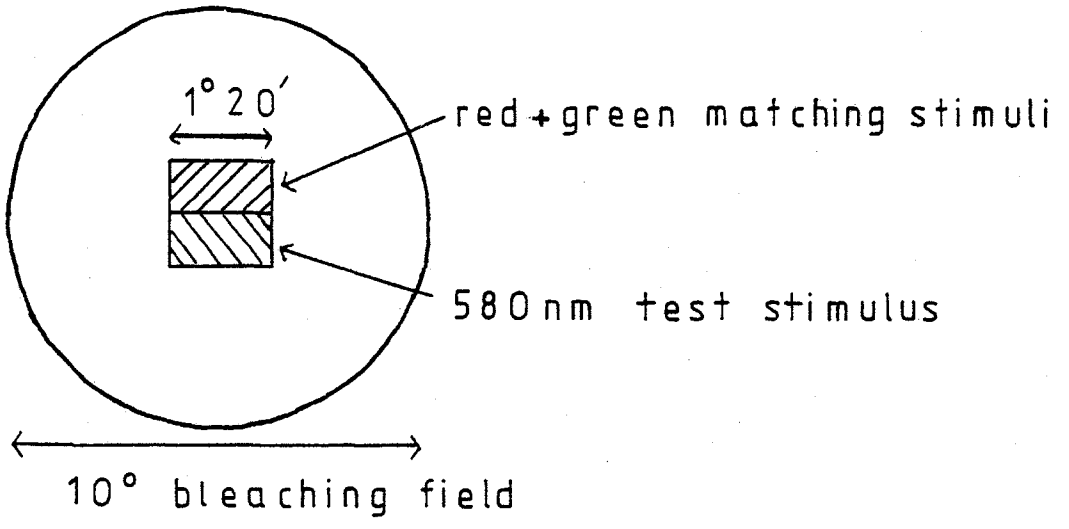


Fig. 2.16 Field configuration for the bleaching experiments.

2.13 Experimental Procedure

Wavelength Discrimination

Wavelength discrimination was measured using the bipartite field illustrated in fig. 2.17.

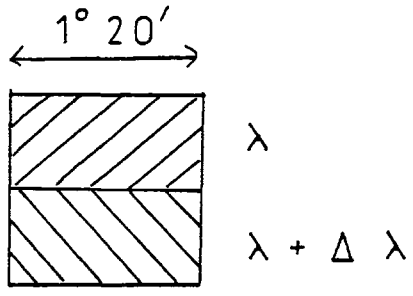


Fig. 2.17 Bipartite field arrangement for wavelength discrimination experiments.

Both halves of the field were set at a wavelength, λ , by the experimenter, two of the reflecting prisms in W2 (fig. 2.7) being blocked off. The observer was instructed to increase the wavelength of the lower half, using a knob connected to the wedge in W1 by a series of weights and pulleys, until he could just detect a difference between the two fields. He then adjusted the intensity of the top half by moving the photometric wedge in front of the reflecting prism in W2, to see if by so doing he could again make the two half fields look identical. If he could do so, the procedure was repeated until it came to the point where no manipulation of the intensity of the top half could make the fields appear identical. This change in wavelength, $\Delta\lambda$, is then a measure of the just noticeable wavelength step, at wavelength λ .The measurement was repeated three or four times to obtain a reliable average. Values of λ ranged from 460 nm to 660 nm, mostly at 20 nm intervals. The observers were instructed not to fixate

the fields for too long as this greatly impaired their discrimination.

Photopic Sensitivity Curves

Spectral sensitivity curves were measured using the secondary white light source, S2, shown in fig. 2.7. The bottom half of the field, from the W1 spectrum, was blocked off, as were two of the beams from W2. A rotating 90° sector coated with magnesium oxide intercepted the beam such that the observer saw a monochromatic 40' x 1°20' field of wavelength λ, flickered alternately with a white light. The observer was instructed to change the intensity of the monochromatic light, by moving the photometric wedge, until the flicker either disappeared or was reduced to a minimum. This setting was taken to be where the luminances of the two lights were equal. The measurement was repeated three times so that an average value could be obtained. The wavelength, λ, of the monochromatic light was changed until the spectrum from 440 nm to 680 nm had been covered in 20 nm steps. The intensity of the white light was kept constant, except for comparison with the extremes of the spectrum which required the insertion of calibrated neutral density filters in front of the source S2. The intensity settings, I_{λ}, for each wavelength were weighted for the spectral output of the primary source at that wavelength, E_{λ} (fig.2.14), and the sensitivity, S_{λ}, was given by the inverse:

$$S_{\lambda} = \frac{1}{E_{\lambda} I_{\lambda}} \qquad \text{Equation 2.2}$$

Colour Matching

Colour matching experiments were performed with the bipartite field illustrated in fig 2.11. In the present study the colorimeter was used for Rayleigh matches only, i.e. a test stimulus of 580 nm, with matching stimuli of red (650 nm) and green (530 nm). The observer viewed the field and was instructed to match the two halves for colour and brightness by varying the intensities of the red and green matching stimuli.

The bleaching experiments are described in Chapter 4.

CHAPTER THREE

Post-Receptoral Inhibitory Responses In Subjects with Normal Colour Vision

	Section	Page
3.1.	Introduction to Shape Selective Adaptation Experiments	58
3.2.	Wavelength Dependent Post-Receptoral Response Mechanisms: General Characteristics Obtained In Previous Experiments.	63
3.3.	Redetermination of the Spectral Responses	71
3.4.	Binocular Organisation of the Response Channel Which Mediates the Inhibitory Interaction.	79
3.5.	Conclusions.	89

3.1 Introduction to Shape Selective Adaptation Experiments

Post-receptoral responses can be investigated by adaptation methods, as explained in chapter 1 (Gilinsky, 1968; Pantle and Sekuler, 1968; Blakemore and Campbell, 1969 a, b; Maudarbocus and Ruddock, 1973). These experiments, which employ grating stimuli, reveal binocularly controlled mechanisms characterised by orientation and width selective responses. In experiments with two-dimensionally structured stimuli, where both the length and width of the bar elements were varied, it was shown that there are two classes of response mechanisms; one tuned to the length of the bars and one that is independent of length (Burton and Ruddock, 1978). The mechanisms which are tuned to bar length determine the adaptation responses for "short"bars, for which length : width ratio is less than three, and which are monocularly driven. The second class of response mechanism determines responses for bars with length : width ratio greater than 3 and is binocularly controlled.

The work described in this chapter is based on the contrast threshold elevation effect (see chapter 1), where adaptation to bright, 100% contrast gratings raises the threshold for detection of a low-contrast test grating of similar spatial frequency and orientation, relative to the threshold obtained after adaptation to a uniform field of the same mean illumination. This is illustrated in fig. 3.1: fig. 3.1a shows the stimulus configuration and fig. 3.1 , point a, shows the threshold illumination level, log I_t, for

detection of the test grating after adaptation to the grating stimulus of mean illumination level I_b. This threshold level is typically some 0.3 log units greater than the value found after adaptation to a uniform field of the same mean illumination, I_b. In the experiments to be described here, the test grating consisted of a 100% contrast grating of low mean illumination, superimposed on a uniform field of the same mean illumination, I_b, as the adaptation grating. When the test and adaptation gratings are matched for orientation and bar width, threshold elevation is observed for a wide range of bar widths (fig.1.10a), e.g. using sinusoidal gratings, Maudarbocus (1973) found that the amplitude of the elevation effect was approximately constant for spatial frequencies up to 15 cyles/deg. (fig.1.11), after which there is a slight reduction as spatial frequency increases to 24 cyles/deg.

The adaptation effect is transferred interocularly, i.e. adaptation of the left eye raises the threshold for detection of a matched test grating presented to the right eye and vice versa (fig.3.1b; fig.3.1 , point b), although there is a slight reduction in the amplitude of the effect for dichoptic presentation as opposed to monoptic presentation of the test and adaptation gratings.

Simultaneous adaptation of both eyes does not increase the adaptation effect by summation, but on the contrary reduces the amplitude of the effect (fig.3.1c; fig.3.1 , point c). Wigley (1977) investigated the characteristics of this inhibitory effect by measuring the threshold for detection of

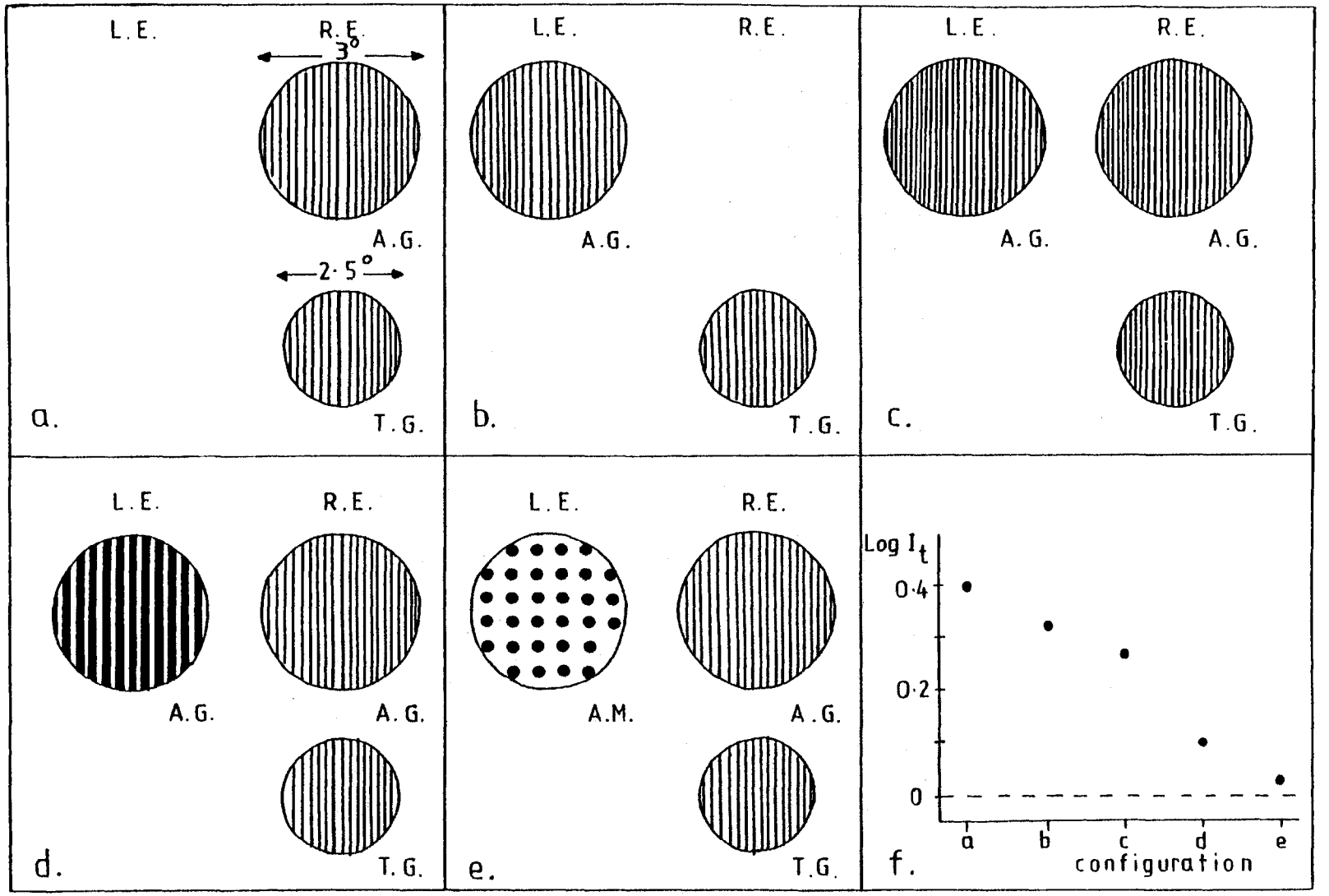

L.E.
R.E.
3°
A.G.
2·5°
T.G.
a.
L.E.
R.E.
A.G.
T.G.
b.
L.E.
R.E.
A.G.
A.G.
T.G.
c.
L.E.
R.E.
A.G.
A.G.
T.G.
d.
L.E.
R.E.
A.M.
A.G.
T.G.
e.
Log I_t
0·4
0·2
0
a
b
c
d
e
configuration
f.

FIG. 3.1

Fig. 3.1 a-e illustrate the various configurations of the adaptation stimuli (AG and AM) and the test stimuli (TG), presented, as shown, to the right eye (RE) and left eye (LE) of the observers.
f, is a schematic representation of the threshold illumination level required for detection of the test, log I_t, after adaptation to each of the configurations a-e. Log I_t = 0 is the value obtained after adaptation to a uniform field presented to the right eye.

the test grating presented to the right eye after simultaneous adaptation of both eyes; the right to a grating matched in bar width and orientation to the test and the left to a vertical grating of variable bar width (fig.3.2).

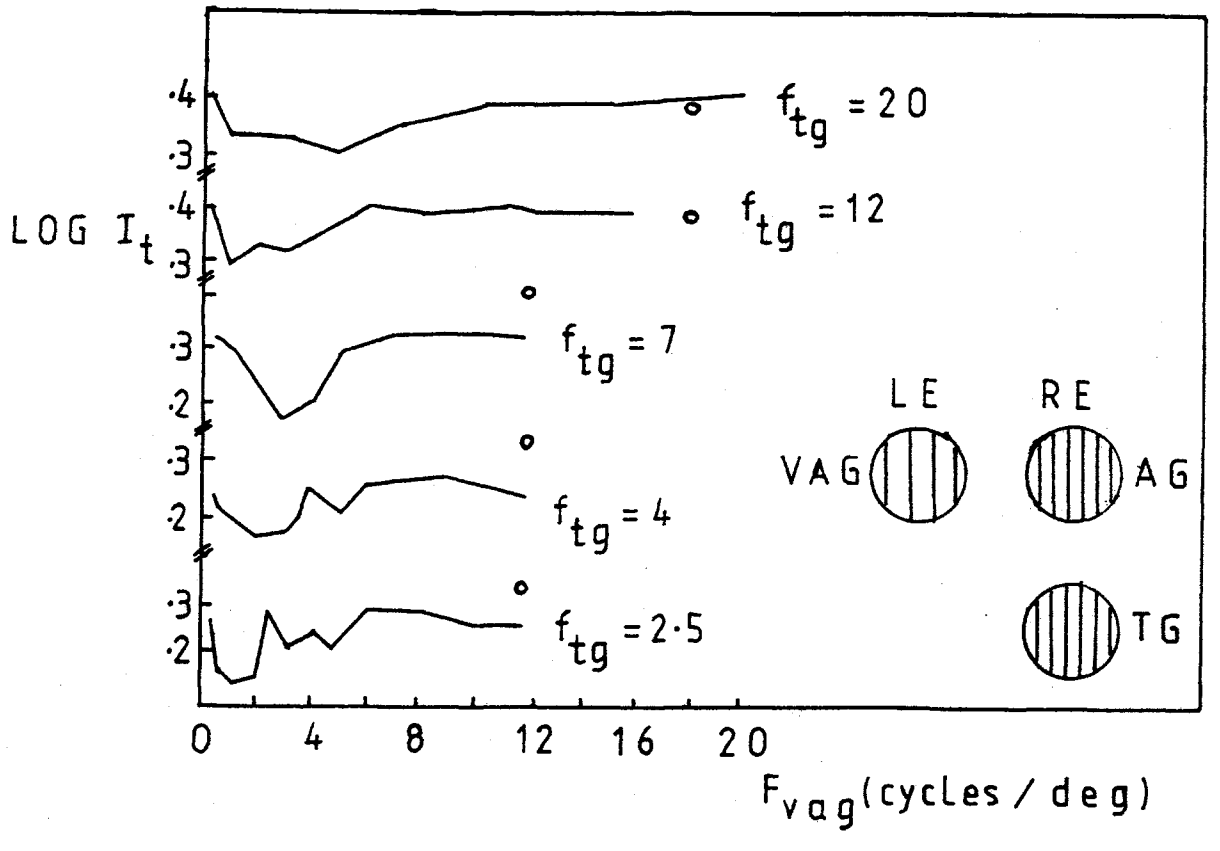


Fig.3.2 Values of the threshold illumination level for the detection of a test grating (TG) presented to the right eye, log I_t, plotted against spatial frequency of the variable adaptation grating (VAG) presented to the left eye. Results are plotted for five spatial frequencies of the test grating, marked in cycles/deg. For each value of ftg = fag, log I_t was also determined in the absence of any stimulus presented to the left eye, and these values are plotted as circles to the right of each plot. The inset shows the stimulus configuration.
From Ruddock and Wigley (1976)

These results show that an adaptation grating of spatial

frequency between 1 and 4 cycles/deg. presented to the left eye significantly reduces the contrast threshold elevation effect exerted by an adaptation grating on a test grating in the right eye. This holds for all spatial frequencies of the test and adaptation gratings presented to the right eye. A similar response can be observed (fig.3.1e; fig.3.1 , point e) when the left eye is adapted to arrays of spots arranged in a matrix (fig.3.3).

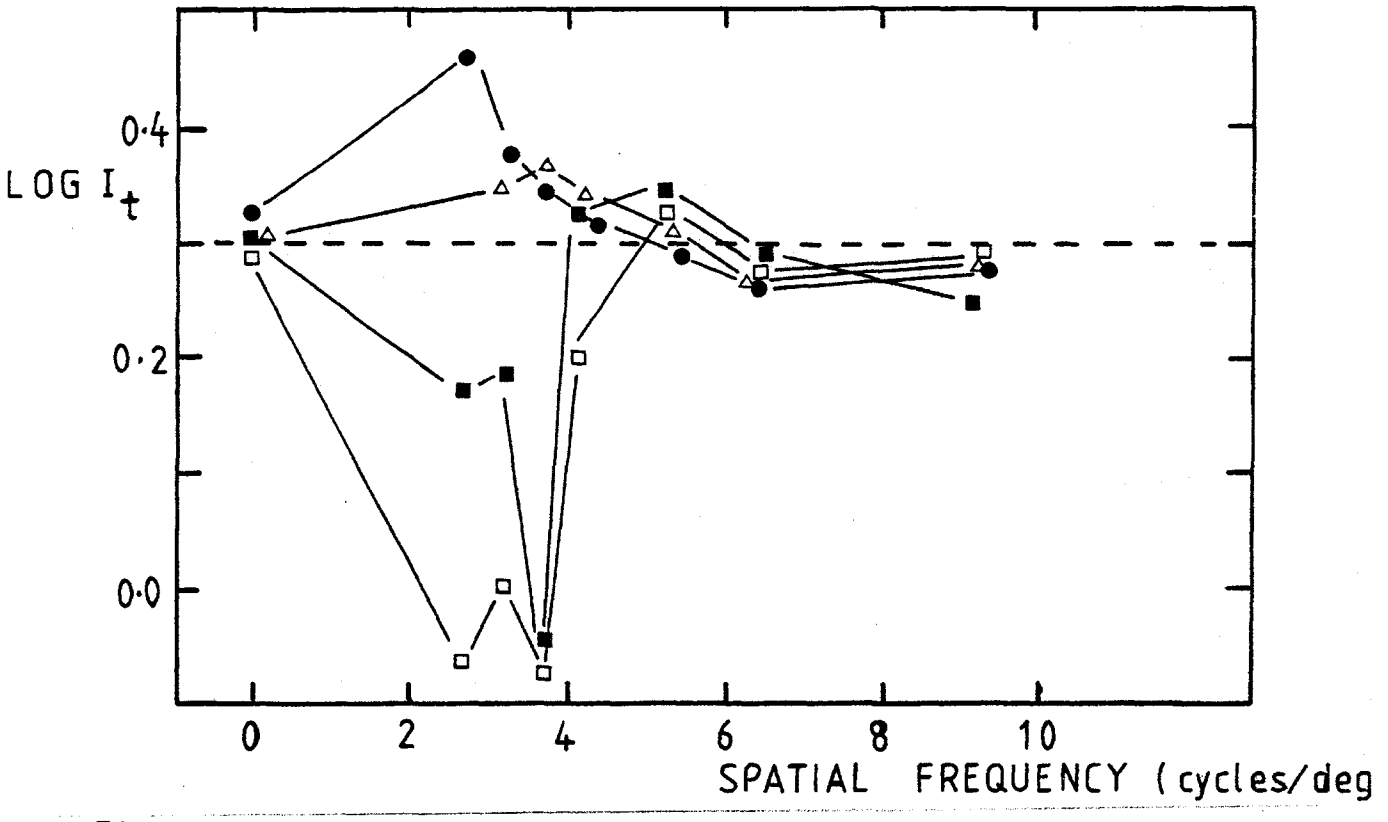


Fig. 3.3 Values of log threshold illumination level, log I_t, plotted against spatial frequency of the adaptation matrix presented to the left eye. The dashed line represents the value of log It found in the absence of the spot matrix, and log I_t = 0 gives the value found after adaptation to a uniform field in the right eye.

Each set of data refer to a different matrix wavelength: ■ 636 nm, □ 610 nm, △ 470 nm and ● 440 nm.

The matrix was of positive contrast, i.e. bright spots on a dark background. The test and adaptation gratings were of bar width 5.7 min. of visual angle (corresponding to a fundamental spatial frequency of 5.26 cycles/deg.) and wavelength 636 nm.

From Hendricks, Ruddock and Waterfield, 1982.

The binocular interaction associated with coarse linear gratings in the left eye is not wavelength dependent (Wigley, 1977), but becomes so when the stimulus presented to the left eye is a matrix of spots, as can be seen in fig. 3.3.

3.2 Wavelength Dependent Post-Receptoral Response Mechanisms: General Characteristics obtained in Previous Experiments

These colour-selective adaptation responses were investigated by Waterfield (1980) using a matrix of spots as the adaptation stimulus presented to the left eye, and a grating adaptation stimulus and a grating test stimulus presented to the right eye. The spots were of diameter 9.3 min.of arc, which corresponds to a fundamental spatial frequency of 3.23 cycles/deg. and gives the minimum value of log I_t (fig.3.3). All stimuli were near monochromatic, with the wavelength of the adaptation matrix, λ , providing the variable parameter. The illumination levels of the adaptation stimuli were set at 4.5 log units above threshold for their detection and the general experimental procedure is described in chapter 2. Threshold for detection of the test grating, log I_t, was measured as a function of λ , the matrix wavelength, and three classes of spectral response were observed, each associated with a different matrix geometry (fig 3.4).

These responses can be obtained with any test wavelength, except that the response illustrated in fig.3.4c is restricted to blue test gratings only, i.e. the spectral responses are independent of the wavelength of the matched test and adaptation gratings presented to the right eye and must therefore be associated specifically with the binocular interaction elicited by the matrix.

Fig. 3.4

Log threshold illumination, log I_t, for detection of the test grating plotted against matrix wavelength, λ .

The test and adaptation gratings were of bar width 5.7 min. of arc in a and b and 10 min. of arc in c, and the matrix spot diameter was 9.3 min. of arc in a and b and 15 min. of arc in c. The adaptation matrix consisted of:

a, bright spots on a dark background, i.e. positive contrast

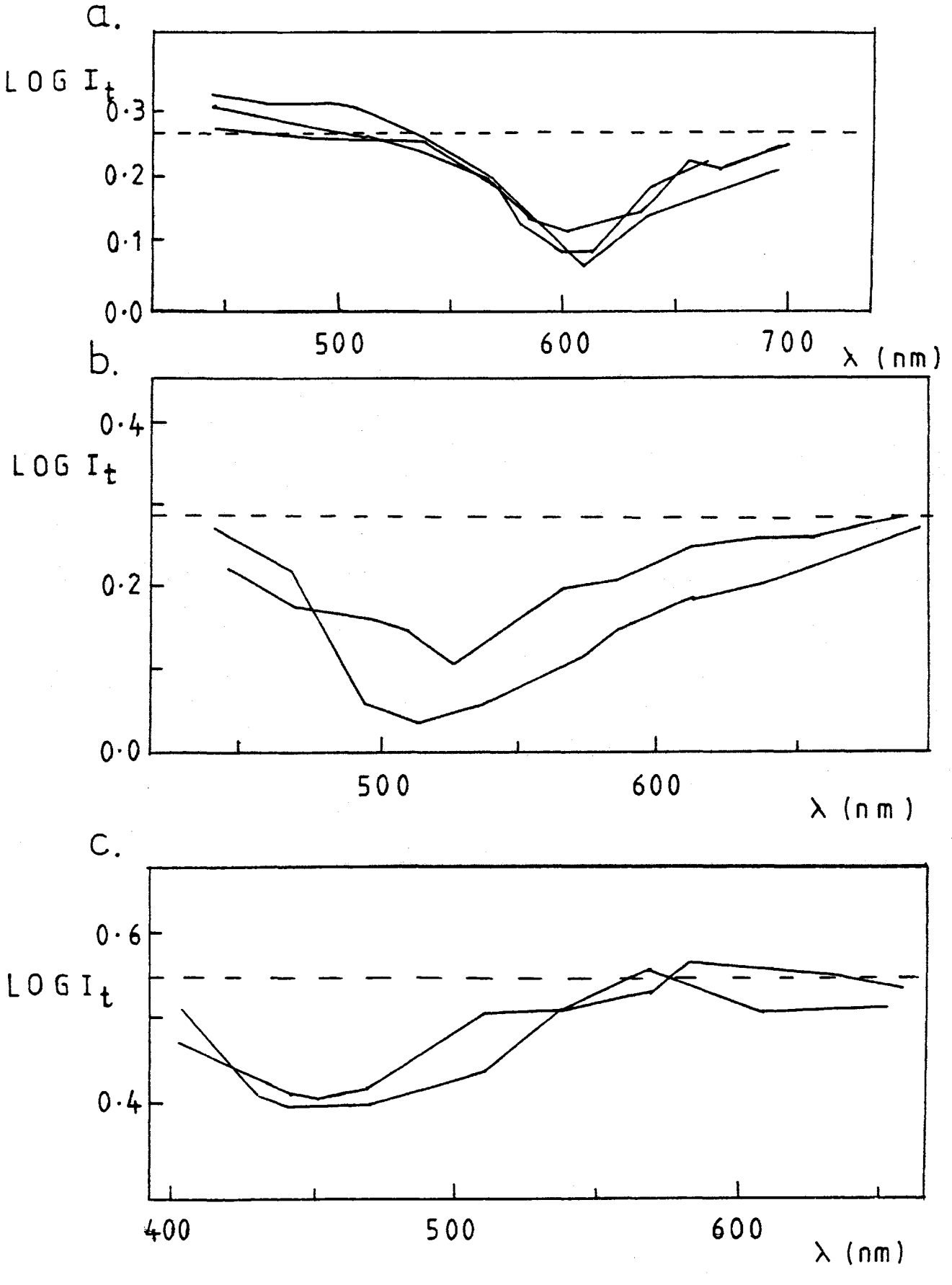
b, dark spots on a bright background, i.e. negative contrast

c, bright spots on a dark background, with the test grating presented on a yellow (580 nm) background.

The dashed lines represent the values of log I_t obtained in the absence of the matrix and log I_t = 0 corresponds to the value found in the absence of structured adaptation. The different plots refer to different subjects.

From Hendricks, Ruddock and Waterfield, 1982.

FIG. 3.4


a.
LOG I_t
0·3
0·2
0·1
0·0
500
600
700
λ (nm)
b.
0·4
LOG I_t
0·2
0·0
500
600
λ (nm)
c.
0·6
LOG I_t
0·4
400
500
600
λ (nm)

These experiments show that it is possible to isolate three independent post-receptoral spectral mechanisms in the human visual system. It should be noted that although in most cases the effect of the matrix is to reduce the effect associated with the adaptation grating presented to the right eye, i.e. log I_t is reduced, in certain cases (i.e. for $\lambda < 500$ nm in fig. 3.4a) log I_t is increased relative to the value found for the grating alone. In the cases where log I_t is reduced, the matrix essentially inhibits or suppresses the effect of the adaptation grating, whereas when log I_t is increased, the adaptation stimuli interact in an excitatory or summating manner. The variation of threshold illumination with change in illumination of the matrix pattern was determined for wavelengths, λ , which produced the the greatest change in log I_t from the value obtained for the adaptation grating alone. Results for the positive contrast matrix are shown in fig. 3.5, in which log I_t is plotted against matrix irradiation level, log E_m.

Log I_t varies approximately linearly with log E_m over the range 1.5 to 4.5 log units above threshold for detection of the adaptation matrix.

The wavelength dependent data of the kind illustrated in fig. 3.4 and the luminance dependent data illustrated in fig. 3.5 can be combined to give spectral response functions, as illustrated in fig. 3.6. The data of fig 3.6a shows schematic wavelength dependent responses for a fixed matrix illumination of 4.5 log units above threshold, corresponding to irradiation levels W_λ at wavelength λ .

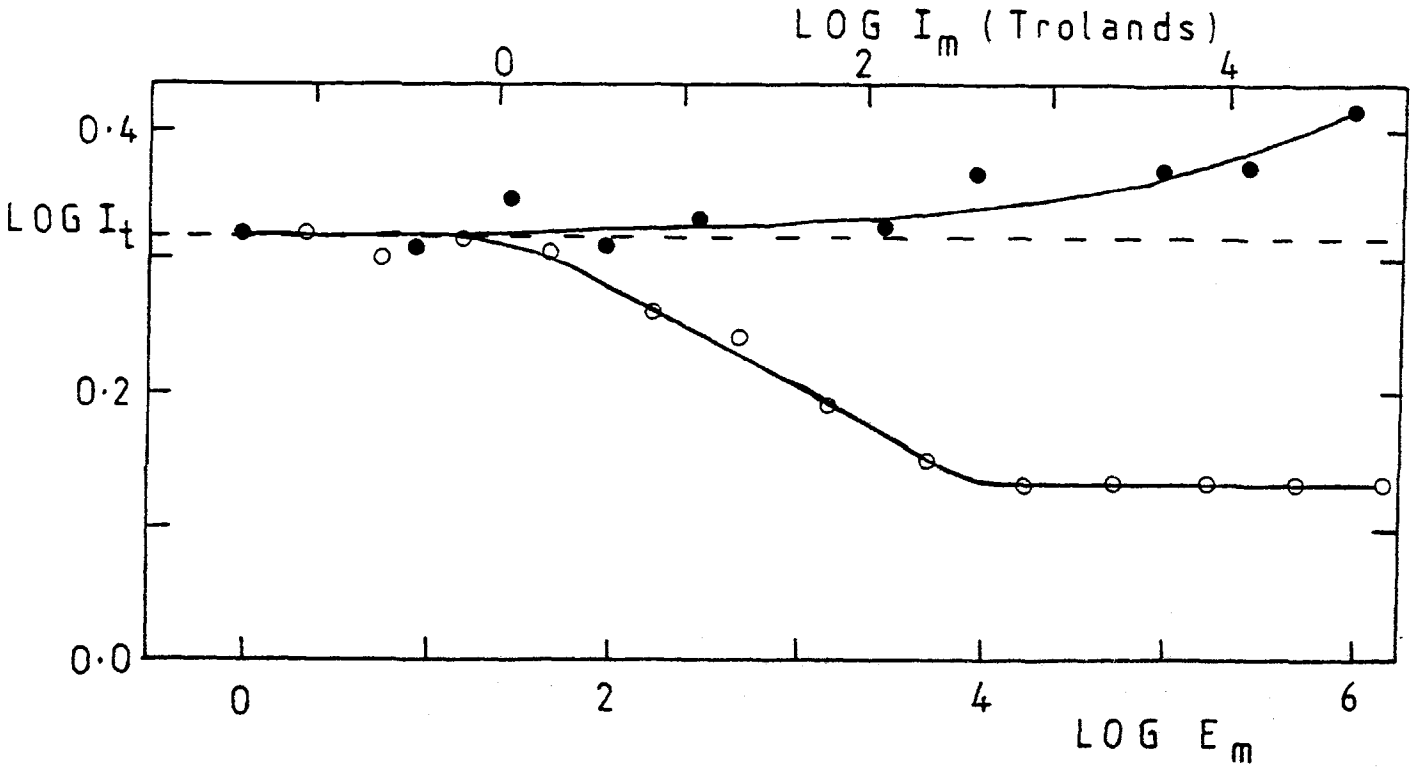


Fig. 3.5. Log threshold illumination level for detection of the test grating, log I_t, plotted against log irradiation of the adaptation matrix, log E_m. Also shown is the corresponding retinal illumination level of the matrix, log I_m, expressed in log trolands. Each point is the mean of thirty measurements.

O data for matrix wavelengths which reduce log I_t relative to the value obtained when E_m = 0 (dashed line).

● data for matrix wavelengths which increase log I_t relative to the value obtained when E_m = 0.

The average illumination level of the adaptation grating presented to the right eye was constant and equal to 3.5 log trolands.

From Hendricks, Ruddock and Waterfield, 1982.

On the assumption that the relation between log I_t and log E_m is similar for all matrix wavelengths which decrease log I_t, and, separately, for all those which increase log I_t, fig.3.6b can be constructed (this applies to matrix wavelengths, λ , which decrease log I_t and a similar figure can be drawn for values of λ which increase log I_t). The positions of the plots for different matrix wavelengths, λ_1, etc, are determined by the known values W_{λ_1}, etc, marked as crosses on fig. 3.6b. The sensitivity, S_{λ_1}, etc, of this response mechanism at a given threshold, log I_t, is then given by,

$$\text{Log } S_{\lambda_1} = - \text{Log } E_{\lambda_1} \qquad \text{Equation 3.1}$$

where E_{λ_1}, etc. are the irradiation values which yield the same value of log I_t for different matrix wavelengths, λ_1, etc.

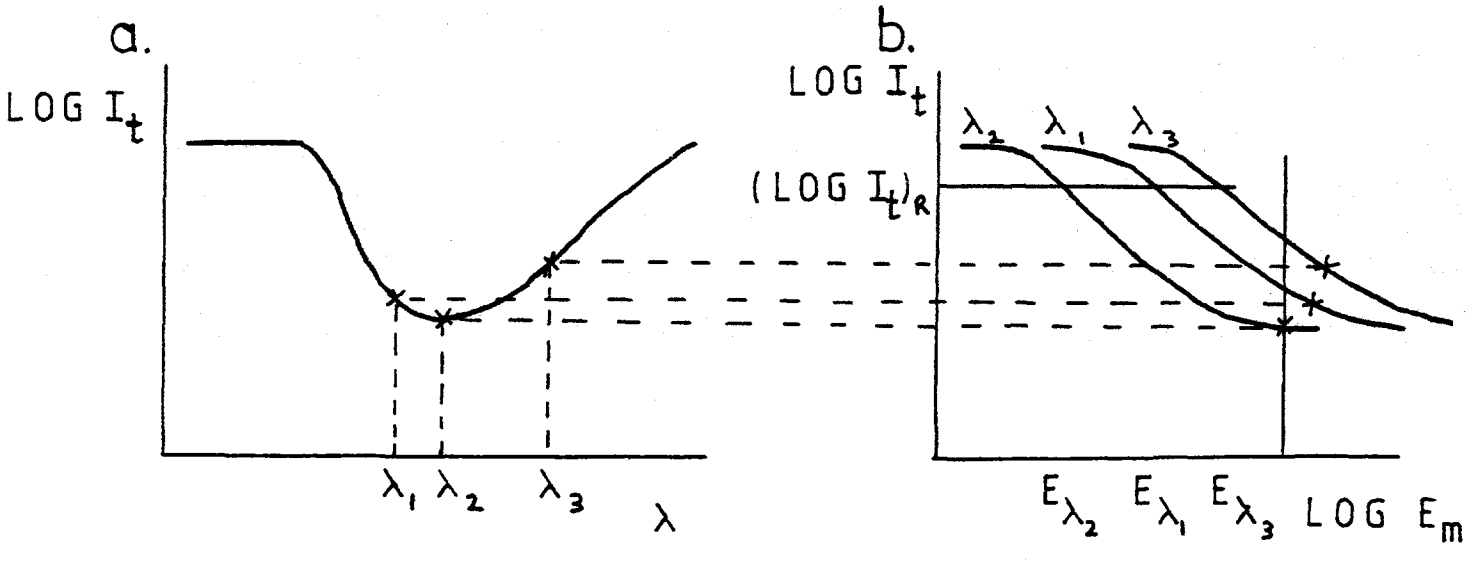


Fig. 3.6a Schematic wavelength dependent responses for a positive contrast matrix of fixed illumination level 4.5 log units above threshold, corresponding to irradiation levels W_λ at wavelength λ . Threshold illumination level, log I_t, is plotted against wavelength, λ .

Fig. 3.6b Schematic luminance dependent responses for different matrix wavelengths, marked λ_1, λ_2, λ_3. Threshold illumination level, log I_t, is plotted against matrix irradiation, log E_m. The values of log W_{λ_1}, W_{λ_2}, W_{λ_3} for wavelengths λ_1, λ_2, λ_3 are marked as crosses. E_1, E_2, E_3 are the irradiation values which yield the threshold value $(\log I_t)_R$.

The resulting normalised spectral sensitivities, derived in this way from the experimental data of fig.3.4 a,b,c, are shown in fig. 3.7 a,b,c.

These spectral sensitivity functions can be represented as linear combinations of the Stiles (1959) π -mechanisms:-

$$S_1 = \pi_5 - \pi_4$$

$$S_2 = \pi_4 - 0.33\,\pi_5$$

$$S_3 = \pi_1$$

The computed sensitivities are plotted as broken lines for comparison with the experimental data on fig. 3.7.
The sensitivities of these response mechanisms are remarkably similar to those obtained by Sperling and Harwerth (1971) from behavioural studies on macaques, following spectrally selective bleaching of the different cone photopigments with coloured lights. They showed that spectral sensitivity in the primate eye can be regarded as the upper envelope of three spectral sensitivity functions, namely

channel 1: $S_1 = \pi_5 - \pi_4$

channel 2: $S_2 = \pi_4 - 0.3\pi_5$

channel 3: $S_3 = \pi_1$

These three channels correspond to the three chromatic mechanisms observed in this psychophysical study.

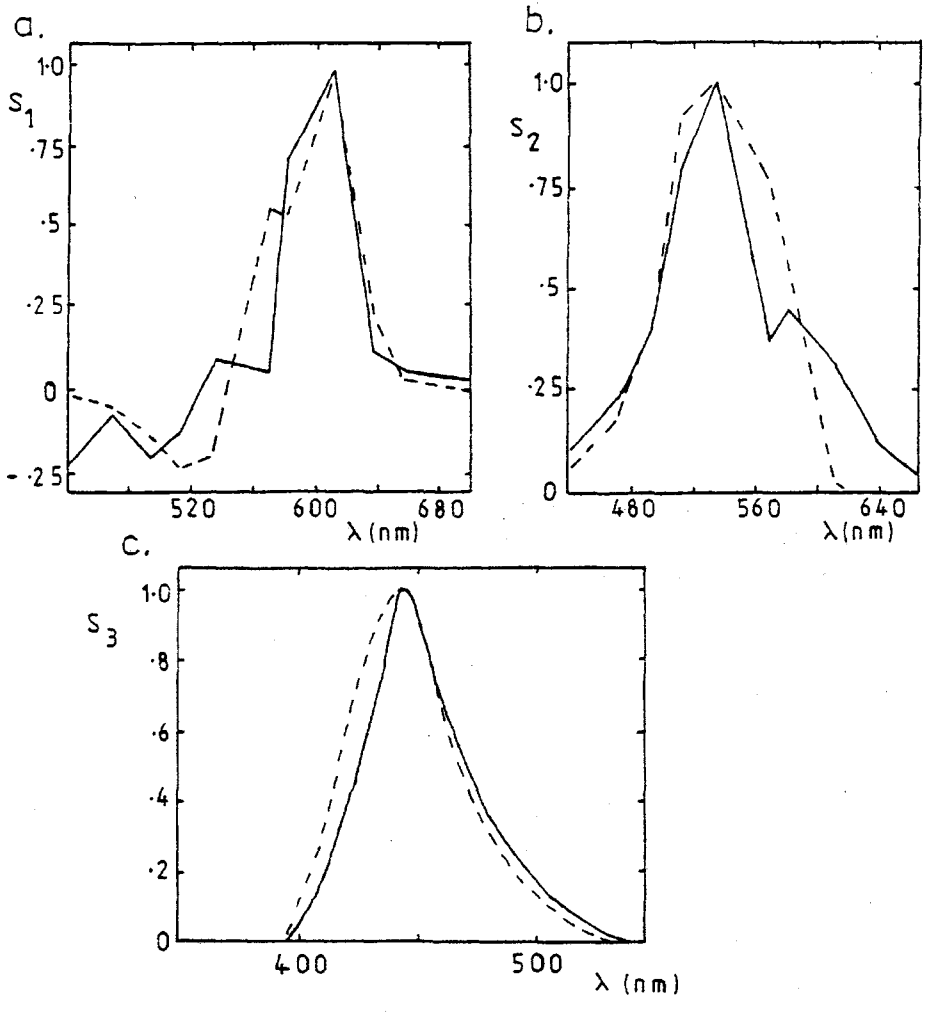


Fig.3.7 The spectral sensitivity profiles of the three response mechanisms. Normalised sensitivity is plotted against wavelength, λ. The continuous lines are the experimental profiles, showing the best mean fit to the data obtained from figs. 3.4 and 3.5 using equation 3.1. The dashed lines are computed profiles based on linear combinations of the Stiles π - mechanisms: a, $\pi_5 - \pi_4$; b, $\pi_4 - 0{\cdot}33\pi_5$; c, π_1 .

From Waterfield, 1980.

The following conclusions can be drawn from these experiments:

(1) The threshold for detection of the test grating depends upon the wavelength of the spot matrix used to adapt the left eye (fig. 3.4). In most cases, the presence of the spot matrix inhibits the effect of the adaptation grating. In a few cases, however, ($\lambda < 500$ nm for the positive contrast matrix) the matrix increases the effect.

(2) The results obtained for three subjects with normal colour vision demonstrate three independent classes of spectral response, with maximum sensitivity at 600 nm (S_1), 530 nm (S_2) and 450 nm (S_3).

(3) The S_3 response closely follows the blue-sensitive π_1- mechanism (Stiles, 1959), whilst the other two responses are narrow-band and can be fitted by linear combinations of the green-and red-sensitive cone mechanisms.

The data of fig. 3.4 were obtained with all the adaptation stimuli set to the same suprathreshold level. The derivation of the spectral sensitivity functions depends, however, on the assumption that the relationship between $\log I_t$ and the matrix irradiation, $\log E_m$, is independent of λ. New experiments were performed to check this point by direct measurement.

3.3 Redetermination of the Spectral Responses

In order to examine more systematically the dependence of the binocular adaptation effect on the irradiation level of the adaptation matrix, and hence to determine the spectral responses, measurements were made with the 4-channel Maxwellian viewing system described in chapter 2.

The stimulus configuration is shown in fig.3.8, and measurements were made for both positive and negative contrast matrices.

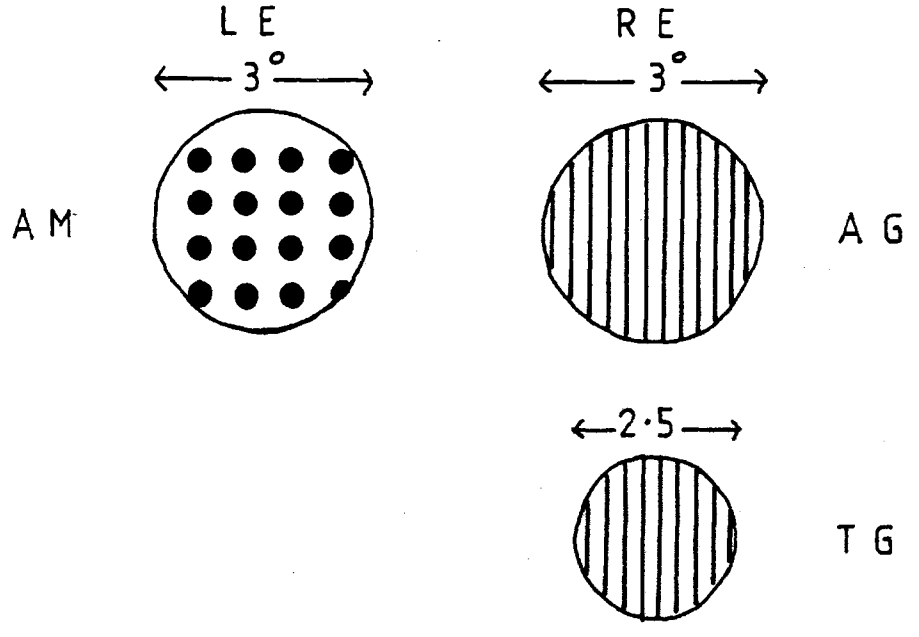


Fig.3.8 Schematic diagram showing the stimulus configuration used in these experiments. The adaptation matrix (AM) and adaptation grating (AG) were viewed binocularly. The test grating (TG) presented to the right eye (RE) consisted of a low contrast grating superimposed on a uniform field of mean illumination level equal to that of the adaptation grating.

The adaptation and test gratings presented to the right eye were of a fixed bar width, equal to 5.0 min. of arc (corresponding to a fundamental spatial frequency of 6.0 cycles/deg) and wavelength 656 nm, and the spot matrix diameter was 9.5 min of arc (fundamental spatial frequency 3.16 cycles/deg) and wavelength λ . The illumination level of the adaptation grating was kept at 4.0 log units above its threshold detection level, whilst the matrix illumination level was varied

between its threshold level and a level of 5-6 log units above threshold. The test consisted of a grating of low illumination superimposed on a uniform field of mean illuminance equal to that of the adaptation grating.

The observer was initially adapted to the grating and spot matrix for two minutes. The stimuli were viewed binocularly and appeared spatially coincident. Consequently, there was a degree of binocular rivalry, a phenomenon which in itself does not influence detection threshold levels (Blake and Fox, 1974) nor the adaptation effect (Ruddock and Wigley, 1976). The experimental procedure is described in chaper 2 and section 3.1. During each experimental session the matrix wavelength was kept fixed and threshold illumination for detection of the test grating, log I_t, was measured for different matrix irradiations, log E_m. Data obtained for matrices of bright spots on a dark background (positive contrast) are illustrated in fig 3.9. Corresponding data for matrices of dark spots on a bright background (negative contrast) are shown in fig. 3.10.

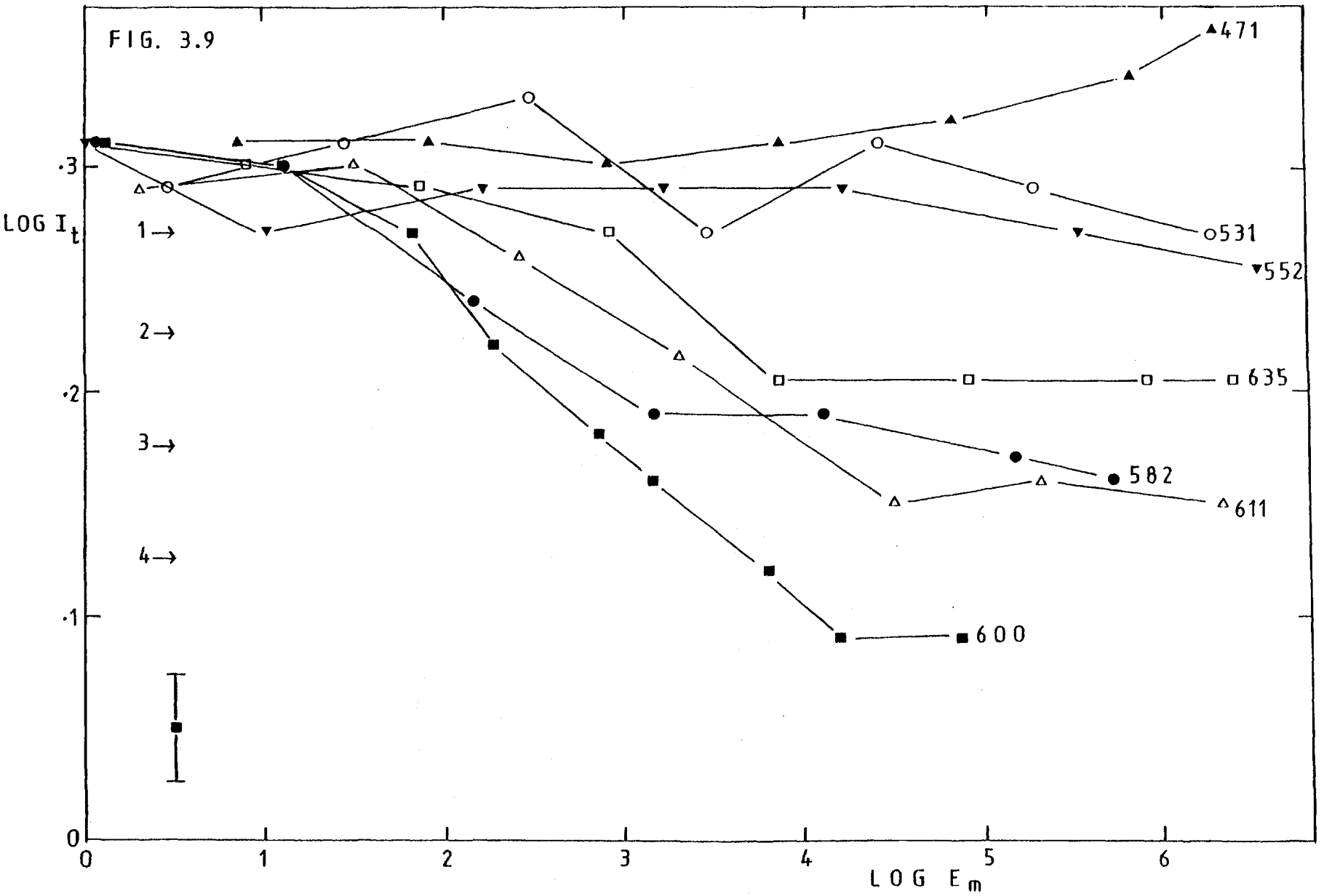
The data of figs. 3.9 and 3.10 show that for those values of λ which produce a significant change in log I_t, the response curves are roughly parallel and saturate at different values of log I_t. In each case, the saturation level of E_m corresponds to a level of approximately 4 log units above detection threshold for each spot matrix wavelength. The spectral sensitivity, S_λ, for this binocular response is defined as $(E_m)_\lambda^{-1}$, where $(E_m)_\lambda$ is the matrix irradiation level required to produce a given threshold level $(\log I_t)_R$ for matrix wavelength λ, and values of S_λ were obtained for four different threshold levels, denoted 1-4, as marked on figs. 3.9 and 3.10.

Fig. 3.9 Log threshold illumination level for the detection of the test grating, log I_t, plotted as a function of matrix irradiation. The adaptation matrix was of positive contrast and each set of data, denoted by a different symbol, refers to a different matrix wavelength, as marked in nm. Log I_t = 0.3 is the threshold level when there is no adaptation stimulus presented to the left eye, and log I_t = 0 is the threshold level when the adaptation grating in the right eye is replaced by a uniform field of the same mean retinal illuminance. Each data point is the average of seven measurements and the average standard error is marked.
Subject IMB.

Fig.3.10 As in fig. 3.9, but the adaptation matrix is of negative contrast.
Subject IMB.

For a given threshold level, $(\log I_t)_R$, a line is drawn parallel to the log E_m axis, and $(E_m)_\lambda$ for a particular matrix wavelength is found at the point where this line and the data curve intersect. Values of log S_λ calculated in this way for the four different values of $(\log I_t)_R$ are plotted against λ in fig 3.11a,b.

The data of fig. 3.11a, b are consistent with those of fig. 3.7a,b, i.e. they reveal two narrow-band functions with peaks at 600 nm and 530 nm. The spectral sensitivity curves become progressively narrower as $(\log I_t)_R$ decreases, due to the different saturation values of log I_t for different wavelengths. Thus, it is only possible to obtain sensitivity functions covering a significant spectral range for small adaptation effects, i.e. for $(\log I_t)_R$ close to its value in the absence of the matrix presented to the left eye.


FIG. 3.9
471
531
552
635
582
611
600
LOG I_t
1→
2→
3→
4→
·3
·2
·1
0
0
1
2
3
4
5
6
LOG E_m

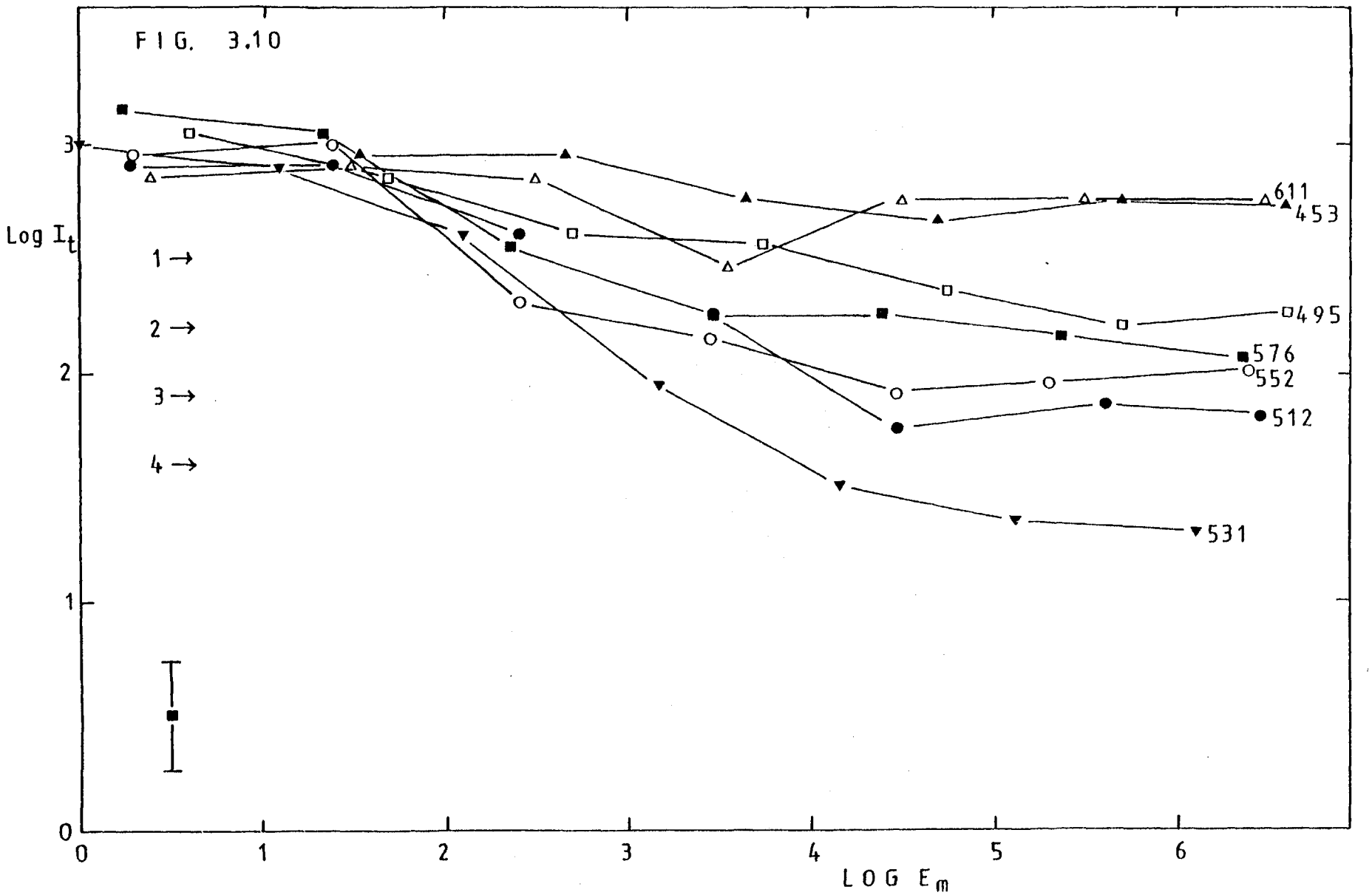

FIG. 3.10
Log I_t
LOG E_m
0
1
2
3
4
5
6
1 →
2 →
3 →
4 →
611
453
495
576
552
512
531

Fig.3.11

Normalised spectral sensitivity, log S , plotted against matrix wavelength , λ .

a. Response curves derived from data of fig. 3.9, i.e. positive contrast matrix configuration, and normalised such that log S_λ = 0 at λ = 600 nm. Each curve, denoted by a different symbol and reference number, defines log S_λ for a different value of $(\log I_t)_R$ namely:

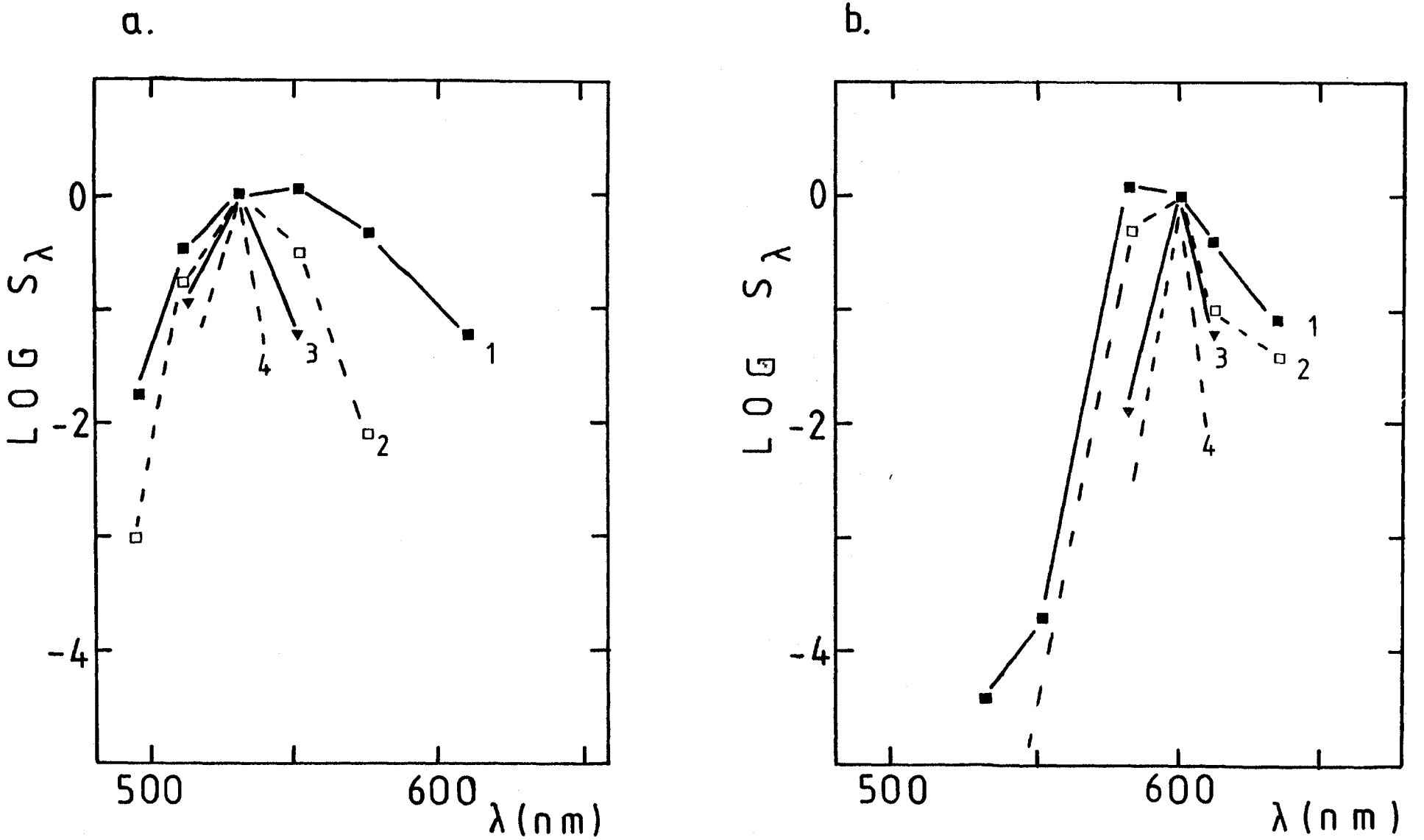
(1) 0.27
(2) 0.225
(3) 0.175
(4) 0.125

b. Response curves derived from data of fig. 3.10, i.e. negative contrast matrix configuration, and normalised such that log S_λ = 0 at λ = 531 nm. Each curve defines log S_λ for a different value of $(\log I_t)_R$ namely:

(1) 0.25
(2) 0.22
(3) 0.19
(4) 0.16

Subject IMB

FIG 3·11



3.4 Binocular Organisation of the Response Channel which mediates the Inhibitory Interaction

The adaptation experiments described in section 3.1 reveal two classes of response mechanism; one orientation selective and binocularly controlled, and the other non-orientation selective and monocularly controlled. Naghshineh and Ruddock (1978) showed that with monocular viewing, it is possible to raise the threshold for detection of a test grating with an adaptation spot matrix of spot diameter equal to the grating bar width, although the reverse is not possible. The experiments described in this section were designed to investigate the stimulus requirements for the production of the inhibitory interaction, by using different combinations of the spot and grating adaptation stimuli presented to the two eyes.

The observer was required to set the threshold for detection of a test grating of spatial frequency 7.4 cycles/deg. and wavelength 635 nm presented to the right eye, after adaptation to a grating or spot matrix, matched in spatial frequency and wavelength to the test, presented to the right eye, and a grating or spot matrix of wavelength 600 nm and variable spatial frequency, f, presented to the left eye (see fig. 3.12 a-d , insets). The spot matrices were of positive contrast only, and the wavelengths were chosen from fig.3.4a to obtain the maximum inhibitory interaction, i.e. the minimum value of log I_t. The adaptation stimuli were all set to an illumination level of 4 log units above detection threshold. The test stimulus was composed of a low illumination grating superimposed on a uniform field

which was of the same average retinal illumination as the adaptation stimulus presented to the right eye. The experimental procedure is described in chapter 2 and the results are shown in fig 3.12; log I_t is plotted against spatial frequency of the stimulus presented to the left eye, and the adaptation configurations are illustrated on each diagram. Thus, for fig. 3.12a the left eye is adapted to a matrix of spots and the right eye to a grating; for fig.3.12b the left and right eyes are adapted to gratings; for fig.3.12c the left and right eyes are adapted to matrices of spots; for fig.3.12d the left eye is adapted to a grating and the right eye to a spot matrix.

The data of fig.3.12 show that the threshold for detection of the test can be raised monocularly by adaptation to a spot matrix as well as by adaptation to a grating (which confirms the results of Naghshineh and Ruddock, 1978), and that this adaptation effect can be inhibited by the presentation to the other eye of a spot matrix or grating of spatial frequency between 1 and 4 cycles/deg. This inhibitory interaction is observed with either a spot matrix or grating of the appropriate spatial frequency, presented to the left eye, combined with either a spot matrix or grating presented to the right eye.

Naghshineh and Ruddock (1978) showed that it is possible to raise the threshold for detection of a spot matrix by monocularly adapting to a matrix of the same spot diameter as the test, but that no corresponding dichoptic adaptation occurs. It was therefore of interest to discover whether it is possible to influence this monocular adaptation effect for a spot matrix with an adaptation stimulus presented to the

Fig.3.12

Log threshold illumination level for detection of the test grating, log I_t, plotted as a function of the spatial frequency of the stimulus presented to the left eye, f. The different adaptation configurations for a-d are illustrated on each diagram. The test grating and adaptation stimulus presented to the right eye are of spatial frequency 7.4 cycles/deg. and wavelength 635 nm, and the adaptation stimulus presented to the left eye is of wavelength 600 nm. The dotted line is the detection threshold in the absence of the adaptation stimulus in the left eye, and log I_t = 0 is the threshold after adaptation to a uniform field. Each point is the average of five measurements and the error bars show the standard deviation from the mean.

■ subject IMB : O subject IPB

other eye. An experiment was therefore performed in which the observer was required to set the threshold for detection of a spot matrix of spatial frequency 7.6. cycles/deg. and wavelength 635 nm presented to the right eye, after adaptation to a spot matrix matched in spatial frequency and wavelength to the test presented to the right eye, and a spot matrix of wavelength 600 nm and variable spatial frequency presented to the left eye (see fig.3.13, inset). The same conditions were observed as in the previous experiment and the results are shown in fig. 3.13.

FIG 3·12

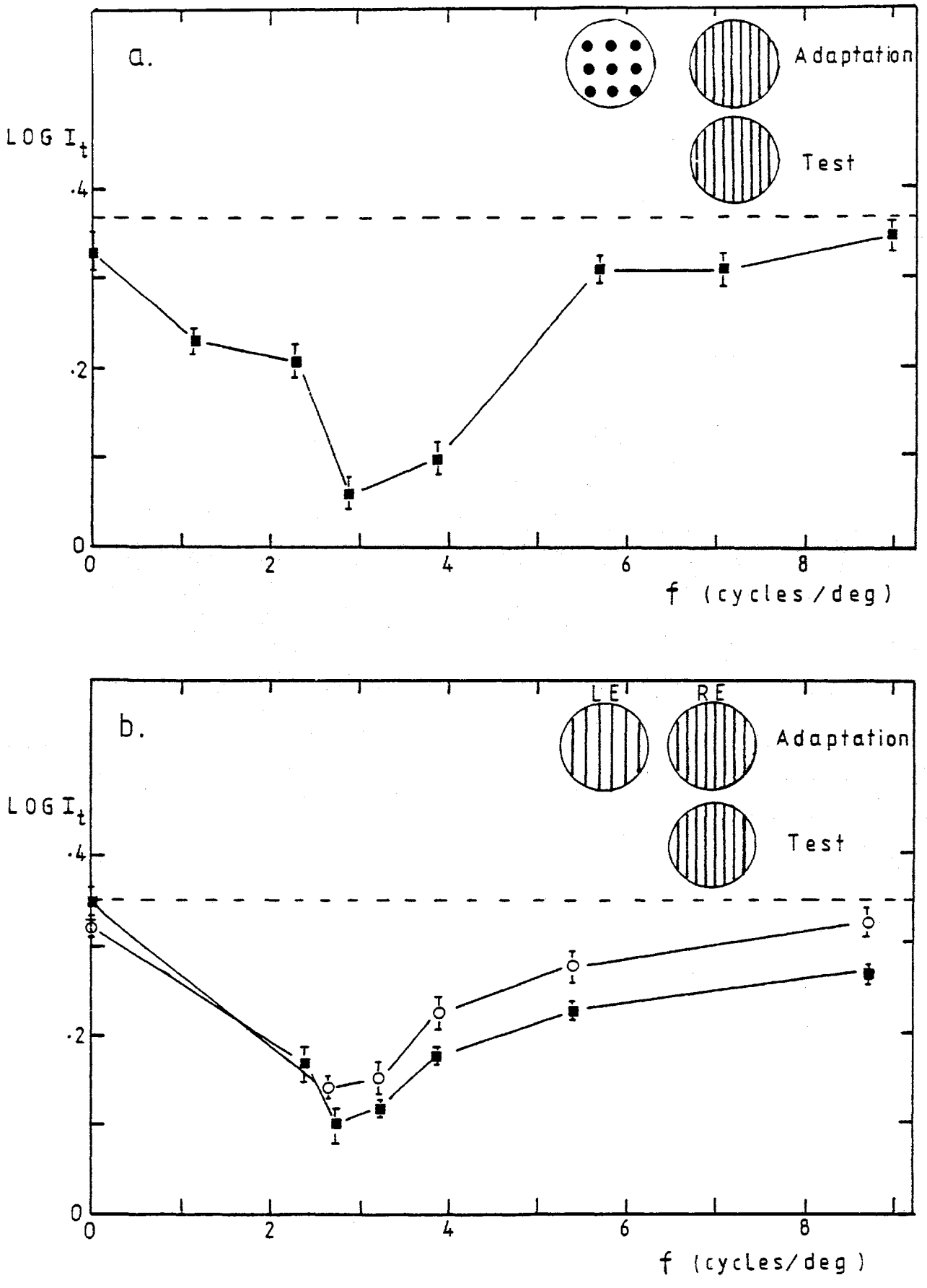
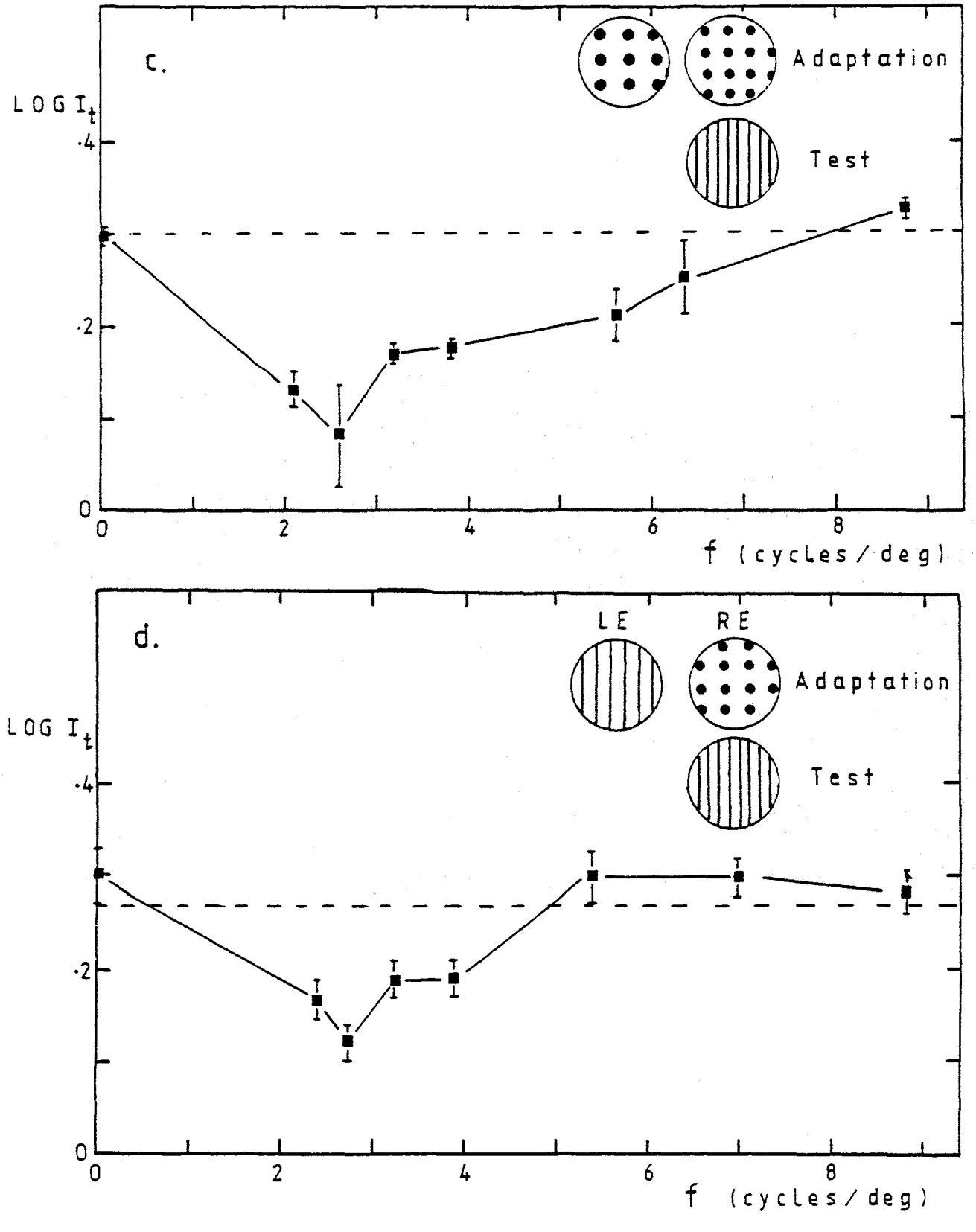

a.
Adaptation
Test
LOG I_t
·4
·2
0
0
2
4
6
8
f (cycles/deg)
b.
LE
RE
Adaptation
Test
LOG I_t
·4
·2
0
0
2
4
6
8
f (cycles/deg)

FIG 3·12


c.
Adaptation
Test
LOG I_t
·4
·2
0
0
2
4
6
8
f (cycles / deg)
d.
LE
RE
Adaptation
Test
LOG I_t
·4
·2
0
0
2
4
6
8
f (cycles / deg)

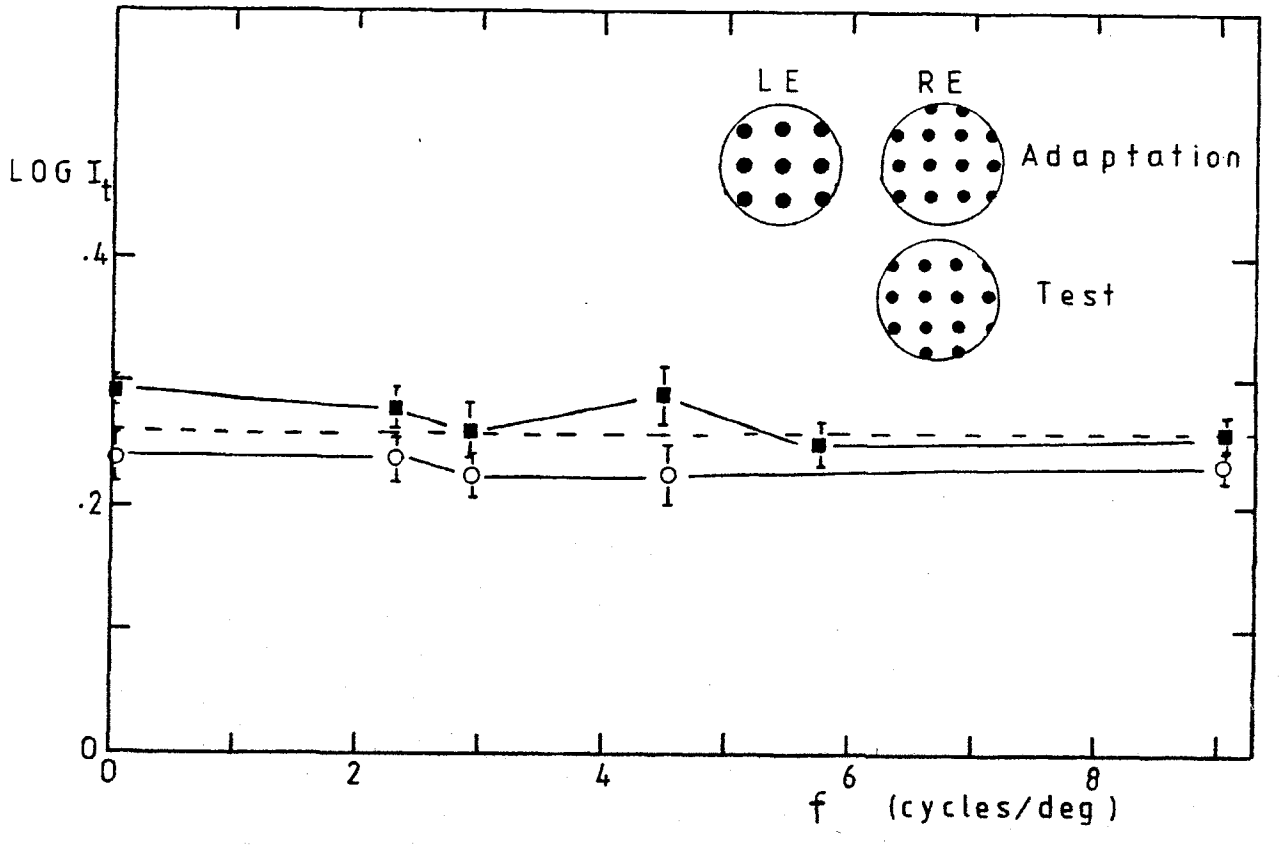


Fig.3.13 Log threshold illumination for detection of the test matrix, log I_t, plotted against the spatial frequency of the matrix presented to the left eye. The test and adaptation matrix presented to the right eye were of spatial frequency 7.6 cycles/deg and wavelength 635 nm. The dotted line is the detection threshold in the absence of the adaptation stimulus presented to the left eye. Each point in the mean of five measurements and the error bars show the standard deviation. The adaptation configuration is shown in the inset.

■ subject IMB: ○ subject IPB

It can be seen from fig.3.13 that no binocular interaction is observed when the test is a two-dimensional matrix structure.

Wavelength dependent responses, of the kind shown in fig.3.4, have previously only been observed when the coarse

stimulus presented to the left eye was a matrix (the configuration illustrated in fig.3.12a). Wavelength selective cortical cells tend to have circularly symmetric receptive fields (Gouras, 1974). It is possible, therefore, that wavelength dependent inhibitory responses may be elicited by a coarse grating structure when the adaptation stimulus presented to the test eye is a matrix (the configuration illustrated in fig.3.12d). This was checked in an experiment similar to the ones previously described in this section, where the threshold for detection of a test grating of 7.4 cycles/deg. and wavelength 635 nm is measured after adaptation to each of the four stimulus configurations illustrated in fig.3.12. The spatial frequency of the structure presented to the left eye was chosen from fig 3.12 to give the largest inhibitory effect, i.e. the smallest value of log I_t, threshold measurements were made for two different wavelengths, 524 nm and 600 nm. The adaptation stimulus presented to the right eye was matched in spatial frequency and wavelength to the test. The results are shown in table 3.1.

As in fig.	LE	RE	Log I_t(λ= 600nm)	Log I_t(λ= 524 nm)
3.12a	Matrix	Grating	.13	.31
3.12b	Grating	Grating	.14	.12
3.12c	Matrix	Matrix	.11	.25
3.12d	Grating	Matrix	.20	.23

Table 3.1 Threshold illumination levels for detection of the test, log I_t, are given for the four different adaptation stimulus configurations, listed in columns 2 and 3. The test and adaptation stimuli presented to the right

eye (RE) were of spatial frequency 7.4 cycles/deg. and wavelength 635 nm. The adaptation stimulus presented to the left eye (LE) was of spatial frequency 2.75 cycles/deg. and wavelength λ.

Subject IMB

These data show that a wavelength dependent response is observed only when a spot matrix is presented to the 'non-test' eye (the first and third configurations), regardless of the adaptation stimulus presented to the test eye.

The results shown in figs. 3.12 and 3.13, and presented in table 3.1, can be represented by a network diagram showing the transmission of signals along the paired visual pathways, implicit in the experimental data (fig.3.14). The network is composed of chromatic channels (C) which transmit information associated with spot stimuli, spot detectors (S.D.), which are monocularly driven, and line detectors (L.D.), which are binocularly driven by summating units (Σ) which pool signals from the luminance channel (L). The spot detectors receive inputs from one eye only, via a direct channel. This is consistent with the results of Naghshineh and Ruddock (1978) who showed that it was only possible to adapt for spots monocularly and that adaptation to bars does not raise the threshold for detection of a spot matrix. The summating units, Σ, combine the outputs of several spot detecting mechanisms to form a channel which transmits signals associated with bar shaped stimuli. The line detectors are driven by excitatory signals (+) from the summating units of both eyes and from the C-channel of the

ipsilateral eye. Thus, it is possible to raise the threshold for detection of bars by monocularly adapting to spot stimuli or by adapting either monoptically or dichoptically to bar stimuli (Naghshineh and Ruddock, 1978). The line detectors (L.D.) and spot detectors (S.D.) on the diagram represent a multiplicity of detectors, each tuned to different stimulus parameters (i.e. size and orientation) and driven by multiple parallel excitatory channels (marked as continuous lines on fig.3.14). In addition to the excitatory inputs, the line detectors also receive inhibitory inputs (-) from the contralateral eye. The inhibitory channels (dashed lines) are associated with bar and spot shaped stimuli. They have a single spatial characteristic which yields the constant spatial responses associated with spatial frequencies in the range 1-4 cycles/deg (fig 3.12). Thus, the line detectors receive excitatory signals from bar stimuli seen by either eye and spot stimuli seen by the ipsilateral eye, and inhibitory signals from the contralateral eye associated with bars (L-response) and spots (C-response), which is consistent with the data presented in table 3.1 and fig. 3.12. The spot detectors do not receive any inhibitory input and this is consistent with the data of fig.3.13, which show that binocular inhibition cannot be elicited with spot matrix targets.

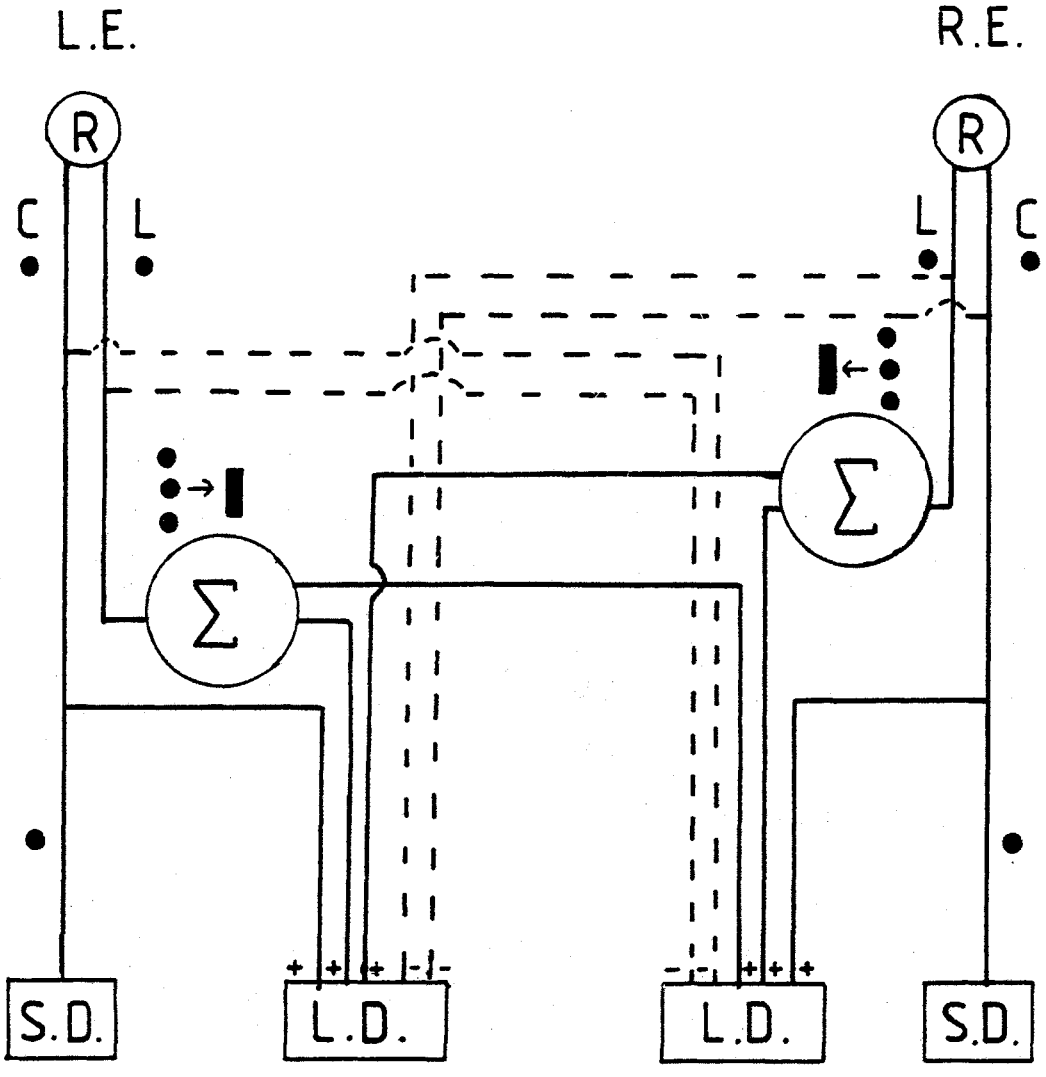


Fig. 3.14 Network diagram representing the arrangement of elements associated with the contrast threshold elevation effect and the inhibitory binocular interaction. R, receptors; S.D., spot detectors; L.D., line detectors; Σ , summating units. Excitatory signals (+) are marked as continuous lines and inhibitory signals (-) are marked as dashed lines.

3.5 Conclusions

The spectral sensitivity data of fig.3.11 reveals that there are two independent binocular response classes, one elicited by positive contrast matrices and one by negative contrast matrices. The spectral response curves closely resemble those of fig. 3.7 a,b, but the new experiments have revealed that the bandwidth of the sensitivity curves becomes increasingly narrow as the reference amplitude of the adaptation effect is increased. This method of evaluating the spectral sensitivities of the binocular mechanisms is more complete than the previous method (fig.3.6) as it does not require any assumptions of the shape of the response curves at high intensities. It is, however, a time-consuming method and, as the two methods have produced essentially the same results, it is the method described in section 3.2 which will subsequently be applied in later sections (chapter 4).

CHAPTER FOUR

Visual Responses of Congenital Red-Green Colour Defective Subjects.

Section		Page
4.1	Introduction	91
4.2	Subjects	94
4.2.1	Wavelength Discrimination Data	95
4.2.2	Rayleigh Matches	96
4.2.3	Spectral Sensitivity	102
4.3	Post-Receptoral Spectral Response Functions in Colour Defective Subjects	103
4.4	Colour Matching under Adaptation	127
4.5	Pigment Mixture Theory of Anomalous Trichromacy	133
4.5.1	Rayleigh Match Shifts Induced by Bleaching	138
4.5.2	Post-Receptoral Response Functions	139
4.6	Single Anomalous Pigment Model	147
4.7	The "Cluster" Theory of Anomalous Trichromacy .	151
4.8	Conclusions	154

4.1 Introduction

The typical abnormal colour vision responses of congenital red-green colour defective subjects have been described in chapter 1. It is commonly accepted that dichromats lack one of the three photopigments present in the normal retina, whilst the two remaining cone photopigments are considered to be normal (Baker and Rushton, 1965; Mitchell and Rushton, 1971; Wald, 1966). A number of hypotheses have been proposed to account for the differences between normal and anomalous trichromatic vision. Some of these theories have been refuted. For example, Alpern and Torii (1968) and Wald (1966) showed, by inserting artificial solutions of macular pigment behind the eyepiece of an anomaloscope, that anomalous colour matches are not due to differences in density of the macular pigment. Alpern and Torii went on to show that protanomaly cannot be due to any inert filter lying between the cone outer segments and the cornea, by applying the method of trans-scleral illumination (Brindley and Rushton, 1959). Protanomalous subjects were found to need more red than normal in a Rayleigh match, even when their cones were illuminated from behind through the sclera (thus bypassing the ocular media). A hypothesis of neural fusion has also been proposed to account for anomalous trichromacy (Ingling and Drum, 1973). Neural fusion of cone signals could account for dichromacy (Leber, 1873; Fick, 1879; Hurvich, 1972), although Rushton's retinal densitometric experiments (Rushton 1963, 1965) suggest that dichromats possess only one photopigment effectively absorbing light at

wavelengths $>$ 500 nm. (Hurvich suggests, however, that as Rushton's method is too insensitive to detect a third photopigment in anomalous observers, one might expect that it would also fail to detect a third pigment in 'dichromatic' observers). However, neural fusion cannot account for anomalous trichromacy because of the Principle of Univariance (Rushton, Powell and White, 1973a), which is that "the intrinsic response of a receptor depends upon its effective quantum catch, but not upon what quanta are caught". If a normal subject makes a Rayleigh match so that the quantum catch by each of the cone pigments involved is the same from the yellow field as from the red + green mixture, then each field will affect each pigment identically and neither pigment will be able to distinguish one from the other. It follows that if the pigments cannot distinguish the fields, nothing else in the visual system can (Rushton, Powell and White, 1973b). Therefore, if the anomalous trichromat has the normal cone pigments, a Rayleigh match that was indistinguishable to the normal pigments would be indistinguishable to him, no matter what fusion mechanisms may occur at a later stage in the system. This is not what is observed; anomalous trichromats do not accept normal Rayleigh matches.

Most studies suggest that alterations in the spectral absorption of at least one photopigment are required to account for anomalous colour vision. Jameson and Hurvich (1956), (Hurvich and Jameson, 1962), proposed that anomalous trichromacy is due to progressive displacements from the normal spectral loci of the three photo-sensitive distribution functions. This theoretical model also

includes a reduction postulate that applies to the post-receptoral neural response level and provides for varying degrees of 'neural efficiency'.

The most common hypothesis, however, is that anomalous observers possess two 'normal' photopigments and one 'abnormal' pigment (Wald, 1966; Alpern and Torii, 1968). Thus, deuteranomals have an abnormal green-sensitive pigment instead of the usual chlorolabe, and protanomals have an abnormal red-sensitive pigment instead of the usual erythrolabe. Most of these theories contain the assumption that there is only one 'deuteranomalous' pigment, common to all deuteranomals, and one 'protanomalous' pigment (Mitchell and Rushton, 1971; Rushton, Powell and White, 1973b; Pokorny, Smith and Katz, 1973; Piantanida and Sperling, 1973a, b; Pokorny and Smith, 1977). MacLeod and Hayhoe (1974) have even proposed that the protanomalous and deuteranomalous pigments are the same molecular species. Pokorny, Moreland and Smith (1975) repeated MacLeod and Hayhoe's analysis and found that the derived functions did not predict the colour matching functions on which they were based. Thus, although they could not refute the theory completely, they showed that the single function derived by MacLeod and Hayhoe is not the pigment that mediates anomalous colour vision. All these theories require the existence of at least one alternative photopigment. Walls and Matthews (1952), however, proposed that the abnormal pigment in deuteranomaly consists of a mixture of normal chlorolabe and erythrolabe. Ruddock and Naghshineh (1974) suggested that both protanomalous and deuteranomalous cones contain mixtures of the normal red- and green- sensitive photopigments. This hypothesis is

economical in that it only requires the three normal photopigments, and the variation in Rayleigh matches amongst different anomalous observers can be explained by a range of erythrolabe/chlorolabe ratios.

A completely different approach to the problem of anomalous trichromacy comes from Alpern's "cluster theory". Alpern and Wake (1977) and Alpern and Pugh (1977) suggested that deuteranopes do not have a single erythrolabe common to all. Colour matching results led Alpern and Moeller (1977) to propose that there are clusters of erythrolabe, chlorolabe and (possibly) cyanolabe. Thus, a normal trichromat is one whose long-wavelength sensitive pigment is from the erythrolabe cluster and whose middle-wavelength sensitive pigment is from the chlorolabe cluster. Deuteranomalous trichromats, however, have both their middle- and long-wavelength sensitive pigments from the erythrolabe cluster, whilst protanomalous trichromats have two pigments from the chlorolabe cluster. This theory is able to predict the variability in colour matching amongst anomalous observers, but requires a large number of different photopigments and thus might be difficult to explain genetically.

In the present study the techniques described in chapter 3 for isolating post-receptoral response functions are applied to colour defective observers, and the results are discussed in relation to the above models. Also presented for some anomalous observers are colour matching data obtained after bleaching the retina.

4.2 Subjects

Subjects were all volunteers from the students and staff at Imperial College, aged between 18 and 30. The existence

of a colour deficiency was first established using the standard Ishihara colour plates, and the subjects stereoscopy was tested using the Julesz (1971) random dot stereograms (plates 8.1-2). Only subjects with stereovision at 80% correlation were chosen for further experiments. Subjects were then required to make a Rayleigh match on the Wright colorimeter and classified as one of the four categories: deuteranomalous, protanomalous, deuteranopic, protanopic. To quantify the degree of colour deficiency, wavelength discrimination curves were obtained for the anomalous trichromats, and each subject made several Rayleigh matches to determine his R/G ratio and the degree of accuracy of his match. In some cases, the photopic spectral sensitivity ($V\lambda$) functions were also measured.

4.2.1 Wavelength Discrimination Data

Wavelength discrimination curves show the change in wavelength required at any reference wavelength in the visible spectrum to just detect a difference in two adjacent near-monochromatic fields. The results, obtained using the method described in chapter 2, are shown in figs. 4.1 - 4.3. In fig 4.1 the data for two dichromats and a normal trichromat are plotted, and show that the dichromats, SH (a deuteranope) and DC (a protanope), are unable to distinguish spectral colours of wavelength $>$ 530 nm. Fig. 4.2 shows the wavelength discrimination data for 9 deuteranomalous subjects. The degree of deficiency ranges from quite a mild loss of discrimination for subjects P.D., D.S., and M.T. (fig 4.2g-i) to a fairly severe defect in the case of subject A.F. (fig. 4.2c). Data for 4 protanomalous subjects are plotted in fig 4.3.

Fig. 4.1 Wavelength discrimination curves. The just detectable change in wavelength, $\Delta\lambda$, is plotted against wavelength, λ . Data is for (a) a deuteranope, (b) a protanope, (c) a normal subject.

Fig. 4.2 Wavelength discrimination curves for 9 deuteranomalous subjects.

4.2.2 Rayleigh Matches

Rayleigh matches were made with the bipartite field provided by the Wright colorimeter (see fig 2.11). Subjects were required to match a mixture of red (650 nm) and green (530 nm) to a fixed yellow (580 nm) stimulus. The match was repeated at least seven times and the mean red : green ratio , log R/G, was calculated along with the mean standard deviation. The results are given in table 4.1.

Obs	Def	Log R/G	S.D.	$\Delta\lambda$ (λ = 600 nm)
AF	DA	-.355	.269	24
AG	DA	-.555	.101	
JH	DA	-.088	.088	10.5
DS	DA	-.482	.056	7
CM	DA	-.24	.090	30
PD-L	DA	-.552	.060	8
MT	DA	-.172	.018	6
EP	DA	-.185	.085	15
IMB	N	0	.017	2.5
CR	N	-.042	.035	
PS	PA	.738	.273	20
SC	PA	.765	.325	40

Table 4.1 Ratio of 650 nm (R) to 530 nm(G)required to match a yellow (580 nm) stimulus. Column 1 gives the observer; column 2 is the colour deficiency: DA - deuteranomaly, PA - protanomaly,N - normal. Column 3 is the mean red : green ratio,log R/G, normalised such that log R/G = 0 for observer IMB. Column 4 is the standard deviation from the mean. Column 5 is the just noticeable change in wavelength ($\Delta\lambda$) in nm at λ = 600 nm. obtained from figs 4.1 - 4.3.

FIG. 4.1

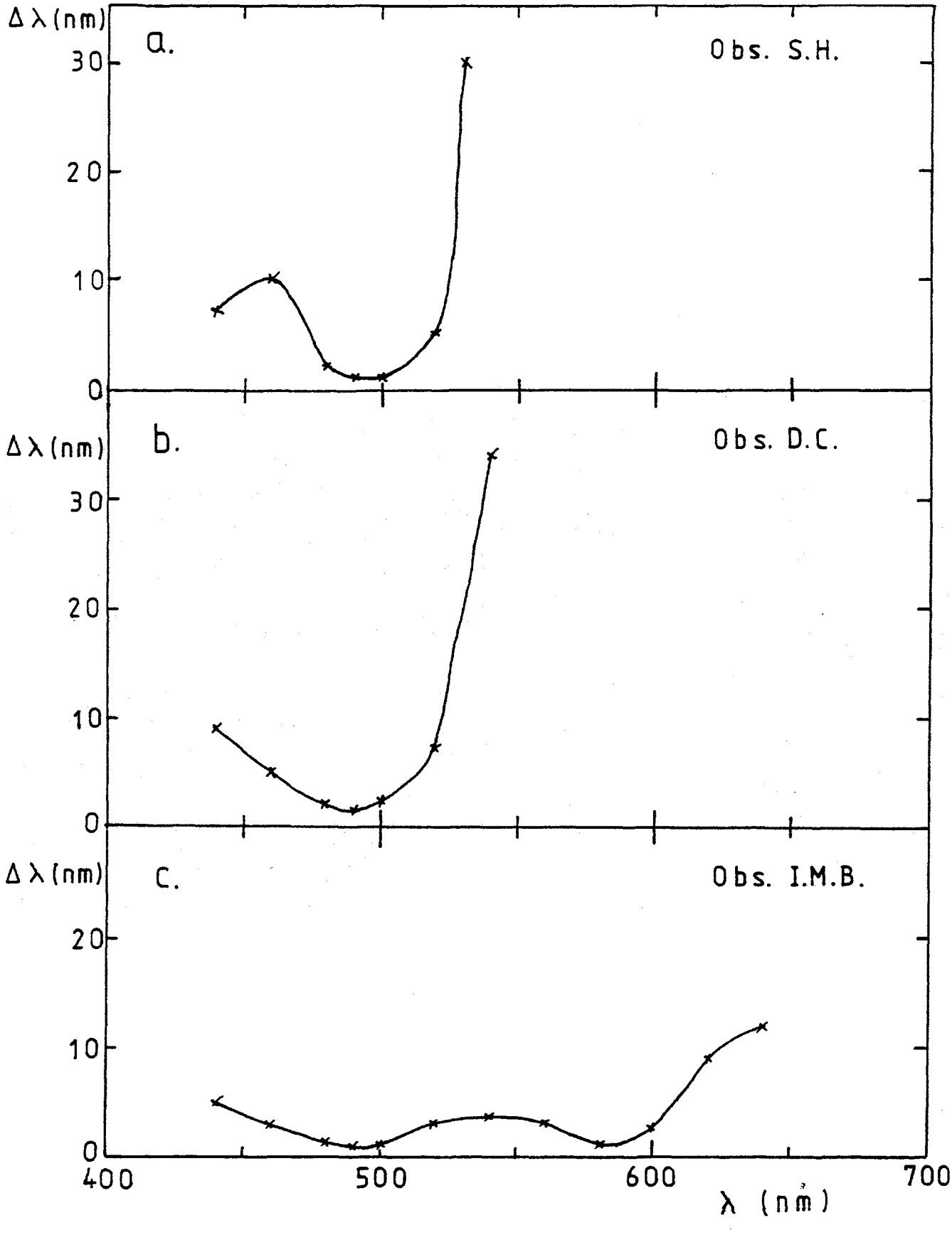

Δλ(nm)
a.
Obs. S.H.
30
20
10
0
Δλ(nm)
b.
Obs. D.C.
30
20
10
0
Δλ(nm)
c.
Obs. I.M.B.
20
10
0
400
500
600
700
λ (nm)

FIG. 4.2

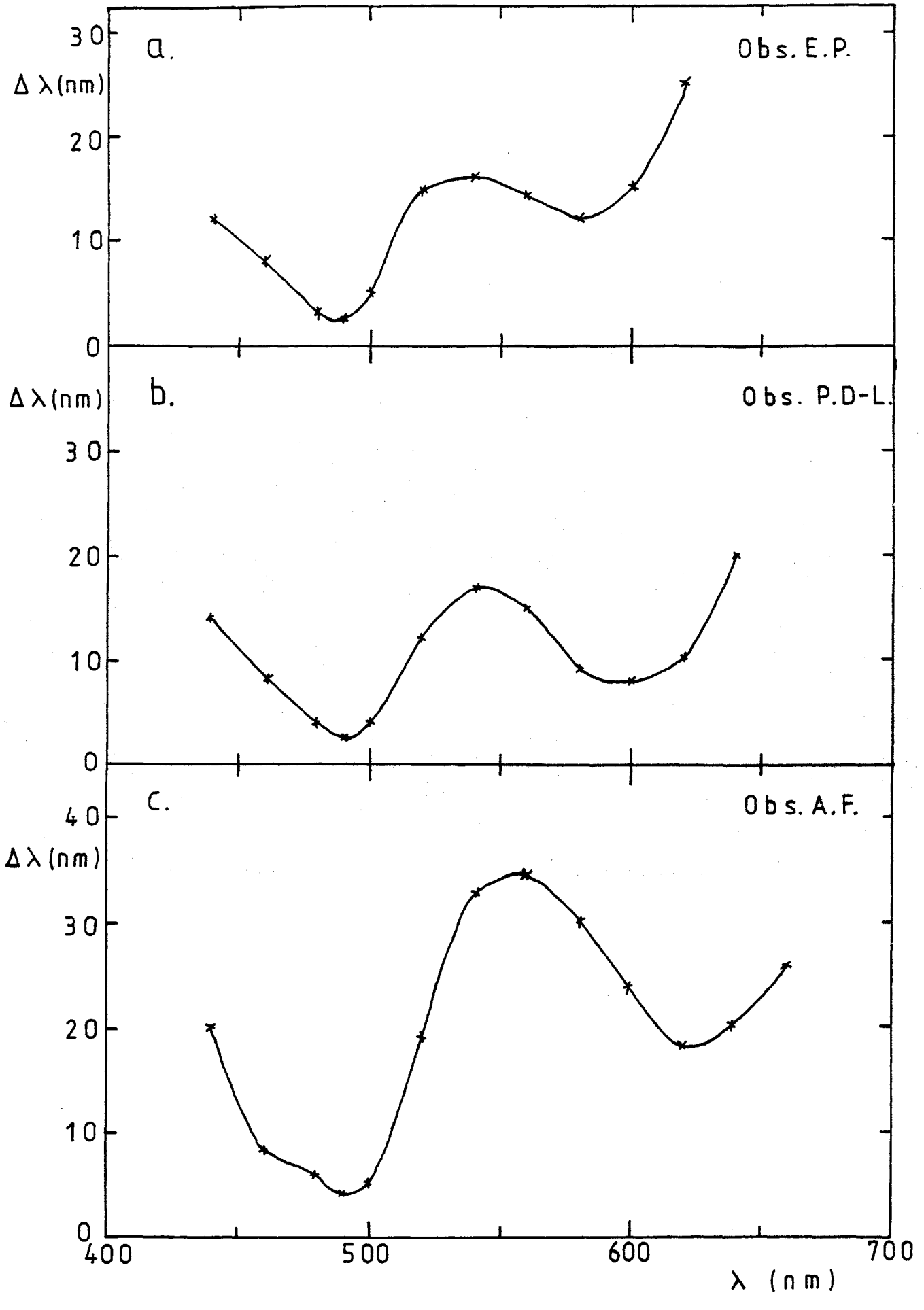

a.
Obs. E.P.
Δλ(nm)
30
20
10
0
b.
Obs. P.D-L.
Δλ(nm)
30
20
10
0
c.
Obs. A.F.
Δλ(nm)
40
30
20
10
0
400
500
600
700
λ (nm)

FIG. 4.2

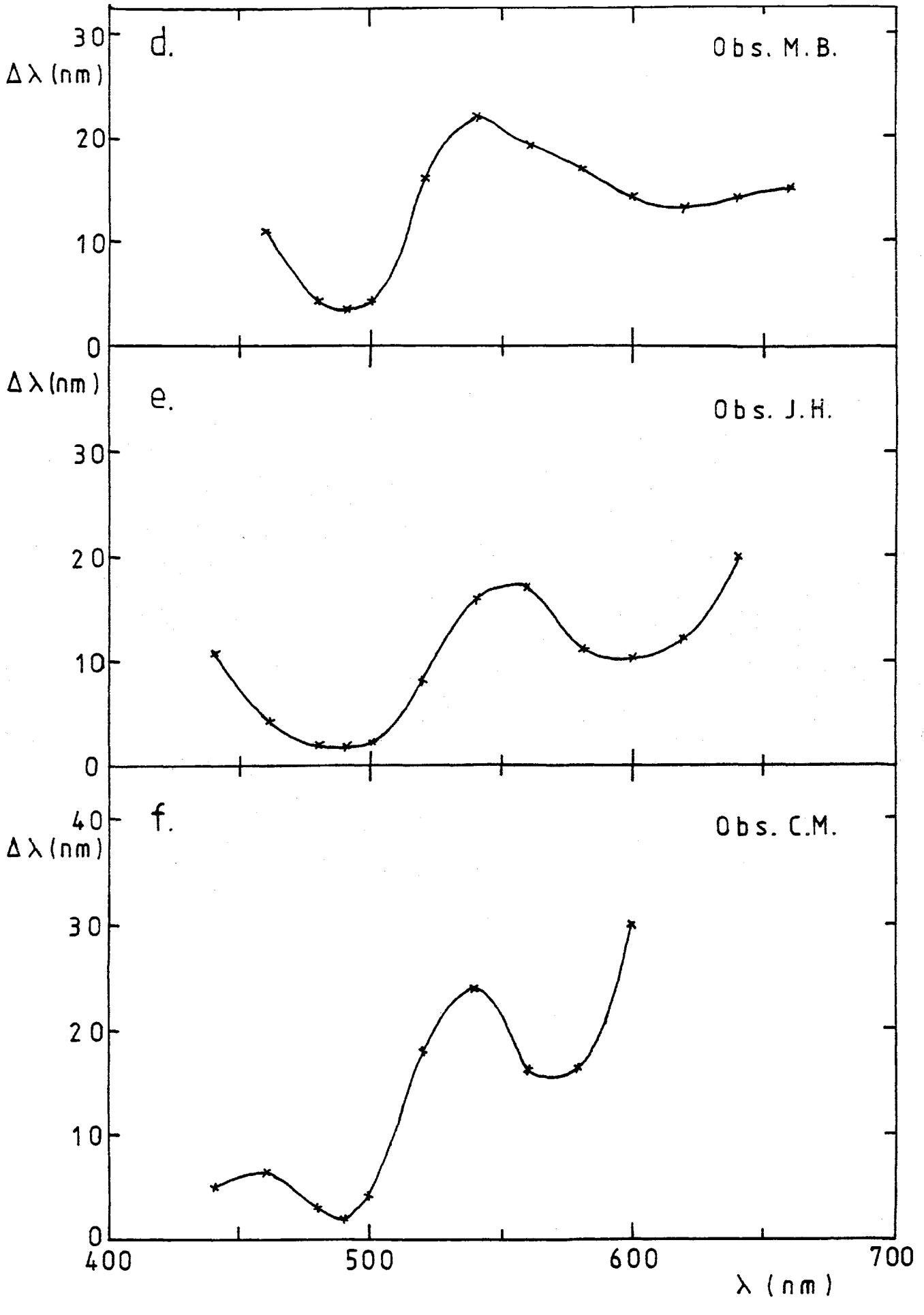

d.
Obs. M.B.
Δλ (nm)
30
20
10
0
e.
Obs. J.H.
Δλ (nm)
30
20
10
0
f.
Obs. C.M.
Δλ (nm)
40
30
20
10
0
400
500
600
700
λ (nm)

FIG. 4.2

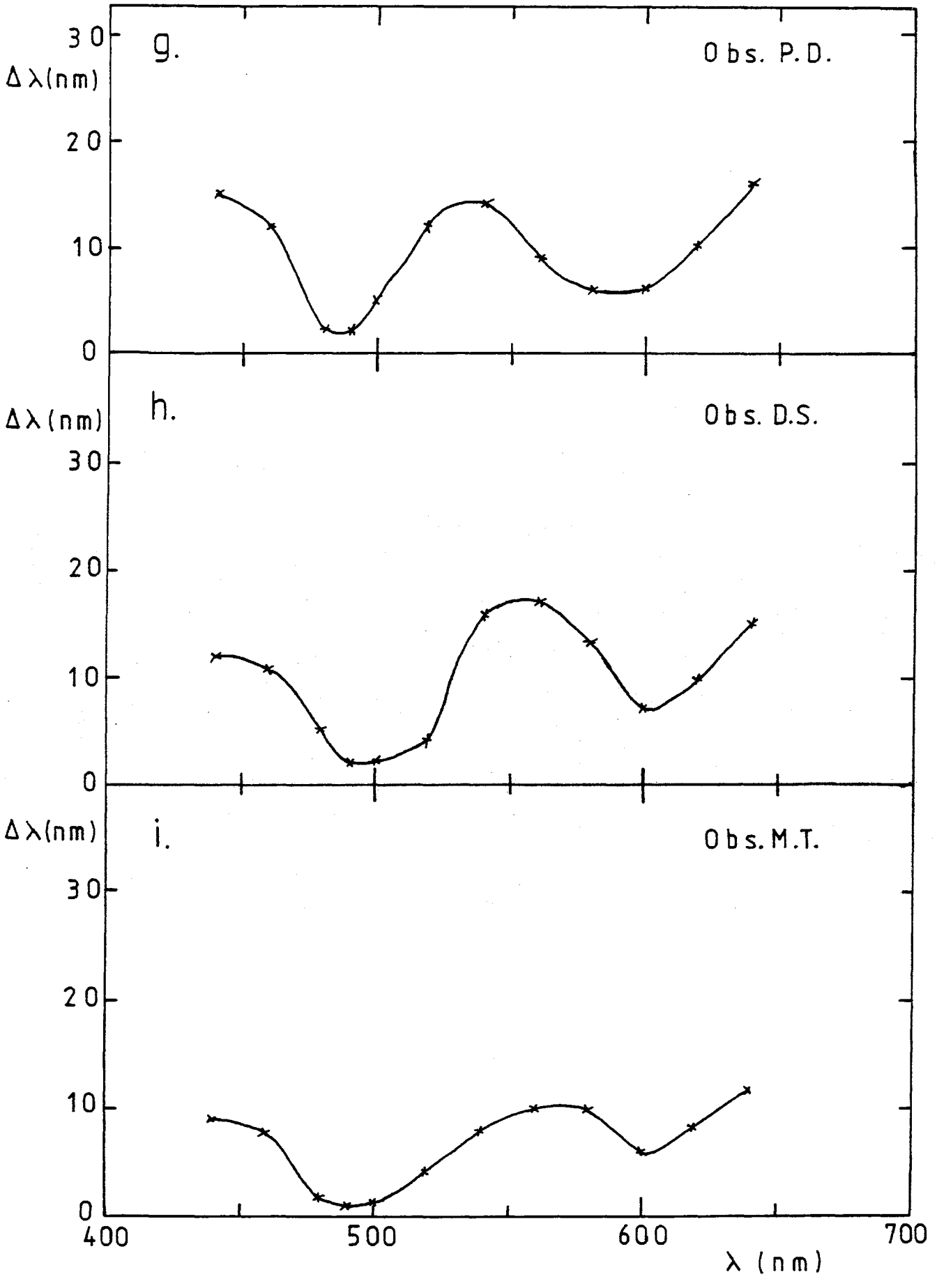
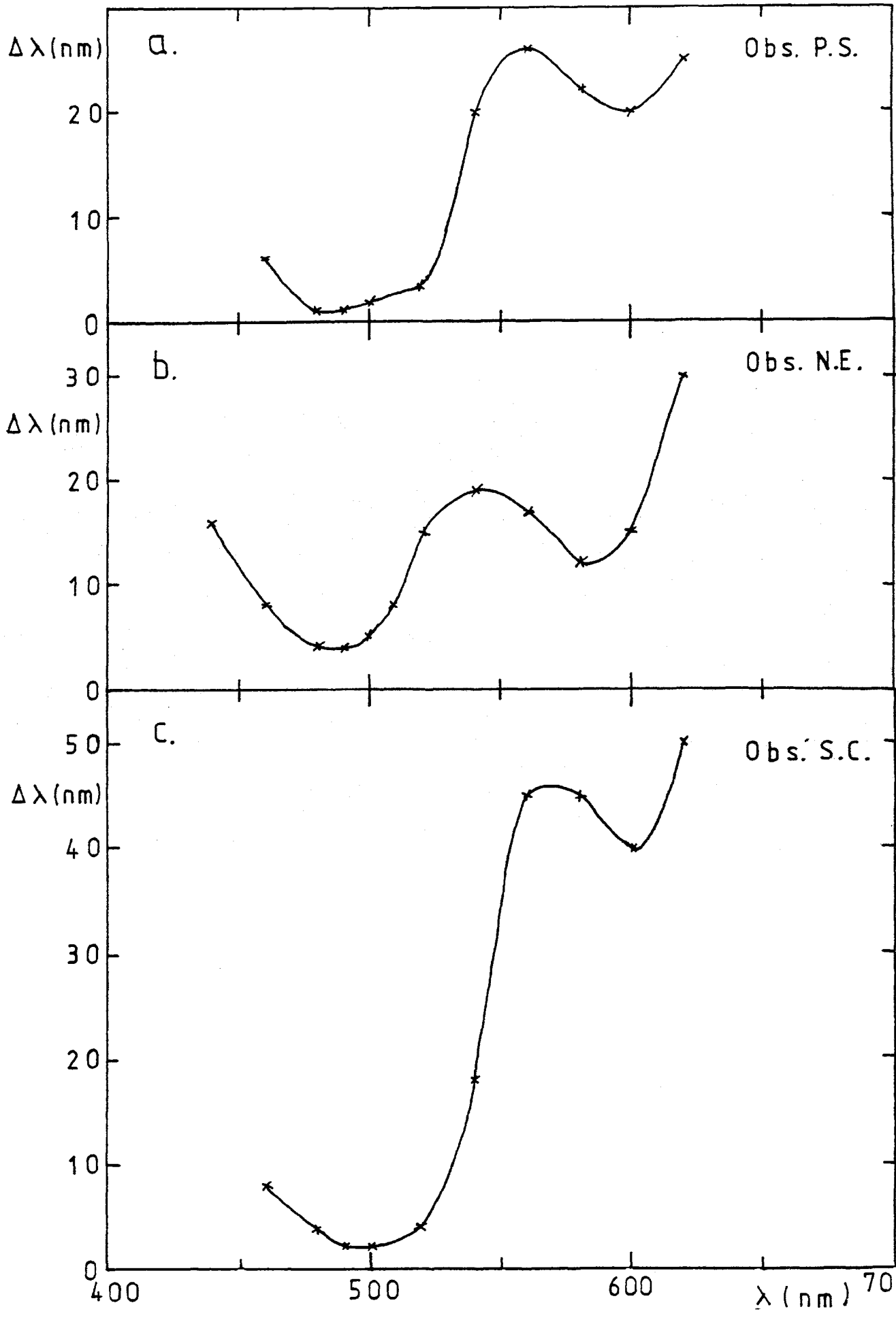

g.
Obs. P.D.
Δλ(nm)
30
20
10
0
h.
Obs. D.S.
Δλ(nm)
30
20
10
0
i.
Obs. M.T.
Δλ(nm)
30
20
10
0
400
500
600
700
λ (nm)

FIG. 4.3


a.
Obs. P.S.
Δλ(nm)
20
10
0
b.
Obs. N.E.
Δλ(nm)
30
20
10
0
c.
Obs. S.C.
Δλ(nm)
50
40
30
20
10
0
400
500
600
λ(nm)
700

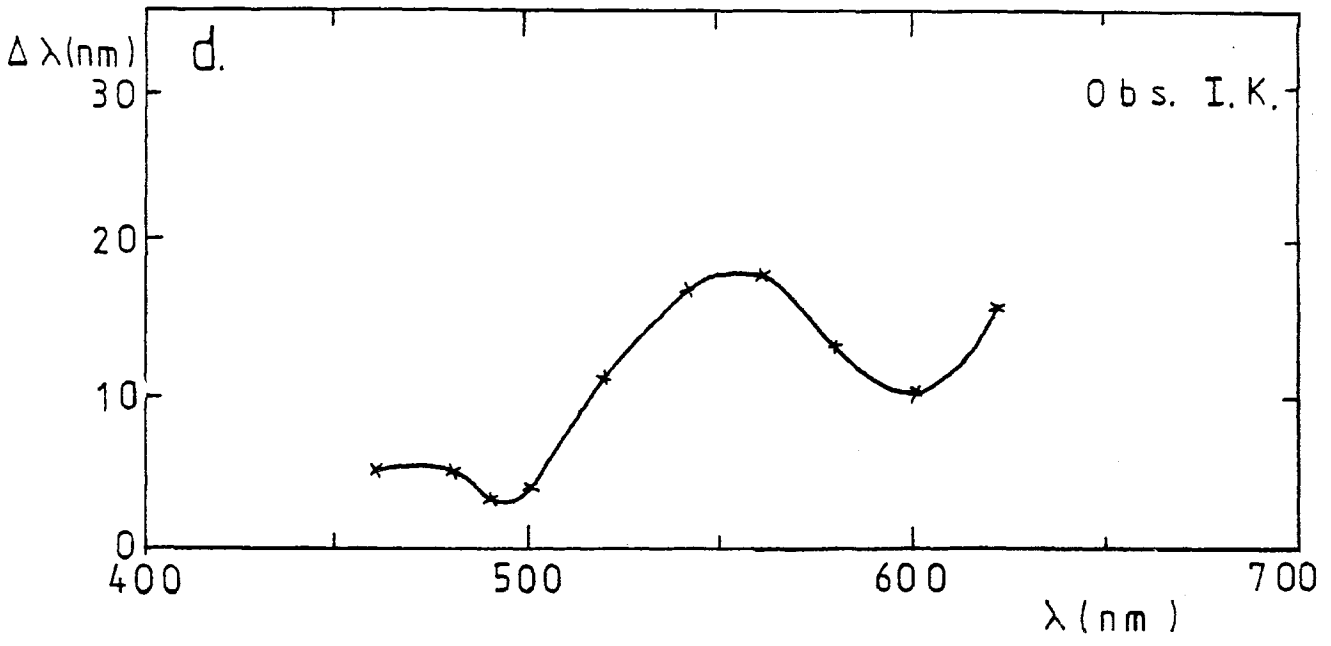


Fig 4.3 Wavelength discrimination curves for 4 protanomalous subjects.

It can be seen from columns 3 and 5 of table 4.1 that the degree of deficiency, as measured by the wavelength discrimination data, does not correlate directly with the Rayleigh match data, i.e. the most severe anomalous subjects do not necessarily have the greatest deviation of log R/G from the normal. This is in agreement with the findings of Nelson (1938).

4.2.3 Spectral Sensitivity

Photopic spectral sensitivity curves were measured on the Wright colorimeter by flicker photometry, as described in chapter 2. Curves were obtained for a few subjects only, namely 4 deuteranomalous, 1 deuteranopic, 1 protanopic and 1 normal subject. The results, illustrated in figs 4.4 and 4.5 show that the normalised sensitivity curves for the deuteranopic and deuteranomalous subjects are shifted towards slightly longer wavelengths than the normal, whilst the sensitivity for the protanope is shifted towards shorter wavelengths and falls off rapidly at long wavelengths.

Fig. 4.4 Photopic spectral sensitivity curves. Normalised log sensitivity, log S , is plotted against wavelength, λ . Data are plotted (continuous lines) for 4 deuteranomalous subjects: a, M.T.; b, MB ; c, DS ; d, JH. Data for a normal subject IMB (dashed line) are plotted for comparison.

4.3 Post-Receptoral Spectral Response Functions in Colour Defective Subjects

A method for the determination of narrow band-width post-receptoral spectral responses (Waterfield, 1980) has been described in chapter 3. Two of the response functions can be reproduced by linear combinations of the red - and green - sensitive cone mechanisms: R-G and G-0.33R. In this section the post-receptoral colour vision responses of red-green anomalous trichromats are investigated and the results analysed in terms of the different theories of anomalous trichromacy. The responses of several dichromats are also investigated.

The experiments were all performed on the 4-channel Maxwellian viewing system described in chapter 2. The stimulus configuration used in the experiments is illustrated in fig 4.6

The test stimulus presented to the right eye consisted of a square-wave grating superimposed on a spatially uniform background of fixed illumination level, I_b. The adaptation stimulus presented to the right eye was a square-wave grating of high contrast (> 98%) and average illumination level, I_b, which was 4 log units above threshold for detection of its structure (corresponding to approximately 3 log trolands).

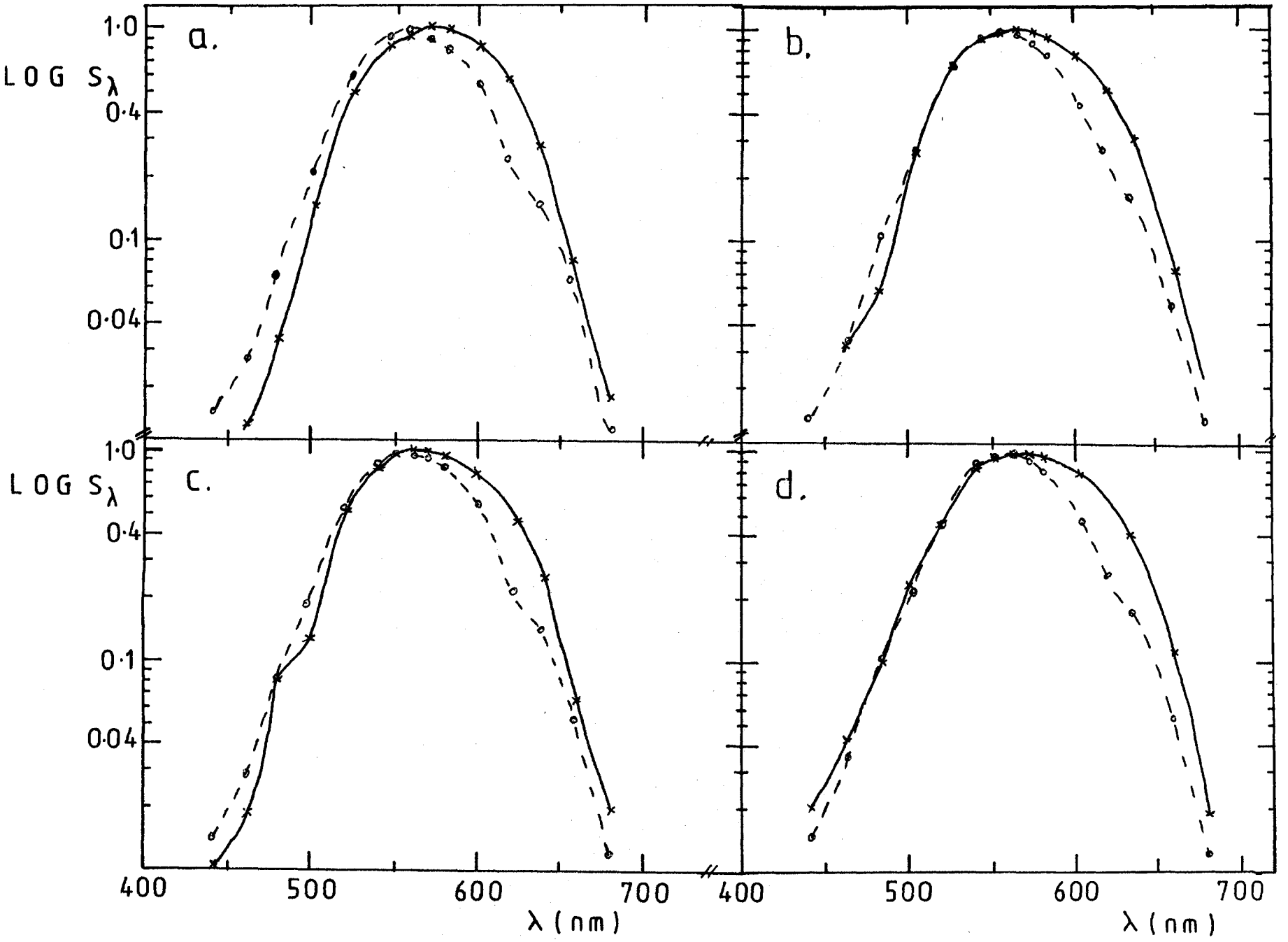


FIG. 4.4

FIG. 4.5

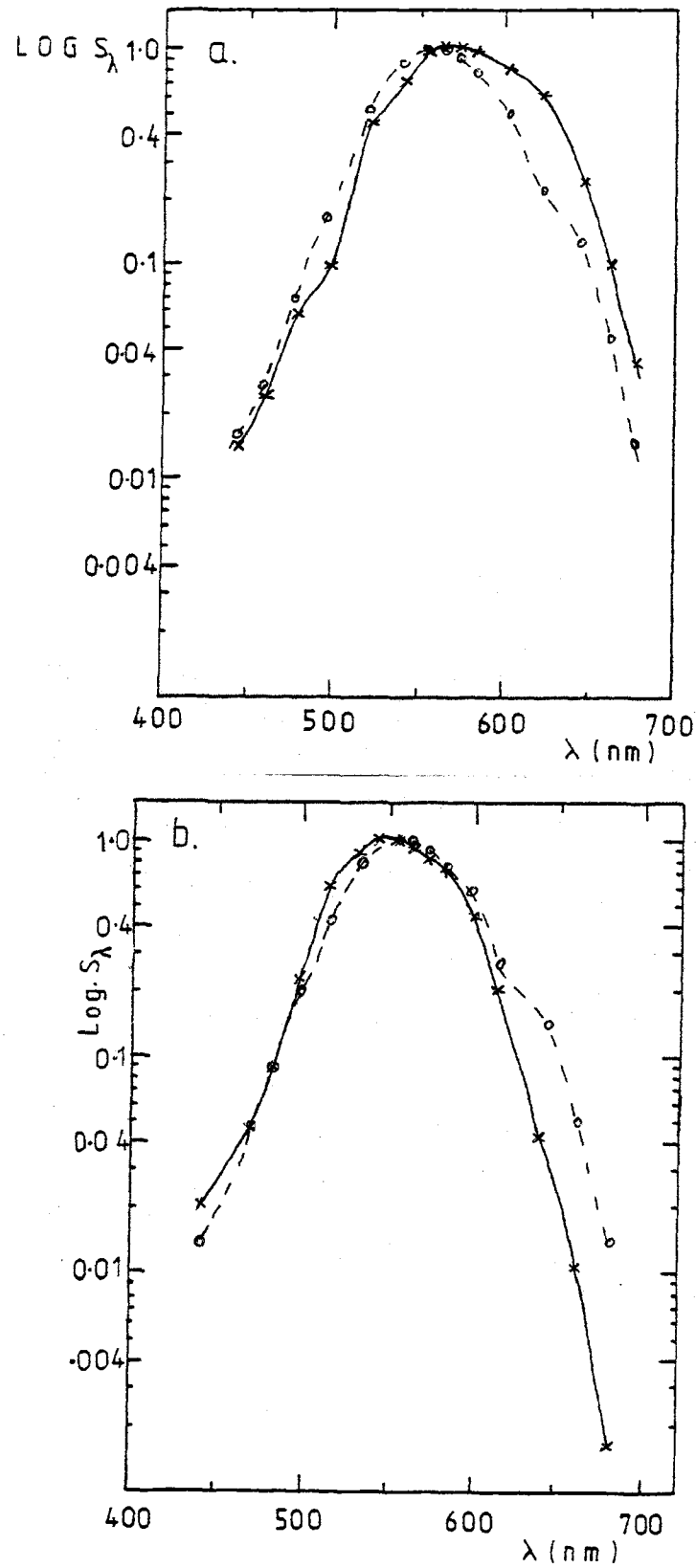


Fig.4.5 As in fig. 4.4 but for (a) the deuteranope SH, and (b) the protanope, DC. Data for normal subject IMB (dashed line) are plotted for comparison.

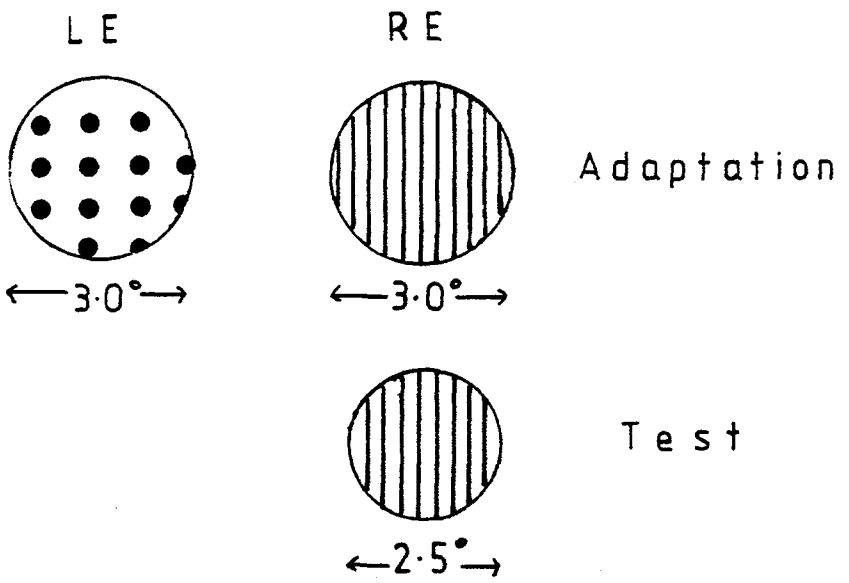


Fig. 4.6 Stimulus configuration used in the binocular adaptation experiments. The test and adaptation gratings presented to the right eye are of spatial frequency 5.68 cycles/deg and wavelength 635 nm. The adaptation matrix, which is of positive contrast, is spatial frequency 2.93 cycles/deg and variable wavelength.

Both the gratings presented to the right eye were of spatial frequency 5.68 cycles/deg and wavelength 635 nm. The adaptation stimulus presented to the left eye was a positive contrast matrix of circular spots, of high contrast ($< 98\%$), and spatial frequency 2.93 cycles/deg. Measurements were made for a number of different matrix wavelengths, λ, and for each value of λ the matrix was set 4.5 log units above threshold for detection of the spots. The subject viewed the adaptation stimuli binocularly, such that they appeared spatially coincident, and was initially adapted for two minutes. The test and adaptation stimuli were then viewed cyclically for 2 sec and 15 sec respectively, and the subject reduced the illumination level of the structured component of the test, I_t, until he could just no longer detect the grating structure (see chapter 2). Values of log I_t were determined both

with and without the matrix pattern presented to the left eye. The value of log I_t obtained in the absence of the matrix was taken as the reference against which the effect of the matrix is measured, and was thus redetermined frequently throughout each series of measurements.

The experimentally determined values of log I_t are plotted as a function of matrix wavelength, λ, for 8 deuteranomalous subjects (fig.4.7 a-h), 4 protanomalous subjects (fig. 4.8 a-d), 3 deuteranopes (fig.4.9 a-c) and 2 protanopes (fig.4.10 a-b). Results for normal subject, IMB, are plotted for comparison.

Fig.4.7 Log threshold illumination, log I_t, for detection of the test grating plotted against the wavelength of the spot matrix, λ. Log I_t = 0 is the threshold level after adaptation to a uniform field, of mean illumination I_b. The dashed line is the value of log I_t obtained in the absence of the matrix. Each point is the mean of 5 measurements and the average standard error is marked. ▼ Data for 8 deuteranomalous subjects.
● Data for normal subject, IMB, plotted for comparison.

Fig.4.8 As for fig. 4.7. ▼ Data for 4 protanomalous subjects.

Fig.4.9 As for fig. 4.7. ▼ Data for 3 deuteranopes.

Fig. 4.10 As for fig. 4.7. ▼ Data for 2 protanopes.

FIG. 4.7

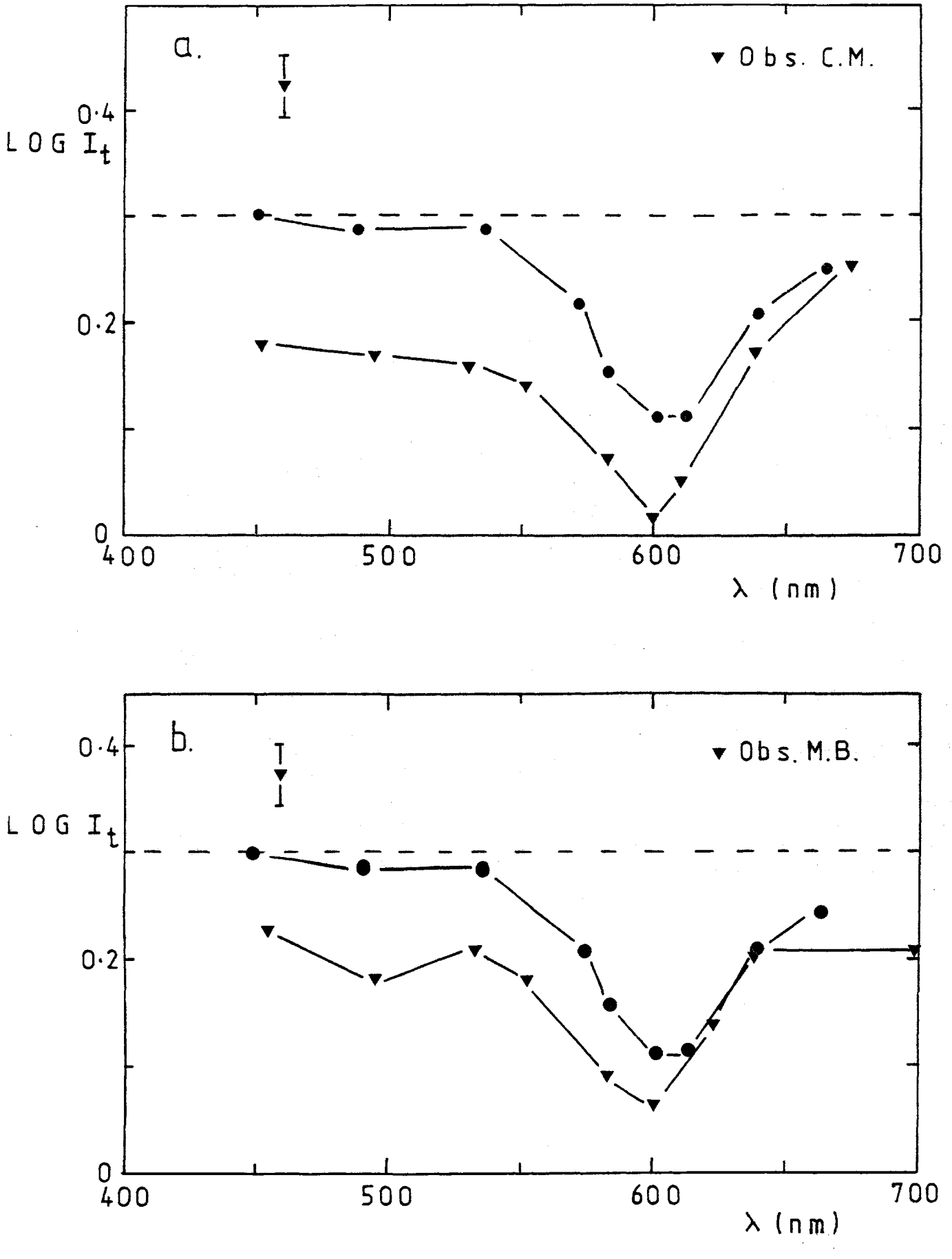
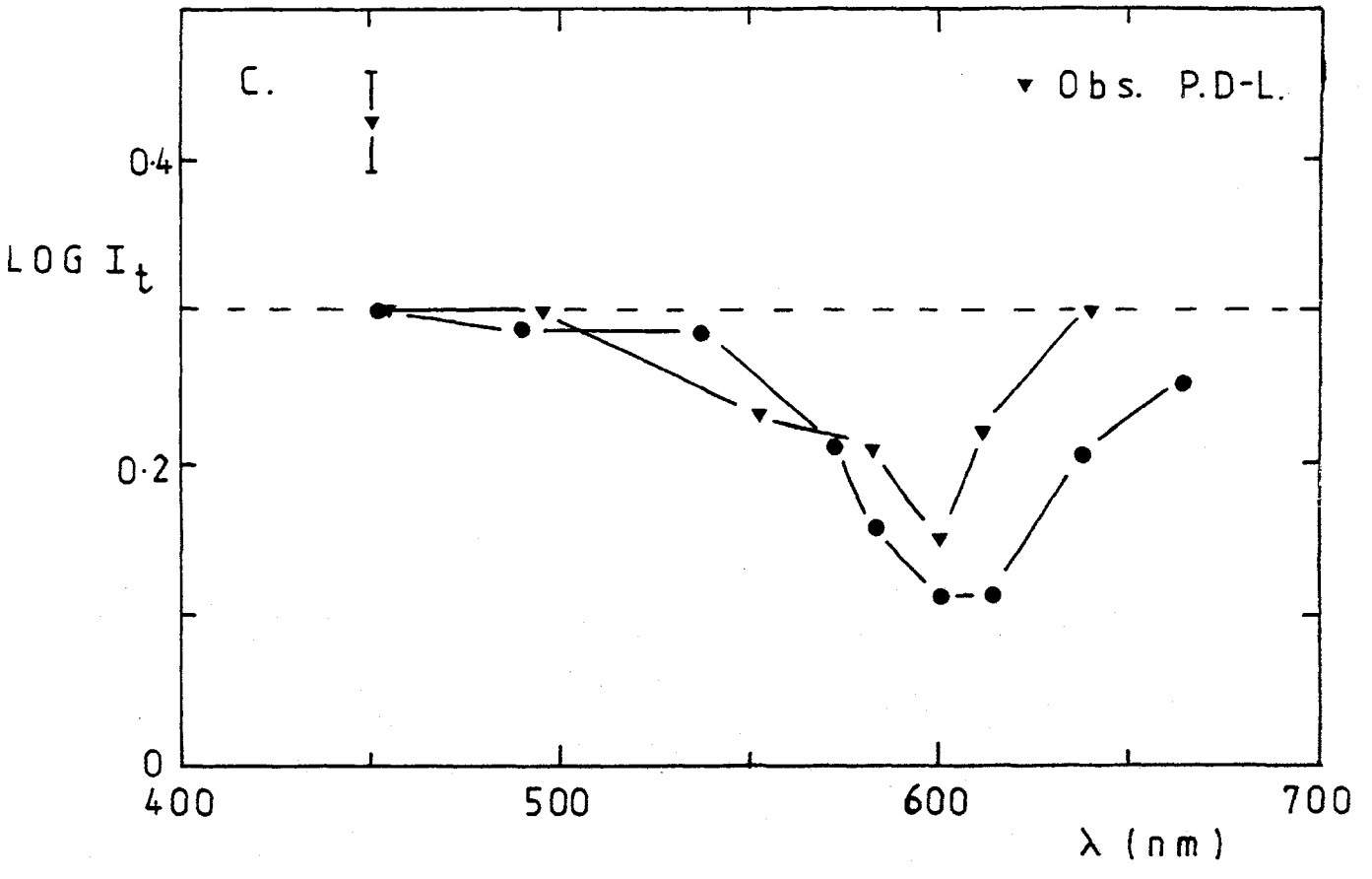

a.
▼ Obs. C.M.
0·4
LOG I_t
0·2
0
400
500
600
700
λ (nm)
b.
▼ Obs. M.B.
0·4
LOG I_t
0·2
0
400
500
600
700
λ (nm)

FIG. 4.7


C.
Obs. P.D-L.
0·4
LOG I_t
0·2
0
400
500
600
700
λ (nm)

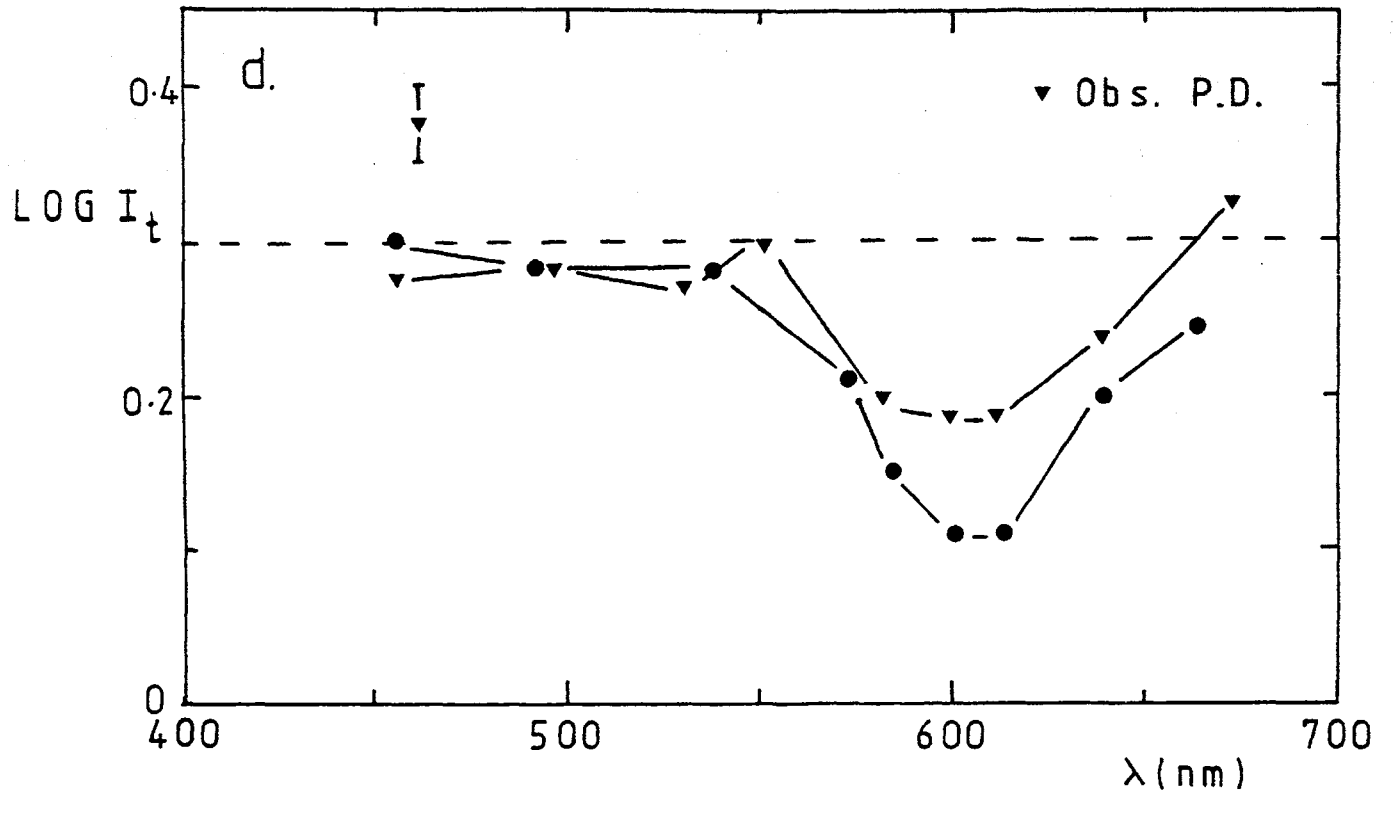

d.
Obs. P.D.
0·4
LOG I_t
0·2
0
400
500
600
700
λ (nm)

FIG. 4.7

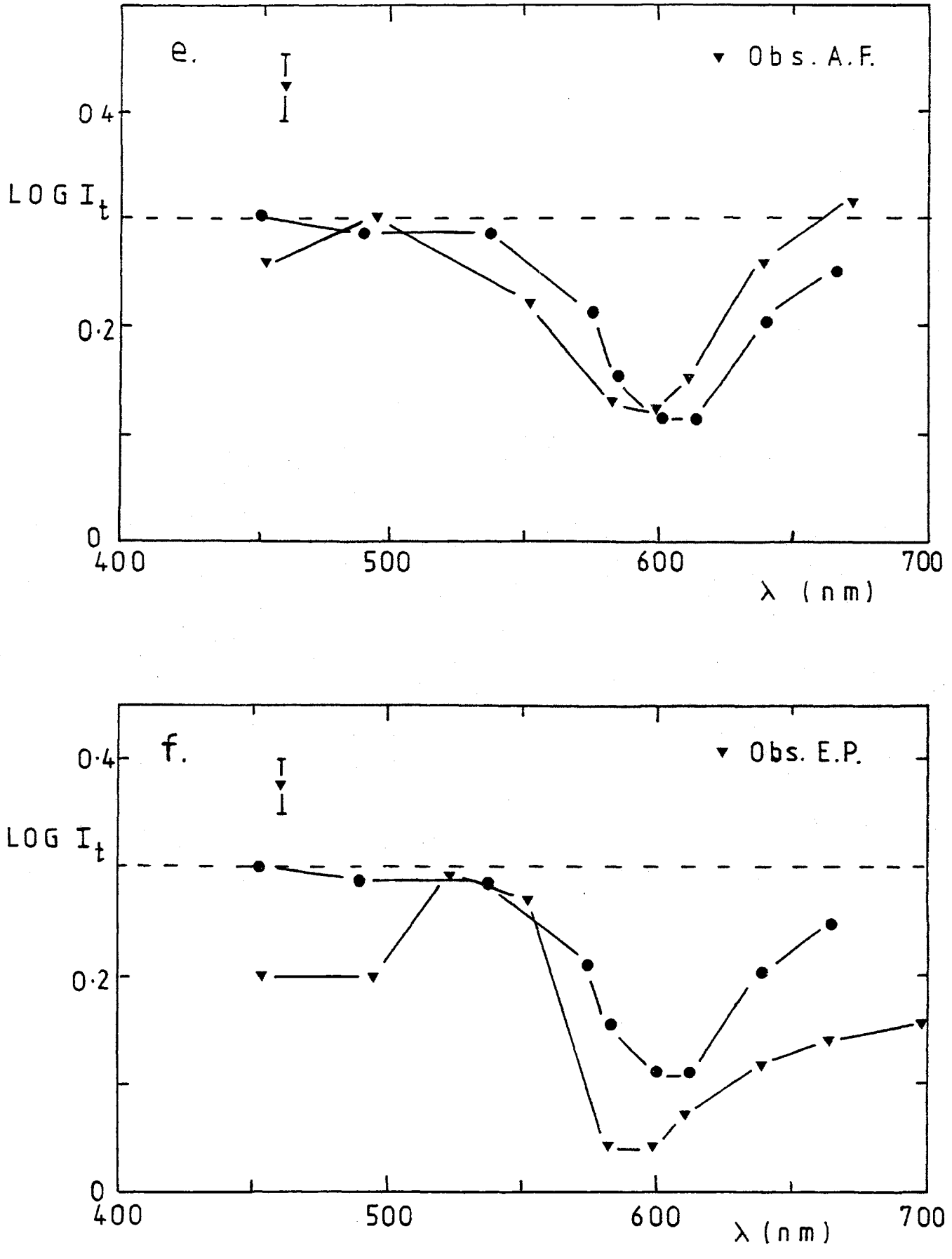
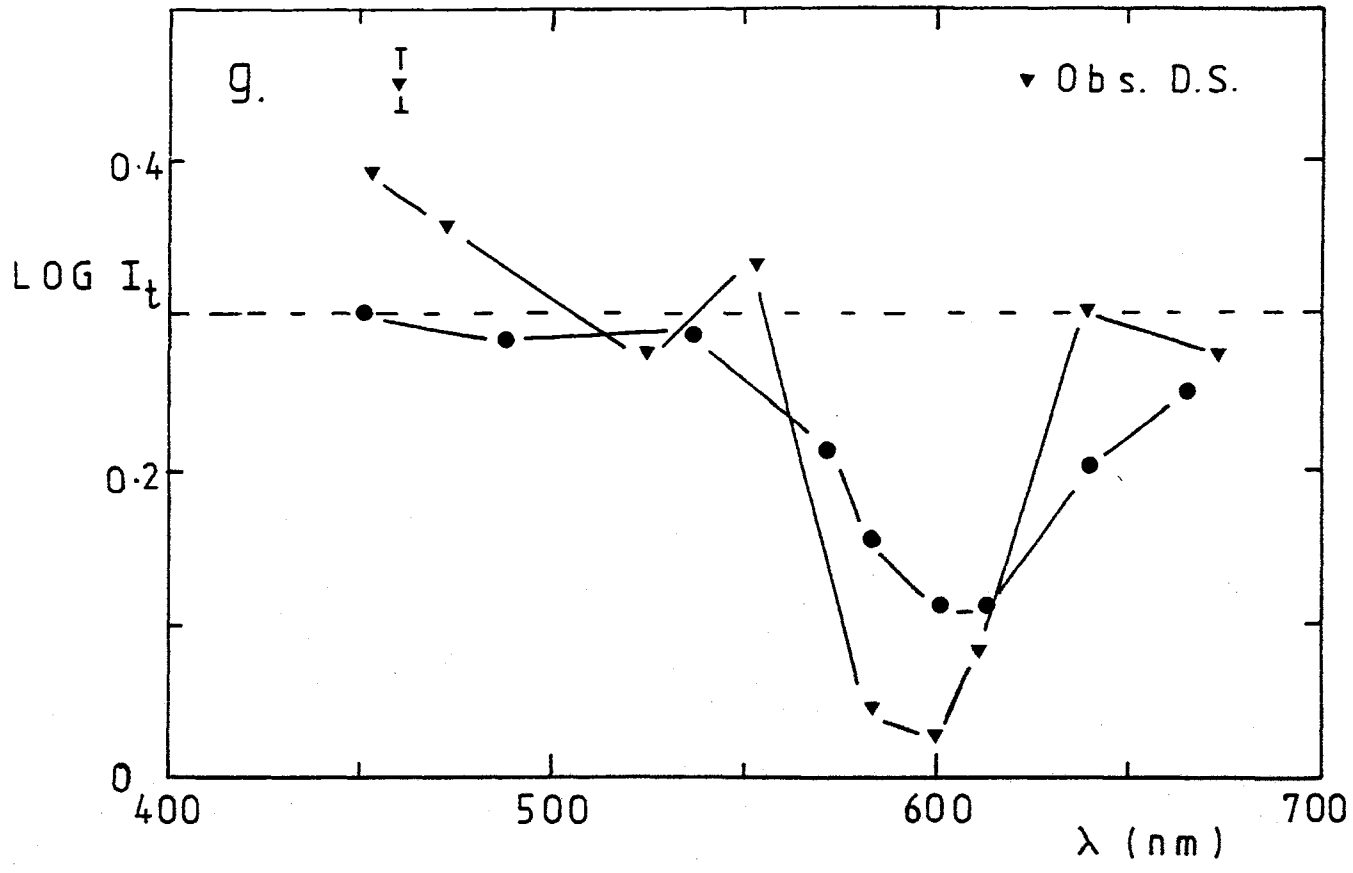

e.
Obs. A.F.
0·4
LOG I_t
0·2
0
400
500
600
700
λ (nm)
f.
Obs. E.P.
0·4
LOG I_t
0·2
0
400
500
600
700
λ (nm)

FIG. 4.7


g.
Obs. D.S.
0·4
LOG I_t
0·2
0
400
500
600
700
λ (nm)

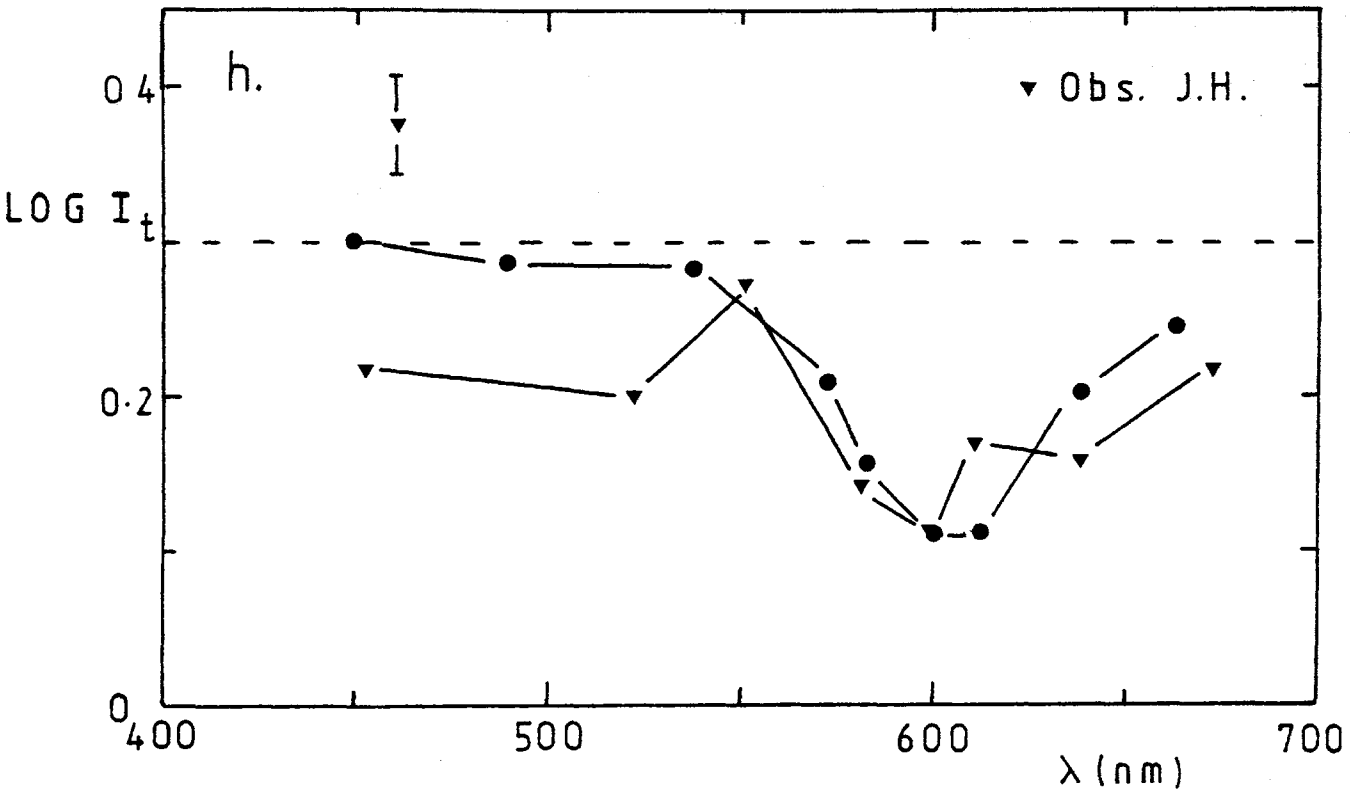

h.
Obs. J.H.
0·4
LOG I_t
0·2
0
400
500
600
700
λ (nm)

FIG. 4.8

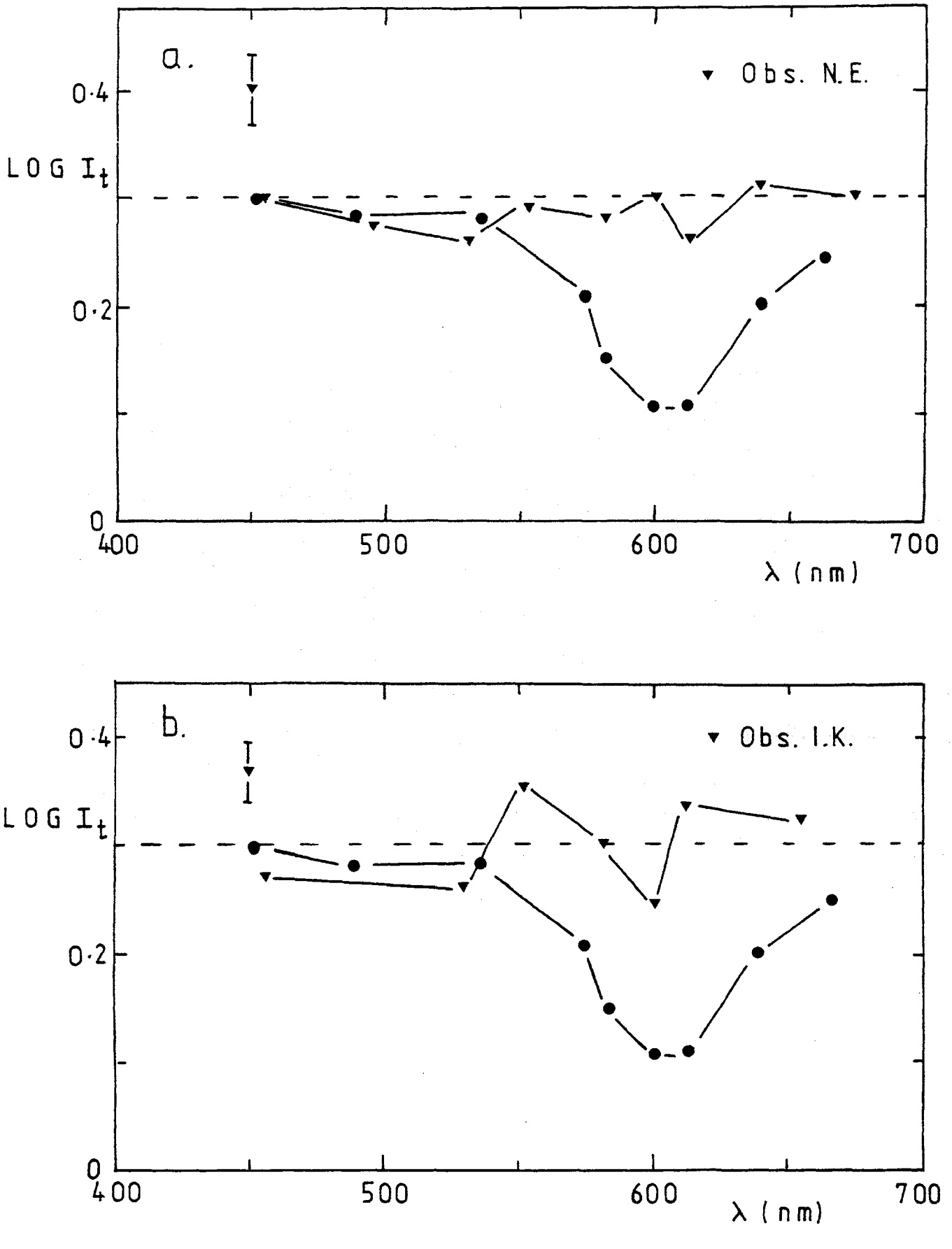
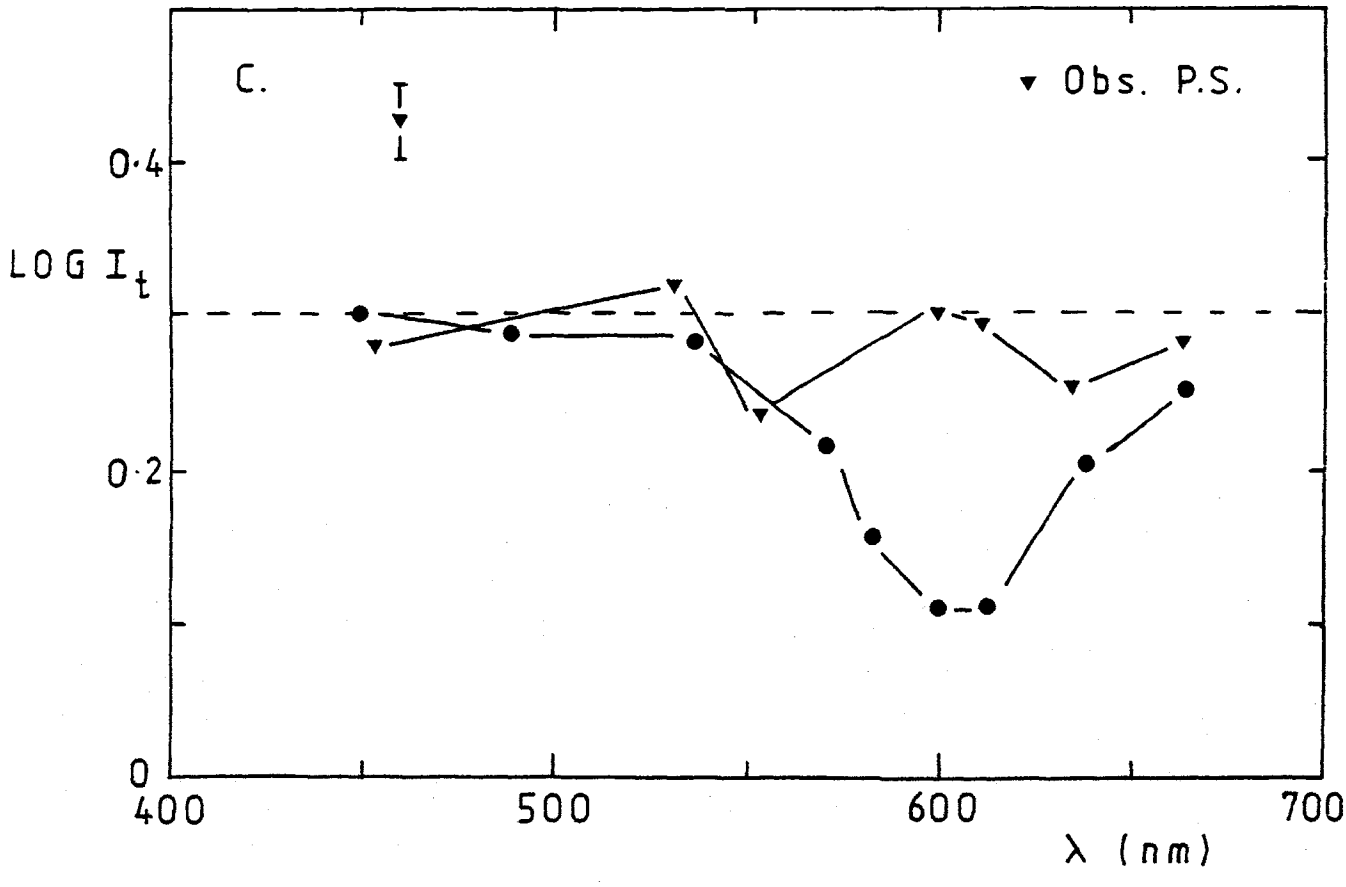

a.
Obs. N.E.
0·4
LOG I_t
0·2
0
400
500
600
700
λ (nm)
b.
Obs. I.K.
0·4
LOG I_t
0·2
0
400
500
600
700
λ (nm)

FIG. 4.8


C.
Obs. P.S.
0·4
LOG I_t
0·2
0
400
500
600
700
λ (nm)

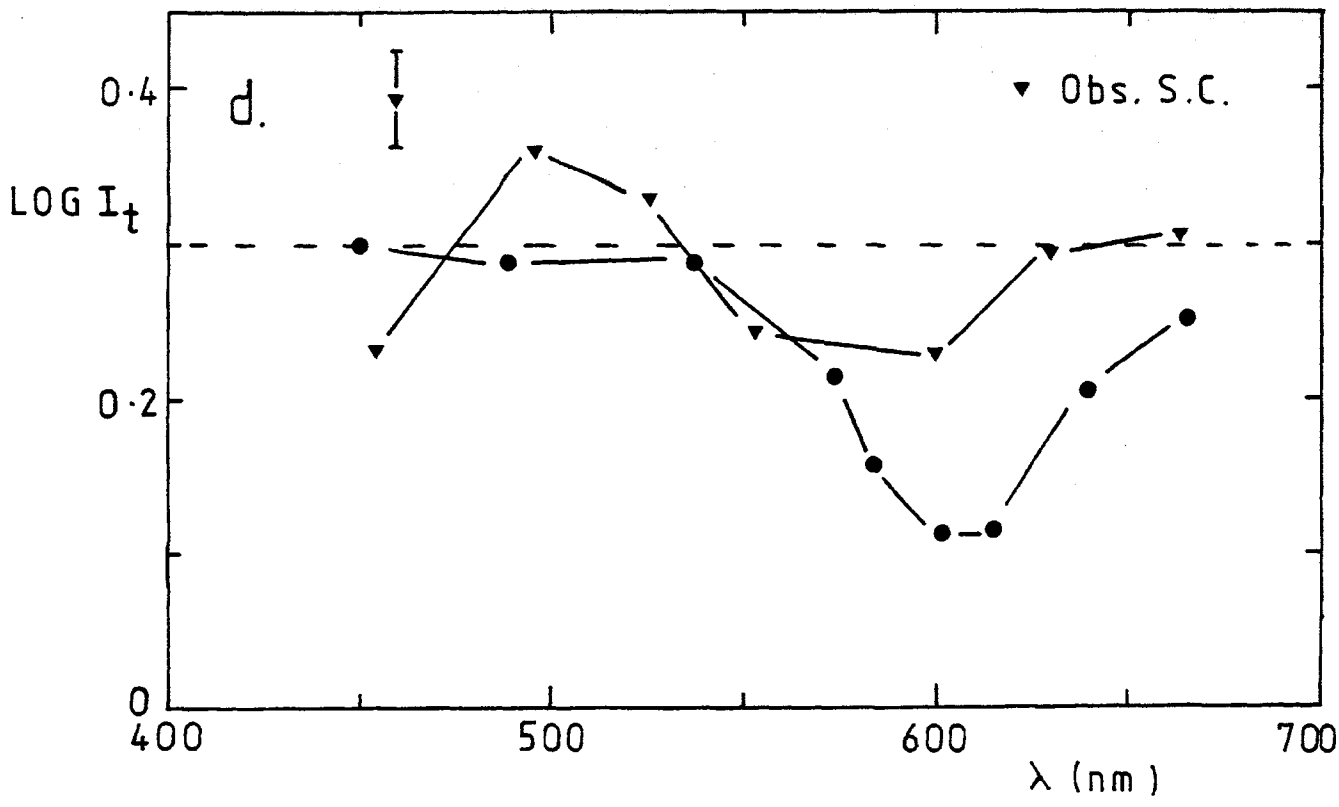

d.
Obs. S.C.
0·4
LOG I_t
0·2
0
400
500
600
700
λ (nm)

FIG. 4.9

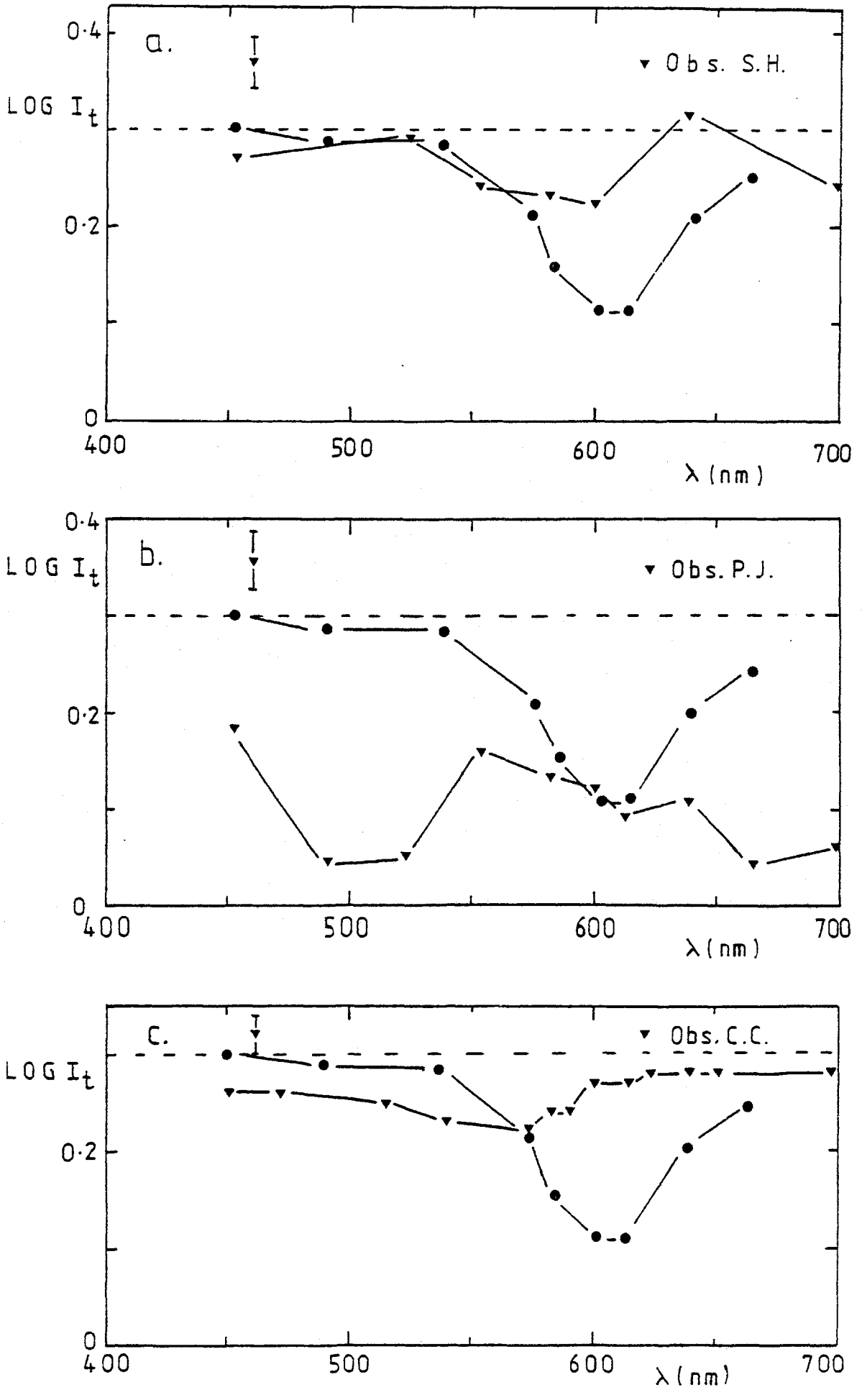
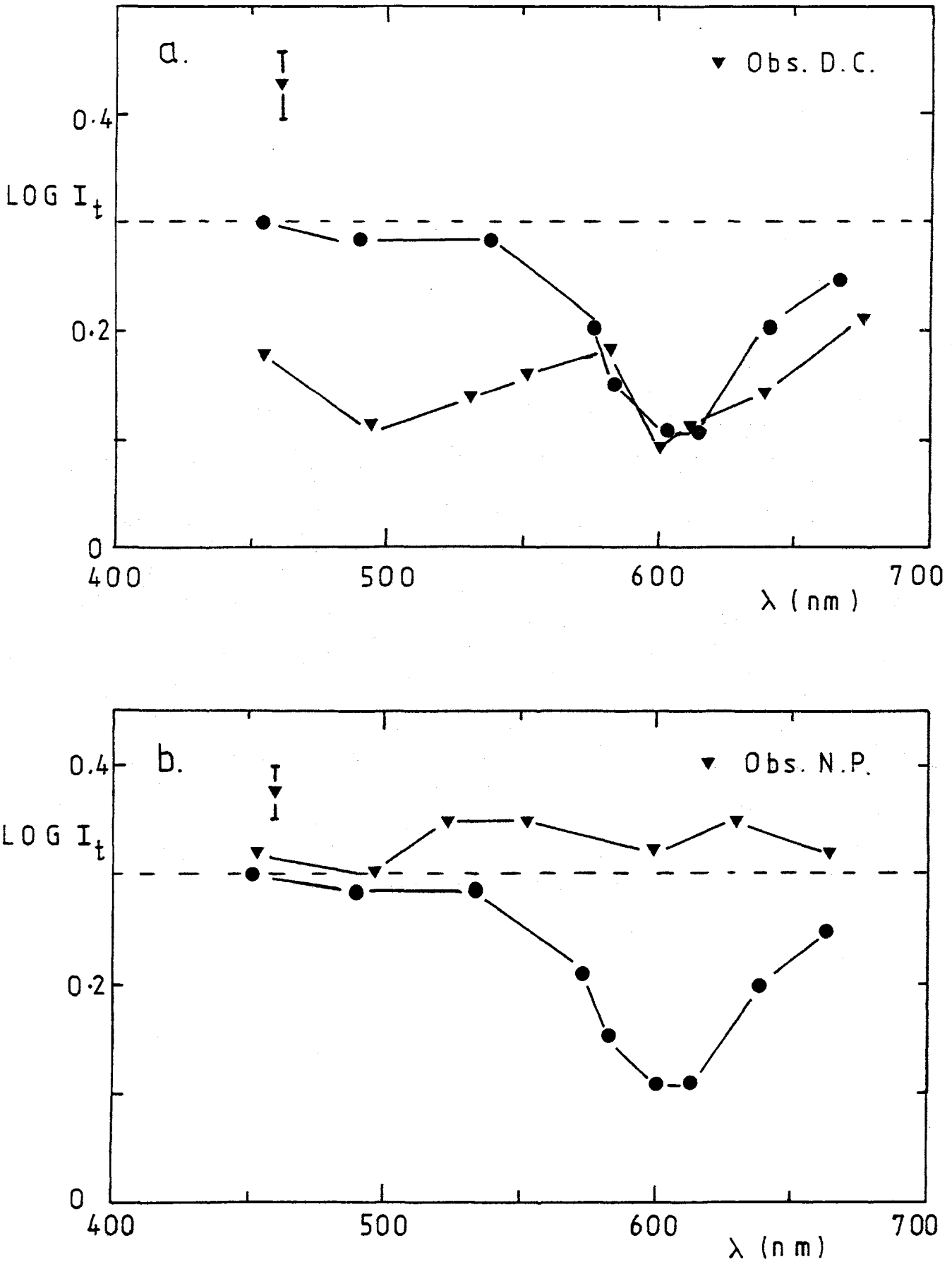

a.
Obs. S.H.
LOG I_t
0·4
0·2
0
400
500
600
700
λ (nm)
b.
Obs. P.J.
LOG I_t
0·4
0·2
0
400
500
600
700
λ (nm)
C.
Obs. C.C.
LOG I_t
0·2
0
400
500
600
700
λ (nm)

FIG. 4.10


a.
Obs. D.C.
0·4
LOG I_t
0·2
0
400
500
600
700
λ (nm)
b.
Obs. N.P.
0·4
LOG I_t
0·2
0
400
500
600
700
λ (nm)

The values of log I_t for the deuteranomalous subjects (fig.4.7) are similar to those for the normal subjects in their dependence on the matrix wavelength, with a sharp minimum around $\lambda \approx 600$ nm. The amplitude of the changes in log I_t with wavelength was in most cases similar to normal, although there was some inter-observer variation. It appears that the amplitude of the effect does not correlate with the degree of colour deficiency. For instance, subjects D.S. and J.H. have very similar wavelength discrimination curves but whereas D.S. produced a very strong binocular effect, J.H.'s wavelength-dependent response was only just significant. The response curves for some observers (noticeably CM and MB) are translated down the log I_t axis with respect to the normal. The reason for this is not apparent. In addition, the curves of all the observers (with the exception of P.D. and J.H.) seem to be shifted to slightly shorter wavelengths than normal. Only one observer, DS, obtained the enhancement of the monocular elevation for shorter wavelength matrices observed in normal subjects. (Hendricks, Ruddock and Waterfield, 1982).

In contrast to these results, the protanomalous subjects do not appear to produce any wavelength-dependent effect (fig.4.8). For all four subjects, the value of log I_t is unaffected by the presence of the matrix at any wavelength. The dichromatic subjects also give abnormal responses. The data for protanope NP (fig.4.10b), and deuteranopes CC (fig.4.9c) and SH (fig.4.9a) are essentially independent of wavelength, i.e. the matrix has no effect on the value of log I_t at any wavelength. For deuteranope PJ (fig.4.9b) and protanope DC (fig.4.10a) the value of log I_t at all matrix

wavelengths is depressed below the value obtained in the absence of the matrix, the data for both subjects varying non-systematically with wavelength.

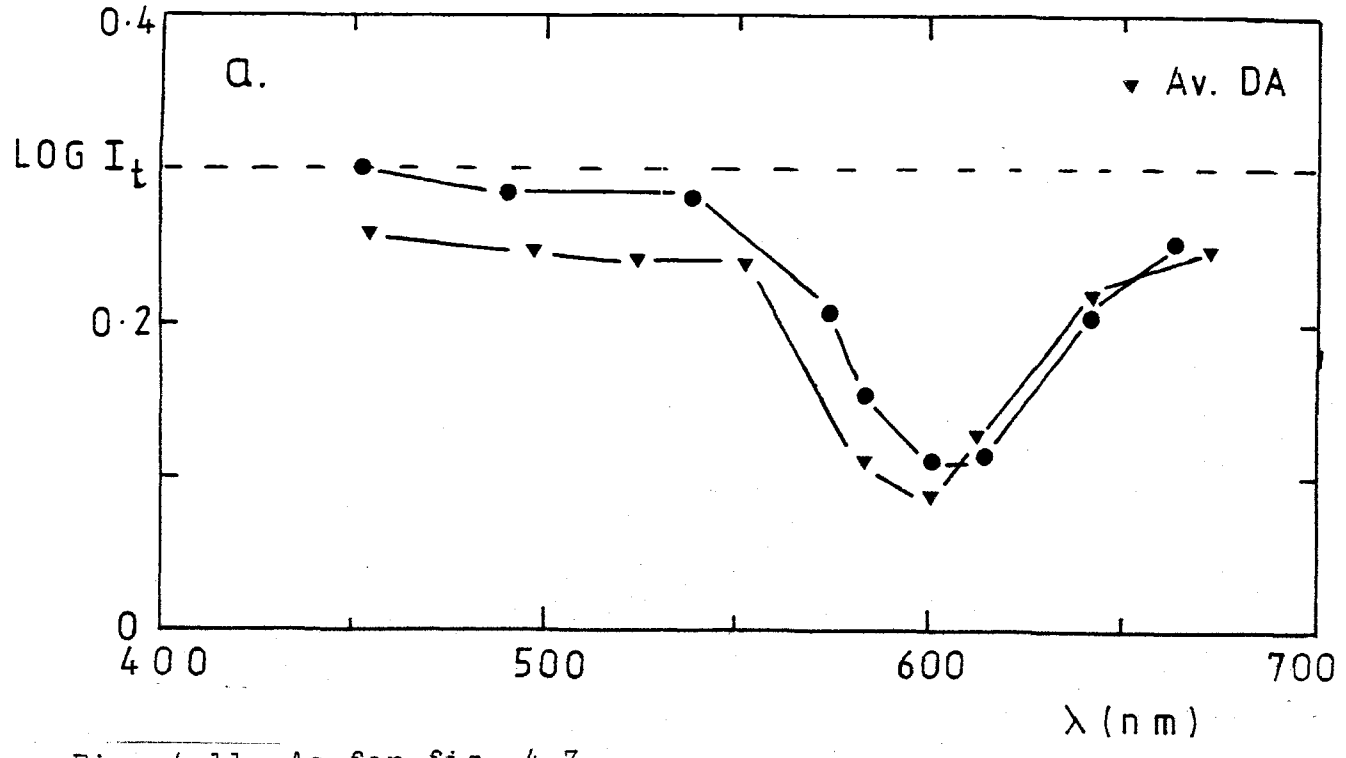
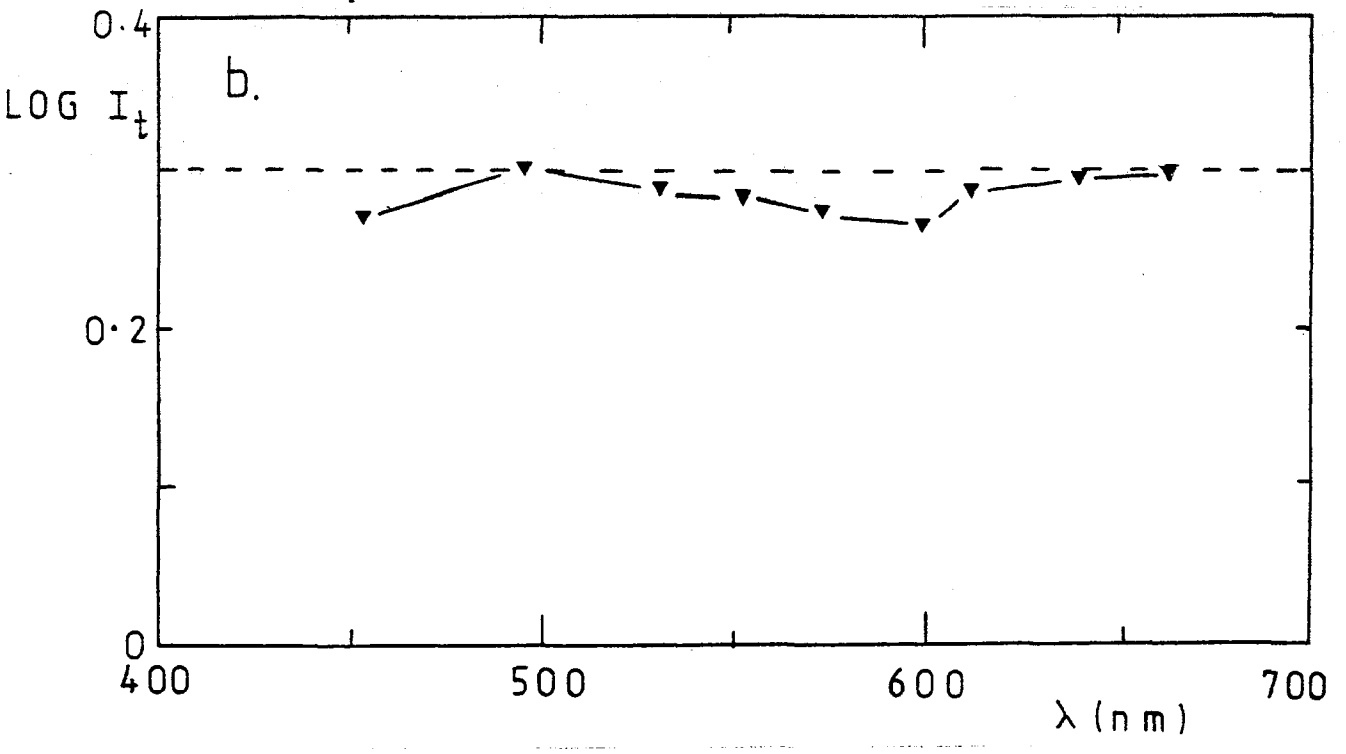
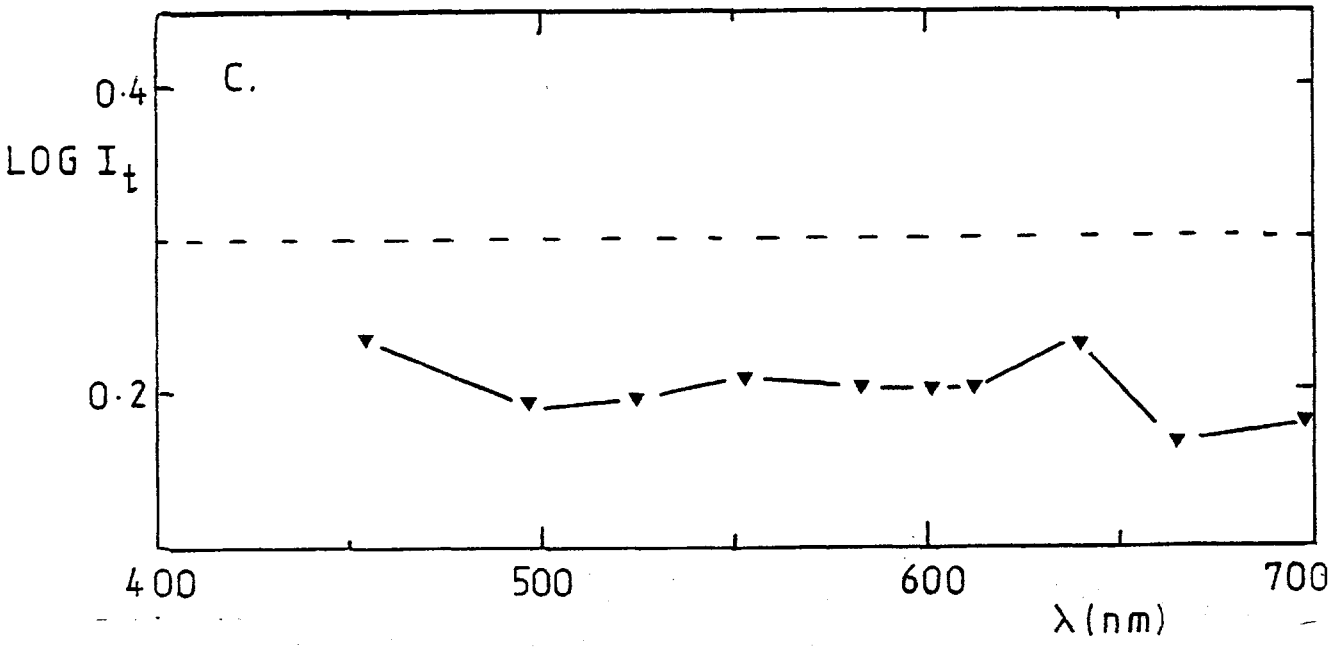


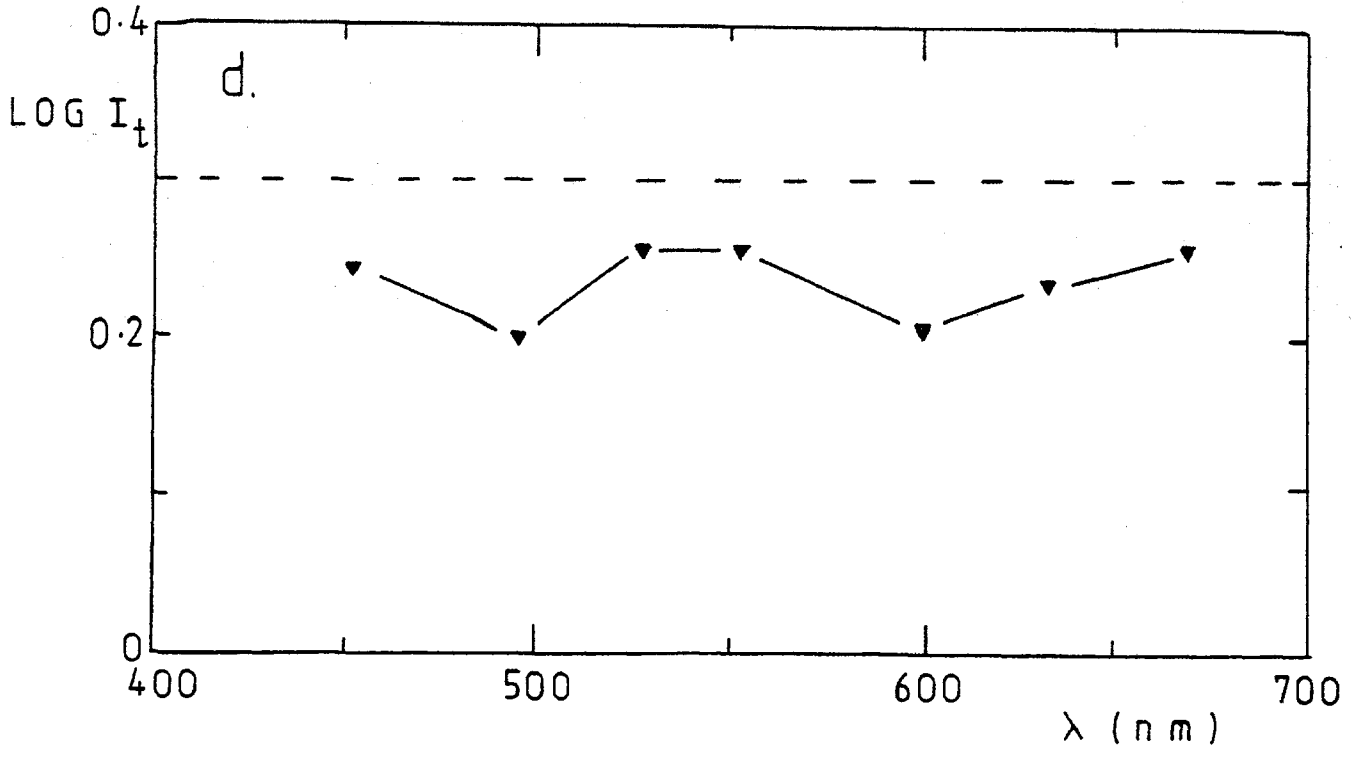
Fig. 4.11 As for fig. 4.7
a, ▼ Average data for 8 deuteranomalous subjects
● data for normal subject, IMB, plotted for comparison.



b, average data for 4 protanomalous subjects



c, average data for 3 deuteranopes



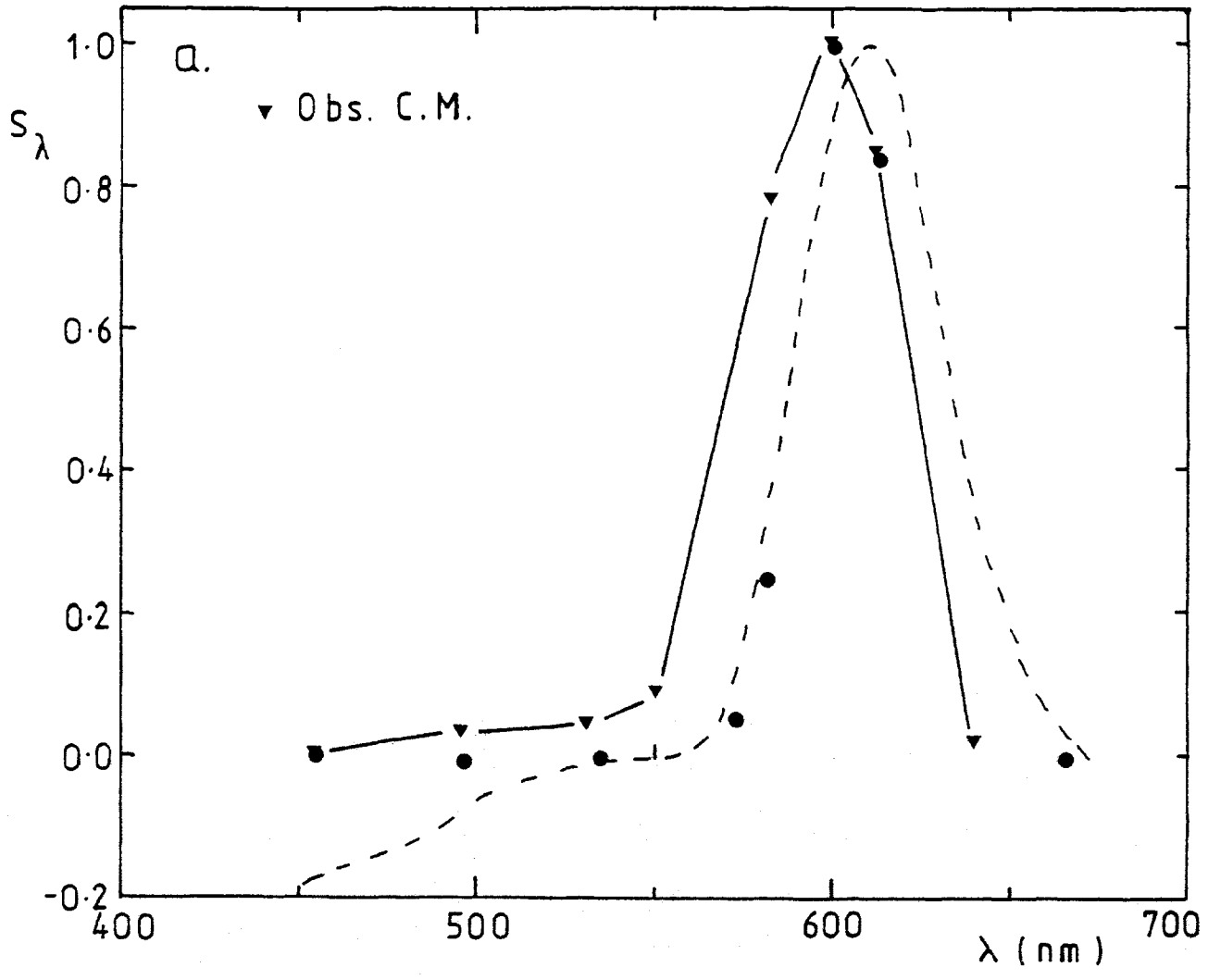
d, average data for 2 protanopes

The average data for each of the four different classes of subjects are plotted in fig.4.11. These data demonstrate that the deuteranomalous subjects (fig 4.11a) have a wavelength-dependent response which is very similar to the normal response, with a slight shift to shorter wavelengths. Fig.4.11 b-d show that the protanomalous, deuteranopic and protanopic subjects produce responses which do not vary in a systematic way with wavelength.

The spectral sensitivities of the post-receptoral mechanisms of the deuteranomalous subjects were calculated using the method described in chapter 3 (see fig.3.6), and the resulting response curves are illustrated in fig.4.12 a-h. The spectral sensitivity curves for the post-receptoral mechanisms in the deuteranomalous subjects, isolated by this technique, are narrow-band response functions with the maximum response at 580 nm - 600 nm. The shapes of the curves are generally similar to normal, although some subjects (noteably JH, fig.4.12h and P.D-L, fig.4.12c) have much narrower response functions than normal. It should be noted that the response curve (dashed line) for normal subject VW is the best mean fit to data obtained over a large number of experimental runs. The data for normal subject IMB were obtained over just two experimental runs, and are a more appropriate comparison for the scatter of points of the deuteranomalous subjects.

The average of the eight spectral sensitivity curves of fig.4.12 is plotted in fig.4.13. It can be seen that this average response for the deuteranomalous subjects has approximately the same bandwidth as the normal curve and peaks at 600 nm.

FIG. 4.12


a.
▼ Obs. C.M.
S_λ
1·0
0·8
0·6
0·4
0·2
0·0
-0·2
400
500
600
700
λ (nm)

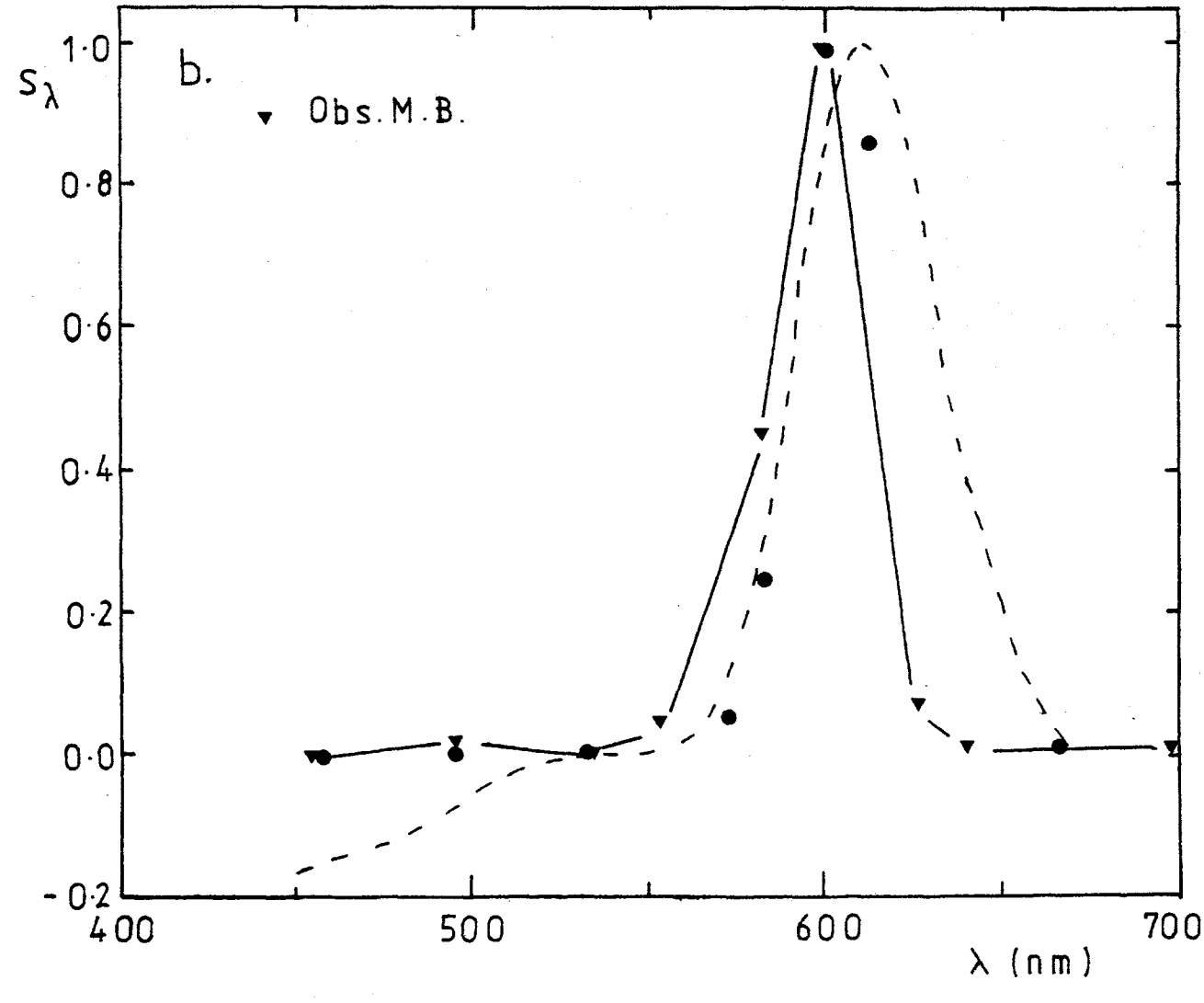
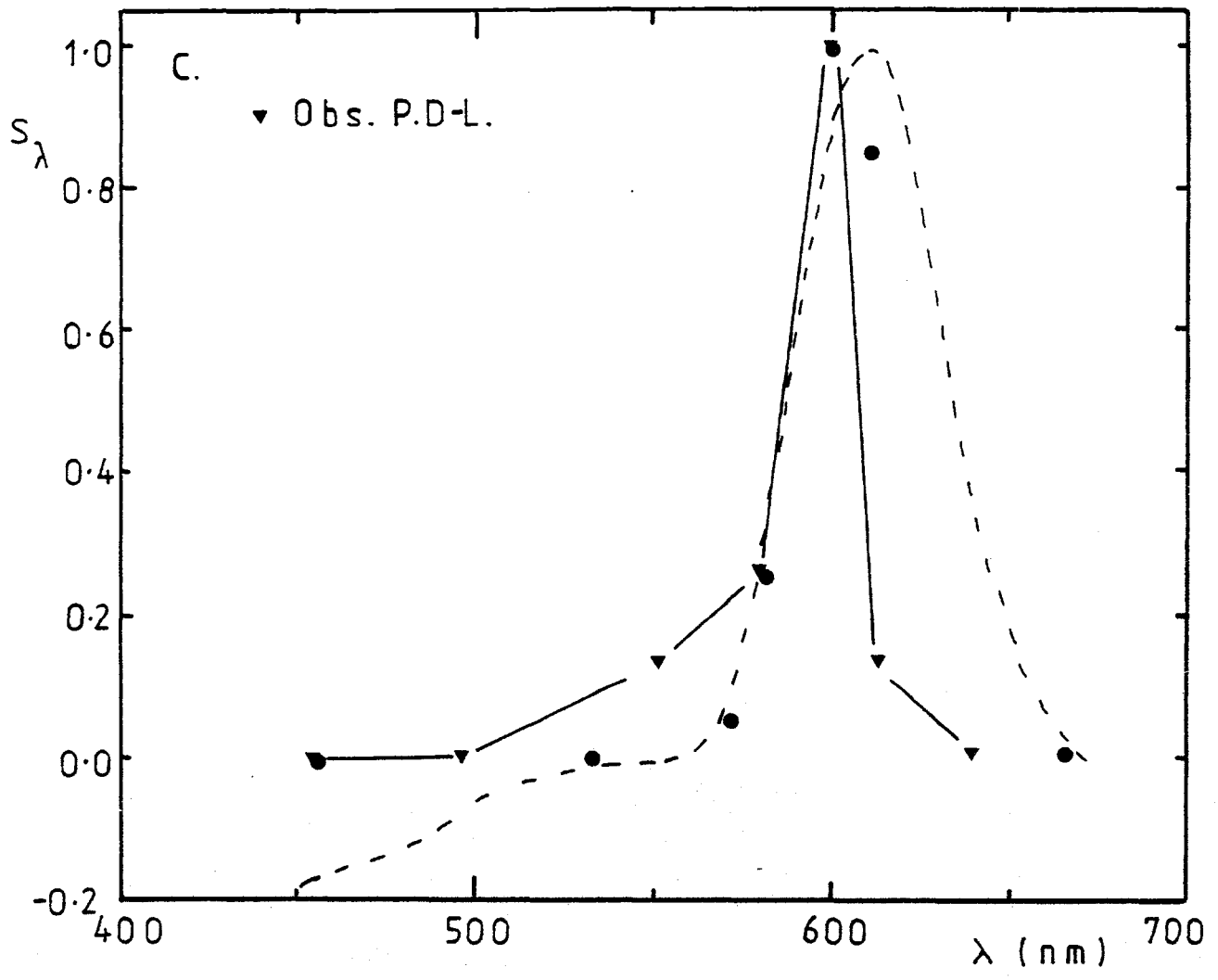

b.
▼ Obs.M.B.
S_λ
1·0
0·8
0·6
0·4
0·2
0·0
-0·2
400
500
600
700
λ (nm)

FIG. 4.12


C.
▼ Obs. P.D-L.
S_λ
1·0
0·8
0·6
0·4
0·2
0·0
-0·2
400
500
600
700
λ (nm)

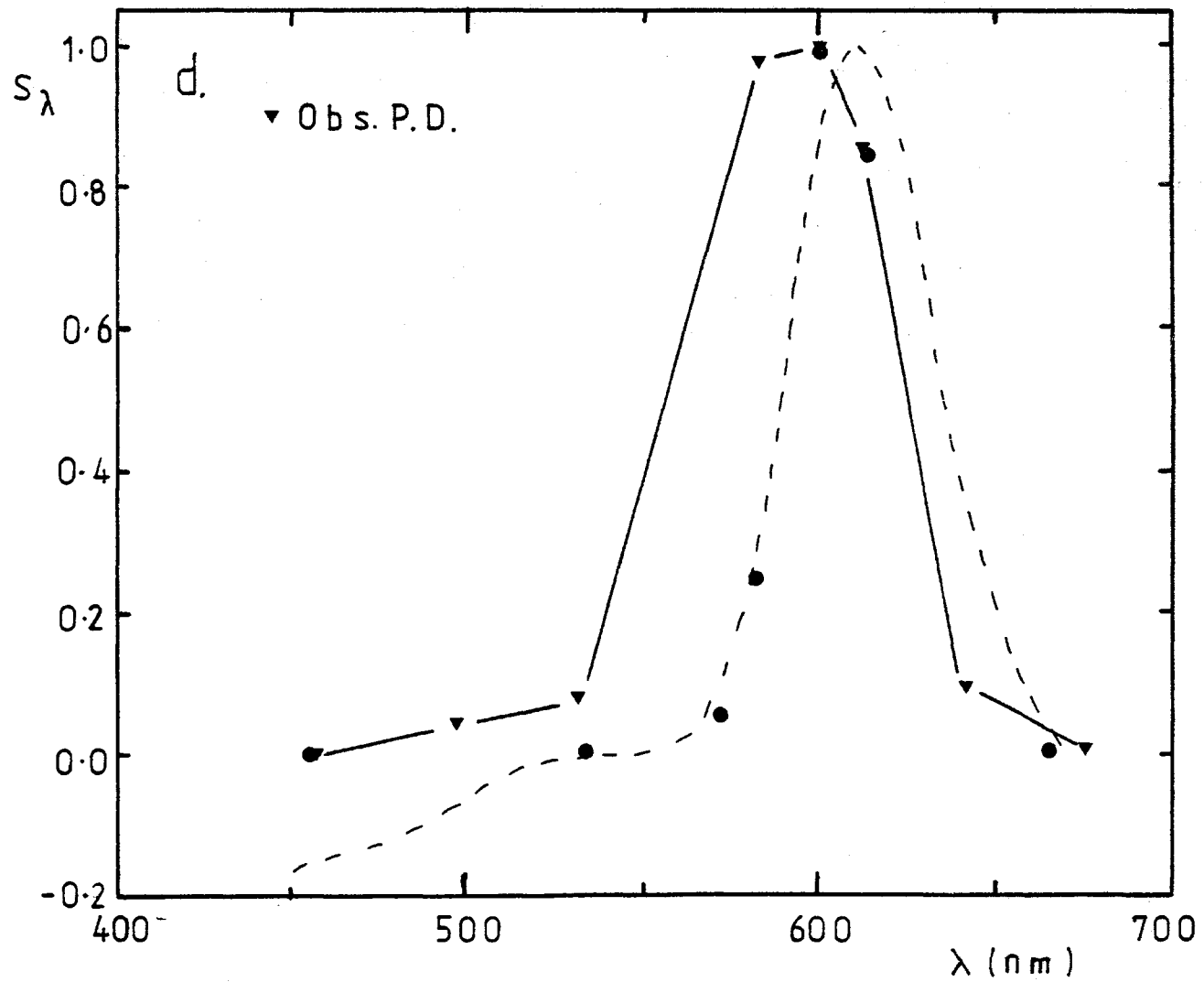
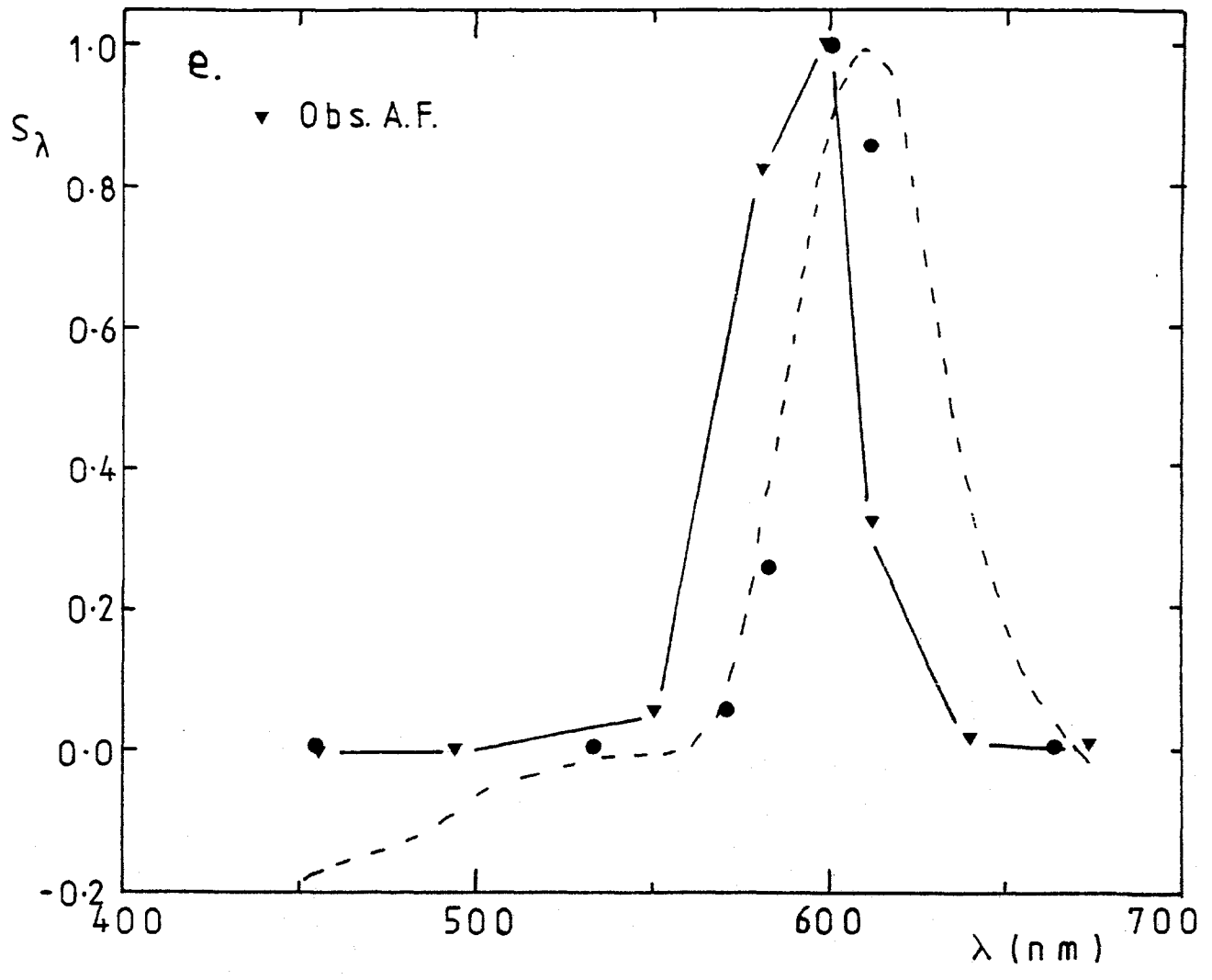

d.
▼ Obs. P.D.
S_λ
1·0
0·8
0·6
0·4
0·2
0·0
-0·2
400
500
600
700
λ (nm)

FIG. 4.12


e.
Obs. A.F.
S_λ
1·0
0·8
0·6
0·4
0·2
0·0
-0·2
400
500
600
700
λ (nm)

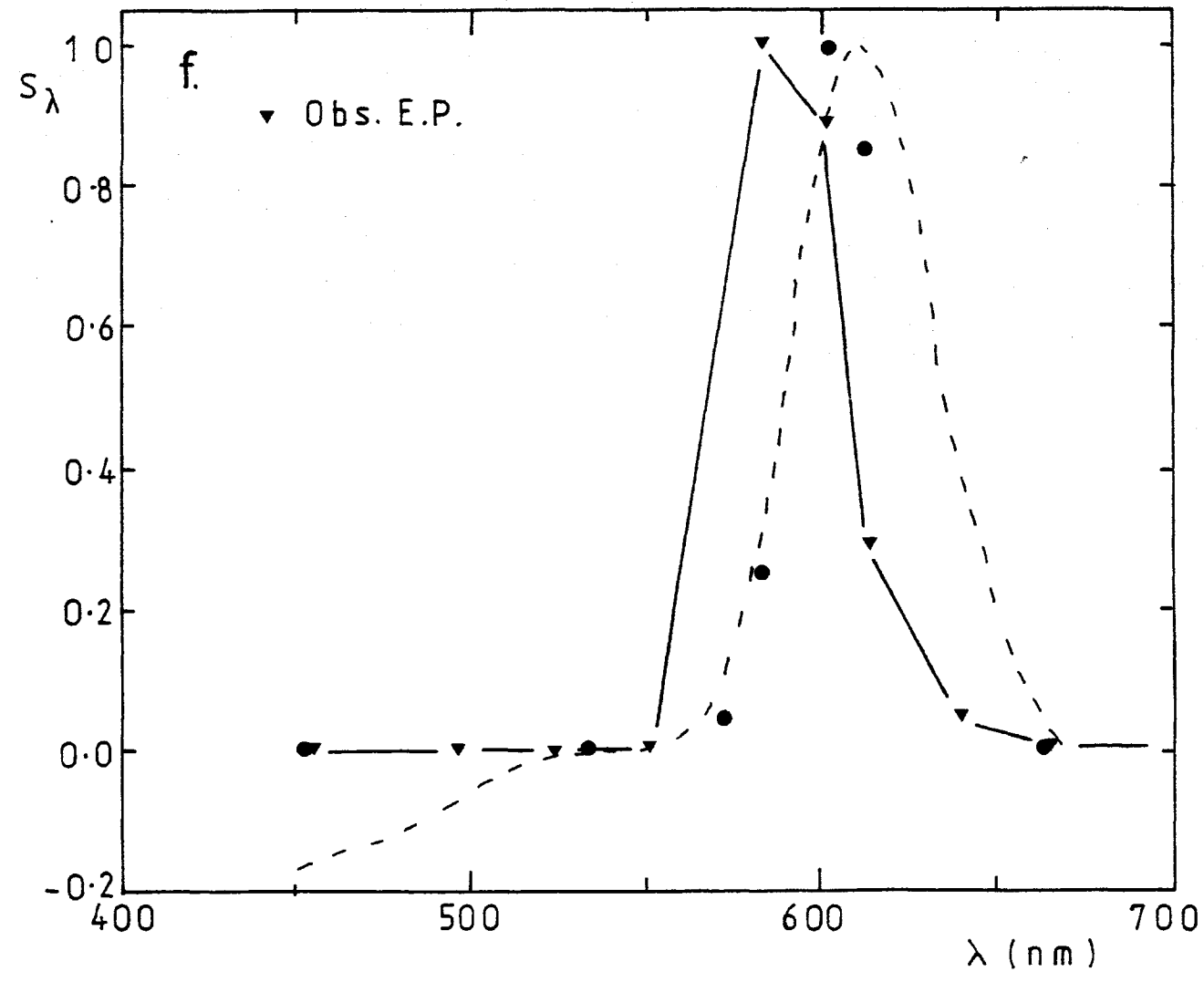
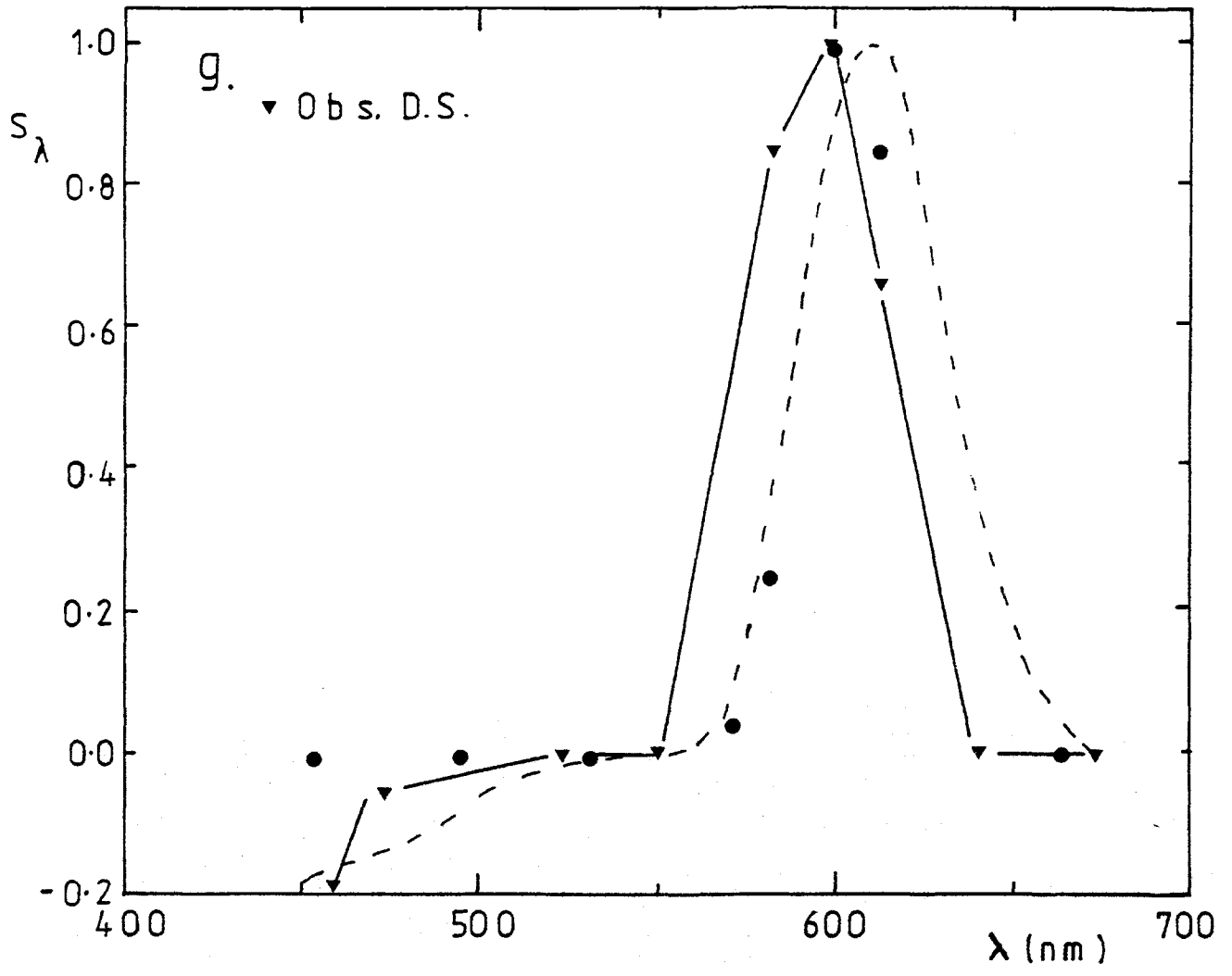

f.
Obs. E.P.
S_λ
1·0
0·8
0·6
0·4
0·2
0·0
-0·2
400
500
600
700
λ (nm)

FIG. 4.12


g.
▼ Obs. D.S.
S_λ
1·0
0·8
0·6
0·4
0·2
0·0
-0·2
400
500
600
700
λ (nm)

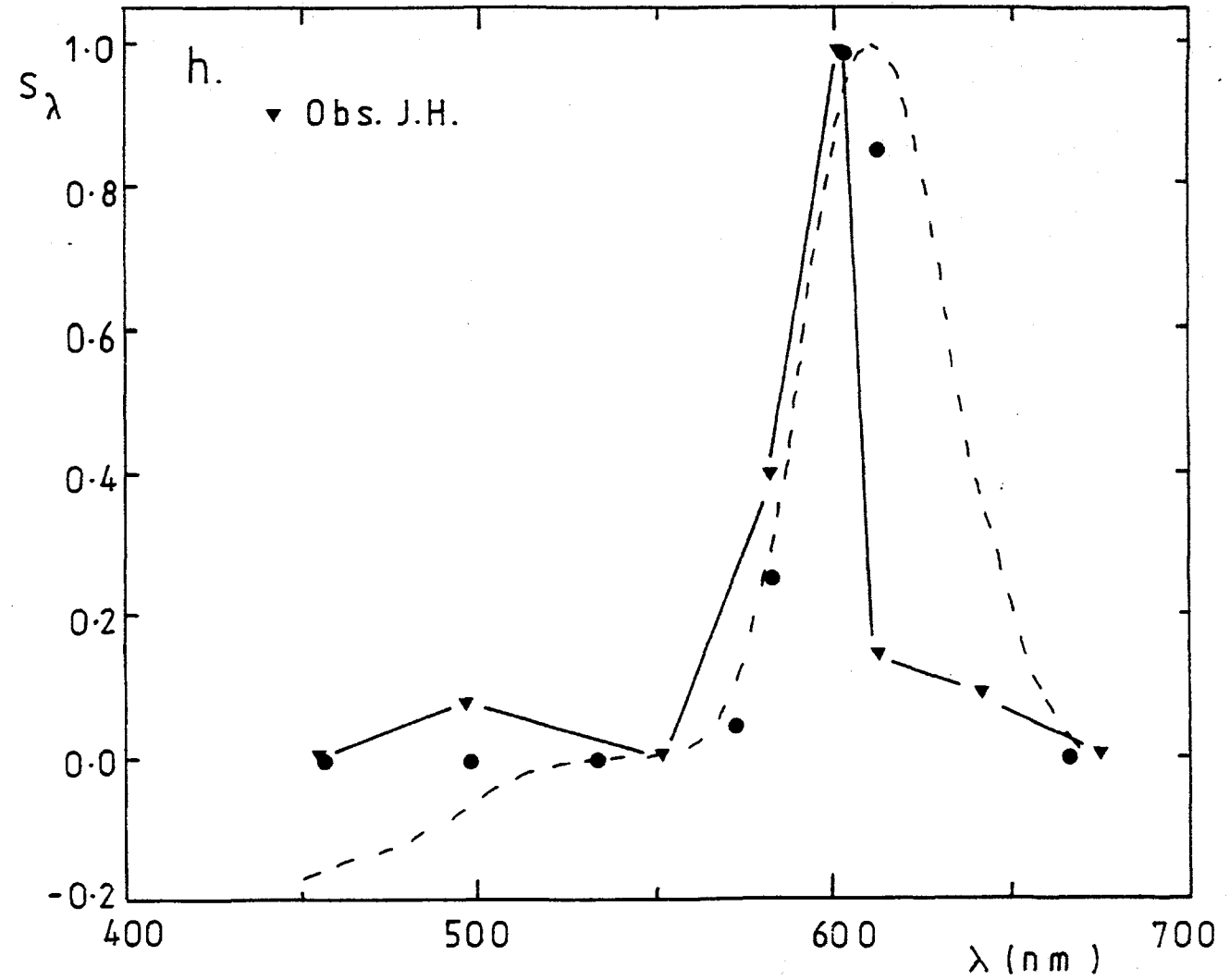

h.
▼ Obs. J.H.
S_λ
1·0
0·8
0·6
0·4
0·2
0·0
-0·2
400
500
600
700
λ (nm)

Fig. 4.12 Normalised spectral sensitivity, S_λ, derived from the data of fig.4.7, plotted against wavelength, λ. a-h ▼ data for 8 deuteranomalous subjects. The best mean fit curve for normal subject VW (dashed line) taken from fig.3.7a, and data for normal subject IMB (full circles) are plotted for comparison on each graph.

FIG. 4.13

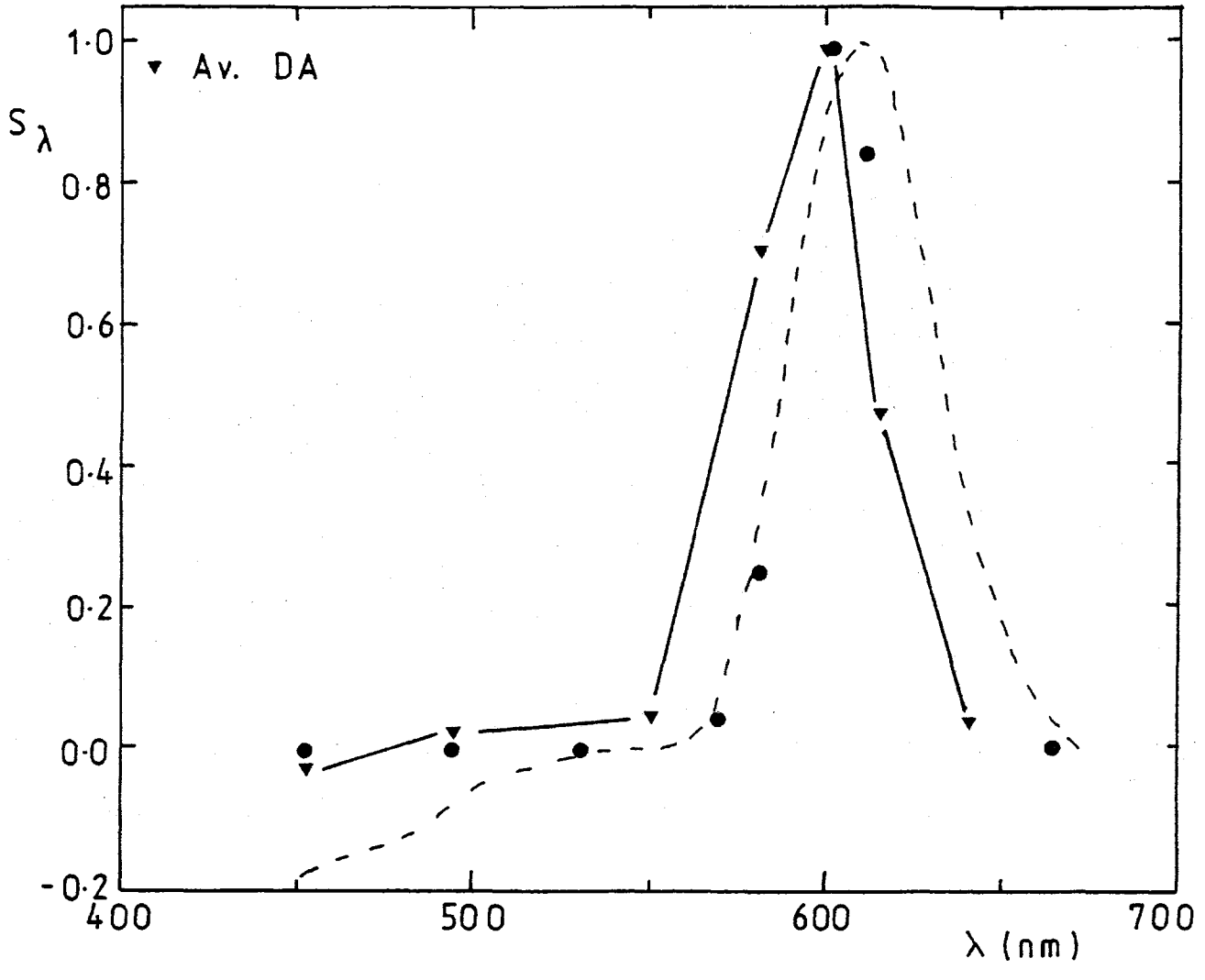


Fig.4.13 As for fig.4.12

▼Average data for 8 deuteranomalous subjects. Data for normal subjects VW (dashed line) and IMB (full circles) are plotted for comparison.

The green-sensitive post-receptoral response mechanism, illustrated in fig.3.7b, which can be fitted by the combination of the normal red (R) and green (G) mechanisms 'G-0.33R', was also investigated for two deuteranomalous subjects. The stimulus configuration was as illustrated in fig.4.6, except that the spot matrix was of negative contrast. Threshold measurements were made for a number of different matrix wavelengths, λ, under the conditions described earlier in this section.

Both these deuteranomalous subjects had obtained wavelength dependent responses for the configuration which isolates the 'R-G' mechanism. In this experiment, however, subject CM's response was independent of wavelength, i.e. the matrix suppressed the effect of the adaptation grating regardless of the matrix wavelength. Data for subject DS, however, shows a wavelength dependent response which is similar to normal. This can be seen more clearly from the calculated spectral sensitivity illustrated in fig.4.15.

The results from this section can be summarised as follows:

(1) Protanomalous, protanopic and deuteranopic subjects show no wavelength-dependent response when tested with the stimuls configuration which isolates an 'R-G' response in normal subjects.

(2) 8 deuteranomalous subjects obtain responses which are similar to normal, although some are shifted to slightly shorter wavelengths and have narrower bandwidths.

(3) Of two deuteranomalous subjects tested with the stimulus configuration which isolates a 'G-0.33R' response in normal subjects, one obtained a response which was similar to normal whilst the other produced no wavelength-dependent response.

FIG. 4.14

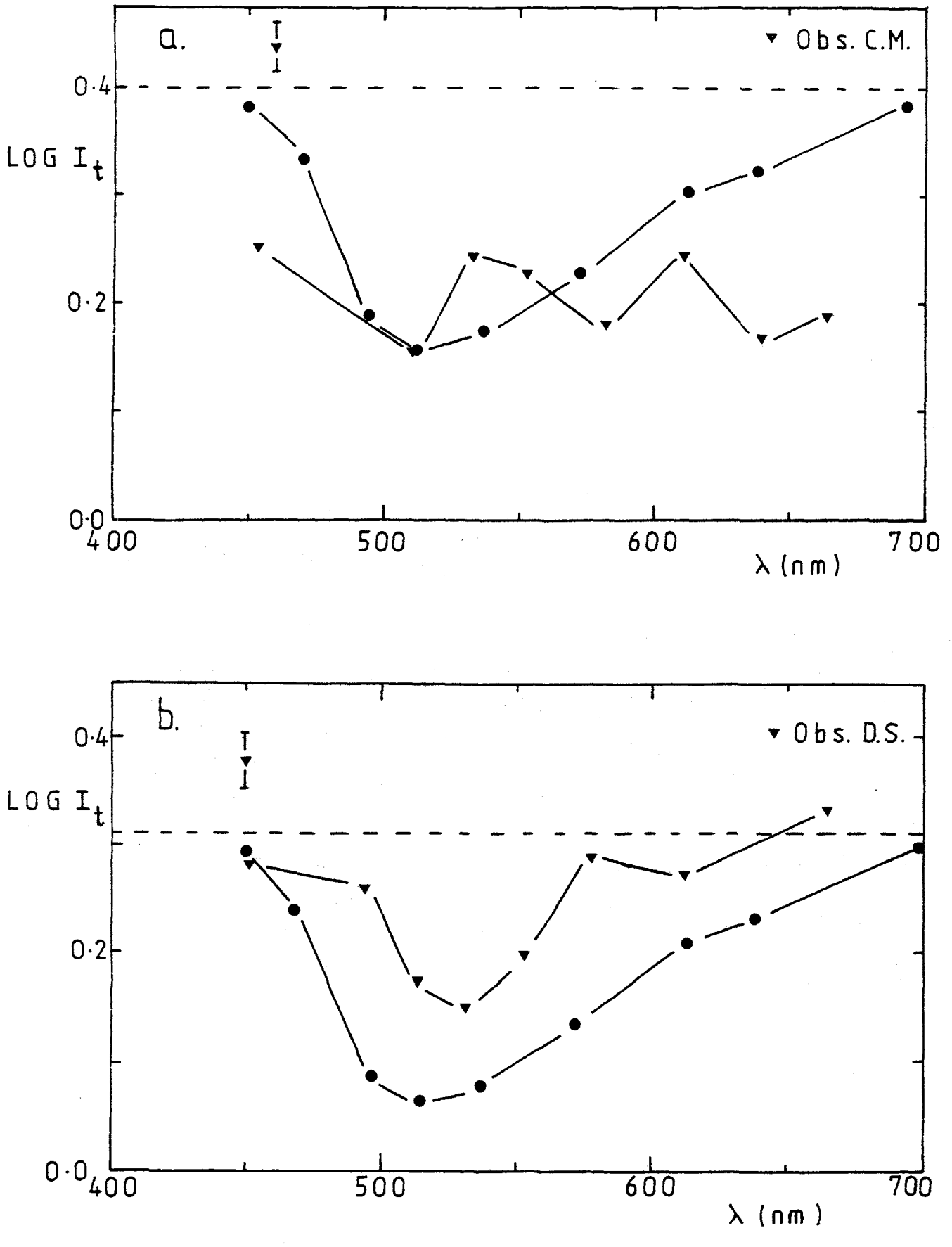


Fig. 4.14. As for fig 4.7 but with the adaptation matrix of negative contrast. ▼ Data for two deuteranomalous subjects. ● data for normal subject VW (taken from fig. 3.4b) is plotted for comparison.

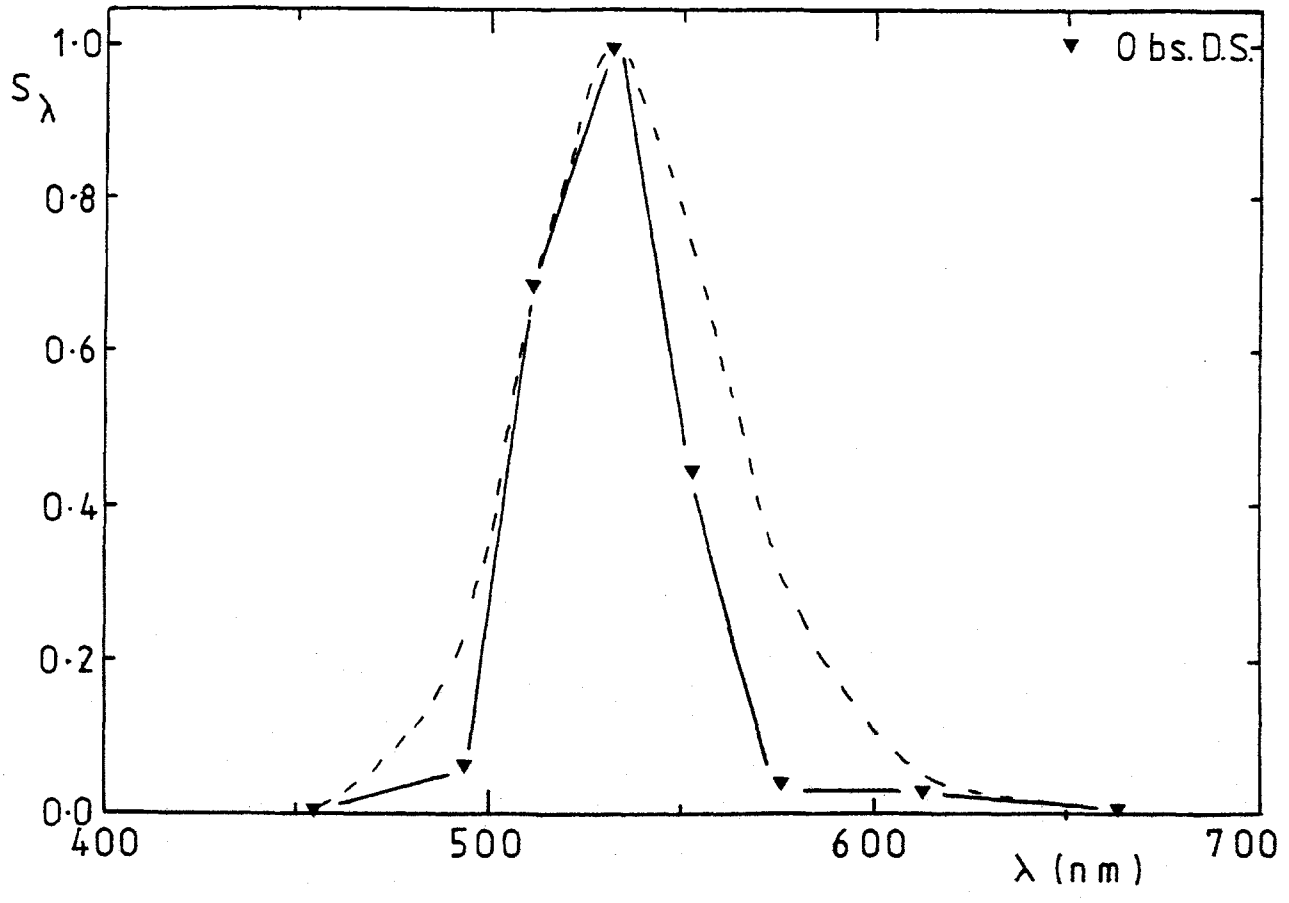


Fig.4.15 As for fig.4.12 but for the negative contrast matrix configuration.

4.4 Colour Matching Under Adaptation

Conspicuous changes in the appearance of colours can be produced by adaptation to coloured lights without upsetting colour matches. Colour matches, can, however, be disturbed by adaptation to very bright lights (Wright, 1936; Brindley, 1953). All adapting lights, whatever their wavelength, cause an increase in the amount of red required in a Rayleigh match and a decrease in the amount of green. Brindley interpreted these observations in terms of the bleaching of the visual photopigments by the adaptation lights. If these pigments

are of sufficiently high peak optical density, their absorption spectrum is modified by partial bleaching (Dartnall, 1957) with consequent modification of the colour-matching functions. Nunn and Ruddock (1978) investigated the effects of adaptation to bright lights on the colour matches of anomalous trichromats. They found that the Rayleigh matches of 3 deuteranomalous subjects tended towards the normal match at high bleaching intensities (4-5 log trolands); the results for 3 protanomalous subjects were similar, although the change from protanomalous matches at low bleaching intensities to normal matches at high intensities was not so straightforward and the errors were greater. Alpern (1979), performing a similar experiment but using a disk-annulus matching field configuration instead of a bipartite field, did not find that the matches of anomalous trichromats tended towards the normal at high intensities. In this section the experiments of Nunn and Ruddock (1978) have been repeated with red-green anomalous trichromats.

The experiments were performed on the modified Wright colorimeter described in chapter 2, and the stimuli are illustrated in fig.4.16. The bipartite field consisted of a near-monochromatic yellow (580 nm) test stimulus and matching stimuli R(650 nm) and G(530 nm). The 10^{o} adaptation field was illuminated by the source S3 (fig.2.15) passed through a broad-band red filter ($\lambda > 600$ nm). The observer was dark adapted for 10 minutes and then adapted to the 10^{o} field for 2 minutes. The experimenter then operated the shutters to allow cyclic presentation of the adaptation field for 15 sec, 3-4 sec darkness for recovery

and 2 sec presentation of the matching field. The observer adjusted the matching stimuli until a satisfactory match was obtained. Five matches were established for each illumination level, Ia, starting at Ia = 0 and proceeding to successively higher illumination levels of the adaptation field.

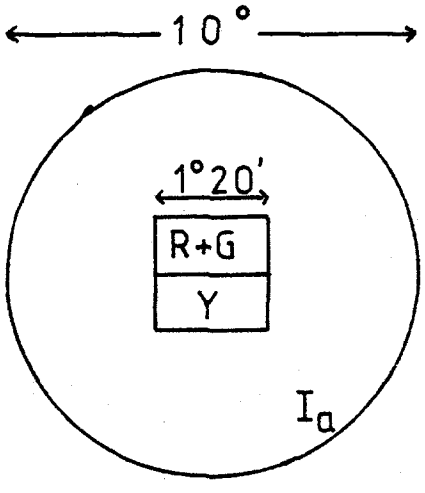
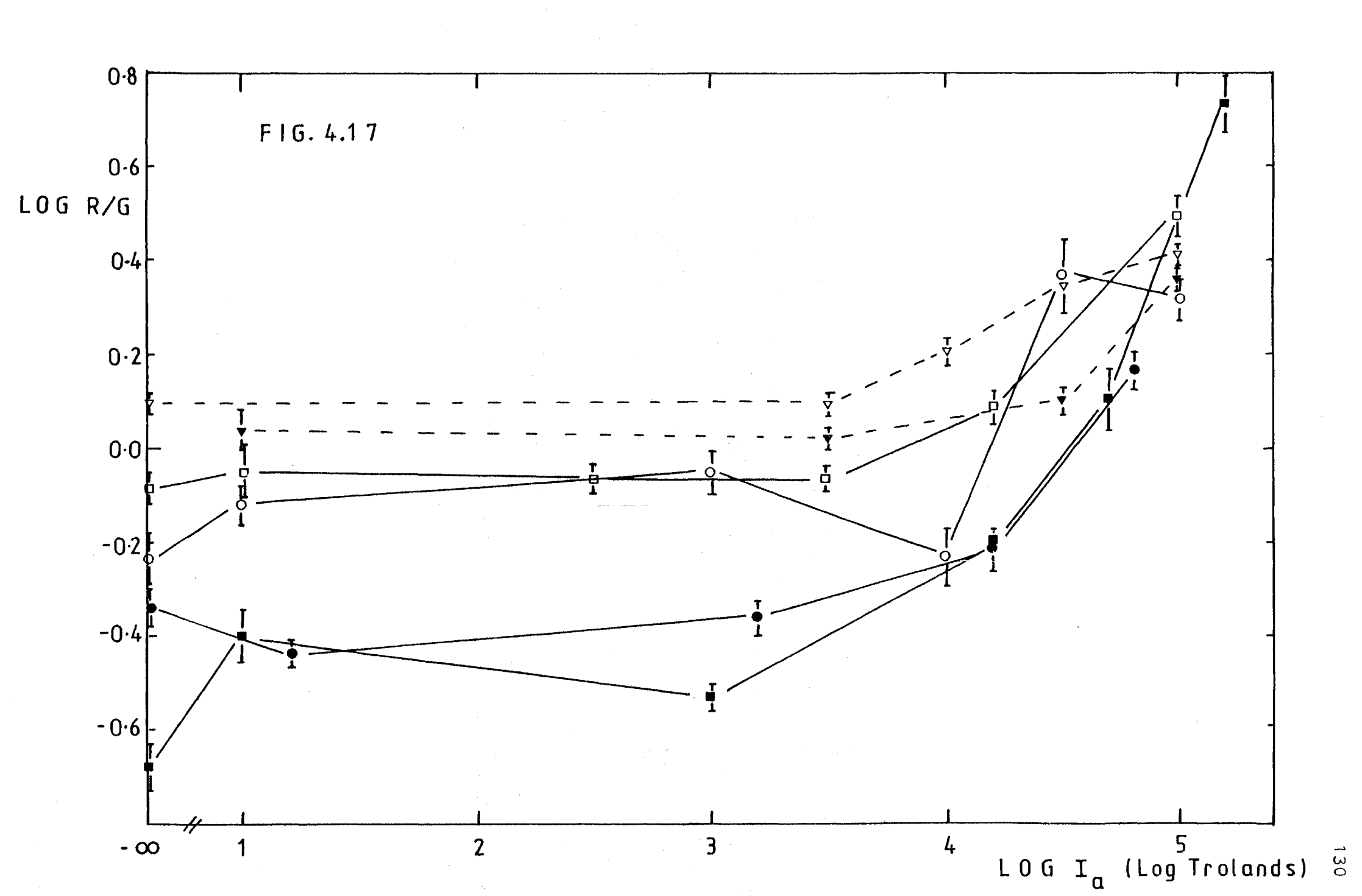


Fig. 4.16 Field configuration for the bleaching experiments. The 1°20' probe field consisted of a 580 nm test stimulus (Y) and matching stimuli 650 nm (R) and 530 nm (G). The 10° red adaptation field was of variable intensity, Ia.

Fig. 4.17 The red:green ratio , log R/G, required to match the near-monochromatic yellow (580 nm) stimulus, plotted against log Ia, the logarithm of the illumination level of the adaptation stimulus. Data for 2 normal subjects (dashed lines), ▽ IMB, ▼ CR. Data for 4 deuteranomalous subjects (continuous lines), □ MT, ■ DS, ○ JH, ● AG. Each point is the average of 5 measurements. The standard deviations are marked.


FIG. 4.17
LOG R/G
0·8
0·6
0·4
0·2
0·0
-0·2
-0·4
-0·6
-∞
1
2
3
4
5
LOG I_a (Log Trolands)

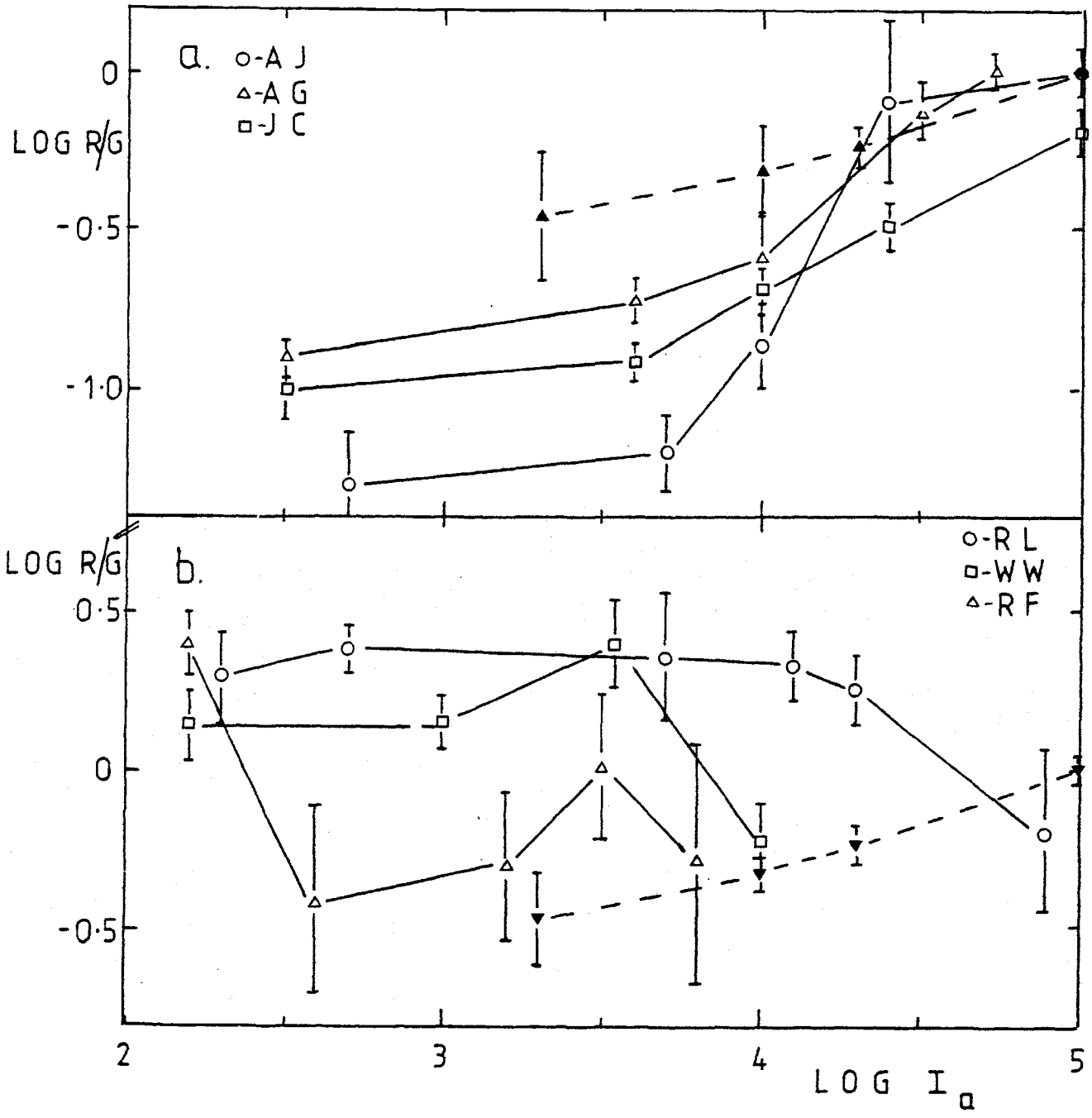


Fig. 4.18 As in fig. 4.17

a, data for 3 deuteranomalous subjects;
b, data for 3 protanomalous subjects.
Data for normal subject BN (dashed lines) are plotted for comparison.
Data taken from Nunn, 1978.

The results for 2 normal subjects (dashed lines) and 4 deuteranomalous subjects (continuous lines) are shown in fig.4.17. The 4 deuteranomalous observers all have lower log R/G values than normal at low levels of adaptation. The data for all observers, however, tend towards log R/G = 0.4 at an adaptation level of 5 log trolands. These results imply that deuteranomalous trichromatic colour vision and normal colour vision approach similar states under high levels of adaptation.

A similar experiment was attempted with 3 protanomalous subjects, using both red and green adaptation stimuli. It was found, however, that at high levels of adaptation, the protanomalous matches became wildly inaccurate. This was probably due to the poor red-sensitivity of these subjects. At high levels of adaptation, the bipartite field appears rather dim even to normal observers. The protanomalous subjects found that there was insufficient red available, and so it was impossible to obtain any significant data with this experimental arrangement.

The results obtained by Nunn (1978) in his similar study on the effects of bleaching on colour matching are illustrated in fig.4.18. The responses of the three deuteranomalous subjects (fig.4.18a) are similar to those obtained in the present study (fig.4.17), i.e. they have lower log R/G values than normal at low levels of adaptation but tend towards the normal match at high adaptation levels. The log R/G values of two protanomalous subjects, WW and RL, (fig.4.18b) are higher than normal at low adaptation levels and tend towards the normal match at high adaptation levels. The third protanomalous subject, RF, shows a similar response although the error bars (showing the standard deviation) are very large.

4.5 Pigment Mixture Theory of Anomalous Trichromacy

The pigment mixture model (Ruddock and Naghshineh, 1974) assumes that red-green anomalous trichromacy is the result of admixture of the red-and green-sensitive photopigments of normal colour vision in single receptors. There are thus three possible classes of red-green colour vision, illustrated in fig.4.19. (α_λ, β_λ) is the normal system in which α_λ and β_λ are the spectral absorption coefficients of the normal red-and green-sensitive mechanisms (fig.4.19a). (α_λ', β_λ) is a system in which a fraction (1-f) of the normal α_λ photopigment is replaced by the β_λ photopigment (fig.4.19b) and (α_λ, β_λ') is a system in which a fraction (1-f) of the normal β_λ photopigment is replaced by the α_λ photopigment (fig.4.19c).

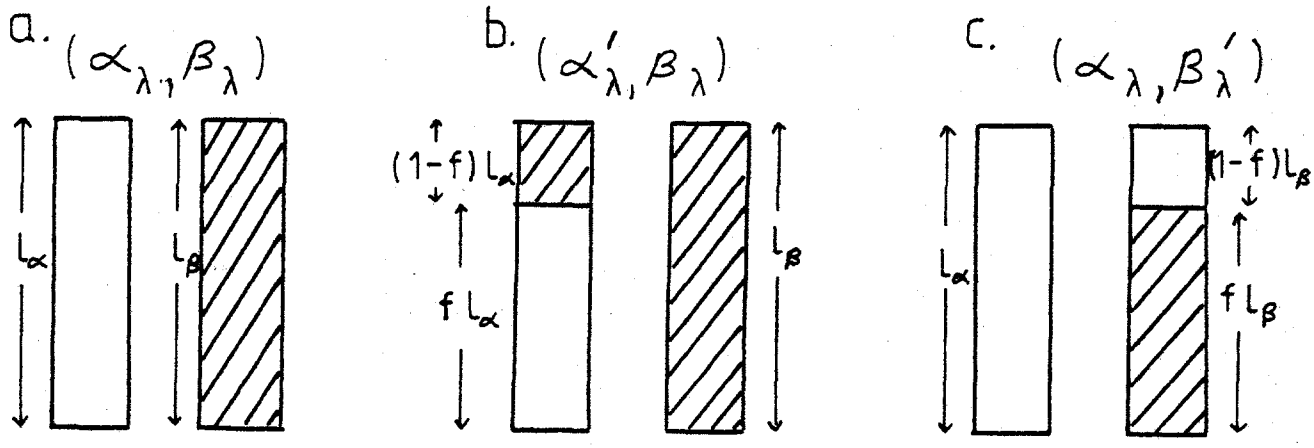


Fig.4.19 Schematic representation of the 3 classes of colour vision predicted by the pigment mixture model. a, corresponds to normal vision; b, corresponds to protanomaly and c, corresponds to deuteranomaly. The effective path-lengths through the pigments are represented by L_α etc.
From Ruddock and Naghshineh, 1974.

The optical densities (D) of the α_λ and β_λ pigments are given

by Beer's Law:

$$D(\alpha)_\lambda = \alpha_\lambda C_\alpha l_\alpha$$

$$D(\beta)_\lambda = \beta_\lambda C_\beta l_\beta \qquad \text{Equations 4.1}$$

where C_α and C_β are the concentrations of, and l_α and l_β are the optical path lengths through, the red-and green-sensitive photopigments respectively. The optical densities of the pigment mixtures are additive, so that the optical density of the α' pigment mixture is given by

$$D_\lambda(\alpha') = f l_\alpha C_\alpha \alpha_\lambda + (1-f) l_\alpha C_\beta \beta_\lambda$$

$$\text{then } D_\lambda(\alpha') = fD_\lambda(\alpha) + (1-f)D_\lambda(\beta)\, l_\alpha / l_\beta \qquad \text{Equation 4.2}$$

More explicit expressions may be obtained on the basis of further assumptions:-

If $l_\alpha = l_\beta$ then,

$$D_\lambda(\alpha') = fD_\lambda(\alpha) + (1-f)D_\lambda(\beta) \qquad \text{Equation 4.3}$$

If $\alpha_\lambda \max C_\alpha = \beta_\lambda \max C_\beta$ then,

$$D_\lambda(\alpha') = fD_\lambda(\alpha) + (1-f)D_\lambda(\beta) \frac{D(\alpha)\ max}{D(\beta)\ max} \qquad \text{Equation 4.4}$$

Similar expressions can be obtained for D(B ').

The analysis in terms of this model is performed with the following assumptions:

(1) In the calculation of colour matches, the effect of the blue-sensitive mechanism is neglected. This is a reasonable approximation as the blue mechanism has very low sensitivity for wavelengths $>$ 520 nm (Stiles, 1959). Absorption curves of the visual pigments are not corrected for the absorption of the ocular media, as these non-photolabile elements do not absorb significantly at wavelengths $>$ 500 nm. (Geeraets et al, 1960; Boettner and Wolter, 1962).

(2) Normal colour vision in the red-green region of the spectrum is mediated by two classes of cone which are distinguished by the optical densities $D(\alpha)_\lambda$, $D(\beta)_\lambda$ of the visual

pigments (α, β) contained within each class of cone. The optical densities determine the spectral sensitivities of the red and green mechanisms of normal colour vision.

(3) The sensitivity curves for the red and green colour mechanisms derived by Pitt (1944) are used in this analysis. These curves, which are illustrated in fig.4.20, were derived from colour matching experiments and were chosen in preference to the increment threshold spectral sensitivity curves measured by Stiles (1959), as the threshold measurements are inherently less precise than colour matching measurements (Stiles,1946; Rodieck, 1973), although the relative curves derived by both methods are similar. The precision with which absorption spectra can be determined using objective methods such as fundus reflectometry (Mitchell and Rushton, 1971) and single-cone microspectrophotometry (Marks, Dobelle and MacNichol, 1964; Brown and Wald, 1964; Bowmaker et al, 1978) is also lower than that of the colour-matching determinations.

(4) Estimates of the peak optical densities of the cone photopigments, based on psychophysical measurements, range between 0.5 and 1.0 (Brindley, 1953; Enoch and Stiles, 1961). The microspectrophotometric studies of Marks, Dobelle and MacNichol (1964) and Brown and Wald (1964) on single cones in monkey and man yielded very low optical densities of the bleachable pigments, i.e. 0.01- 0.03. Brindley (1970) attributed these low values to the effects of stray light reaching the recording photocell without having passed through the cone, and distortion of the retina such that the light does not pass along the whole length of the cone. More recent microspectrophotometric measurements on single cones of the rhesus monkey yield densities of 0.5 for both red and green cones; with the assumption that the cone outer segment

length is 35μm (Bowmaker et al, 1978).

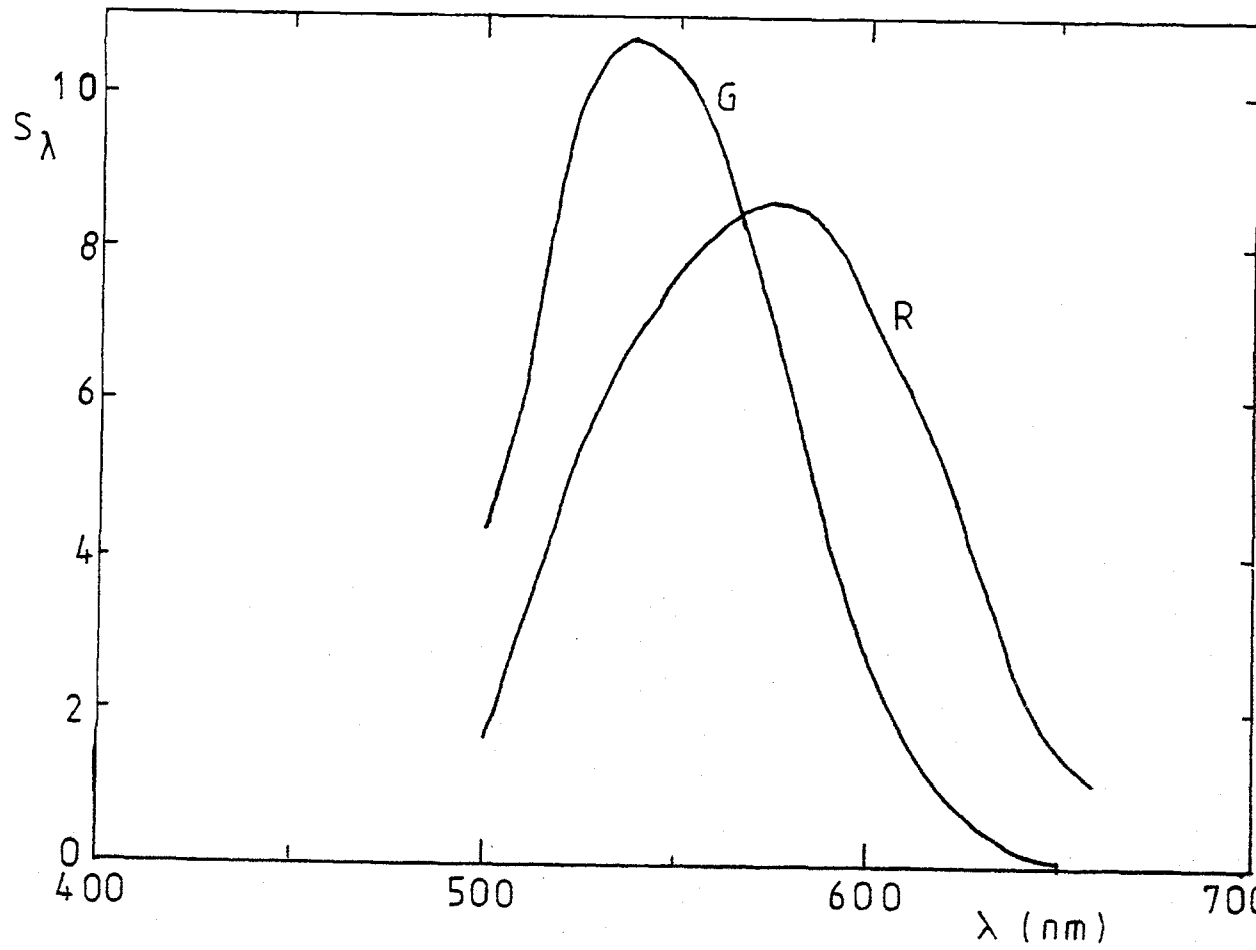


Fig. 4.20 The fundamental response curves for the green-and red-sensitive mechanisms. Relative sensitivity, S_λ, is plotted against wavelength . Data taken from Pitt (1944) and weighted for equal quantum efficiency at all wavelengths.

Rayleigh colour matches for the systems (α_λ', β_λ) and (α_λ, β_λ') have been calculated using equations 4.3 and 4.4 (Ruddock and Naghshineh, 1974). Figs. 4.21 and 4.22 show the values of the ratios of the colour matching coefficients, R/G, as a function of the variable f for the two systems corresponding to protanomaly and deuteranomaly respectively. It can be seen that the changes in colour matches for the protanomalous system (fig.4.21) and the deuteranomalous system (fig 4.22) with change in f are not

symmetrical relative to the normal match. Smaller values of f are required in the protanomalous case to reproduce the experimental values of R/G for protanomalous subjects (marked as circles on fig.4.21).

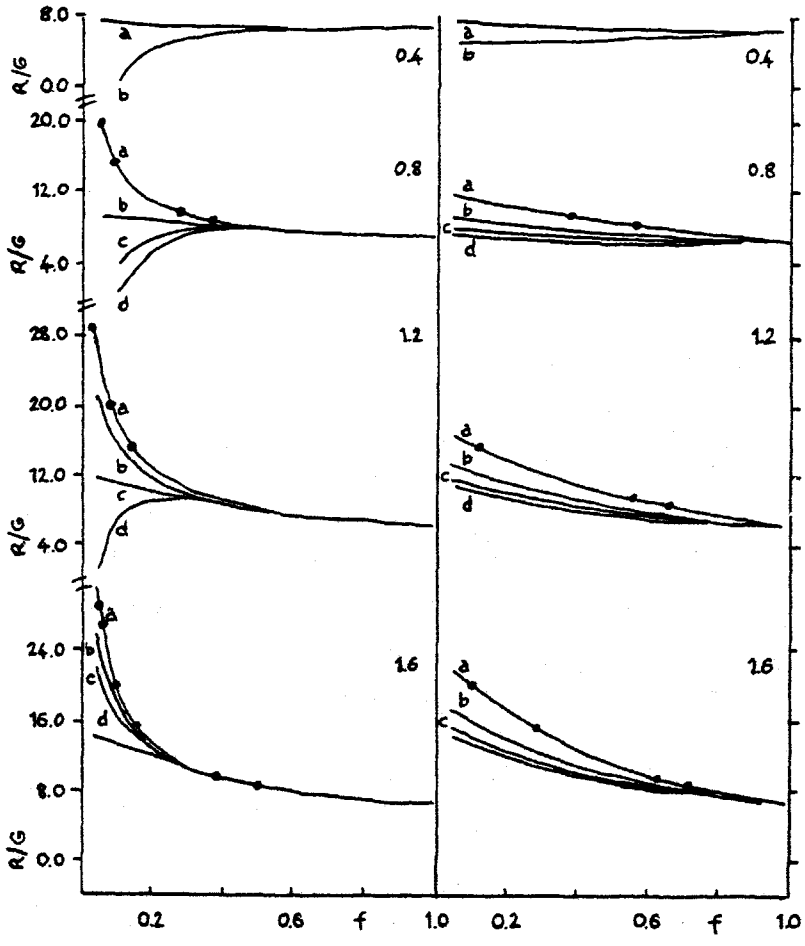


Fig.4.21 Rayleigh colour matches for the system (α_λ', β_λ) calculated on the basis of equation 4.4 (left hand column) and 4.3 (right hand column). Values of the ratio of the colour matching coefficients R/G are given as a function of the variable f. Values 0.4 etc. given with each set of data refer to the peak optical density of the α_λ pigment. a, b, c and d refer to peak optical density values of 0.4, 0.8, 1.2 and 1.6 for the β_λ pigment. Points give experimental values of R/G for protanomalous subjects.
From Ruddock and Naghshineh, 1974.

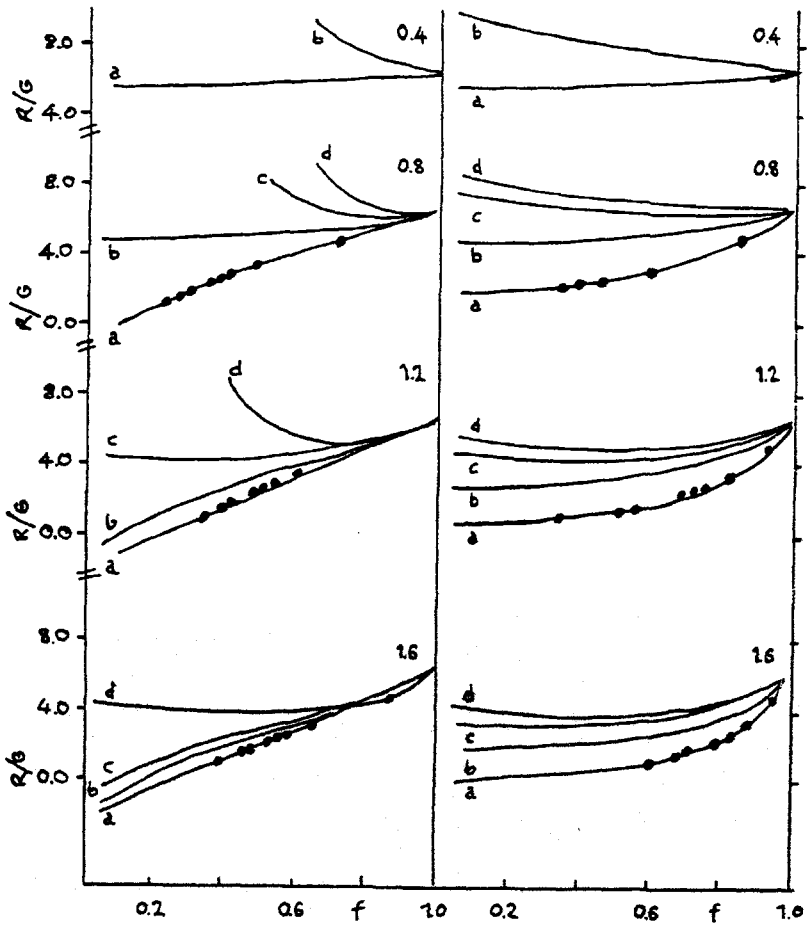


Fig. 4.22 As fig 4.21, but for the system (α_λ, β_λ'). Points refer to experimental values of R/G for deuteranomalous subjects.

4.5.1. Rayleigh Match Shifts Induced by Bleaching

The shifts in Rayleigh matches of normal and deuteranomalous trichromats induced by bleaching have previously been discussed by Alpern (1979) and Nunn (1978). Nunn's analysis showed that his experimental results (which are the same as those in this study for normal and deuteranomalous subjects, and which are illustrated in fig.4.18) could be quantitatively explained in terms of the pigment mixture model. He deduced a range of values for D (α) max and D(β) max, using equation 4.4, which corresponded to Rayleigh match shifts of up to Δ log R/G = 0.35 following

bleaching for normal subjects (consistent with the shift observed in fig.4.17). This range of D(α) max, D(β) max, illustrated in fig.4.23, will be used in the present analysis.

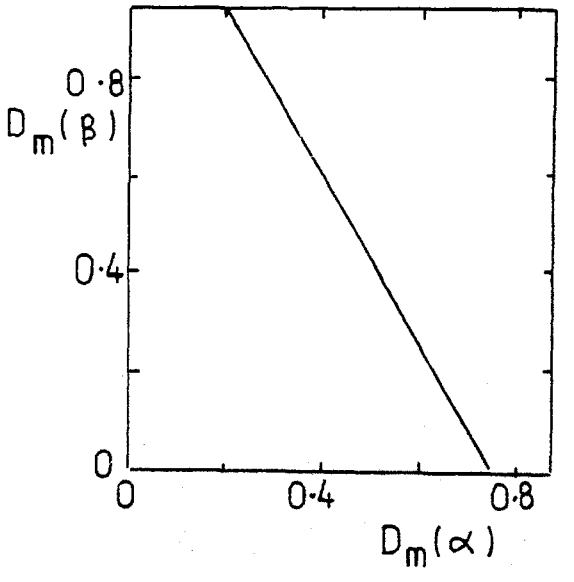


Fig.4.23 The range of D(α) max, D(β) max values which give rise to Rayleigh match shifts of Δ log R/G = 0.35 following bleaching for normal subjects.
From Nunn (1978).

4.5.2 Post-Receptoral Response Functions

Two expressions have been obtained which relate the optical densities of the pigment mixtures, α_λ' and β_λ', to the optical densities of the normal, α_λ and β_λ, photopigments (equations 4.3 and 4.4). The case where $\alpha_\lambda \max C_\alpha = \beta_\lambda \max C_\beta$ is first considered. D(α) max was chosen to be 0.5; this gives a value of D(β) max of 0.42 (from fig.4.23). To obtain the spectral optical density of the α and β pigments, the logarithm of the spectral sensitivity data of fig.4.20 was calculated. This gives directly the relative shape of the optical density curves, as $D(\alpha) \propto \alpha_\lambda$ and $D(\beta) \propto \beta_\lambda$ (equations 4.1), and the absolute values are fixed by the chosen values

of D(α) max and D(β) max; the resulting curves are illustrated in fig.4.24.

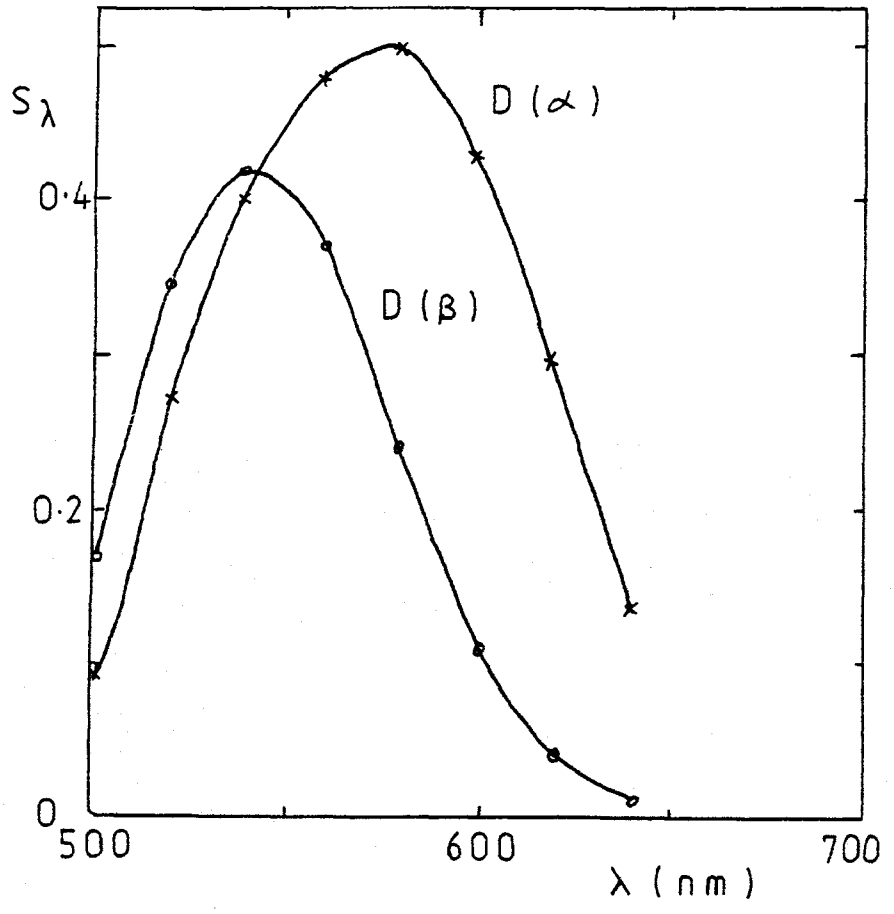


Fig.4.24 Optical densities of the α and β pigments, D(α), D(β), with D(α) max = 0.5, D(β) max = 0.42.

Equation 4.4 then becomes,

$$D(\alpha') = fD(\alpha) + 1.14(1-f)D(\beta) \quad \text{Equation 4.5}$$

and,

$$D(\beta') = fD(\beta) + 0.88(1-f)D(\alpha) \quad \text{Equation 4.6}$$

The curves generated by these equations for f = 0.8, 0.6, 0.4, 0.2 are shown in fig. 4.25 a-d.

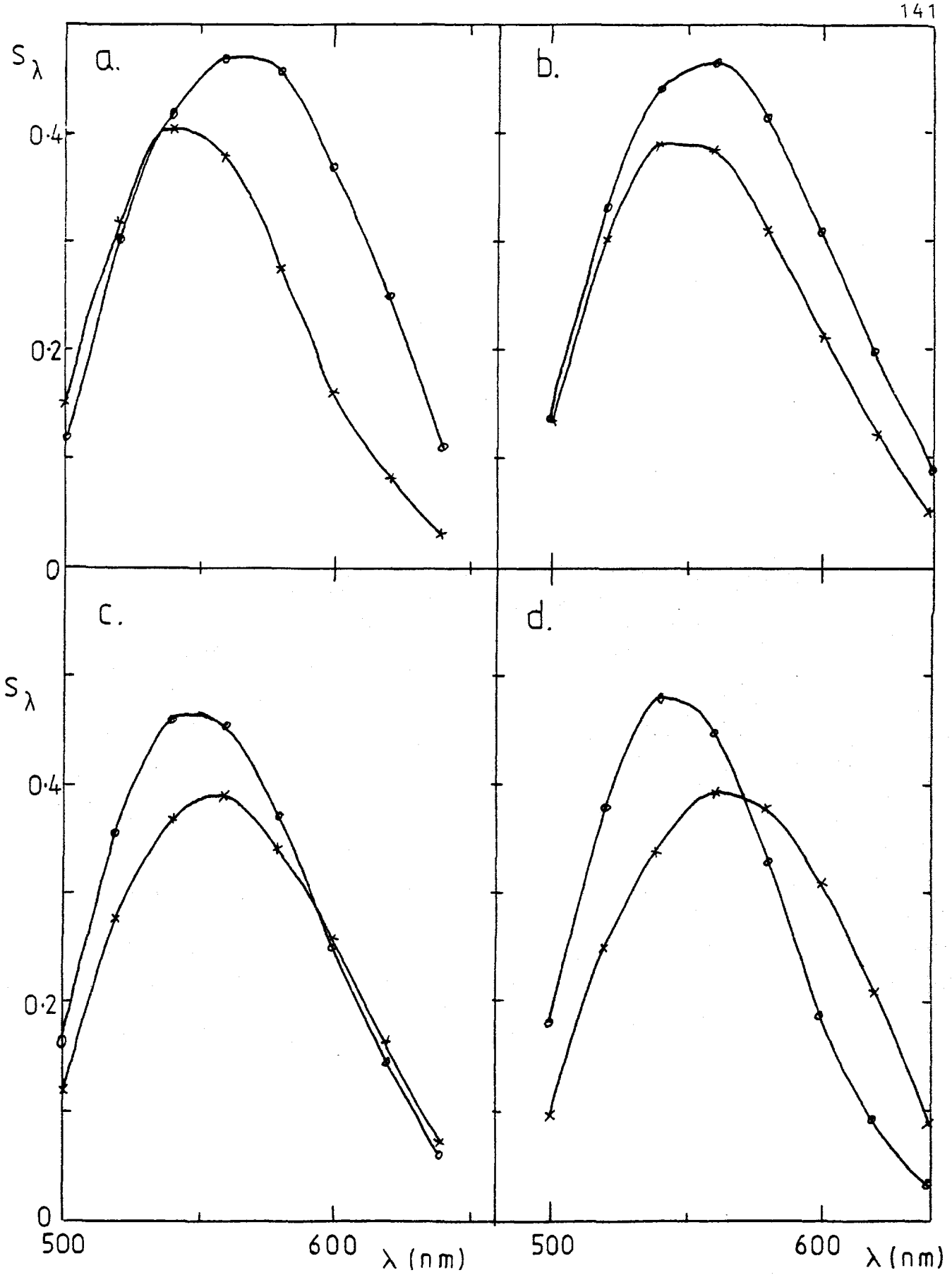


Fig. 4.25 Optical densities of the α' and β' pigment mixtures, calculated from equations 4.5 and 4.6, for a, f = 0.8; b, f = 0.6; c, f = 0.4; d, f = 0.2

o $D(\alpha')$
× $D(\beta')$

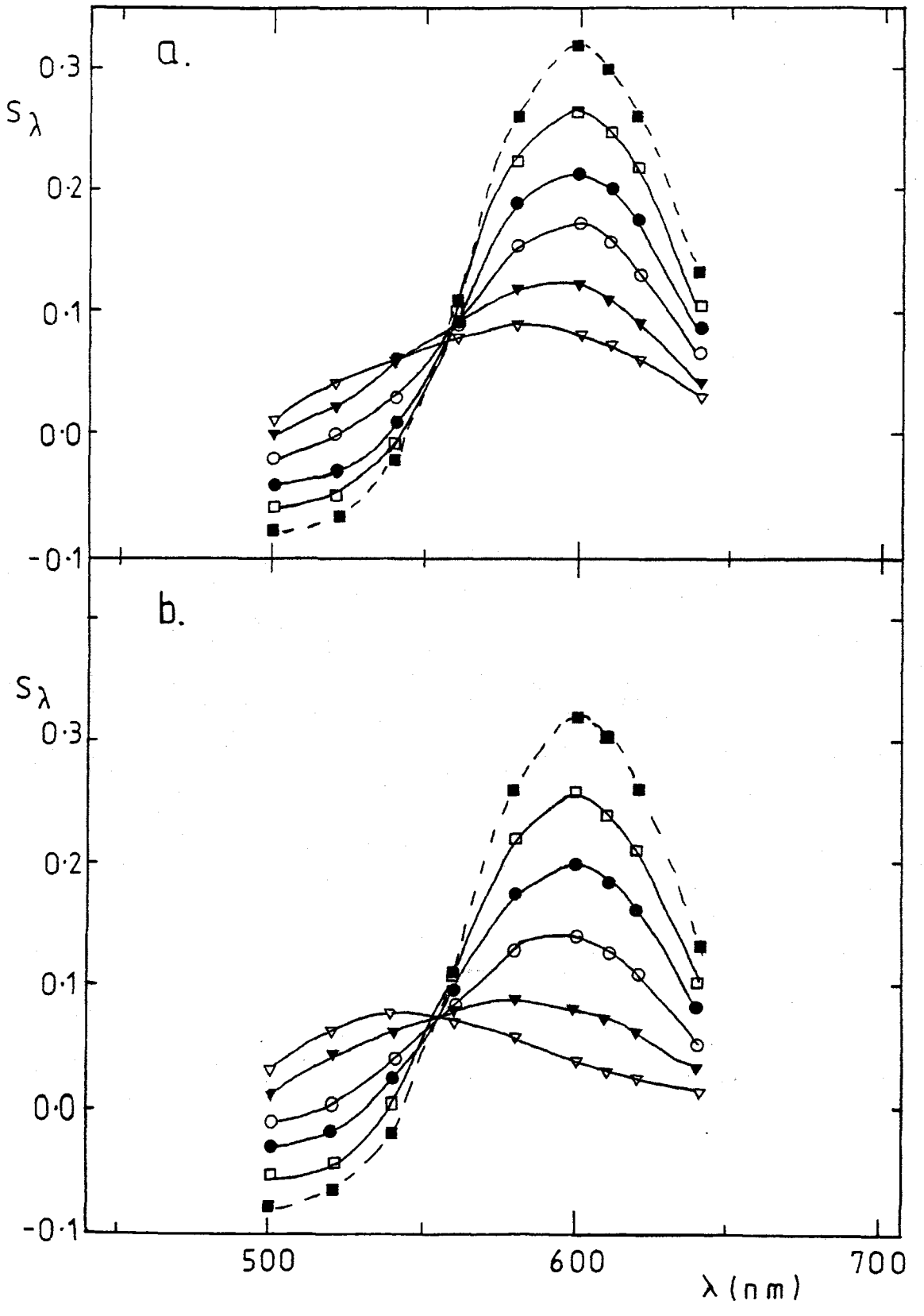


Fig.4.26 Spectral sensitivity curves for the 'R-G' mechanism. a, data for the deuteranomalous case, D(α) - D(β'); b, data for the protanomalous case, D(α') - D(β). The different curves are for different values of f : □, 0.8; ●, 0.6; ○, 0.4; ▼, 0.2; ▽, 0.05. The predicted normal curve, D(α) - D(β), is plotted for comparison (■, dashed line).

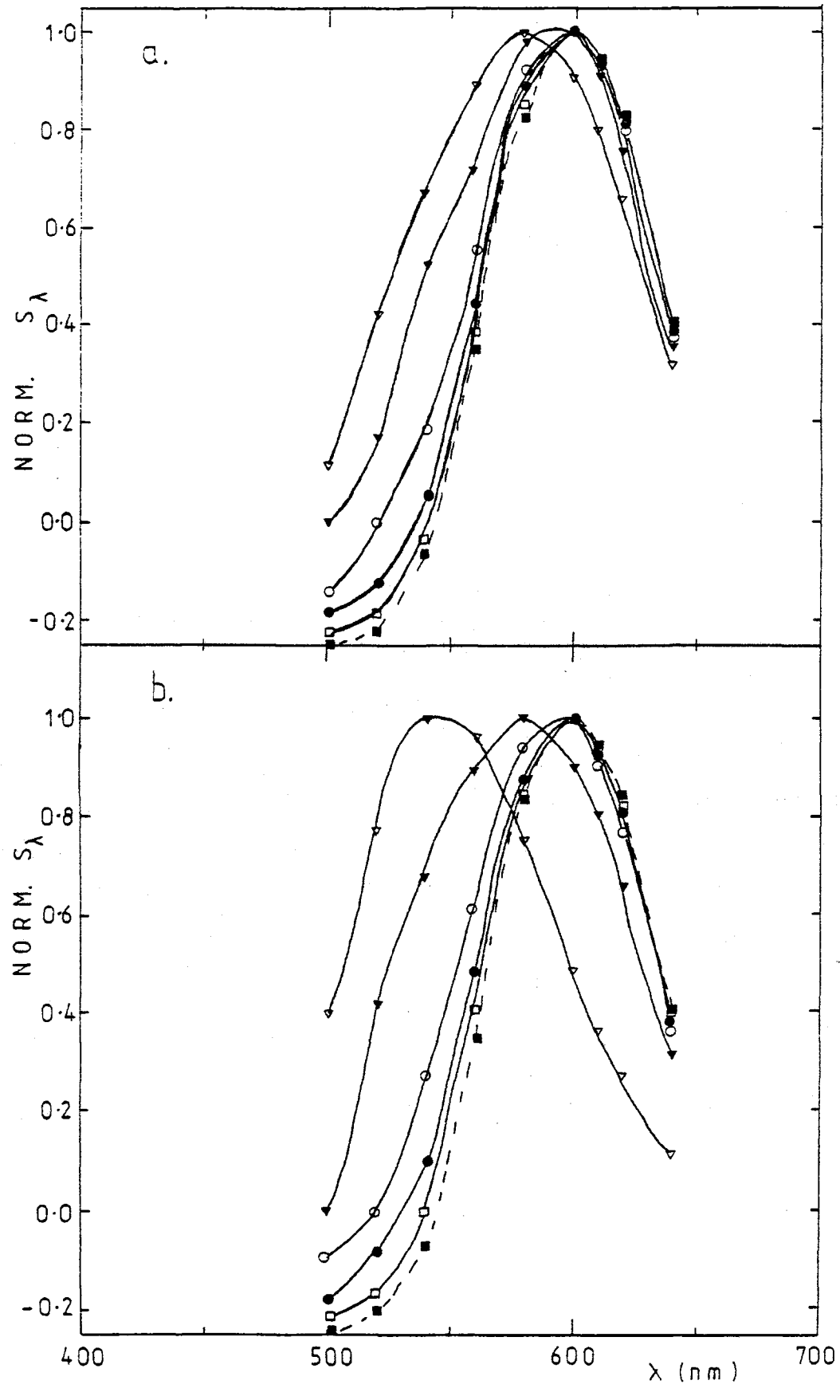


Fig. 4.27 As for fig. 4.26 except that the curves have been normalised.

The spectral sensitivities of the 'R-G' mechanism can be calculated by subtracting these photopigment optical densities, i.e. for the normal case $D(\alpha) - D(\beta)$; for the deuteranomalous case $D(\alpha) - D(\beta')$; for the protanomalous case $D(\alpha') - D(\beta)$. Sensitivity curves obtained in this way are plotted for deuteranomals in fig.4.26a and protanomals in fig.4.26b, for $f = 0.8$, 0.6, 0.4, 0.2 and 0.05. Data for the normal case, $D(\alpha) - D(\beta)$, (dashed line) are plotted for comparison. The corresponding normalised curves are plotted in fig.4.27 a,b.

It can be seen from fig. 4.27a that the normalised deuteranomalous curves are very similar to normal for values of $f > 0.4$. For low values of f (i.e. for more extreme cases of deuteranomaly where a large proportion, 1-f, of the normal green-sensitive pigment is replaced by the red-sensitive pigment) there is a broadening of the sensitivity curve and a shift to shorter wavelengths. This is more noticeable in the non-normalised data (fig.4.26a) where the amplitude of the response curve decreases as f decreases. The normalised protanomalous curves (fig.4.27b) are similar to normal for values of $f > 0.6$. For lower values of f there is a broadening of the curves anda marked shift to shorter wavelengths. This again can be clearly seen from the non-normalised curves (fig.4.26b) which are virtually flat for $f < 0.2$.

Spectral responses for the second red/green mechanism ($G - 0.33R$) were also calculated using the anomalous mechanisms predicted by this theory: $D(\beta) - 0.33D(\alpha)$ for the normal case and $D(\beta') - 0.33D(\alpha)$ for the deuteranomalous case. The results for values of f equal to 0.8, 0.6, 0.4 and 0.2 are plotted in fig.4.28. The data for $f = 0.8$

(i.e. a fairly mild degree of deuteranomaly) are exactly the same as the data predicted for the normal case. As f decreases (i.e. the amount of red-sensitive pigment replacing the green-sensitive pigment in the normal green cones increases) the sensitivity curve is displaced to longer wavelengths and becomes broader.

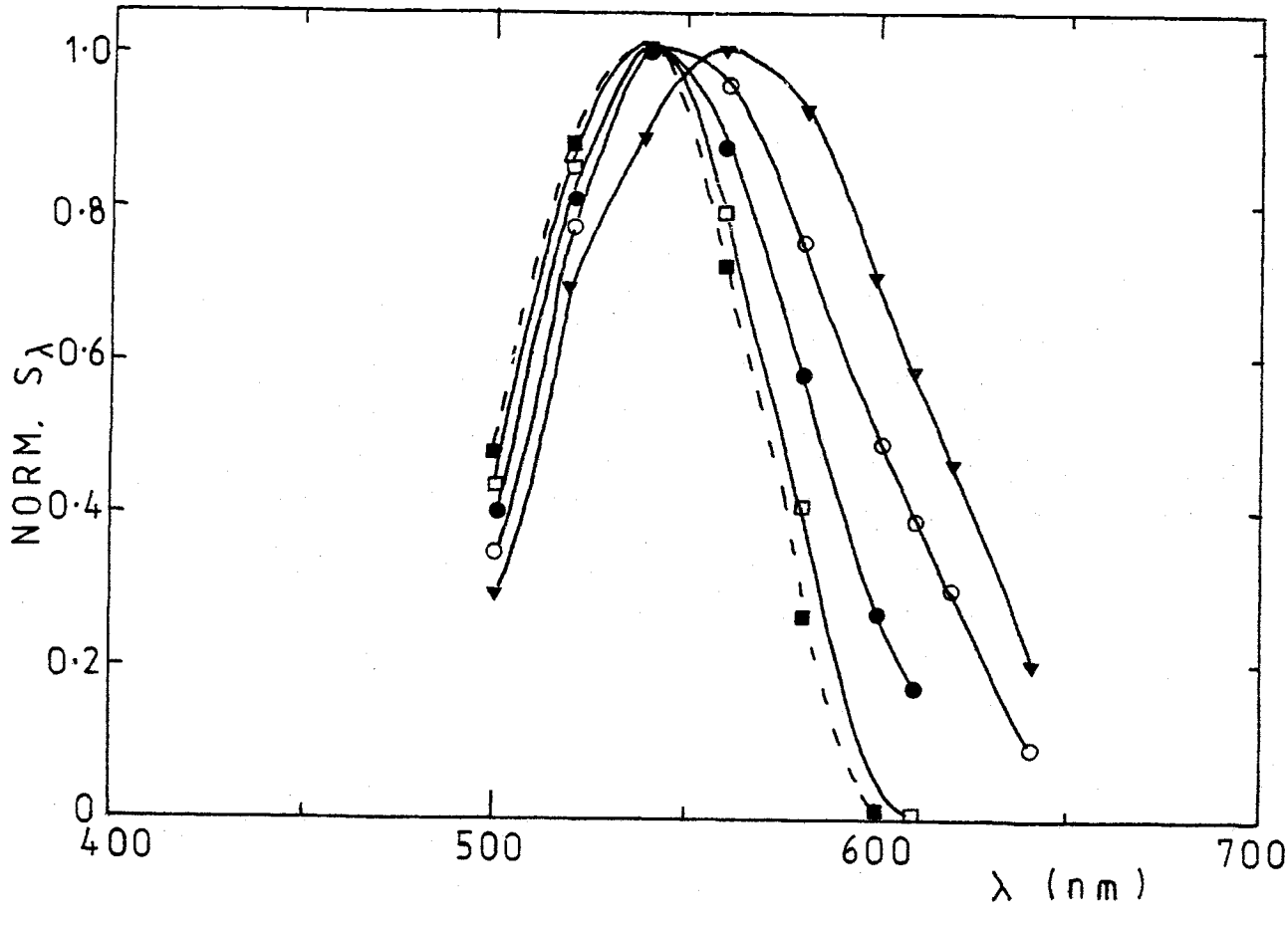


Fig.4.28 Normalised sensitivity curves for the 'G-0.33R' mechanism predicted for the deuteranomalous system, D(β') - 0.33D(α). The different curves are for different values of f: □ , 0.8; ● , 0.6; ○ , 0.4; ▼ , 0.2. The predicted normal curve is plotted for comparison (■ , dashed line).

Another pair of values of D(α) max, D(β) max were chosen to perform this analysis; i.e. D(α) max = 0.6, D(β)max = 0.25. The curve predicted for the normal case (D(α) - D(β)), however, was inconsistent with the observed normal response

of fig.3.7, having a maximum sensitivity at 580 nm rather than 600-610 nm. It was thus not appropriate to make any predictions using the pigment mixture model with these data.

The predictions so far have been made using equation 4.4 which contains the assumption that $\alpha \max C_\alpha = \beta \max C_\beta$. The alternative expression (equation 4.3) where $l_\alpha = l_\beta$ is now considered.

Equation 4.3 $D(\alpha') = fD(\alpha) + (1-f)D(\beta)$

Similarly $D(\beta') = fD(\beta) + (1-f)D(\alpha)$

The sensitivity of the 'R-G' mechanism for the deuteranomalous case will then be given by

$$D(\alpha) - D(\beta') = D(\alpha) - fD(\beta) - (1-f)D(\alpha)$$
$$= f(D(\alpha) - D(\beta))$$

which will produce exactly the same normalised sensitivity curves as in the normal case, although the non-normalised data will have a reduced amplitude. Similarly for the protanomalous case,

$$D(\alpha') - D(\beta) = fD(\alpha) + (1-f)D(\beta) - D(\beta)$$
$$= f(D(\alpha) - D(\beta))$$

Thus, the pigment mixture model can successfully predict the response curves of fig.4.12 for the deuteranomalous subjects. If it is assumed that $l_\alpha = l_\beta$ (i.e. the lengths of the cone outer segments of the red and green cones are equal), then the model predicts that the normalised deuteranomalous response will be the same as normal, i.e. a narrow-band response peaking at 600 nm. If it is assumed that $\alpha \max C_\alpha = \beta \max C_\beta$ (i.e. the absorption per unit path length is the same for the red-and green-sensitive photopigments), then the model predicts that the normalised response will be similar to normal but shifted slightly to

shorter wavelengths, which is the observed experimental response (see the average deuteranomalous data, (fig.4.13)). The model also successfully predicts the deuteranopic and protanopic results (figs. 4.9 and 4.10 respectively): if, in the case of the deuteranope, the 'green' cones are filled solely with the red-sensitive photopigment, then R-G = 0 and no wavelength-dependent response is predicted, and similarly for the protanopes.

The model can also be used to interpret qualitatively the experimental results of the protanomalous subjects (figs 4.8 and 4.11b). Fig.4.27b shows that at low values of f the normalised protanomalous response becomes broadened and shifted to shorter wavelengths, and the non-normalised response curves become virtually flat for values of $f \lesssim 0.2$. Figs. 4.21 and 4.22 show that most of the experimental colour matches of the protanomalous observers can only be reproduced with low values of f($f \lesssim 0.2$), whereas the deuteranomalous system predicts most experimental matches with $f \gtrsim 0.6$. The low values of f required to predict the protanomalous colour matches give rise to very broad 'R-G' curves (fig.4.26b) with low amplitude. This suggests that the protanomalous 'R-G' response is more difficult to measure than that for the corresponding deuteranomalous subjects (the experimental data for protanomalous subjects show no variation of response with wavelength, fig.4.8).

4.6 Single Anomalous Pigment Model

Several independent attempts have been made to isolate the abnormal 'deuteranomalous' and 'protanomalous' pigments required by the single anomalous pigment model. Rushton, Powell and White (1973b), using the technique of 'exchange

thresholds', measured an abnormal pigment, 'deutanolabe' in their deuteranomalous observers, with peak sensitivity at 555 nm. and 'protanolabe' in their protanomalous observers, with peak sensitivity at 550 nm. Piantanida and Sperling (1973a) measured increment thresholds against a violet background (410 nm) and obtained anomalous pigments peaking at 545 nm (protanomalous) and 560 nm (deuteranomalous).

Pokorny, Smith and Katz (1973) combined colour matching data with a standard shape for the pigment absorption curve to predict a deuteranomalous pigment (λmax at 554.6 nm) and a protanomalous pigment (λmax at 541.6 nm). The data of Pokorny et al (1973) are illustrated in fig.4.29, and have been used to calculate the post-receptoral spectral response functions. Thus the functions 'R-G' and 'G-0.33R' were calculated for all three classes of observer, using the photopigment sensitivities illustrated in fig.4.29, and are plotted in fig.4.30 a and b respectively. Fig.4.30a shows that the 'R-G' response is as expected, with peak sensitivity at 600 nm. The result calculated for deuteranomaly, however, is not the same as that observed with the 8 deuteranomalous subjects in this study (fig.4.12; average data, fig 4.13). The predicted response is similar in shape to the normal but is displaced by 10 nm to longer wavelengths, whereas the observed response is shifted to slightly shorter wavelengths. The predicted protanomalous response is again similar to normal, but with a 10 nm shift to shorter wavelengths. The 'G-0.33R' mechanism is difficult to predict as data is only available for wavelengths $>$ 530 nm. The deuteranomalous response is again shifted to longer wavelengths; this time by 20 nm to peak at 550 nm (fig.4.30b). This is not consistent with the response curves of the two

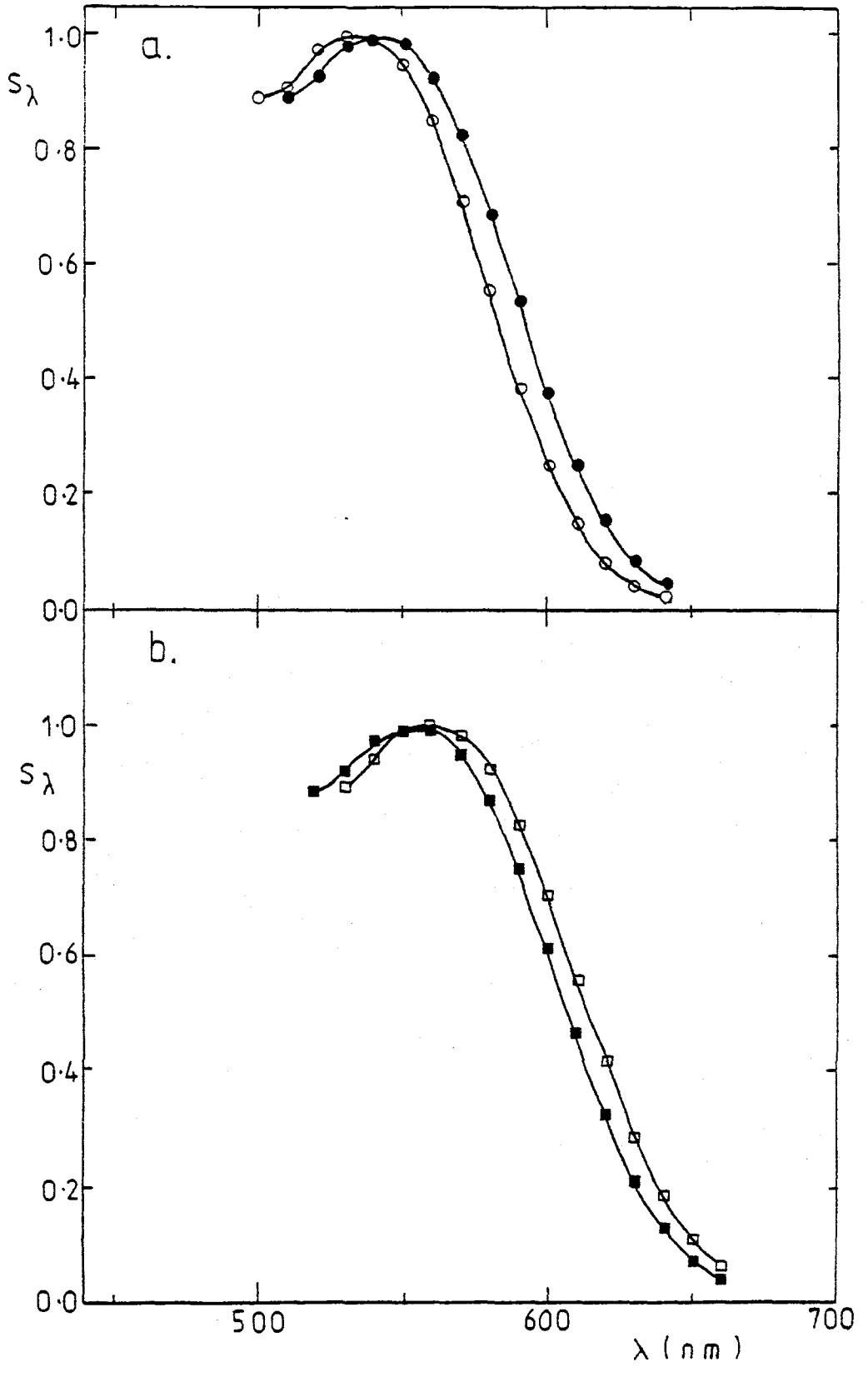


Fig.4.29 Normalised sensitivity as a function of wavelength for the middle - and long - wavelength sensitive pigments.
a, protanomalous trichromats
b, deuteranomalous trichromats
From Pokorny, Smith and Katz (1973)

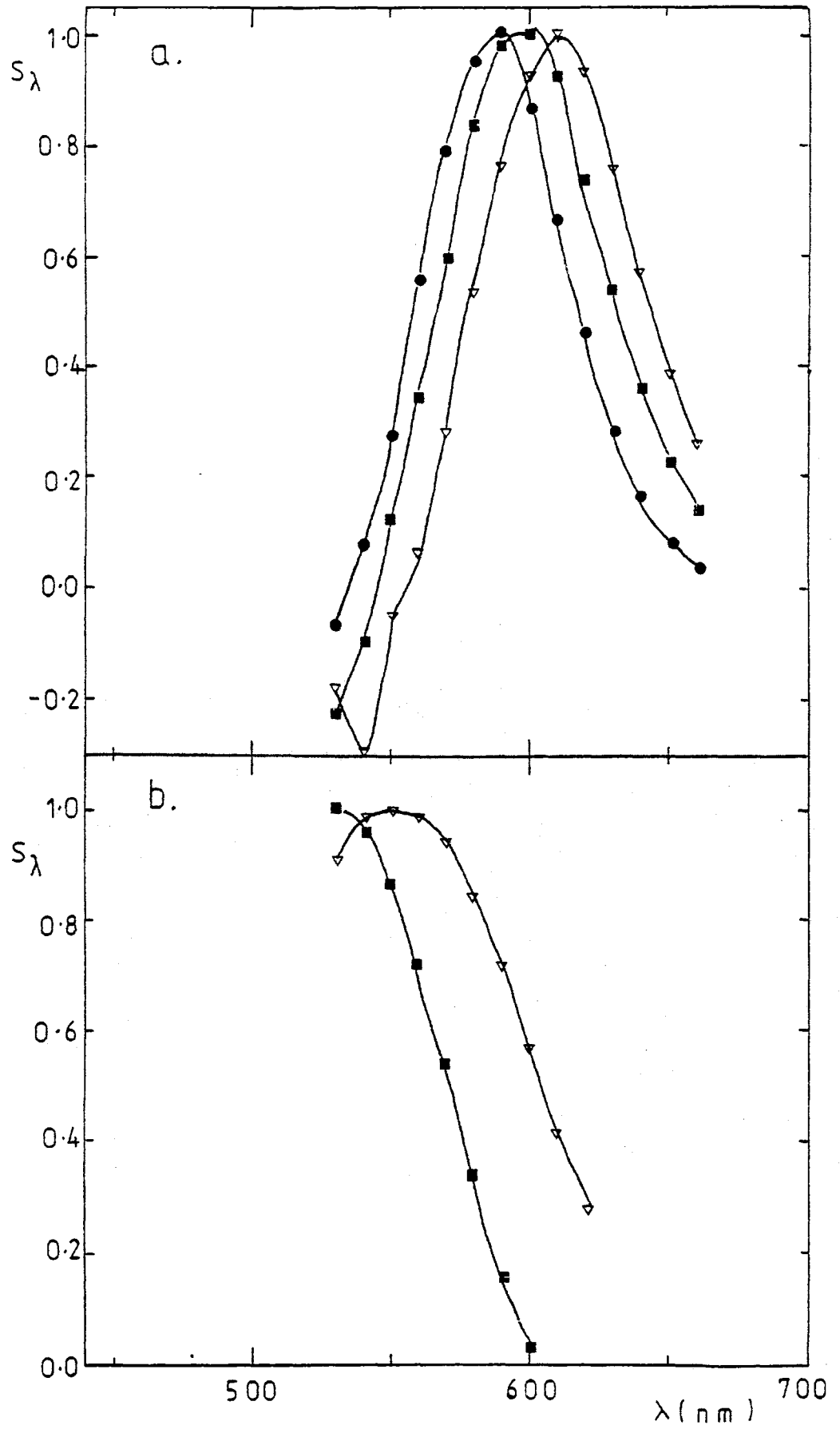


Fig.4.30 Normalised sensitivity curves predicted for (a) the 'R-G' mechanism and (b) the 'G-0.33R' mechanism by the single-pigment model.
■ using the normal pigments 'R' and 'G'.
▽ using the deuteranomalous pigments 'R' and 'G'
• using the protanomalous pigments 'R' and 'G'.

deuteranomalous subjects who performed this experiment (fig.4.15); one of whom produced a normal response, peaking at 530 nm, whilst the other, who had a more extreme colour deficiency, obtained no wavelength-selective response..

Thus, the single-pigment model does not adequately predict the post-receptoral response mechanisms of either the deuteranomalous or protanomalous subjects. In addition, it fails to predict the variation in anomalous colour matches.

4.7 The "Cluster" Theory of Anomalous Trichromacy

Recent microspectrophotometric experiments on single cones in monkeys have revealed three classes of cone with peak sensitivities at 420 nm, 535 nm and 565 nm (Bowmaker, Dartnall, Lythgoe and Mollon, 1978). The peak sensitivities of 19 'green' cones and 18 'red' cones of 5 different rhesus monkeys are shown in fig.4.31.

Bowmaker and Mollon (1980) suggested that these data made plausible the hypothesis of Alpern and Moeller (1977), i.e. that there are individual variations in the peak sensitivities of 'erythrolabe' and 'chlorolabe' of normal human observers and that in anomalous trichromacy, both long-wave pigments are drawn from the same class. The 'green'-sensitive cone distribution has two maxima, separated by 7 nm, and the'red'-sensitive cone distribution has a maximum with a broad shoulder, spanning 5 nm. Thus, a typical deuteranomalous observer is assumed in this analysis to have two red-sensitive photopigments, with a separation of 7 nm, and a typical protanomalous observer has two green-sensitive photopigments with a separation of 5 nm. The 'R-G' mechanisms calculated for both types of observer are illustrated in fig.4.32 and

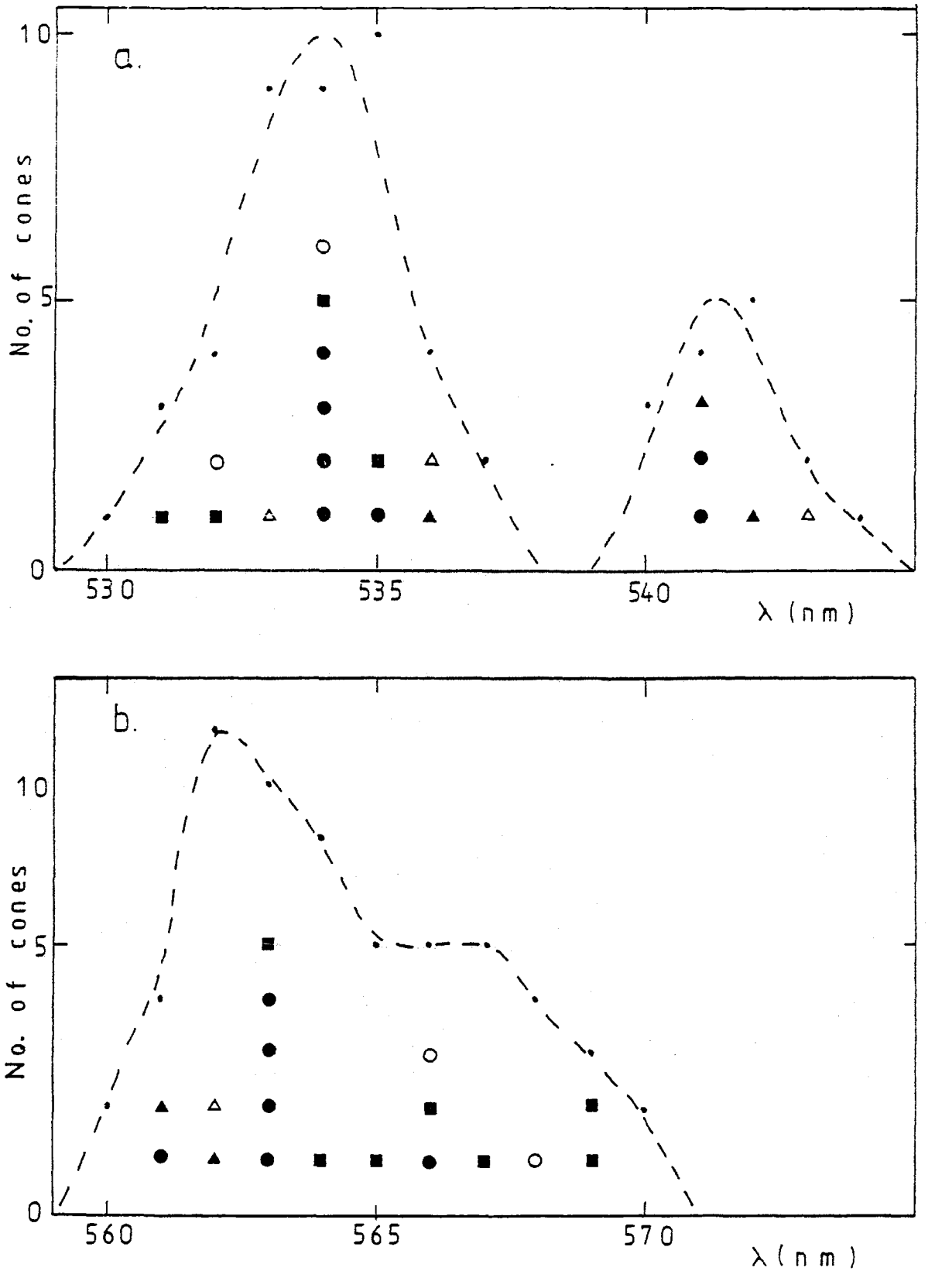


Fig.4.31 Distribution of 19 'green' and 18 'red' cones of rhesus. The symbols represent cones from 5 different animals. The dashed lines are 'running average' curves obtained by averaging the frequencies of cones over 3 consecutive wavelengths. From Bowmaker et al, 1978.

and the 'G-0.33R' mechanism for the 'deuteranomalous' observer is illustrated in fig. 4.33.

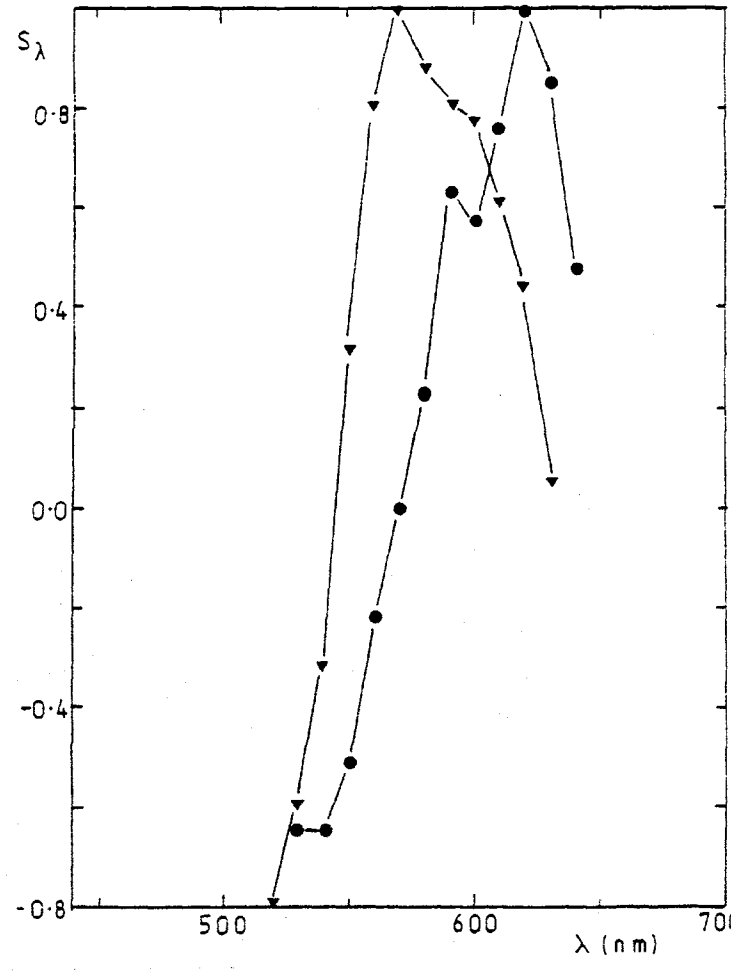


Fig. 4.32 Normalised spectral sensitivity curves for the 'R-G' mechanism predicted by the 'cluster' model. ● deuteranomalous observer, ▼ protanomalous observer.

The predictions of this model are similar to those of the 'single-pigment' model, but more extreme. The 'R-G' spectral response of the deuteranomalous observer is a narrow-band response, with a sharp peak at 620 nm (the experimental data of fig.4.13 shows a maximum sensitivity at 600 nm). The protanomalous response is slightly broader but peaks at 570 nm. The 'G-0.33R'response for deuteranomalous observers has a maxiumum at 565 nm (compared with the experimentally observed maximum at 530 nm,

(fig.4.15) and is rather broad.

This model does not satisfactorily predict the post-receptoral responses obtained with the deuteranomalous or protanomalous observers.

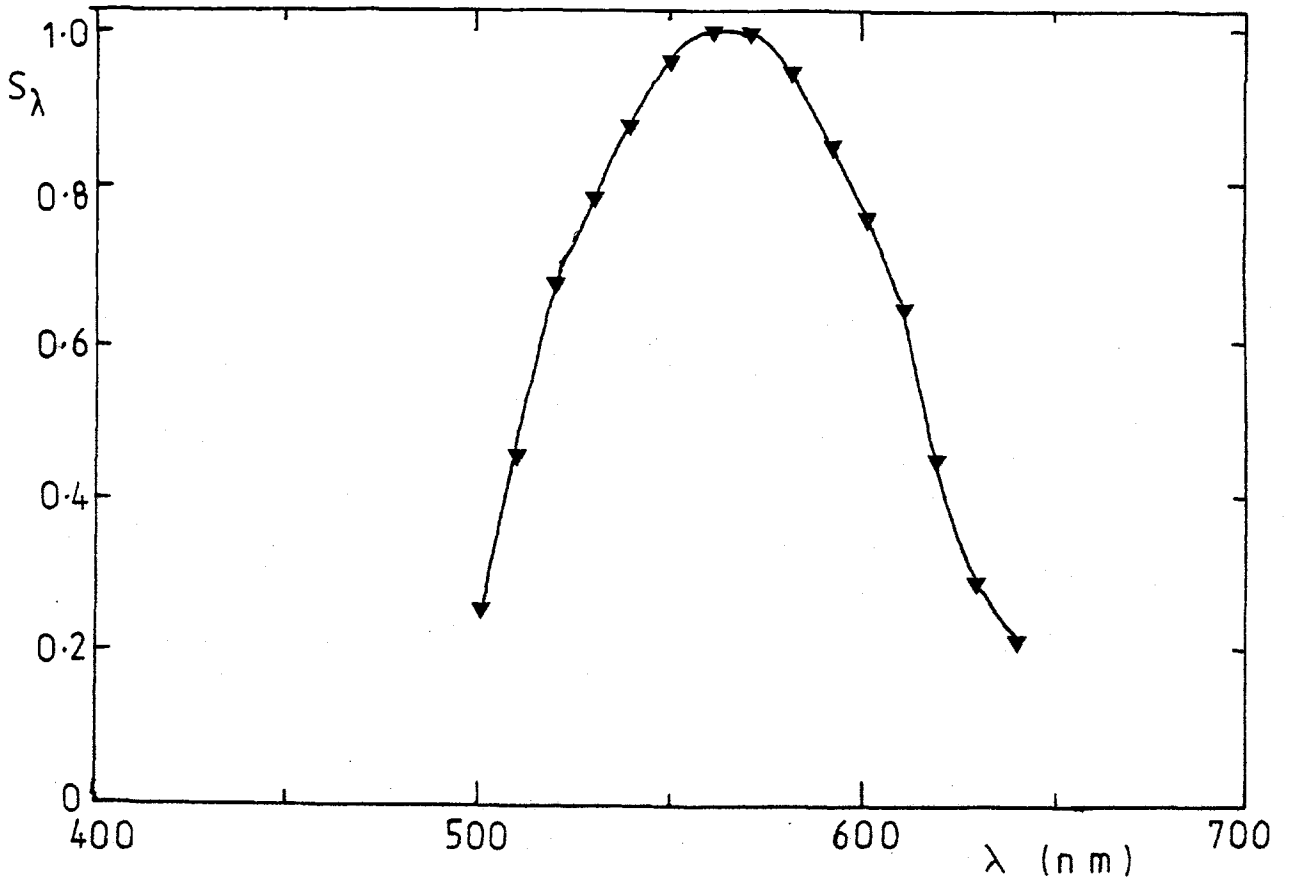


Fig.4.33 Normalised spectral sensitivity curve for the 'G-0.33R' mechanism predicted by the 'cluster' model for deuteranomalous observers.

4.8 Conclusions

The binocular spectral responses of red-green colour defective observers (figs.4 7-4.10; average data, fig.4.11) and the corresponding spectral sensitivity functions (figs. 4.12 and 4.13) have been discussed in terms of the three most plausible hypotheses of anomalous trichromacy: the pigment-mixture model; the single-pigment model; and the 'cluster'

model. None of these models predicts a wavelength-independent 'R-G' response for all protanomalous subjects, although the pigment-mixture model implies that the normal wavelength-dependent response may only be measured for subjects with a very mild degree of protanomaly. The pigment-mixture model also successfully predicts the responses of the deuteranomalous, deuteranopic and protanopic subjects, and has already been shown (Nunn, 1978) to successfully predict colour matching results similar to those of fig.4.17.

The single-pigment and 'cluster' models are unsatisfactory, in that they predict a shift to longer wavelengths of the 'R-G' mechanism for deuteranomalous subjects with respect to the normal responses, whereas the experimental data tend to show a slight shift to shorter wavelengths. They also predict a very different response than normal for the deuteranomalous 'G-0.33R' mechanism, whereas it was found experimentally that one subject, a mild deuteranomal, obtained the normal response, whilst a second subject, a more extreme deuteranomal, obtained no wavelength-dependent response.

CHAPTER FIVE

Visual Responses of a Subject with an Unusual Defect Associated with Chromatic Light Stimuli

Section		Page
5.1	Introduction	157
5.2	The Inhibitory Spreading Effect	161
5.3	Further Visual Threshold Sensitivity Measurements	171
5.4	Temporal Characteristics of the Spreading Inhibition	175
5.5	Conclusions	178

5.1 Introduction

Congenital colour vision defects, such as those described in chapter 4, are caused by abnormal characteristics of the cone photopigments. They result in reduced discrimination and abnormal colour matching, but do not give rise to loss of other visual functions, such as visual acuity. In this chapter, data are presented for a subject who has a rare central colour defect which affects both chromatic and achromatic visual responses.

MW is a 30 year old male who was initially referred to Imperial College by an employer because of problems associated with his colour vision. Extensive ophthalmic investigation revealed no trace of abnormality in the ocular media or fundus and his acuity in black and white corresponds to 6/4 vision in each eye. He has been aware of his abnormal vision since childhood, but there is no record of treatment with unusual drugs, no unusual medical history and no recorded accident. The defect has remained stable throughout the 10 years of study at Imperial College and tests carried out on his family, including a single male offspring, have revealed no other cases of the defect. There is, however, a congenital red-green deficiency in both maternal and paternal families; probably a deutan defect in both cases.

MW's visual responses have been extensively studied (Bender and Ruddock, 1974; Ruddock and Waterfield, 1978) and some of the principal results are now summarised briefly. Fig.5.1 shows the logarithm of foveal threshold sensitivity to a 1^{o} circular test field, log S , as a function of stimulus wavelength , for subject MW and normal subject BB.

MW's sensitivity is suppressed for all near-monochromatic targets compared with that of the normal observer. There is a large loss of sensitivity for wavelengths > 610 nm.

Fig 5.2a shows the increment threshold values I_t, for a 1^o diameter circular test stimulus superimposed on a 7^o diameter circular background field of illumination level I_b. The test and background stimulus wavelengths were the same and data are given for a number of wavelengths. The data show a sudden fall in log I_t which occurs as the background illumination increases beyond a certain critical value, coinciding approximately with that at which the background field becomes visible to MW. The effect is most marked for long-wavelength stimuli. Fig 5.2b shows that when a 650 nm target is presented on backgrounds of varying wavelengths, this characteristic fall in the value of log I_t is observed for all background wavelengths tested, i.e. 440, 530 and 650 nm.

Fig. 5.3 shows the critical fusion frequency (CFF) as a function of the mean illumination level, I, for a 100% square-wave modulated, 40' x 80' test field of wavelength 590 nm. The CFF values for normal observer BB increase continuously to more than 35 Hz, whereas the CFF values for subject MW saturate at 12-15 Hz.

MW's stereoscopic depth perception was investigated with Julesz' (1971) random dot anaglyphs, which are printed in red and green and viewed through red (630 nm) and green (530 nm) interference filters, placed one before each eye. MW could not resolve the single anaglyph elements when viewing through the red filter alone. When viewing through both filters, however, he was able to correctly identify the stereo-images. Thus, MW's fusion of the stereo-images is not influenced by his inability to perceive the 'red' component (Ruddock and Waterfield, 1978).

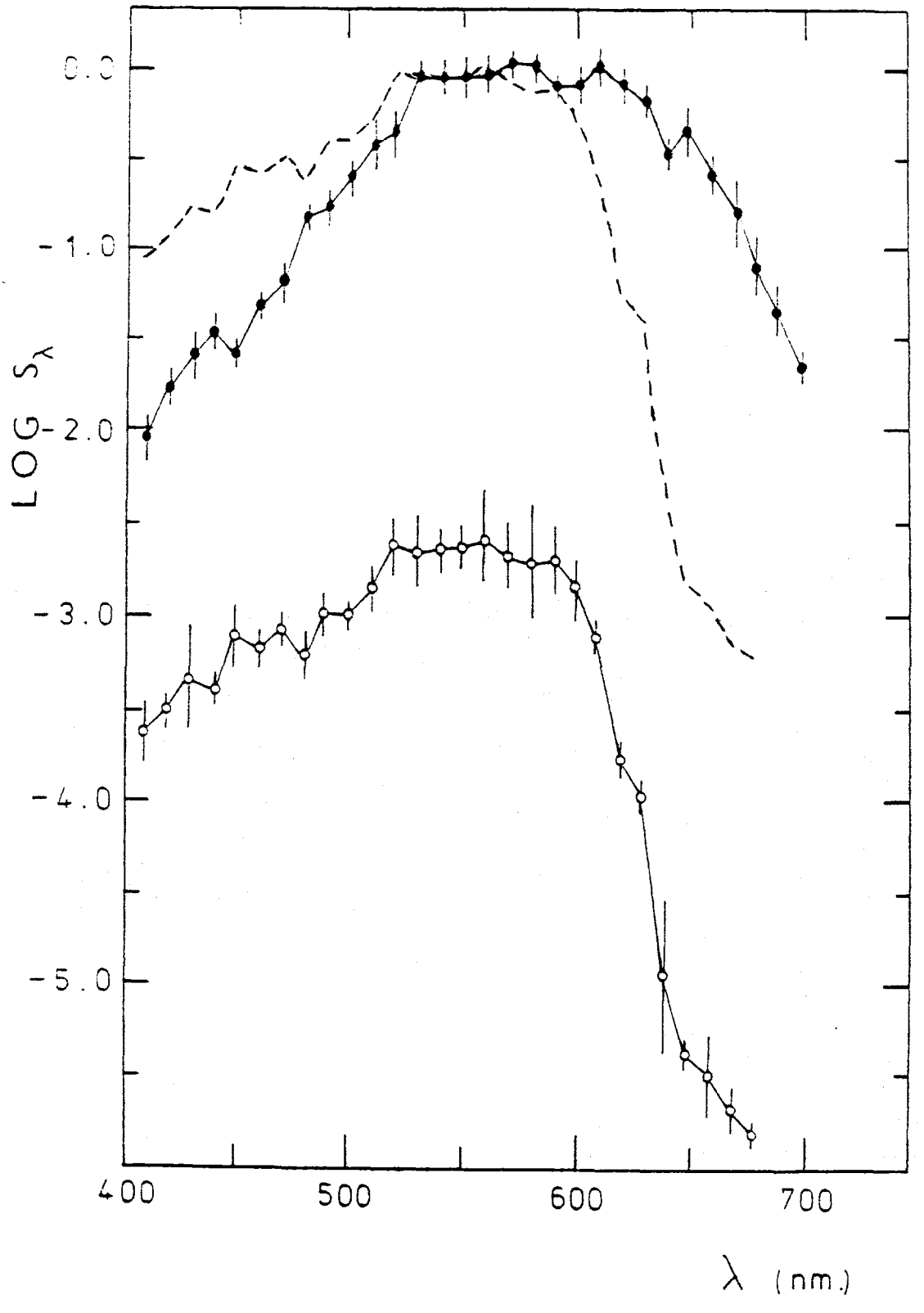


Fig 5.1 Normalised threshold sensitivity, log S_λ, for detection of a foveally fixated, 1^o diameter circular target of wavelength, λ. Sensitivity is in relative units. The target was presented in a $^1/_2$ s on, $^1/_2$ s off, flash and recovery cycle and located by four dim white fixation points forming a square around the target. Each point is the mean of 3 readings and the error bars show the standard deviation. ○ subject MW; ● normal subject BB. The broken line represents MW's data redrawn for comparison. From Bender and Ruddock, 1974.

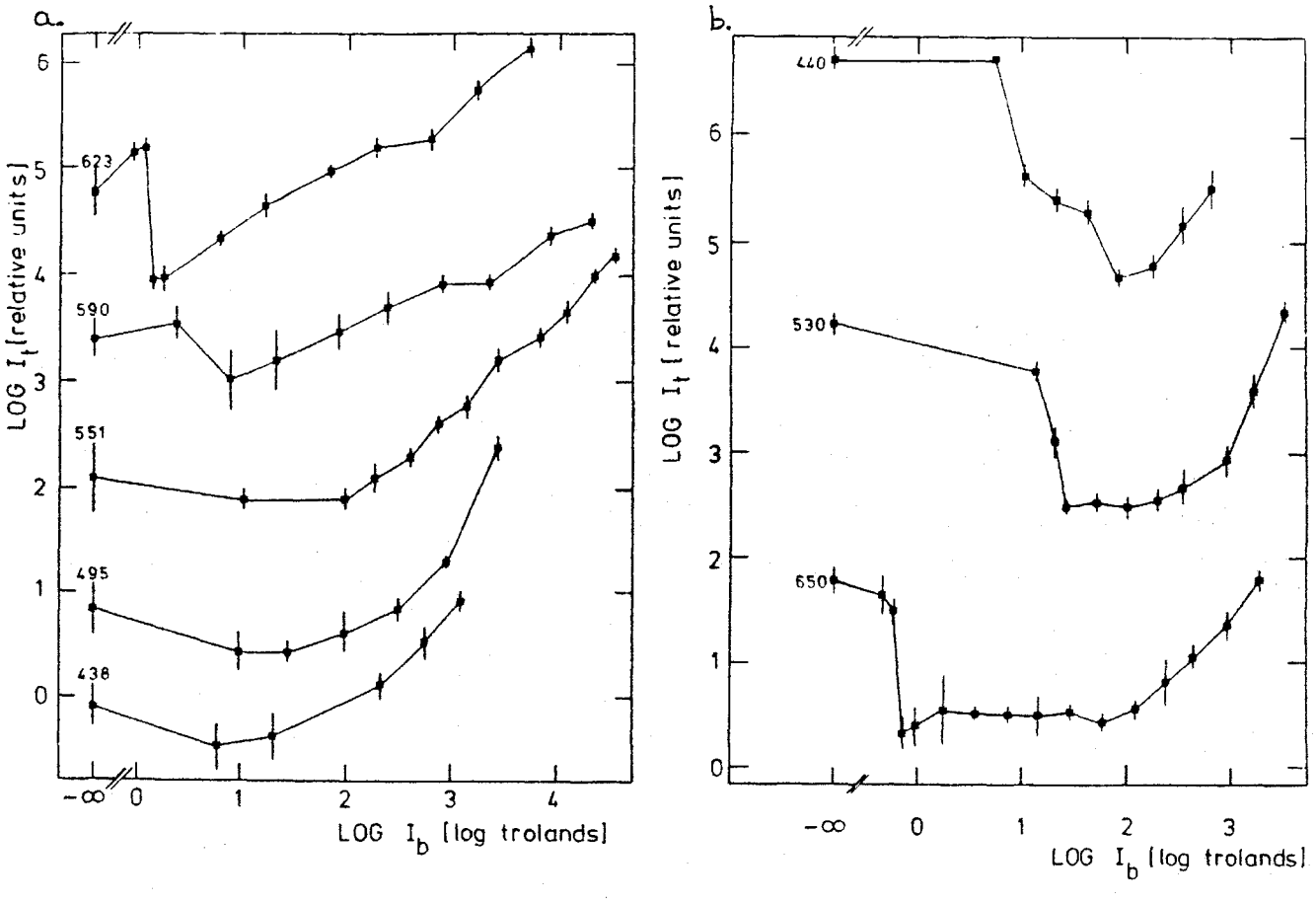


Fig. 5.2a, log threshold illumination level, log I_t, for the detection of a 1^o diameter circular test target, superimposed on a 7^o diameter circular background, is plotted against the background illumination level, log I_b. The wavelengths of the test and background fields were the same for each set of data and the value of this wavelength in nm is given with each set.
b, as in (a) but the test was of wavelength 650 nm in all three cases, and the background wavelengths are marked in nm. Each point is the mean of three readings and the total spread is denoted by the error bars. Subject MW
From Bender and Ruddock, 1974.

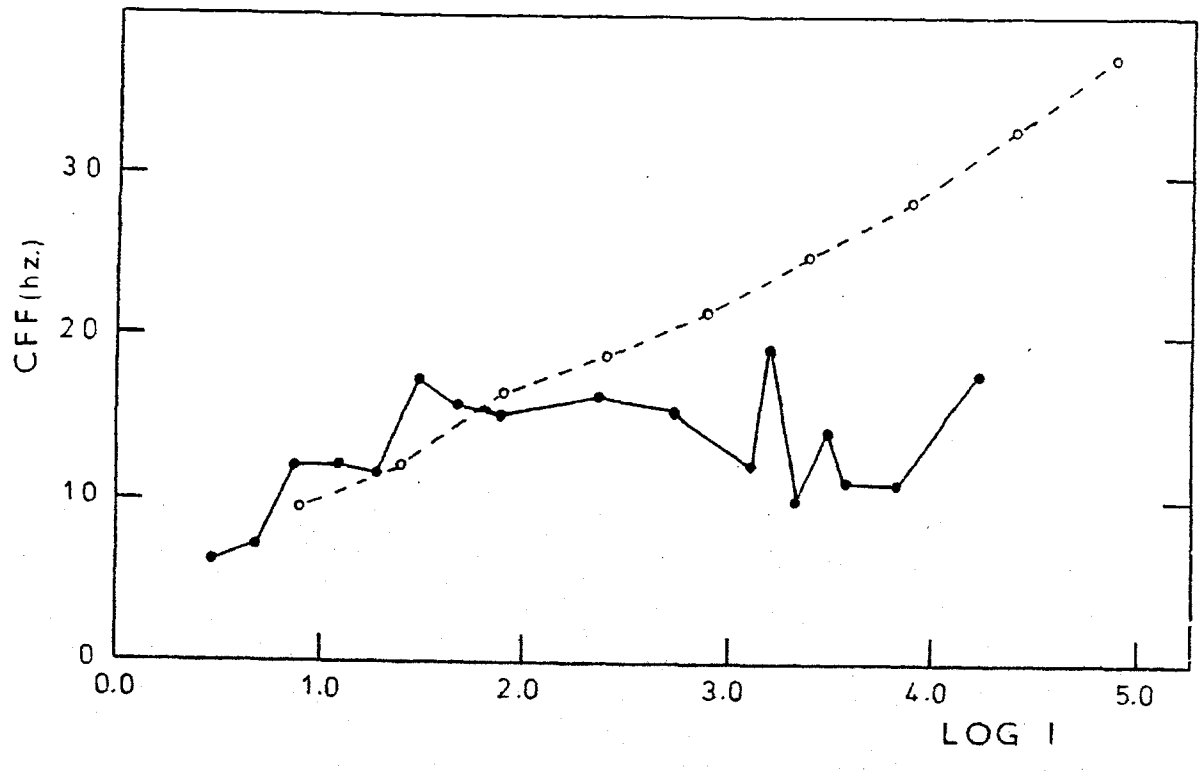


Fig. 5.3 Critical fusion frequency (CFF) for foveal viewing of a 100% square-wave modulated, 40' x 80' test field of wavelength 590 nm and mean illumination level, I. Each point is the mean of 3 readings with typical spread of 2-4 Hz.
● subject MW; O normal subject BB.
Scales of illumination level for the two subjects were adjusted so that log I = 0 defines threshold level for each subject.
From Bender and Ruddock, 1974.

5.2 The Inhibitory Spreading Effect

It had been noted in previous studies (Bender and Ruddock, 1974; Ruddock and Waterfield, 1978) that MW cannot detect small or dim red targets, and when these targets are made larger and brighter, he reports that they appear as a 'diffuse grey area, with a metallic, silvery sheen'. In the new study it was found that his detection of high contrast black and white targets is affected when these targets are either superimposed

on, or located adjacent to, a red surface colour. This is illustrated in fig 5.4 in which MW has sketched the appearance of high contrast black on white targets located near red areas Small red stimuli are undetected (fig 5.4a) but as their size increases they are seen as diffuse grey areas which spread outside the stimulus boundaries (e.g. fig 5.4c). High contrast targets are obscured when located within this grey area (fig 5.4d). The effect also occurs under dichoptic presentation of the stimuli, i.e. when the black and white target is presented to one eye and the red stimulus to the other. The area over which MW perceives the 'silvery-grey' effect depends on the size of the red stimulus; for example, note the difference between fig 5.4d and fig 5.4e.

The variation in the spread of the inhibition with change in size of the red stimulus was examined more quantitatively. Two rows of high contrast black targets, one full and the other open circles, were printed on to a white card. This card was placed against a coloured square, which provided the inhibitory stimulus, as illustrated in fig 5.5.

The subject was asked to identify the position at which the large circular targets could just not be detected (distance l_s from the edge of the inhibitory stimulus) and at which the targets first appeared to have blurred edges (distance l_b from the edge of the inhibitory stimulus). These two distances were determined for a red stimulus card (chromaticity coordinates, x = 0.492, y = 0.316; luminance factor Y = 12.6) in the shape of a square of variable area. The change of the inhibitory area with change in the size of the red card is shown in fig 5.6, in which the inhibitory area, A_i (equal to the stimulus area added to the surround

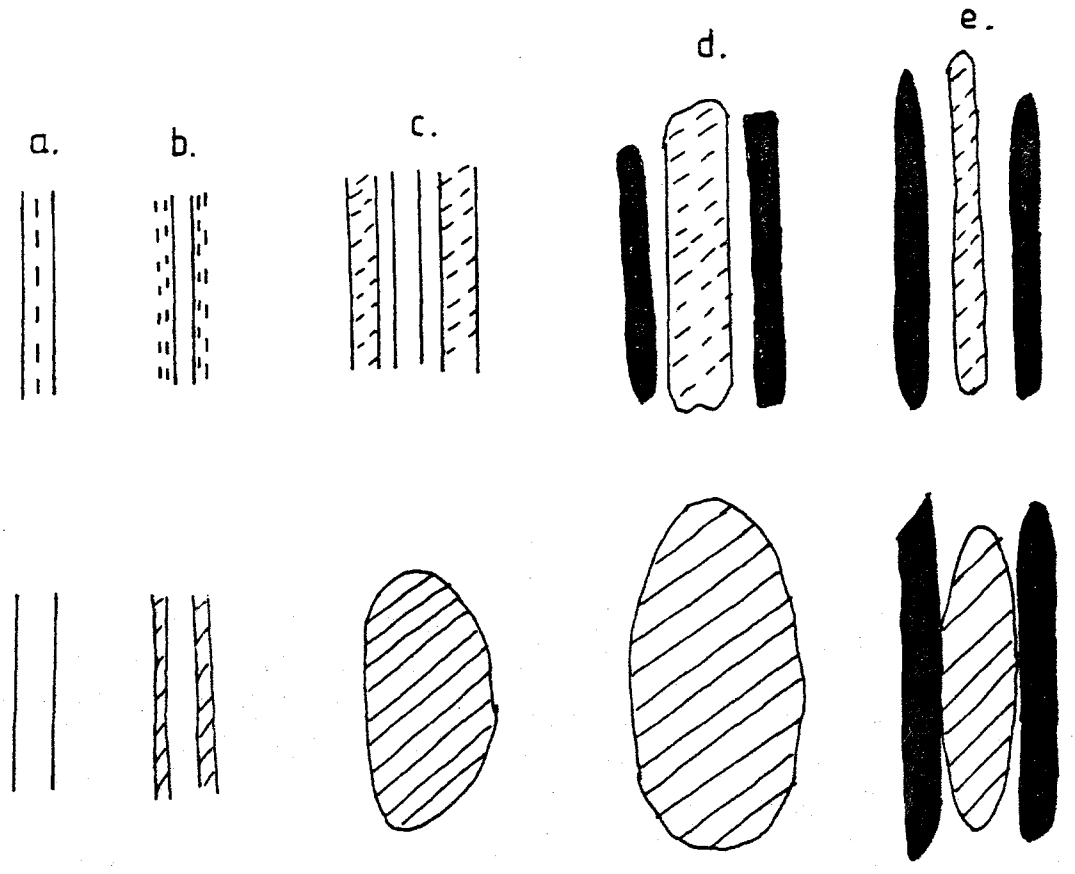


Fig 5.4 The upper row shows a set of 5 stimulus patterns (a-e), consisting of black bars, denoted by the continuous lines or fully shaded areas and red bars, denoted by the broken lines or hatched areas. The lower row shows MW's hand-drawn illustration of the appearance of these patterns; the hatched areas denoted regions which appeared 'silvery-grey' and the fully shaded areas appeared black, with well-defined edges.

area extending to a distance l_s or l_b from the stimulus edge) is plotted against the area of the red inhibitory stimulus, A_s. A_i is linearly related to A_s for much of the range, implying extensive summation over the area of the inhibitory stimulus. It was also noted, however, that when the inhibitory stimulus was an oblong, the inhibition extended further from the short than from the long edge of the stimulus, thus it is not simply area which determines the spread of the effect.

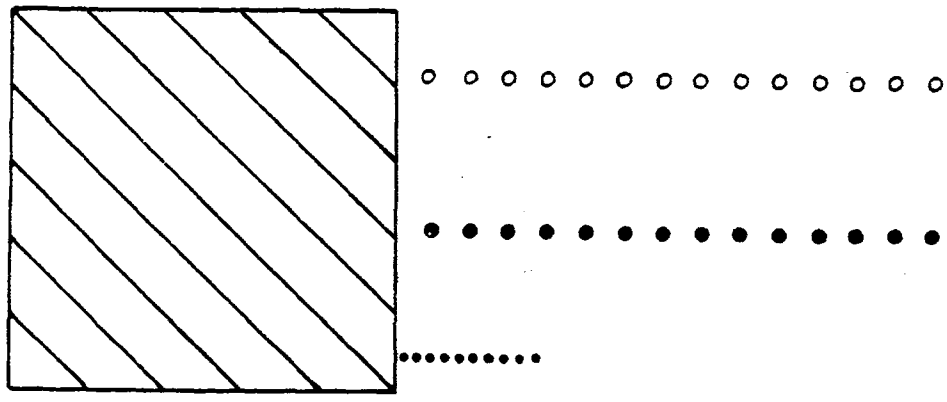


Fig 5.5. illustrates the method used to measure the spread of inhibition around a coloured stimulus, represented by the hatched square. The large full circles and open circles were of 12 min of arc diameter and centre to centre separation 34 min. The small full circles were of diameter 3.4 min of arc.

The dependence of this inhibitory effect on the colour of the stimulus was also investigated. Colour samples from the Royal Horticultural Society colour chart were viewed at a fixed distance, such that they subtended an area of 5^{o} x 3.7^{o} at the subject's eye. The effect was measured as before, using the card illustrated in fig 5.5. The small circular targets (3.4 min diameter) were used for those inhibitory stimuli which gave small effects, in order to obtain more accurate results. The results are illustrated in fig 5.7, in which the different symbols, plotted at points corresponding to the chromaticity of the inhibitory stimulus card on the CIE 2^{o} chromaticity chart (CIE, 1931), indicate the distances over which the inhibition extends from the edge of the colour samples, with zero effect denoted by a full triangle. It can be seen that the inhibitory effect is associated with colours in the red-purple region of the chromaticity chart and is greater for saturated than

desaturated colours. No effect was observed for yellow samples, but there is as small effect for a green (x = 0.266, y = 0.515) and a blue (x = 0.275, y = 0.20) sample.

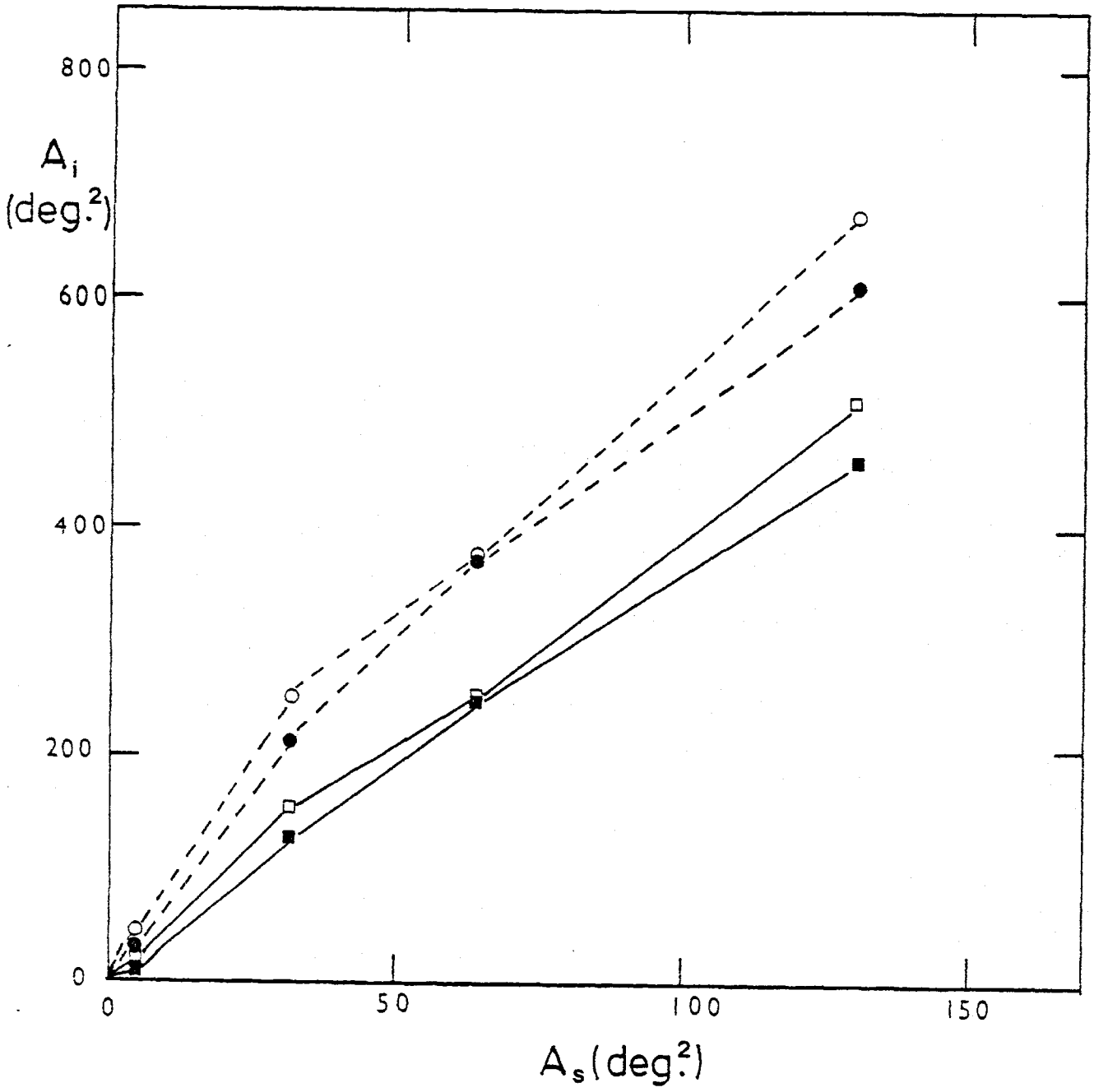


Fig 5.6 The area, A_i, covered by the inhibitory responses plotted against the area of the square inhibitory stimulus, A_s. Squares correspond to the area of a square with side length $(2\,l_s + \sqrt{A_s})$ and circles to the area of a square with side length $(2\,l_b + \sqrt{A_s})$. Data were measured for 12 min diameter circular targets; open symbols for open targets, full symbols for full targets. Subject MW.

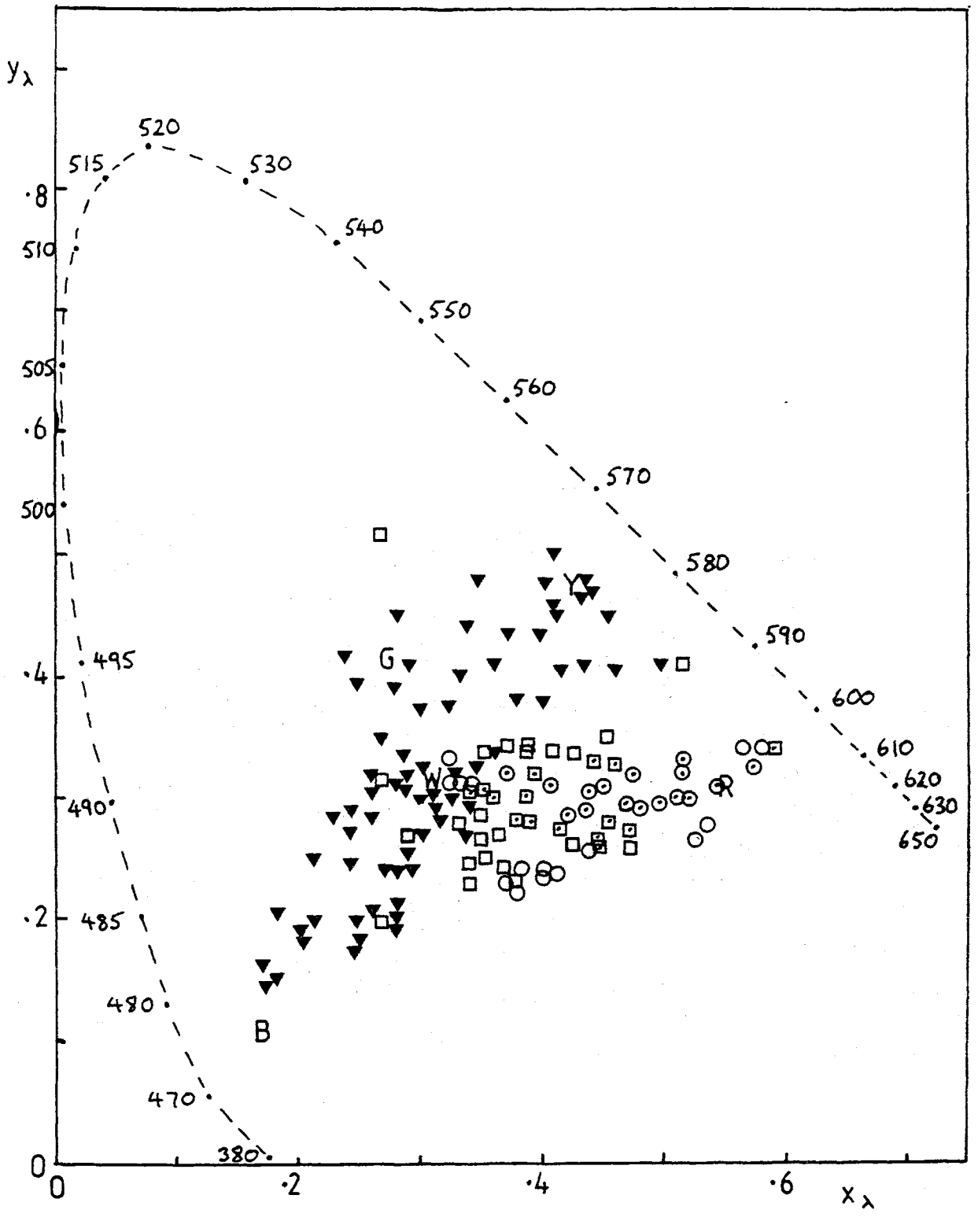
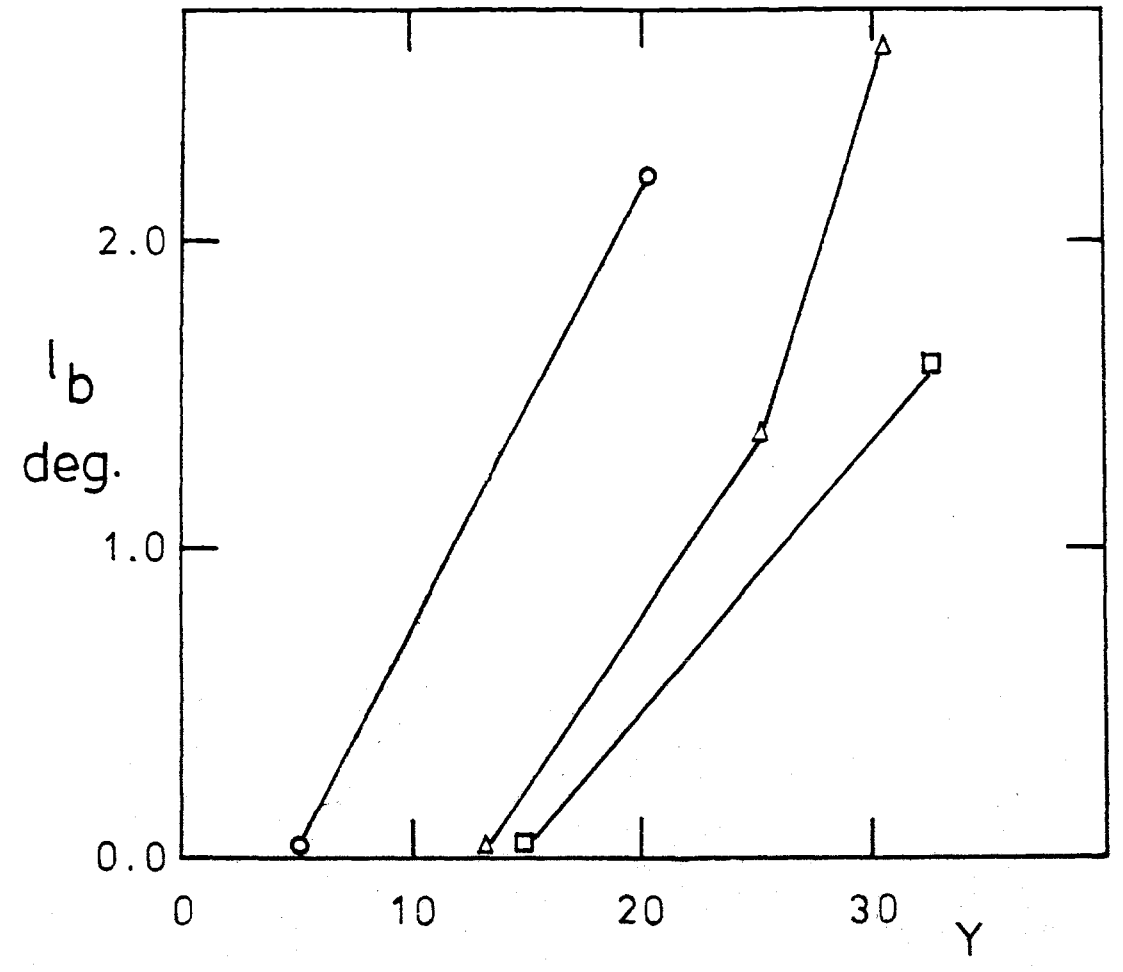


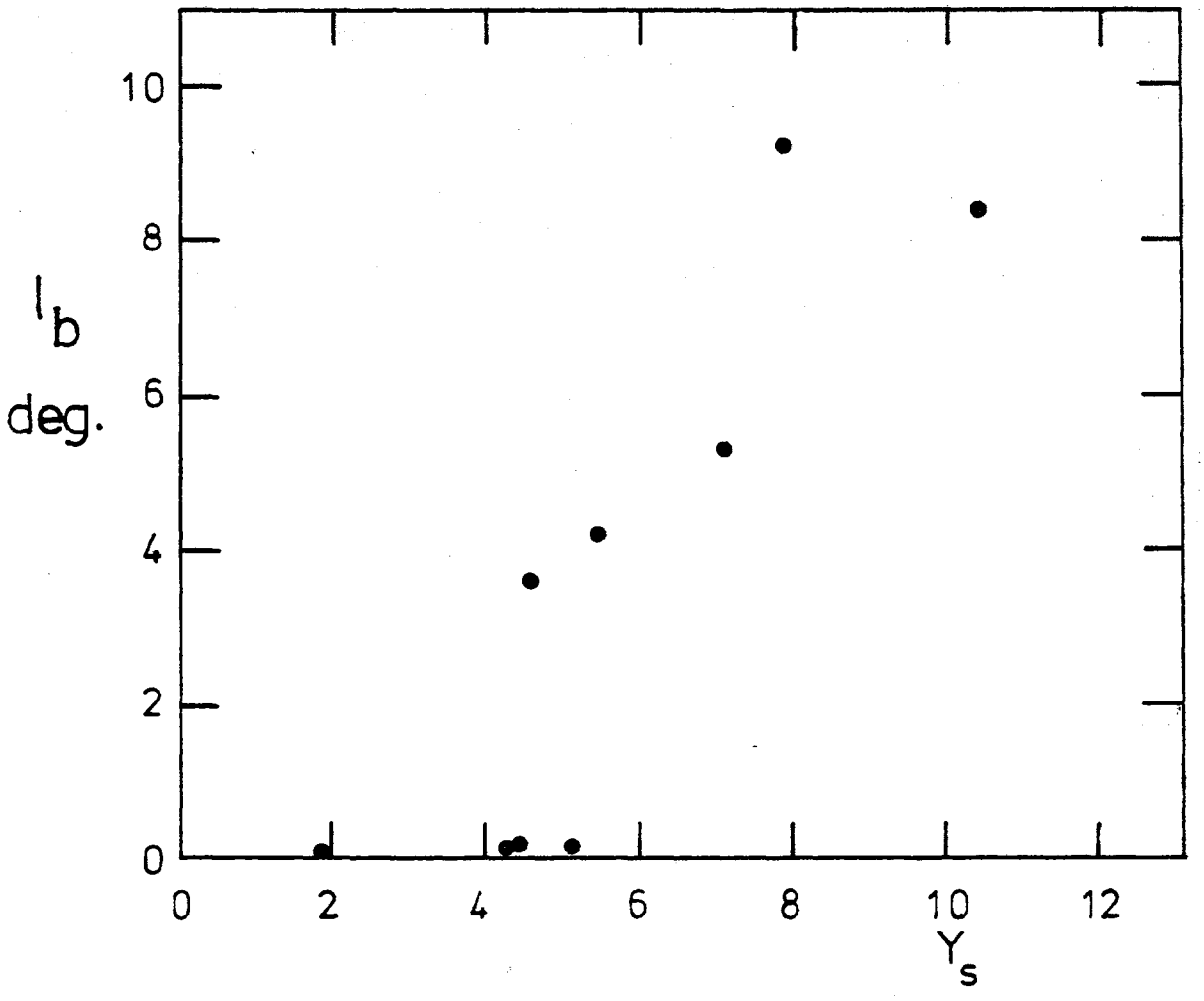
Fig 5.7 CIE 2° x-y chromaticity chart showing the value of l_s for 5 x 3.7 deg stimuli with chromaticity coordinates denoted by the data points. Values of l_s were measured from the short side of the stimulus, for 12 min circular black targets. Different symbols denote different ranges of values of l_s: ⊙, $l_s > 3°$; ⊡, $1.7° < l_s \leq 3°$; ○, $0.23 < l_s \leq 1.7°$; □, $l_s \leq 0.23°$. ▼, zero effect. W denotes the white point (source C). R,G, B and Y are the co-ordinates of four 23.5 x 17 deg stimuli (see text) and the numbers denote the wavelength (nm) of spectral stimuli on the spectrum locus. Subject MW.

To examine the dependence of this inhibitory effect on brightness and saturation, measurements of l_b were made for (i) samples of approximately the same saturation and chromaticity (i.e. constant colour coordinates x and y), but of different luminance factor, Y, the variable which correlates with the apparent brightness of the sample (fig 5.8a), and (ii) samples of constant luminance factor (Y = 12) lying on a straight line between the white point, W, and a fixed point (620 nm) on the spectrum locus (fig 5.8b). The data of fig 5.8a show only the general trend of the relationship between Y and l_b, as the number of available samples with constant chromaticity but different Y-factor was very limited. The data demonstrate, however, that l_b increases as Y increases, i.e. the brighter the sample the greater the spread of the inhibitory effect. The variation of l_b with saturation is illustrated in fig. 5.8b. The degree of saturation is expressed in terms of the variable, Y_s, the luminance of the chromatic component of the desaturated stimulus (see Appendix B). As Y_s, and therefore the saturation, increases, the value of l_b rises rapidly after a threshold value (Y_s = 5) has been exceeded. Thus the spread of the inhibition increases with stimulus saturation.

Fig 5.8a Values of l_b plotted against the luminance factor, y, of the stimulus. Each symbol refers to stimuli with different chromaticity coordinates:
○, x = 0.475, y = 0.296; △, x = 0.423, y = 0.286;
□, x = 0.445, y = 0.330
b. Values of l_b plotted against the luminance factor Y_s (which is a measure of saturation, see Appendix B) of stimuli with constant Y-factor, equal to 12, lying on a line joining the white point, W, to the wavelength 620 nm on the spectrum locus.
Subject MW.

FIG. 5.8





A few check measurements were made with four large (23.5^{o} x 16.5^{o}) colour samples; one red (x = 0.553, y = 0.312, Y = 11.4), one yellow (x = 0.425, y = 0.472, Y = 9), one green (x = 0.274, y = 0.415, Y = 15.8) and one blue (x = 0.167, y = 0.105, Y = 6). The locations of these colours on the CIE chromaticity chart are denoted by R, Y, G and B on fig 5.7. The colour samples were mounted on white card, on which black targets were printed, as illustrated in fig 5.9. The large targets (open squares and full circles) subtended 37.1 min of arc at the subject's eye, and the small targets (open triangles, open squares and full circles) subtended 14.8 min of arc. When viewing the blue and green cards MW had slightly reduced acuity on the coloured area, i.e. the two concentric rings appeared as one, he was unable to perceive the targets located on the border, and the small targets which were located immediately adjacent to the edge appeared blurred. When viewing the red card, MW was unable to perceive any of the targets located with 5^{o} of the edge of the card; outside this distance he could perceive the larger targets only as 'blurred'. All the targets on and adjacent to the yellow card were clearly visible. This is consistent with the results obtained with the smaller samples (fig 5.7), i.e. there is a large inhibitory effect for the red sample, small effects for the green and blue, but no effect for the yellow.

The effect of placing two colours together was also investigated. A large (30.9^{o} x 21.7^{o}) red card (colour coordinates, x = .553, y = .312, Y = 11.4) was used as a coloured background on which four different colour samples were mounted in turn. The coloured targets

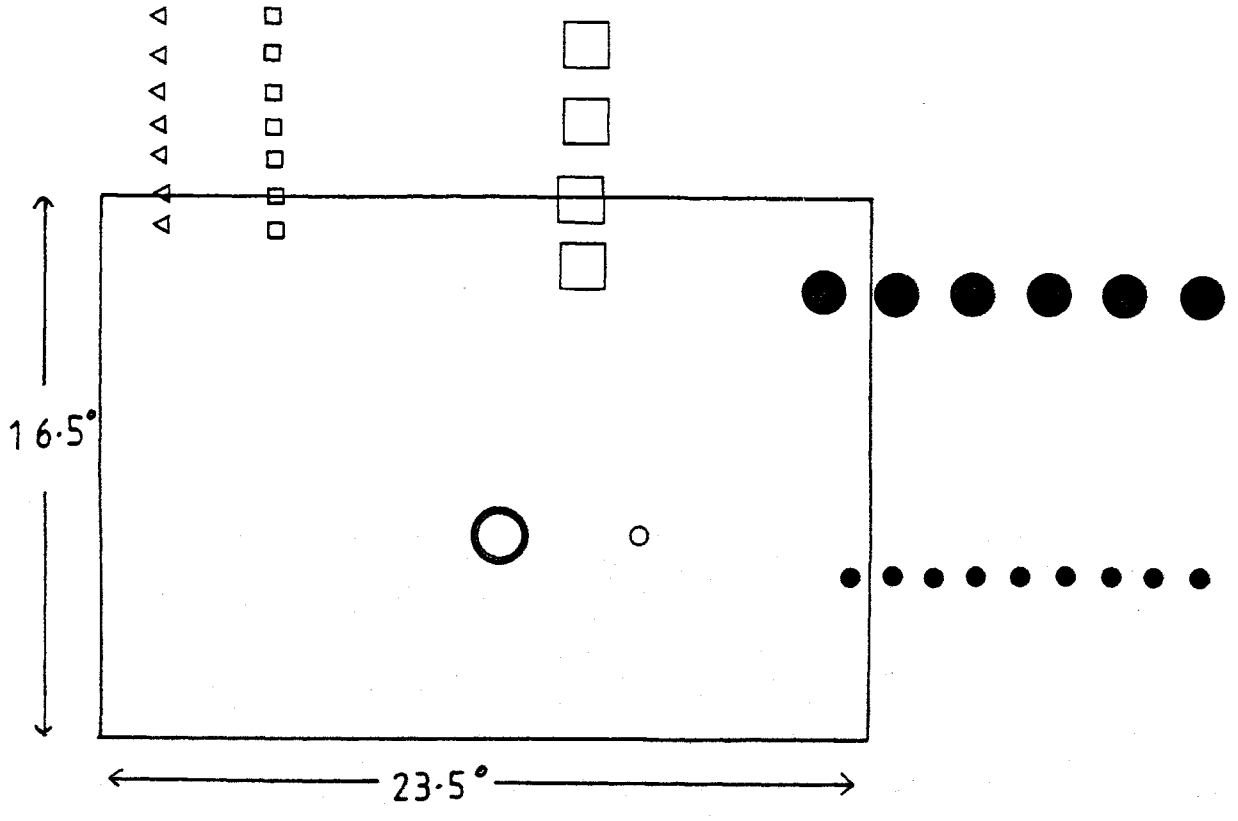


Fig 5.9 Shows one of the large (23.5° x 16.5°) coloured stimulus cards mounted on a white background and the black targets used to check the measurements made with the smaller Royal Horticultural Society colour samples. The large targets subtended 37.1 min of arc at the eye and the small targets subtended 14.8 min.

had dimensions 5° x 3.7°and were blue (x = .175, y = .146, Y = 5.9), green (x = .266, y = .515, Y = 19.2), violet (x = .455, y = .282, Y = 5.6) and yellow (x = .439, y = .473, Y = 63.9). The blue and violet targets were completely unseen by MW and the yellow target was perceived as a very ill-defined "lighter grey" patch. Green, however, was perceived as much better defined, although the edges were still spread out over an area greater than that occupied

by the stimulus, and MW was able to correctly identify the colour. Thus there appears to be some form of selectivity in the detection of the targets superimposed on the red card, which is not simply dependent on the value of 'Y', as the yellow card, which has the largest Y-value, is seen poorly and with no detectable colour, whereas the colour of the green card was detected. It appears, therefore, that there is some form of colour specificity in the target detection, which may reflect colour opponency in the visual pathways. There was, unfortunately, no further opportunity to investigate this effect as the subject was not available.

5.3 Further Visual Threshold Sensitivity Measurements

It has already been shown (fig 5.1) that MW's threshold sensitivity demonstrates a marked loss in the detection of near-monochromatic targets, which is greatest for $\lambda > 610$ nm. Increment thresholds were also measured for a circular white light target of diameter 3.5 deg. flashed for 300 ms once every 3s in the centre of a steady 17 deg. background field, which was either red (636 nm) or white (3000 K). Fig 5.10 shows values of log threshold illumination, log I_t, plotted against log background illumination, log I_b for subject MW and normal subject IH. The two subjects give similar threshold responses for the white background. MW's threshold for the white target on the red background, however, increases much more rapidly than IH's with increase in log I_b. This confirms the results of the previous section (fig 5.7) that red stimuli produce an abnormally large suppression of MW's sensitivity to targets which he can readily perceive in isolation.

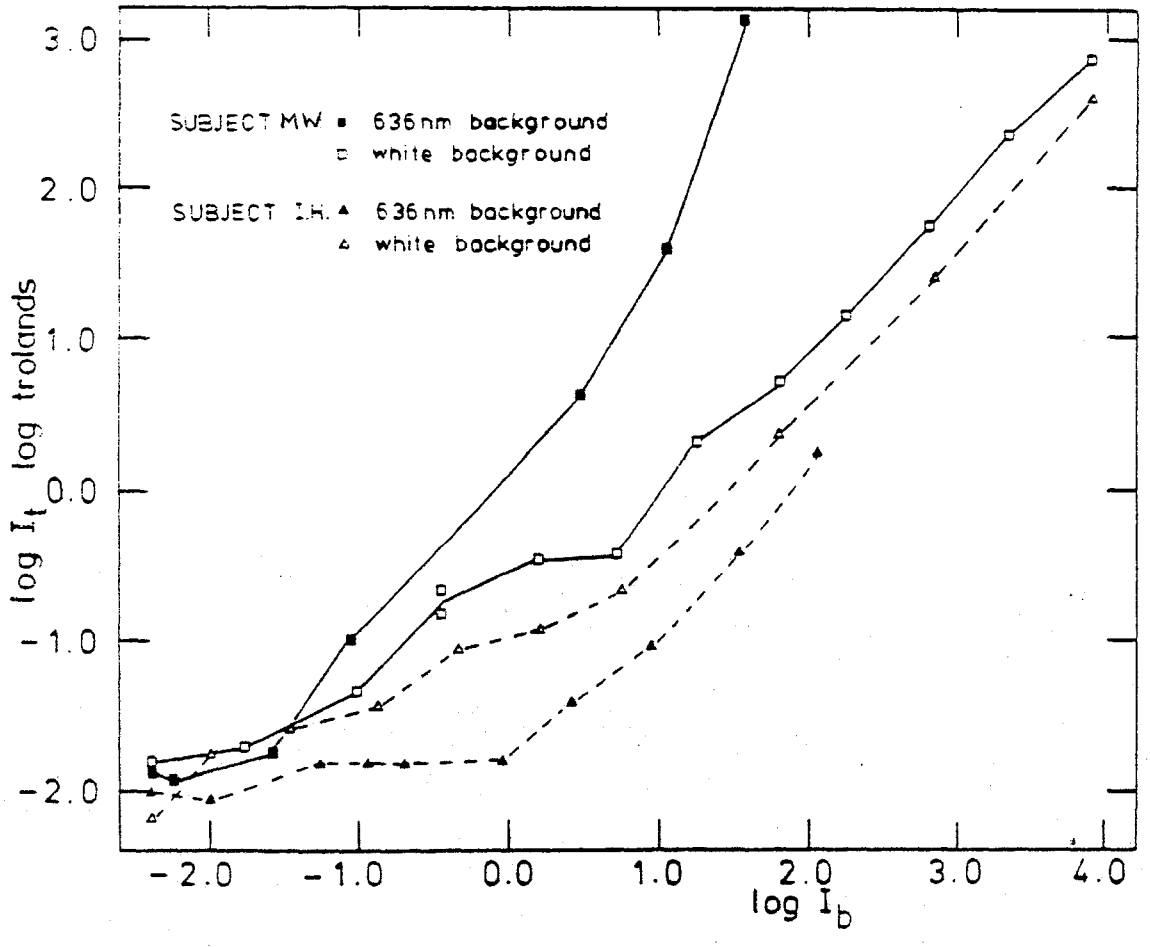


Fig 5.10 Threshold illumination, log I_t for detection of a white 3.5 deg target plotted against the illumination level, log I_b, of the 17 deg background field. Open symbols, white light background; closed symbols, background wavelength 636 nm. Triangles, normal subject IH. Squares, subject MW.

The spatial summation of MW's foveal and non-foveal threshold detection was investigated by measurements of threshold illumination for detection of 635 nm circular targets of different sizes, presented as a 15 ms flash once every 3s. The results are illustrated in fig. 5.11, where log threshold illumination for detection of the target, log I_t, is plotted against the target area, A, and shows that there is no

effective spatial summation in the detection of red light stimuli, either foveally or 30° off-axis. This is in contrast to the inhibitory effect, where considerable spatial summation is observed (fig 5.6).

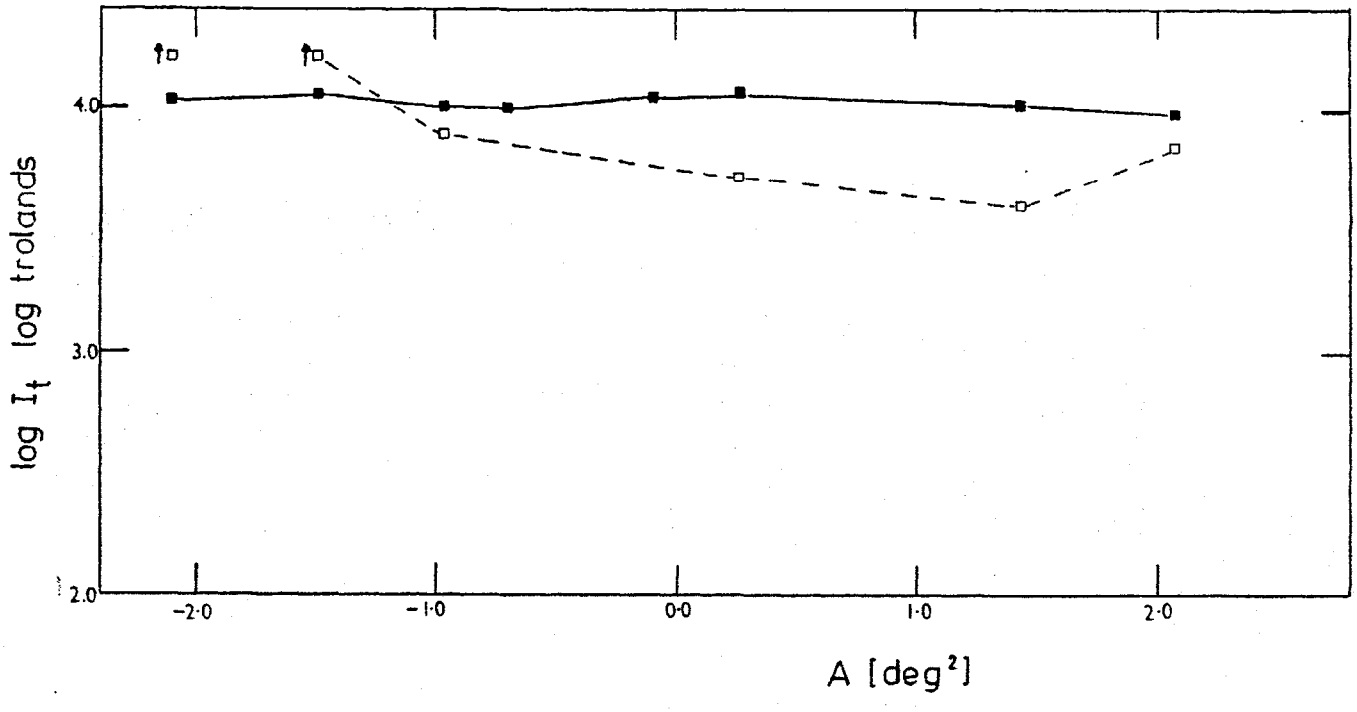


Fig 5.11 Threshold illumination, log I_t for detection of a 635 nm circular target plotted against target area, A. Each point is the mean of 5 readings, with typical standard deviation of 0.03 log units.
■, foveal vision; □, targets located 30° off-axis along the horizontal meridian.
Subject MW.

In order to obtain further data on the spread of inhibition, increment thresholds were also measured for the detection of a green (524 nm) target flashed for 300 ms every 3s, within a steady red (636 nm) or green (536 nm) annulus of illumination level Ia. The results,

illustrated in fig 5.12, show that MW's threshold illumination for detection of the green target is markedly dependent on the illumination level of the surrounding red annulus and, to a lesser extent, on that of the green, whereas for the normal subject IH it is virtually unaffected by the red annulus.

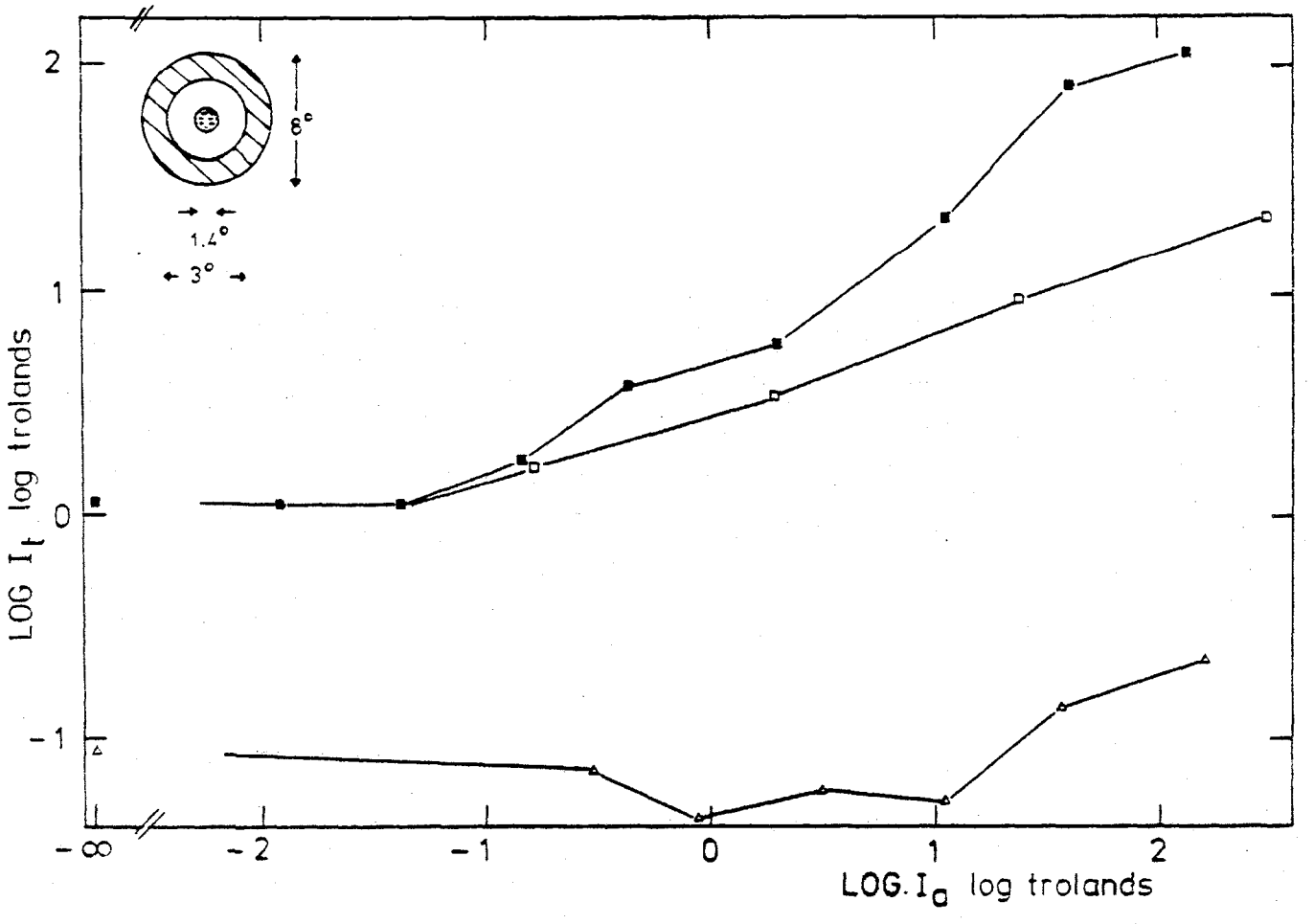


Fig 5.12 Threshold illumination, log I_t, for detection of a 1.4 deg diameter, 524 nm circular target, plotted against the illumination level, log Ia, of a concentric annulus. The inset shows the stimulus configuration. Each point is the mean of 3 readings, with typical standard deviation of 0.03 log units.
■ , subject MW, 636 nm annulus;
□ , subject MW, 536 nm annulus;
△ , normal subject IH, 636 nm annulus.

These results confirm quantitatively that red stimuli interfere with MW's detection of targets located in adjacent regions of the visual field and that the magnitude of the effect depends on the luminance of the red stimulus. They also confirm that the inhibitory effect can be obtained with other monochromatic stimuli, as it is observed with the green annulus, although the effect is greatest for the red annulus.

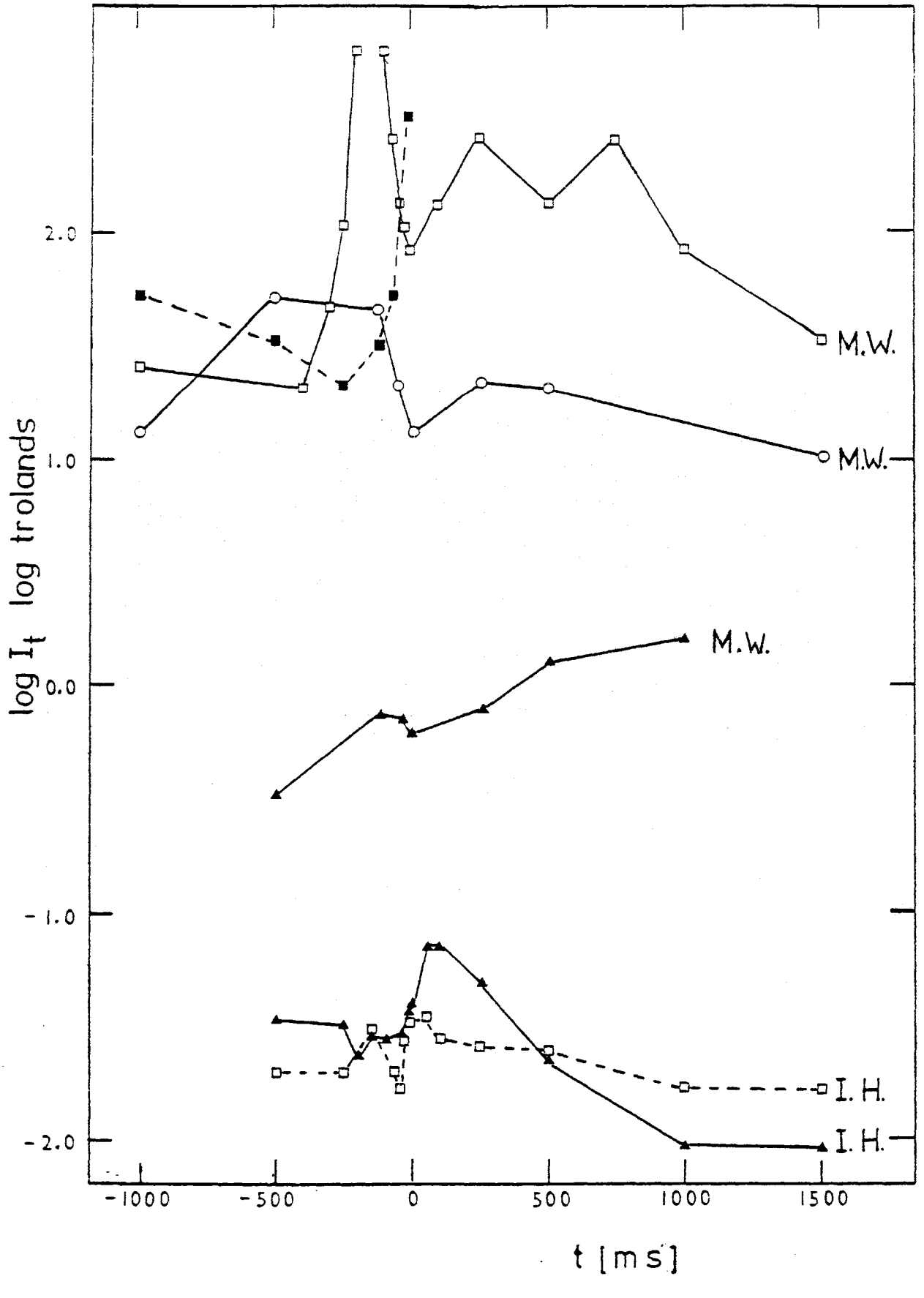
5.4 Temporal Characteristics of the Spreading Inhibition

Measurements of MW's critical fusion frequency (CFF) have shown that his CFF saturates at 12-15 Hz, whereas for normal vision it increases continuously with mean illumination level to a value > 35 Hz (fig 5.3). As red flickering lights cause MW extreme discomfort, the following two-flash experiment was performed. The threshold illumination level for detection of a 20 ms green (524 nm) test flash was measured as a function of delay time between the onset of the test and that of a conditioning flash of 500 ms duration. The 17° diameter circular conditioning field was concentric with the 1.4° diameter circular test flash, and 3 different conditioning colours were investigated; red (635 nm) green (536 nm) and white (3000 K). The results are illustrated in fig 5.13 where log threshold illumination level, log I_t, is plotted against the time delay, τ, between the onset of the two stimuli, with negative values of τ denoting that onset of the test flash precedes that of the conditioning flash. A red conditioning field of illumination level -1.02 log trolands causes a large increase in MW's threshold detection level for values of τ in the range -250 ms to 750 ms. For τ in the range - 200 ms to - 100 ms MW was unable to

detect the green flash at the maximum value of log I_t provided by the instrument. Measurements were also made for a red conditioning field of mean illumination level 2.2 log trolands, but MW was unable to detect the test at any available log I_t level for $\tau > 0$. The green conditioning flashes also influence the threshold values, but to a much lesser extent than the red, and the white conditioning flashes give a very small effect. Data for normal subject IH, plotted for comparison, show a relatively small variation of log I_t with , and his threshold levels for detection of the green flash are much lower than MW's. These results show that MW's threshold for detection of the green flash are significantly different in experiments with coloured conditioning stimuli than in those with white conditioning stimuli. It should be noted that a large inhibitory effect was observed even with a red conditioning field of -1.02 log trolands, which is near to the threshold level. Thus a very strong inhibitory response can be generated by a red conditioning field which is only just visible.

Fig 5.13 Threshold illumination level, log I_t, for detection of a 524 nm, 3.5° diameter test flash of 20 ms duration, plotted against the delay, τ, between the onset of a conditioning test flash of 500 ms duration and the test flash. Negative values of τ denote the test preceding the conditioning stimulus. Each point is the mean of 5 readings, with typical standard deviation 0.1 log units. The two lowest sets of data refer to normal subject IH, the others to subject MW. Different symbols refer to different parameters of the conditioning field:
■ , 636 nm, 2.12 log troland;
□ , 636 nm, -1.02 log troland;
○ , 524 nm, -1.02 log troland;
▲ , white light, -1.1 log troland.

FIG. 5.13


log I_t log trolands
2.0
1.0
0.0
-1.0
-2.0
-1000
-500
0
500
1000
1500
t [ms]
M.W.
M.W.
M.W.
I. H.
I. H.

5.5 Conclusions

In the Introduction to this chapter it was noted that MW's sensitivity in detection of long-wavelength light stimuli is very low and that he makes grossly abnormal threshold settings for monochromatic stimuli, although his acuity for black and white targets is normal. In the present study it has been shown that red light has a considerable inhibitory effect on his vision, such that he is unable to perceive high contrast black and white targets when they are located near a red surface colour. It is shown that this inhibitory effect is observed most readily with red and purple colours, although small effects can be observed with blue and green (fig 5.7). The spread of the effect from the edge of the inhibitory stimulus depends linearly on the area of the stimulus (fig 5.6), and is increased when either the saturation or the brightness of the inhibitory surface colour is increased (fig 5.8).

Measurements of visual threhold sensitivity confirm that red stimuli, and to a lesser degree other monochromatic stimuli, produce an abnormally large suppression of MW's sensitivity to targets which he can readily perceive in isolation (figs 5.10, 5.12). It was also established that there is no effective spatial summation in the detection of red lights (fig 5.11), in contrast to the extensive spatial summation observed with the inhibitory effect.

A possible site of MW's defect is the pre-striate area V4, which contains a high proportion of colour-selective cells (Zeki, 1978). Receptive fields of single neurons in V4 are generally large (up to 5 deg square, Zeki, 1980), but they are not as extensive as is implied by the

spatial summation observed in the spreading inhibition (fig 5.6). Thus it is likely that more central mechanisms are also involved.

CHAPTER 6

Summary and General Conclusions

A method of binocular adaptation which isolates three independent post-receptoral responses in subjects with normal colour vision (Hendricks, Ruddock and Waterfield, 1982) is reviewed in chapter 3. This method involves setting threshold for detection of a test grating after adaptation to a grating (presented to the test eye) and a spot matrix (presented to the non-test eye). The three mechanisms can be represented by linear combinations of the Stiles (1959) π - mechanisms, namely $\pi_5 - \pi_4$, $\pi_4 - 0.33\pi_5$ and π_1. New data are presented which relate the irradiation level of the matrix (for a series of wavelengths) to the threshold for detection of the grating (figs 3.9 3.10) and it is observed that the response curves saturate at different wavelengths. This new method shows that the spectral response curves for the two red/green opponent mechanisms become progressively narrower as the size of the adaptation effect increases, and thus sensitivity functions covering a significant spectral range can be recorded only for small adaptation effects. The binocular organisation of the adaptation effect was also investigated (figs 3.12, 3.13) and a network diagram constructed on the basis of the results (fig 3.14).

Data for congenital red/green colour defective subjects are presented in chapter 4. Wavelength discrimination curves were measured for each subject in order to assess the degree of the defect. The adaptation experiment which isolates the post-receptoral 'R-G' mechanism in normal subjects was performed by 8 deuteranomalous, 4 protanomalous,

3 deuteranopic and 2 protanopic subjects. The deuteranomalous subjects (fig 4.7, average data fig 4.11a) yield response curves that are similar to those for normal subjects, but with a slight shift in some cases to shorter wavelengths. The protanomalous, deuteranopic and protanopic subjects (figs 4.8 - 4.10) all give responses that are wavelength-independent. Four deuteranomalous subjects also carried out colour matching experiments, in which they established Rayleigh matches under adaptation to a series of bleaching lights of different illumination levels. The 'deuteranomalous' colour matches approached the colour matches of two normal subjects at high bleaching levels of 4.5 - 5.0 log trolands (fig 4.16).

The adaptation data for the colour defective subjects was analysed in terms of three different models of anomalous trichromacy: the pigment-mixture model (Ruddock and Naghshineh, 1974); the single anomalous pigment model (Mitchell and Rushton, 1971; Alpern and Torii, 1968; Piantanida and Sperling, 1973a, b; Pokorny, Smith and Katz, 1973); and the 'cluster model' (Alpern and Moeller, 1977; Alpern, 1979). The pigment-mixture model which asserts that anomalous trichromats possess the three 'normal' photopigments with one set of cones containing a mixture of two pigments, predicts that the 'R-G' response curves for both protanomalous and and deuteranomalous subjects are similar to normal, but flatten out and shift to shorter wavelengths as the degree of the deficiency increases, which is consistent with the results observed in the deuteranomalous case. The absence of any wavelength-dependent responses in the protanomalous subjects can be explained qualitatively by the fact that large proportions of the 'green' photopigment are required in the protanomalous 'red'

cones to predict the colour matching results (Ruddock and Naghshineh, 1974). The single anomalous pigment model and the 'cluster' model both predict anomalous 'R-G' responses which shift to longer wavelengths, which is inconsistent with the observed data. Thus, the pigment-mixture model of anomalous trichromacy is the only one of the three examined which is capable of predicting the experimental results presented in chapter 4.

In chapter 5, the visual responses of MW, a subject with an unusual defect associated with chromatic light stimuli, were examined. MW's thresholds for red targets are much higher than normal (fig 5.1) and it was discovered that red stimuli induce a spreading inhibition which can obscure black and white targets located on or adjacent to the red stimulus (fig 5.4). The magnitude of this inhibitory effect depends linearly on the area of the stimulus (fig 5.6). The inhibitory effect can also be obtained with blue and green stimuli, but the effect is much greater for red and purple stimuli (fig 5.7) and increases with both saturation and brightness. Data for a two-flash experiment (fig 5.13) show that presentation of a red conditioning stimulus can influence the detection of a test flash presented 250 ms - 750 ms before the conditioning flash. It is argued that MW's abnormal visual responses must arise at some central point in the visual system; possibly the pre-striate area V4 (Zeki, 1978),although the spread of the inhibitory effect is greater than that expected from the receptive field sizes of V4 neurones.

APPENDIX A

Data Recording Circuit

In the Maxwellian optical system (fig 2.2), the position of the neutral density wedge was monitored by recording the voltage on the wiper of a 10-turn potentiometer, which was connected by gears to the wedge and had a constant applied voltage. The output from the wiper was measured on a digital multimeter (DANA, model 3800B) and recorded on a digital printer (CREDSHIRE, model DP100). Fig A.1 shows the circuit used to sample the voltage reading on the multimeter and to record it on the printer.

The observer records the position of the wedge by pressing either of two switches, S1 or S2. These two switches are debounced with two monostable multivibrator circuits TTL type 74121, and the active low outputs of these devices are logically NOR'd together using a 7400 NAND gate to clock the counter unit and trigger a further monostable to generate a pulse for the multimeter (DMM) 'read' line. A second NAND gate output is inverted and used to trigger another monostable to drive the printer 'print' line. The output from the debounced switch S1 also triggers the printer 'R/B shift' timing monostable to give an active low output pulse. Thus the observer can initiate two print sequences: 'print red' or 'print black'. A third switch, S3, initiates the 'paper feed' sequence on the printer.

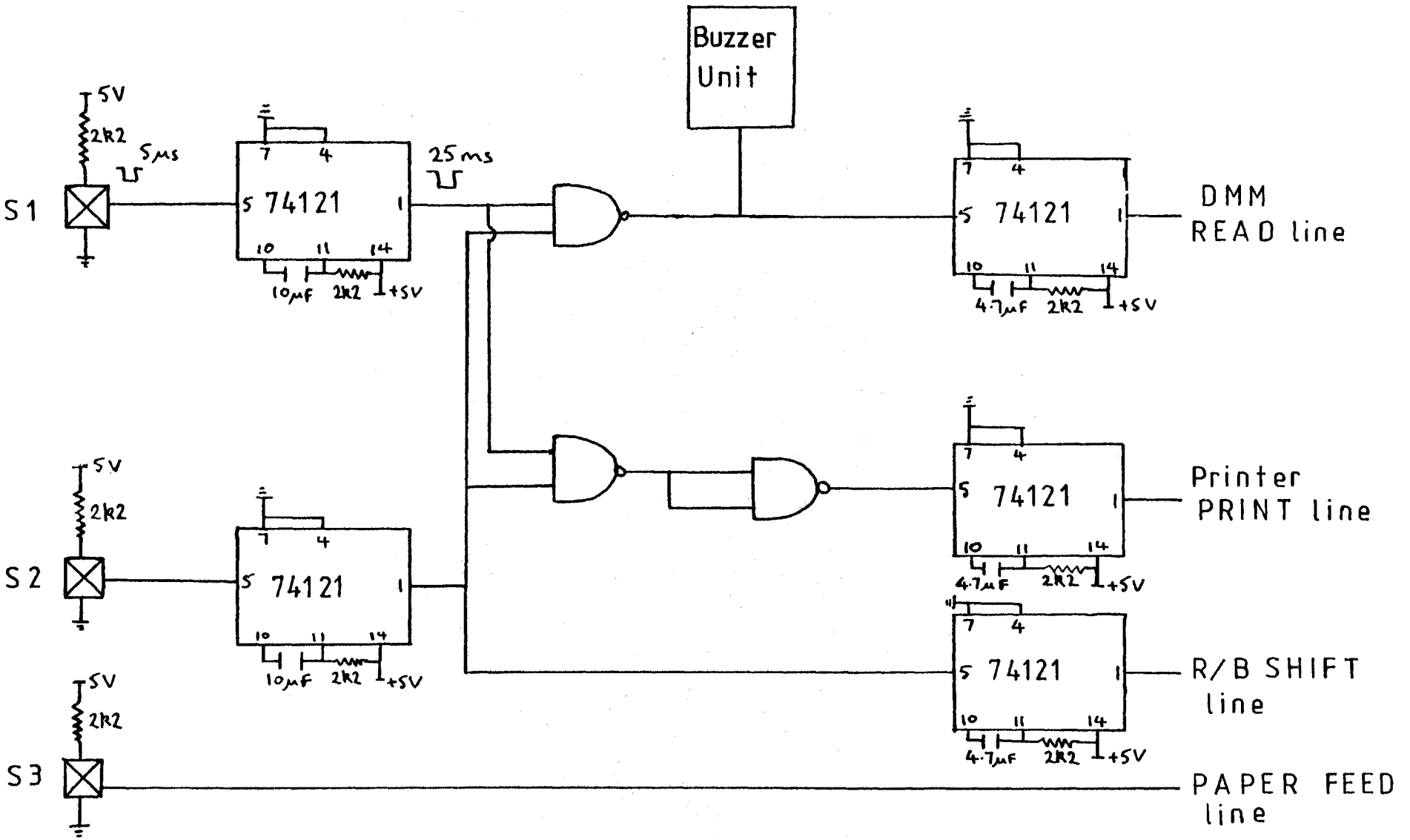


Fig. A.1 Circuit diagram

APPENDIX B

Representation of a desaturated stimulus in terms of chromatic and achromatic components

In order to examine the effect of changes in stimulus saturation on the spreading inhibition exhibited in the visual responses of subject MW, the luminance, Y_S, of the chromatic component of a desaturated stimulus was derived. It is assumed that a desaturated colour (x,y) is represented by a combination of white (x_W, y_W) and a saturated colour (x_S,y_S). If the tristimulus values of the white and saturated stimuli are X_W, Y_W, Z_W and X_S, Y_S, Z_S, respectively, then:

$$x_W = \frac{X_W}{X_W+Y_W+Z_W} \quad , \quad y_W = \frac{Y_W}{X_W+Y_W+Z_W} \qquad \text{Equations B.1}$$

$$x_S = \frac{X_S}{X_S+Y_S+Z_S} \quad , \quad y_S = \frac{Y_S}{X_S+Y_S+Z_S} \qquad \text{Equations B.2}$$

and, by addition of the two colours,

$$x = \frac{X_W+X_S}{X_W+Y_W+Z_W+X_S+Y_S+Z_S} \quad , \quad y = \frac{Y_W+Y_S}{X_W+Y_W+Z_W+X_S+Y_S+Z_S} \qquad \text{Equations B.3}$$

From equations B.1, B.2 and B.3,

$$\frac{x_W}{y_W} = \frac{X_W}{Y_W} = K_W$$

$$\text{and } \frac{x_S}{y_S} = \frac{X_S}{Y_S} = K_S \qquad \text{Equations B.4}$$

where K_W and K_S are constants for fixed values of x_S, y_S, x_W and y_W.

From equation B.3,

$$\frac{x}{y} = \frac{X_W+X_S}{Y_W+Y_S} = \frac{Y_WK_W+Y_SK_S}{Y_W+Y_S}$$

but $Y = Y_S+Y_W$,

therefore $$\frac{x}{y} = \frac{((Y-Y_S)K_W+Y_SK_S)}{Y}$$

i.e. $$Y_S = \frac{(x/y - K_W)Y}{K_S-K_W}$$ Equation B.5

Y, K_W and K_S are all constant for samples of constant luminance which lie on a straight line between the white point and a fixed point on the spectrum locus. Thus Y_S is proportioned to x/y and gives a measure of the saturation of the samples.

REFERENCES

- ALPERN, M. (1979) "Lack of uniformity in colour matching". J. Physiol. (Lond.) 288, 85-105.
- ALPERN, M. and MOELLER, J. (1977) "The red and green cone visual pigments of deuteranomalous trichromacy." J. Physiol. (Lond.) 266, 647-675.
- ALPERN, M. and PUGH, E.N. (1977) "Variation in the action spectrum of erythrolabe among deuteranopes." J. Physiol. (Lond.) 266, 613-646.
- ALPERN, M. and TORII, S. (1968) "Prereceptor colour vision distortions in protanomalous trichromacy". J. Physiol. (Lond.) 198, 549-560.
- ALPERN, M. and WAKE, T. (1977) "Cone pigments in human deutan colour vision defects". J. Physiol. (Lond.) 266, 595-612.
- BAGRASH, F.M., KERR, L.G. and THOMAS, J.P. (1971) "Patterns of spatial integration in the detection of compound visual stimuli." Vis.Res.11,635-645.
- BAKER, H.D. and RUSHTON, W.A.H. (1965) "The red-sensitive pigment in normal cones". J. Physiol. (Lond.) 176, 56-72.
- BENDER, B.G. and RUDDOCK, K.H. (1974) "The characteristics of a visual defect associated with abnormal responses to both colour and luminance." Vis. Res. 14, 383-393.
- BLAKE, R. and FOX, R (1974) "Adaptation to invisible gratings and the site of binocular rivalry suppression." Nature 249, 488-490.
- BLAKEMORE, C. and CAMPBELL, F.W. (1969)a. "Adaptation to spatial stimuli". J. Physiol. (Lond.) 200, 11-13.

- BLAKEMORE, C. and CAMPBELL F.W. (1969)b. "On the existence of neurones in the human visual system selectively sensitive to the orientation and size of retinal images." J. Physiol. (Lond.) 203, 237-260.
- BOETTNER, E.A. and WOLTER, J.R. (1962). "Transmission of the ocular media." Invest. Ophthal.1, 776-783.
- BOWMAKER, J.K., DARTNALL, H.J.A., LYTHGOE, J.N., and MOLLON, J.D. (1978) "The visual pigments of rods and cones in the rhesus monkey, Macaca Mulatta." J. Physiol. (Lond.) 274, 329-348.
- BOWMAKER, J.K. and MOLLON, J.D. (1980) "Primate microspectrophotometry and its implications for colour deficiencies." Colour Deficiencies V, 61-64. Ed. G. Verriest.
- BOYCOTT, B.B. and DOWLING, J.E. (1969) "Organisation of the primate retina: light microscopy." Phil. Trans.R.Soc. 225B, 109-184.
- BRINDLEY, G.S. (1953) "The effects on colour vision of adaptation to very bright lights." J. Physiol. (Lond.) 122, 332-350.
- BRINDLEY, G.S. (1970) "Physiology of the retina and visual pathway." Monographs of the Physiological Society, Ed. Davson, H., Greenfield, H.D.M., Writtam, R. and Brindley, G.S. Edward Arnold (Publ.) Camelot Press.
- BRINDLEY, G.S. and RUSHTON, W.A.H. (1959) "The colour of monochromatic light when passed into the human retina from behind." J. Physiol (London) 147, 204-208.
- BROWN, P.K. and WALD, G. (1964) "Visual pigments in single rods and cones of the human retina." Science 144, 45-52.

- BURTON, G.J. and RUDDOCK K.H. (1978) "Visual adaptation to patterns containing two-dimensional spatial structure." Vis. Res. 18, 93-99.
- DALTON, J. ((1798) "Extraordinary facts relating to the vision of colours." Mem. Lit. Phil. Soc. (Manchester) 5, 28-45.
- DARTNALL, H.J.A. (1952) "Visual pigment 467, a photosensitive pigment present in tench retinae." J. Physiol. (Lond.) 116, 257-289.
- DARTNALL, H.J.A. (1957) "The visual pigments." Methuen, London.
- DAW, N.W. (1968) "Colour-coded ganglion cells in the goldfish retina: extension of their receptive fields by means of new stimuli." J. Physiol.(Lond.) 197, 567-592.
- DE MONASTERIO, F.M. (1978)a "Properties of concentrically organised X and Y ganglion cells of Macaque retina." J. Neurophysiol 41, 1394-1417
- DE MONASTERIO, F.M. (1978)b "Centre and surround mechanisms of opponent-colour X and Y ganglion cells of retina of macaques." J. Neurophysiol.41, 1418-1434.
- DE MONASTERIO, F.M., GOURAS,.P. and TOLHURST,D.J. (1975) "Concealed colour-opponency in ganglion cells of the Rhesus monkey retina." J. Physiol. (Lond.) 251, 217-229.
- DE VALOIS, R.L., ABRAMOV, I. and JACOBS, G.H. (1966) "Analysis of response patterns of LGN cells." J. Opt. Soc. Am. 56, 966-977.
- DOWLING, J.E. and BOYCOTT, B.B. (1966) "Organisation of the primate retina: electron microscopy." Proc. Roy. Soc. B. 166, 80-111.

- ENOCH, J.M. and STILES, W.S. (1961) "The colour change of monochromatic light with retinal angle of incidence." Optica Acta 8, 329-358.
- ENROTH-CUGELL, C. and ROBSON, J.G. (1966) "The contrast sensitivity of retinal ganglion cells of the cat.". J. Physiol. (Lond.) 187, 517-552.
- FICK, A.E. (1879) "Die Lehre von der Lichtempfindung." Handbuch der Physiologie. Hermann, L. (Ed.) Vol.3, 139-234.
- FIORENTINI, A. and MAZZANTINI, L. (1966) "Neural inhibition in the human fovea: a study of interactions between two line stimuli." Atti. Ford. Georgio Ronchi 21, 738-747.
- GEERAETS, W.J., WILLIAMS, R.C., CHAN, G., HAM, W.T., GUERRY, D. and SCHMIDT, F.H. (1960) "The loss of light energy in retina and choroid." Arch. Ophthal. 64, 606-615
- GILINSKY, A. (1968) "Orientation-specific effects of patterns of adapting light on visual acuity." J. Opt. Soc. Am. 58, 13-18.
- GOURAS, P. (1968) "Identification of cone mechanisms in monkey ganglion cells." J. Physiol (Lond.) 199, 533-547.
- GOURAS, P. (1969) "Antidromic responses of orthodromically identified ganglion cells in monkey retina." J. Physiol. (Lond.) 204, 407-417.
- GOURAS, P. (1970) "Trichromatic mechanisms in single cortical neurons." Science 168, 489-492.
- GOURAS, P. (1974) "Opponent-colour cells in different layers of foveal striate cortex." J. Physiol (Lond.) 238, 583-602.
- GUILD, J. (1931) "The colorimetric properties of the spectrum." Phil. Trans. Roy. Soc. A 230, 149-187.
- HENDRICKS, I.M., RUDDOCK, K.H. and WATERFIELD, V.A. (1982) "Spectral sensitivity functions of post-receptoral responses in human vision." J. Physiol (Lond.) 331, 17-33.

- HERING, E (1885) "Uber individuelle verschiedenheiten des Farbensinnes." Lotos, Jb. Naturwiss. N.F. 6, 142-198.
- HUBEL, D.H. and WIESEL, T.N. (1960) "Receptive fields of optic nerve fibres in the spider monkey.". J. Physiol. (Lond.) 154, 572-580.
- HUBEL, D.H. and WIESEL, T.N. (1962) "Receptive fields, binocular interaction and functional architecture in the cat's visual cortex." J. Physiol.(Lond.) 160, 106-154.
- HUBEL, D.H. and WIESEL, T.N. (1968) "Receptive fields and functional architecture of monkey striate cortex." J. Physiol (Lond.) 195, 215-243.
- HURVICH, L.M. (1972) "Colour vision deficiencies". Handbook of Sensory Physiology Vol. VII/4 Visual Psychophysics. Jameson, D. and Hurvich, L.M. (Ed.). Springer-Verlag (publ.) Berlin.

  HURVICH, L.M. and JAMESON, D. (1962) "Colour theory and abnormal red-green vision." Documenta Ophthal 16, 409-442.
- INGLING, C.R. and DRUM, B.A. (1973) "How neural adaptation changes chromaticity coordinates." J. Opt. Soc. Am. 63, 369-373.
- ISHAK, I.G.H. (1952) "The photopic luminosity curve for a group of fifteen Egyptian trichromats." J. Opt. Soc. Am. 42, 529-534.
- JAMESON, D. and HURVICH, L.M. (1956) "Theoretical analysis of anomalous trichromatic colour vision." J.Opt.Soc.Am. 46, 1075-1089.
- JULESZ, B. (1971) "Foundations of cyclopean perception." Univ. of Chicago Press.
- KANEKO, A. (1970) "Physiological and morphological identification of horizontal, bipolar and amacrine cells in goldfish retina. J. Physiol.(Lond.) 207, 623-633

- KUFFLER, S.W. (1953) "Discharge patterns and functional organisation of mammalian retina." J. Neurophysiol. 16, 37-68.
- LEBER, T. (1873). "Uber die Theorie der Farbenblindheit und über die Art und Wëse, wie Gewisse, der Untersuchung von Farbenblinden entrommenen einwände gegen die Young-Helmholtz'sche Theorie sich mit Derselben vereinigen lassen." Klin. Mbl. Augenheilk 11, 467-473.
- LENNOX-BUCHTHAL, M.A. (1962) "Single units in monkey, cercocebus Torquatus Atys, cortex with narrow spectral responsiveness." Vis. Res.2, 1-15.
- MACLEOD, D.I.A. and HAYHOE, M. (1974) "Three pigments in normal and anomalous colour vision." J.Opt.Soc.Am. 64, 92-99.
- MAFFEI, L., FIORENTINI, A. and BISTI,S. (1973) "Neural correlate of perceptual adaptation to gratings." Science 182, 1036-1038.
- MARKS, W.B, DOBELLE, W.H. , MacNICHOL, E.F. (1964) "Visual pigments of single primate cones." Science 143, 1181-1183.
- MAUDARBOCUS, A.Y. (1973) "Response characteristics of the human visual system in the detection of spatially periodic stimuli." Ph.D. Thesis. Univ. of London.
- MAUDARBOCUS, A.Y. and RUDDOCK, K.H. (1973) "The influence of wavelength on visual adaptation to spatially periodic stimuli." Vis. Res. 13, 993-998.
- McKEON,W.M. and WRIGHT, W.D. (1940) "The characteristics of protanomalous colour vision." Proc. Phys. Soc. 52, 464-479.
- MICHAEL, C.R. (1968) "Receptive fields of single optic nerve fibres in a mammal with an all-cone retina III : opponent-colour units.". J. Neurophysiol. 31, 268-281.

- MICHAEL, C.R. (1978) "Colour vision mechanisms in monkey striate cortex: dual-opponent cells with concentric receptive fields." J. Neurophysiol. 41, 572-588.
- MITCHELL, D.E. and RUSHTON, W.A.H. (1971) "Visual pigments in dichromats." Vis. Res. 11, 1033-1043.
- NAGHSHINEH, S. and RUDDOCK, K.H. (1978) "Properties of length-selective and non-length-selective adaptation mechanisms in human vision." Biol. Cybern. 31, 37-47.
- NELSON, J.H. (1938) "Anomalous trichromatism and its relation to normal trichromatism." Proc. Phys. Soc. 50, 661-702.
- NUNN, B.J. (1978) "An investigation into the spectral characteristics of metacontrast phenomena and of adaptation effects in human vision." Ph.D.Thesis Univ. of London.
- NUNN, B.J. and RUDDOCK, K.H. (1978) "Effects of adaptation to bright lights on anomalous trichromatic colour vision". Mod. Probl. Ophthal. 19, 218-221.
- OIKAWA,T., OGAWA, T. and MOTOKAWA, K (1959) "Origin of so-called cone action potential." J. Neurophysiol 22, 102-111
- PADMOS, P. and NORREN, D.V. (1975) "Cone systems interaction in single neurons of the LGN of the Macaque." Vis. Res. 15, 617-619.
- PANTLE, A.J. and SEKULER, R.W. (1968) "Velocity-sensitive elements in human vision. Initial psychophysical evidence." Vis. Res.8, 445-450.
- PANTLE, A.J. and SEKULER, R.W. (1969) "Contrast response of human visual mechanisms sensitive to orientation and direction of motion". Vis. Res. 9, 397-406.
- PIANTANIDA, T.P. and SPERLING, H.G. (1973)a. "Isolation of

a third chromatic mechanism in the protanomalous observer." Vis.Res. 13, 2033-2047.

- PIANTANIDA,T.P. and SPERLING,H.G.(1973)b "Isolation of a third chromatic mechanism in the deuteranomalous observer." Vis. Res.13, 2049-2058.
- PITT, F.H.G. (1944) "The nature of normal trichromatic and dichromatic vision." Proc.Roy.Soc.B.132, 101-117.
- POKORNY, J., MORELAND,J.D. and SMITH, V.C. (1975) "Photopigments in anomalous trichromats" J.Opt.Soc.Am. 65,1522-1524.
- POKORNY, J.and SMITH, V.C. (1977) "Evaluation of single-pigment shift model of anomalous trichromacy." J.Opt.Soc.Am. 67, 1196-1209.
- POKORNY, J.,SMITH, V.C. and KATZ, I.(1973) "Derivation of the photopigment absorption spectra in anomalous trichromats." J.Opt.Soc.Am. 63, 232-237.
- POLYAK, S.L.(1941) "The retina". Univ. of Chicago Press.
- RAYLEIGH, LORD (1881) "Experiments on colour". Nature 25,64-66.
- RODIECK, R.W. (1973) "The vertebrate retina". W.H. Freeman & Co., San Francisco.
- RUDDOCK, K.H. (1963) "Evidence for macular pigmentation from colour matching data." Vis. Res. 3, 417-429.
- RUDDOCK, K.H. (1965) "The effect of age upon colour vision - II. Changes with age in light transmission of the ocular media." Vis. Res. 5, 47-58.
- RUDDOCK, K.H. and NAGHSHINEH, S.(1974) "Mechanisms of red-green anomalous trichromacy: Hypothesis and analysis." Mod. Probl. Ophthal. 13, 210-214.
- RUDDOCK, K.H. and WATERFIELD, V.A.(1978) "Selective loss of function associated with a central visual defect." Neuroscience Letters 8, 93-98.
- RUDDOCK, K.H. and WIGLEY, E. (1976) "Inhibitory binocular interaction in human vision and a possible mechanism

subserving stereoscopic fusion." Nature 260, 604-606.

- RUSHTON, W.A.H. (1963) "A cone pigment in the protanope." J. Physiol. (Lond.) 168, 345-359.
- RUSHTON, W.A.H. (1965) "A foveal pigment in the deuteranope.". J. Physiol (Lond.) 176, 24-37.
- RUSHTON, W.A.H., POWELL, D.S. and WHITE, K.D. (1973)a "Exchange thresholds in dichromats." Vis.Res. 13, 1993-2002.
- RUSHTON, W.A.H., POWELL, D.S. and WHITE, K.D. (1973)b "Pigments in anomalous trichromats." Vis.Res. 13, 2017-2032.
- SPERLING, H.G. and HARWERTH, R.S. (1971) "Red-green cone interactions in the increment-threshold spectral sensitivity of primates." Science 172, 180-184.
- STEINBERG R.H. and SCHMIDT, R. (1970) "Identification of horizontal cells as S-potential generators in the cat retina by intracellular dye injection." Vis. Res.10, 817-820.
- STILES, W.S. (1946) "A modified Helmholtz line-element in brightness-colour space." Proc.Phys.Soc.58, 41-65.
- STILES, W.S. (1959) "Colour vision: the approach through increment threshold sensitivity." Proc.Nat.Acad.Sci. 45, 100-114.
- SVAETICHIN, G. (1953) "The cone action potential". Acta Physiol. Scand. 29, suppl. 106, 565-600.
- SVAETICHIN, G and MacNICHOL, E.F. (1958) "Retinal mechanisms for chromatic and achromatic vision." Annals New York Acad. Sci. 74, 385-404.
- THOMAS, J.P., PADILLA, G.J. and ROURKE, D.L. (1969) "Spatial interactions in identification and detection of compound visual stimuli". Vis.Res.9, 283-292.

- WAGNER, H.G., MacNICHOL, E.F. and WOLBARSHT, M.L.(1960) "The response properties of single ganglion cells in the goldfish retina." J.Gen Physiol 43, suppl 2, 45-62.
- WALD, G. (1966) "Defective colour vision and its inheritance." Proc.Nat.Acad.Sci.U.S.A. 55, 1347-1363.
- WALD, G. (1968) "Molecular basis of visual excitation" Science 162, 230-239.
- WALLS, G.L. and MATTHEWS, R.W. (1952) "New means of studying colour blindness and normal foveal colour vision". Univ. of California Press, L.A.
- WATERFIELD, V.A. (1980) "Colour and spatial pattern discrimination in human vision." Ph.D. Thesis. Univ. of London.
- WESTHEIMER, G. (1965) "Spatial interactions in the human retina during scotopic vision." J. Physiol. (Lond.) 181, 881-894.
- WESTHEIMER, G. (1966) "The Maxwellian view". Vis.Res. 6, 669-682.
- WESTHEIMER, G. (1967) "Spatial interactions in human cone vision." J. Physiol. (Lond.) 190, 139-154.
- WIESEL, T.N.and HUBEL, D.H. (1966) "Spatial and chromatic interactions in the lateral geniculate body of the rhesus monkey." J. Neurophysiol. 29, 1115-1156.
- WIGLEY, E. (1977) "Monocular and binocular responses of the human visual system to spatially structured stimuli.". Ph.D. Thesis. Univ. of London.
- WRIGHT, W.D. (1928) "A re-determination of the trichromatic coefficients of the spectral colours." Trans.Opt.Soc. 30, 141-159.
- WRIGHT,W.D. (1936) "The breakdown of a colour match with high

intensities of adaptation." J. Physiol. (Lond.) 27, 23-33

- WRIGHT, W.D. (1946) "Researches on normal and defective colour vision." Henry Kimpton, London.
- WYSZECKI, G. and STILES, W.S. (1982) "Colour Science". 2nd Ed. John Wiley and Sons, New York.
- YOUNG, T. (1802) "On the theory of light and colours." Phil. Trans. 92, 12-48.
- YOUNG, T. (1807) "Lectures on natural philosophy". Vol.2, Johnson, London.
- ZEKI, S.M. (1978) "Functional specialisation in the visual cortex of the rhesus monkey." Nature 274, 423- 428.
- ZEKI, S. (1980) "The representation of colours in the cerebral cortex." Nature 284, 412-418.

ACKNOWLEDGEMENTS

I am particularly grateful to Dr. K.H. Ruddock for his guidance, patience and encouragement throughout my research, and for his critical reading of this thesis.

I would like to thank Dr. J. Barbur, Dr. I. Holliday and Mr. I. Coole for technical help during this project, Dr. V.A. Barbur for her useful advice in the initial stages and Dr. E. Ike, Mr. P. Skinner and Mr. A. Wilson for many helpful discussions. Many thanks also to all my tireless observers!, particularly to Mr. M. White.

I acknowledge, with thanks, the receipt of a research studentship from the Science and Engineering Research Council which funded this study.

I would like to express my sincere thanks to my parents for their help and encouragement, without which this study would not have been completed, and particularly to my mother for her conscientious typing of this thesis.

Finally, I would like to thank my husband for all his patience and encouragement. This thesis is dedicated to him and to our daughter, Christine, who arrived halfway through this project!